Numerical and Experimental Investigations on Wire Electrode Health during Wire Electric Discharge Machining Process

A Thesis

Submitted in partial fulfillment of the requirements for the degree

of

DOCTOR OF PHILOSOPHY

By

Sanghamitra Das

Roll No. 166103009

Department of Mechanical Engineering
Indian Institute of Technology Guwahati
Guwahati, Assam, India
2021

Indian Institute of Technology Guwahati

Department of Mechanical Engineering

Guwahati – 781039

STATEMENT

The present thesis entitled, **"Numerical and Experimental Investigations on Wire Electrode Health during Wire Electric Discharge Machining Process"** has been carried out by me under the supervision of Prof. Shrikrishna N. Joshi, Department of Mechanical Engineering, Indian Institute of Technology Guwahati. This work has not been submitted elsewhere for the award of any degree.

Sanghamitra Das

Date: 21-12-2021

Sanghamitra Das

Roll. No. 166103009

Department of Mechanical Engineering,

Indian Institute of Technology Guwahati,

Guwahati – 781039, India

Indian Institute of Technology Guwahati

Department of Mechanical Engineering

Guwahati – 781039

CERTIFICATE

It is certified that the work described in this thesis, entitled, **"Numerical and Experimental Investigations on Wire Electrode Health during Wire Electric Discharge Machining Process"** done by **Ms. Sanghamitra Das (Roll No. 166103009),** a Ph.D. student in the Department of Mechanical Engineering, Indian Institute of Technology Guwahati, for the award of degree of **Doctor of Philosophy** has been carried out under my supervision. This work has not been submitted elsewhere for the award of any degree.

Date: 20-4-2022

Prof. Shrikrishna N. Joshi
Department of Mechanical Engineering
Indian Institute of Technology Guwahati,
Guwahati – 781039, India

Dedication

This thesis is dedicated to my parents Mr. Ashok Kumar Das and Mrs. Eva Talukdar

Abstract

Wire electric discharge machining (WEDM) is a widely used high-precision machining process. With growing demands of manufacturing sector, wire erosion and breakage act as major challenges during WEDM process. Although material removal from the workpiece is desirable to achieve the required shape and contour, wire erosion and damage are detrimental to the overall machining process. Wire wear reduces the wire strength and eventually causes the wire to fail, which is a significant disadvantage in the modern manufacturing sector. Frequent wire breakage adversely affects the product geometric precision, surface integrity, and productivity of the manufacturing establishments. The damages undergone by the wire also have a notable effect on the surface quality achieved by the workpiece during machining. To reinforce and enhance the effective utilization of the wire EDM process, it is very much essential to mitigate the frequency of wire failure. Thus, it is imperative to understand the causes of wire breakage and predict the frequency of its occurrence. Prediction and prevention of wire rupture will definitely provide some useful insights in achieving sustainable manufacturing with the desired product quality.

In this research work, a three-dimensional nonlinear transient thermo-mechanical model for a molybdenum wire used during WEDM has been developed to compute the temperature and the induced stresses. The computational ability of the developed model has been verified by conducting systematic experiments. The merit of the work lies in the use of a three-dimensional thermo-mechanical nonlinear numerical model to compute the wire strength based on the stresses generated during machining. A simple and novel method has been developed, which computes the wire safety index based on the residual stresses generated on the wire electrode surface. The stresses produced on the wire were observed to reach values beyond the yield stress (600 MPa) of the molybdenum wire at certain process conditions, which causes the reduction in strength of the wire. The wire safety index was evaluated by calculating a ratio (X) between the maximum value of residual stress induced and the yield stress of the wire. If the equivalent residual stresses produced in the wire during the discharge phenomenon is well below the yield strength of the wire, the wire is said to be within the safe limit. As the residual stress values cross the yield point, the strength of the wire starts deteriorating which is harmful to the health of the wire. Formation of microcracks on the wire surface was considered as indicators of

wire breakage to estimate the threshold value of wire strength beyond which the wire is considered to be unsafe for machining.

A comprehensive analysis of the wire wear and its deformation mechanism, morphology study of the eroded wire samples is very crucial in restricting wire failure and enhancing the overall efficiency of the operation. This section reports an extensive experimental investigation on the measurement and analysis of molybdenum wire erosion after WEDM of Ti-6Al-4V alloy at varying input levels viz. discharge voltage, discharge current, pulse on-time, pulse off-time, and wire speed. An in-depth discussion on various wire damages and deformation during the discharge phenomenon has been demonstrated. Moreover, the influence of different process conditions on wire erosion and on the surface quality achieved by the component has been investigated. The eroded wire surfaces reported damages in the form of craters, globules, microholes. A wire surface quality index for the tolerable limit of wire surface erosion without causing wire failure was estimated using image processing technique. A relationship between wire wear and product surface quality was also established using the developed technique. The mean of wire image histogram was used as an indicative tool to correlate the intensity of wire wear and the workpiece quality. It was observed that as the mean of image histogram decreases, the intensity of wire surface erosion increases. A histogram mean of 122.17 was observed to be the threshold limit below which the damages on the wire surface are critical thus increasing the probability of wire failure. Wire wear have shown a detrimental effect on the surface roughness of WEDMed components and deteriorate the surface quality by approximately 25-35 %. A comprehensive discussion on wire breakage due to excessive erosion is also presented. The findings presented in this work extend the existing area of knowledge in this field and give better insights to understand the wire erosion mechanism and achieve stable machining without wire breakage.

The work has been extended to study the characteristics of coated wires during WEDM cutting operation. Nowadays, coated wires are extensively used in modern manufacturing industries due to improved properties as compared to uncoated wires. A three-dimensional thermo-mechanical finite element model (FEM) of a zinc coated brass wire electrode during WEDM process was developed. The temperature and stresses generated in the wire at different sets of process conditions are computed using the developed model. The crater volume produced in the wire is calculated when the temperature exceeds the melting point of the wire material. The stresses induced in the zinc coated brass wire were noted to be lower than the yield strength of the core brass

material. Thus, the wire strength is estimated based on the amount of material removed from the zinc coated brass wire. In the end, parametric studies to investigate the effects of input parameters on the temperature, residual stresses and crater volume generated in the wire are carried out.

The final part of the work presents a detailed experimental investigation of the erosion and deformation of a zinc coated brass wire during WEDM experiments on Ti-6Al-4V alloy. A comparative study between the characteristics of molybdenum wire and zinc coated brass wire showed that for the same process conditions, the zinc-coated brass wire suffers severe damages as compared to the molybdenum wire. The outer coating layer of zinc erodes faster due to its low melting temperature of 693 K. The zinc layer offers protection for the brass core against thermal shock and arc discharges produced during the discharge phenomenon. Material erodes from the zinc-coated brass wire substantially as soon as the melting point of brass is also reached. The reason behind the higher wear rate of zinc-coated brass wire in comparison to molybdenum wire is the lower melting point of zinc (693 K) and brass (1203 K) as compared to molybdenum (2896 K). The molybdenum wire is also less prone to breakage in comparison to the zinc coated brass wire due to its high tensile strength. The relationship between wire wear and workpiece surface roughness is also established. Thus, despite the zinc coating around the brass core, the performance of the molybdenum wire can be considered better in terms of wire health and workpiece surface quality. The disadvantage associated with molybdenum wire is its high cost and hence industries may prefer zinc-coated brass wire for bulk machining of products and rough cutting operations for a set of optimized process conditions.

Acknowledgements

My research work has been an incredible journey of continuous learning, hard work and perseverance. The constant support, motivation and help that I have received from many people during the entire span of my thesis work have made this journey a zenith of growth.

I would like to thank the Ministry of Education, Government of India, for providing financial support. I sincerely thank the Indian Institute of Technology Guwahati for providing all sorts of infrastructural facilities to carry out this doctoral research work. I also extend my heartfelt gratitude to DPPC secretary, Mechanical office staff and hostel authorities for extending all necessary help during my PhD tenure.

I wish to express my sincere and deep appreciation to my supervisor, Prof. Shrikrishna N. Joshi, for his encouragement, insightful guidance, patience, and enthusiastic support throughout my studies, including the writing of this dissertation. I am especially thankful to him for critically reviewing the reports and research papers despite his busy schedule of academic and other administrative works.

I am highly thankful to my doctoral committee members, Prof. S. Senthilvelan, Dr. Manas Das, and Dr. Arindam Dey, for their continuous academic guidance and for checking my work progress and seminars during my Ph.D. Their valuable discussions and suggestions were truly encouraging for me.

I would like to express my sincere gratitude to Prof. K. S. R. Krishna Murthy, Prof. S. Senthilvelen, Prof. Santosha K. Dwivedy, and Prof. Anoop K. Dass, present and former Heads, Department of Mechanical Engineering, Indian Institute of Technology Guwahati, for providing various laboratory facilities and sanctioning funds without which completion of the work would not have been possible. I am also grateful to all the faculty members of the Mechanical Engineering department.

I would also like to acknowledge the Advanced Manufacturing Laboratory, Material Science Laboratory, Central Workshop, and Central Instruments Facility of Indian Institute of Technology Guwahati and all scientific officers and staff members for providing instruments and helping me to carry out the research work.

I deeply acknowledge the unabated support and counseling provided by my colleagues and friends, Dr. Ravikant, Dr. Borad M. Barkachary, Dr. Gururaj Bolar, Dr. S.

Sunderlal Singh, Ms. Ngangkham Devarani, Mrs. Upasana Sarma, Mr. Brijesh Kumar Singh, Mr. Ritam Sharma, Ms. Swati Singh, Mr. Antash Kishore Sinha, and, Mr. Evenmore Mylliem throughout my studies. I highly appreciate the technical cooperation given by Mr. Jiten Basumatary and Mr. Saiffuddin Ahmed. I am also grateful to the Assistant Workshop Superintendent, Mr. Nandan Kanan Das and other staff members of the workshop, Mr. Chandan Banikya, Mr. Dilip Chetry, Mr. Joykrishna Saikia, and Mr. Gwmchar Baro for their assistance during my experimental work.

My most sincere gratitude and appreciation go to my father, Mr. Ashok Kumar Das, my mother, Mrs. Eva Talukdar, my brother, Mr. Pritam Das for their patience, continuous encouragement, and moral support over the past difficult years. I am deeply indebted to all the other members of my family who gave me constant support and encouragement throughout my life.

Last, but not the least, I am thankful to the Almighty for providing me this wonderful experience and such an awesome aura for research work.

Date: 21-12-2021

Sanghamitra Das

Sanghamitra Das

(RollNo. 166103009)

Contents

List of figures

List of Tables

List of abbreviations

ANOVA	Analysis of variance
EDX	Energy dispersive X-ray
FESEM	Field emission scanning electron microscope
WEDM	Wire electric discharge machining
XRD	X-ray Diffraction

List of symbols

A_0	Original cross-sectional area of the wire
A_c	Cross sectional area of the machined wire sample (μm^2)
A_{rem}	Amount of material removed from the wire cross-section (μm^2)
b_i	Body force vector
$[B]$	Geometry matrix
c	Specific heat (J/kgK)
$[C]$, $[K]$	Global heat capacity matrix and global conductivity matrix respectively
d	Distance between crystallographic planes of a sample
$\{d\}$	Nodal displacement degree of freedom of an element
D	Constitutive matrix
$[D_e]$	Elastic stiffness matrix
$[D_p]$	Plastic stiffness matrix
D_c	Depth of discharge crater (μm).
E	Young's modulus (GPa)
E_0	Energy density
F_a, F_c, F_d	Fraction of energy absorbed by the anode, cathode and dielectric respectively
h	Convective heat transfer coefficient (W/m^2K).
I	Discharge current (A)
k	Thermal conductivity (W/mK)
$[K_{th}]$	Thermal stiffness matrix
L	Distance travelled by the wire during a single pulse cycle
L_{on}	Distance travelled by the wire during a single pulse on-time
$[N]$	Shape function matrix
N_i	Lagrange shape function
Q	Heat flux applied (W/m^2)
$\{Q\}$	Heat flux matrix
r, φ, z	Cylindrical coordinates
R_w	Wire radius (μm)
R	Spark radius (μm)

R_c	Radius of discharge crater (μm)
Ra	Surface roughness (μm)
t_{on}	Pulse on-time (μs)
t_{off}	Pulse off-time (μs)
T	Temperature (K)
T_b	Boiling point temperature of work material (K)
$\{T_e\}$	Element nodal temperature matrix
$\{u\}$	Displacement field
v	Wire velocity (m/s)
V	Discharge voltage (V)
V_c	Crater volume in the wire (μm^3)
W_{av}	Average input power (W)
α	Thermal diffusivity (m^2/s)
α_e	Thermal expansion coefficient (K^{-1})
ρ	Density of wire material (kg/m^3)
ν	Poisson's ratio
$\sigma_{r,T}$, $\sigma_{ax,T}$	Radial and axial stresses originated due to temperature gradients on the wire
$\sigma_{ax,ext}$	Stress produced due to initial tension applied to the wire
σ_{ij}	Stress tensor
σ_y	Yield strength (MPa)
σ_1, σ_2, σ_3	*x, y* and *z* components of stresses respectively
σ_{12}, σ_{23}, σ_{13}	Shear components of stress
$d\sigma$, $d\varepsilon$, dT	Stress, Strain, and Temperature increments
ε	Strain of a sample
θ	Diffraction angle
λ	Specific wavelength of X-ray
ξ, η, ζ	Isoparametric coordinates of the eight noded hexahedral element

CHAPTER 1

Introduction

Wire electric discharge machining (WEDM) is widely used in the manufacture of dies and punches, microsurgical tools, thin-walled structural parts in aerospace industries, semiconductor applications, gauges, cams, etc. Figure 1.1 shows some important applications of WEDM in modern day industries. Many difficult to machine materials like titanium, metal matrix composites, tool steel can be easily machined using this process. WEDMed products have good accuracy and surface finish. A number of factors play an important role in maintaining the precision and quality of the final parts to meet the demands of modern day applications. Apart from the process conditions used during the cutting operation, the wire material and wire properties play a crucial role in determining the quality of the components. The frequent occurrence of wire rupture, however poses a serious threat as it disrupts the entire production line and causes environmental hazards. It increases machining time, human labour and resources. Moreover, the wire damages cause geometrical errors and degrades the surface finish of the workpiece. Thus, it is of utmost importance to predict and limit the occurrence of wire failure in order to achieve sustainability in machining along with the desired machining efficiency.

1.1 Wire electric discharge machining

WEDM is an important non-contact machining process that removes material by generating electric spark discharges in between the wire electrode and workpiece. It is a thermal process that removes material from electrically conductive materials by the method of melting and vaporization. It is advantageous over conventional methods of machining due to its ability to cut electrically conductive materials irrespective of their hardness and melting point, which is otherwise very difficult to cut by traditional machining methods like milling and grinding. WEDM employs a thin moving wire of diameter in the range of 0.05 – 0.3 mm as the cutting tool (Pramanik and Basak (2016)). Deionized water, a dielectric medium is applied in a very narrow interelectrode gap of the order of 12–50 μm between the wire and workpiece (Benedict (1987)). The moving cathodic wire traverses over the workpiece and high frequency electrical discharges are created by a DC power source and a pulse generator.

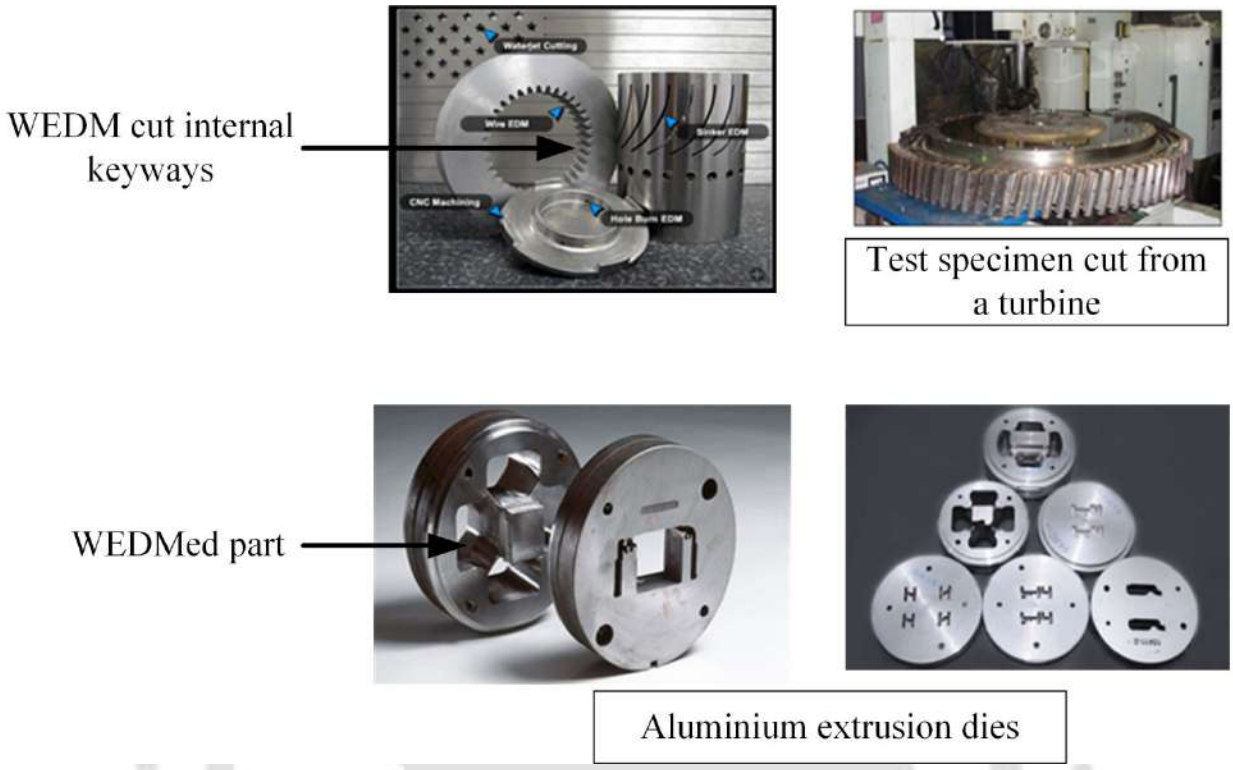

Figure 1.1 Components machined using wire EDM process (http://www.wirecutcompany.com/capabilities_facilities.html as seen on 7/10/2016)

Figure 1.2 shows the process mechanism of a wire EDM cutting process. An enlarged view of the wire workpiece interaction and the formation of the plasma channel is also depicted. When electric current is applied between the wire electrode and workpiece, there is a continuous flow of electrons and positive ions between the cathode and anode. The wire acts as the cathode and the workpiece acts as the anode during the WEDM process. The surrounding dielectric fluid breaks down and the power supply decreases the applied voltage delivered to the gap, but raises the current. This creates an intense electrical field, which causes the formation of a discharge channel in the narrow interelectrode gap. A huge amount of temperature is generated during the spark discharges, which melts and vaporizes material from both the electrodes. The pressure generated causes the formation of a bubble around the plasma channel, which collapses as soon as the discharge stops. This creates a shock wave front and the violent rush of dielectric fluid into the machining zone flushes away the molten material forming small craters in both the wire electrode and workpiece.

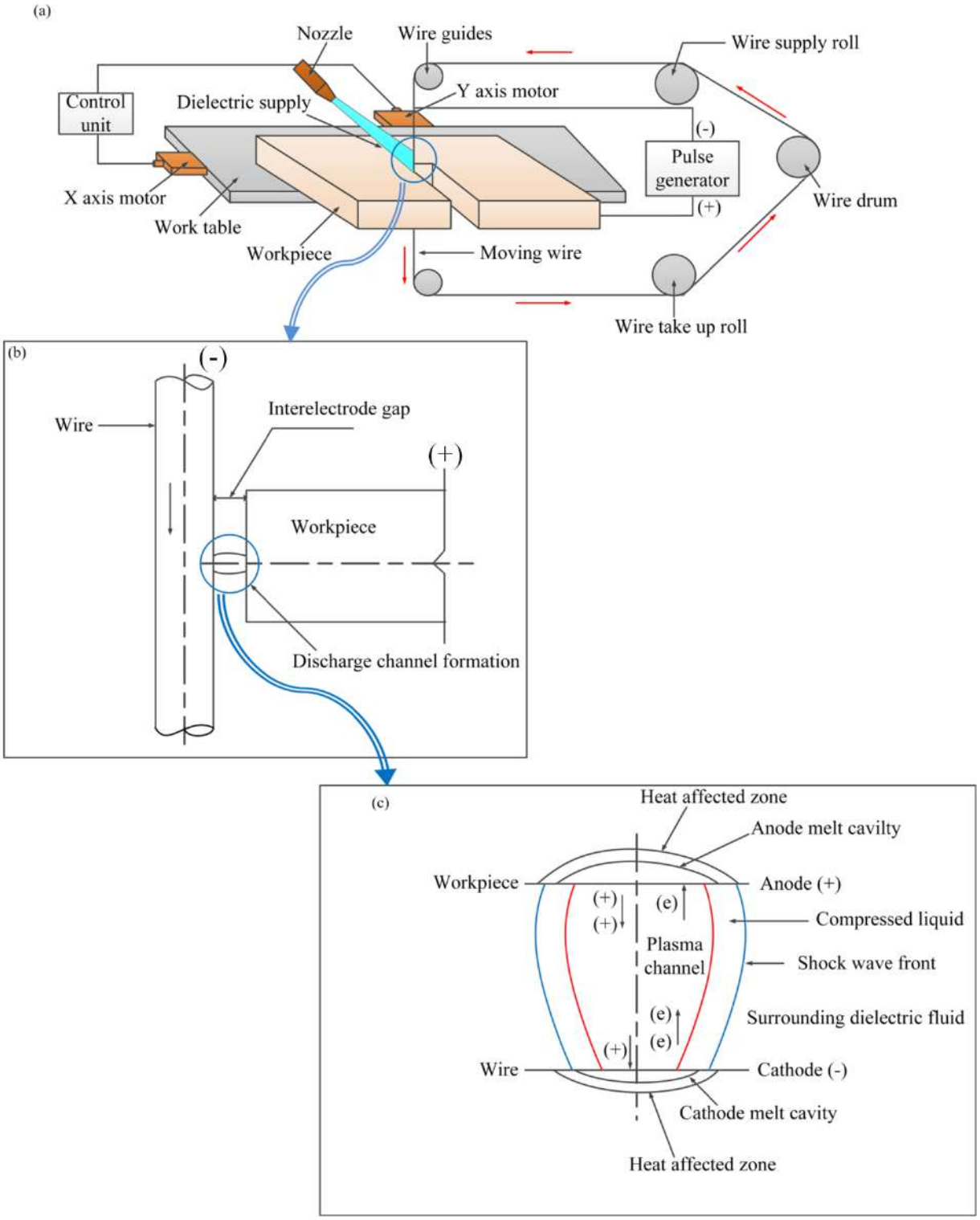

Figure 1.2 (a) Schematic of a WEDM setup (b) Interaction between the wire electrode and workpiece (c) Formation of plasma channel in the interelectrode gap

1.2 Importance of wire health during WEDM cutting

The wire electrode is an important element of the WEDM system. A moving wire with a diameter range of 0.05–0.3 mm acts as the tool electrode and deionized water as dielectric (Benedict (1987)). Brass, copper, tungsten, molybdenum are some of the materials used for a wire electrode. The wire traverses along a predefined path through the workpiece and is held between two tension rollers with a constant tension in order to maintain the straightness and strength of the wire. The wire electrode also plays a significant role in deciding the surface quality and geometrical precision of the machined products.

During wire EDM process, wire experiences combined thermal and mechanical loads, which decreases its strength and may lead to wire breakage. Temperature rise during the repetitive spark discharges is the most critical factor responsible for wire erosion and failure (Dekeyser et al. (1988)). The wire starts eroding when the temperature gradients exceed the melting point of the wire material. Although material removal from the workpiece is desirable to achieve the required shape and contour, wire erosion and damage are detrimental to the overall machining process. Wire wear reduces the strength and eventually causes the wire to fail, which is a significant disadvantage in the modern manufacturing sector. The wire strength further diminishes due to the thermal and residual stresses originated due to temperature rise during the spark cycles. The residual stresses retained in the wire electrode reduce the strength of the wire which may result in the formation of microcracks and eventually cause the wire to rupture. This undesirable situation hampers the overall output of the system causing surface damage to the component, loss of machining time, and resources. Wire failure adversely affects the process productivity and geometrical accuracy of cut parts. The frequent occurrence of wire rupture has tremendously reduced the efficiency and growth of the manufacturing system especially during assembly line operations. The damages undergone by the wire also have a notable effect on the surface quality achieved by the workpiece during machining. Thus, the wire health is an important aspect to be considered during WEDM cutting in order to meet the demands of modern day applications and achieve sustainable machining.

1.3 Motivation for the present research work

The health of the wire tool plays a crucial role in determining the machining efficiency and productivity. During WEDM spark discharges, the generation of huge amount of temperature causes material melting and removal from both the electrodes. Erosion of the wire electrode degrades the wire strength and drastically reduces the wire life. The probability of wire failure increases which hampers the overall manufacturing line in industries. Wire breakage is a great environmental hazard as it increases the energy consumption and resources. Proper disposal or reusability of used wires is still a major challenge, which poses as a serious environmental threat. Thus, the prediction and prohibition of wire failure is essential to achieve sustainable and uninterrupted machining. In order to limit the occurrence of wire failure, we need to have a deeper understanding of the causes of wire rupture. The study of wire health and the factors controlling the life of a wire is of prime importance in order to meet the increasing demands of modern day production sector.

Several WEDM studies have focussed on optimizing the WEDM performance by improving the MRR, surface quality and geometrical precision of the machined products. In comparison to the studies carried out on the workpiece, a very limited amount of research has discussed the importance of wire tool and the methods to limit the wire breakage phenomenon (Banerjee et al. (1993), Saha et al. (2004), Banerjee and Prasad (2010), Fedorov et al. (2018)). The characteristics of the wire during the spark discharges need to be critically analysed. Moreover, an elaborate analysis on the morphology of eroded wire samples as well as workpiece samples is imperative in order to have a deeper understanding of the wire failure process. Pramanik and Basak (2016) and Pramanik and Basak (2018) explained the wear mechanism by investigating the eroded wire samples; however a deeper understanding of the wire behaviour during failure is vital to achieve sustainable manufacturing. A need was thus identified to develop a thermo-mechanical model of the wire tool during the discharge process for accurate prediction and prevention of wire rupture. The development of a numerical model shall provide some useful insights into estimating the wire strength during the metal cutting operation. A health index for the wire tool shall be highly useful to the manufacturers to predict the probability of wire failure. The evaluation of a wire safety factor based on the results predicted by the model shall provide important guidelines to maintain the wire health and hence improve the wire life. Moreover, the wire undergoes severe damages

during the discharge phenomenon. The wire erosion cannot be eliminated completely but can be minimized to maintain the wire strength. Thus, it was thought worthy enough to estimate a wire surface quality index to quantify and minimize the intensity of surface damages undergone by the wire. This cumulatively provided the motivation to carry out the present research work.

1.4 Scope of the present research

The present work primarily focuses on the prediction and prevention of wire erosion and breakage in order to achieve sustainable and efficient WEDM machining. Initially, a realistic three-dimensional thermo-mechanical model is developed for the molybdenum wire tool to estimate a wire safety index for safe metal cutting operation. The developed model could predict the temperature and stresses generated in the wire tool during machining. The model was well validated with experimental data. The wire safety factor was established based on the thermally induced stresses in the molybdenum wire in order to predict the occurrence of wire failure.

Extensive experimental analysis was carried out on the WEDM setup with molybdenum wire as the tool and Ti-6Al-4V alloy as the workpiece. This study was carried out to understand the wire erosion mechanism and the detrimental influence of wire wear on product quality. A wire surface quality index was developed using the image processing technique to estimate the extent of damages on the wire samples. The developed technique proved to be a useful tool in establishing a tolerable limit of wire surface erosion to minimize breakage and maintain the desired surface quality of the components. The histogram mean of the collected images of eroded wire samples could also establish the interrelationship between wire wear and the surface finish of the workpiece.

With increasing demands of high productivity, coated or stratified wires are utilized with excellent sparking abilities. Zinc-coated brass or zinc-coated copper wires were developed which improved the cutting speed along with better flushing and debris removal characteristics (Prohaszka et al. (1997)). Thus, the research work was extended to study the characteristics of zinc coated brass wires during WEDM operation. Both numerical and experimental studies were carried out to investigate the erosion and rupture pattern of coated

wires. A comparative study was further performed to analyse the behaviour of both the molybdenum wire and the zinc coated brass wire during machining.

1.5 Organization of the thesis

The organization of chapters in this thesis in detail is as follows.

Chapter 1 presents the fundamentals of the WEDM process and the importance of wire electrode during cutting. It also discusses the various challenges faced due to wire breakage and the motivation behind the work.

Chapter 2 presents a detailed literature survey of the experimental as well as theoretical research work reported on various aspects of wire electrode erosion such as the effect of heat generated in spark plasma, thermal stresses, wire rupture phenomena, wire fatigue. It also presents important research findings on the causes of wire failure and advancements to reduce wire breakage with various wire health monitoring and control systems. The chapter concludes by summarizing important observations from the literature survey and stating the research objectives.

Chapter 3 presents the three-dimensional thermo-mechanical finite element modeling of a molybdenum wire electrode. The numerical model is presented in detail, in terms of its governing equations, assumptions, boundary conditions, heat flux model, material properties and solution methodology. The model is well validated with published results and experimental data. In the end, a case study on the numerical simulation of the thermo-mechanical characteristics of the wire electrode, which computes the temperature and stresses generated in the wire, is presented.

Chapter 4 presents the estimation of the strength of a molybdenum wire based on thermally generated residual stresses induced in the wire electrode during the pulsed discharges. The stresses are computed from the developed numerical model presented in chapter 3. A wire safety factor is evaluated to predict and limit the probability of wire failure.

Chapter 5 presents a detailed experimental investigation of the molybdenum wire erosion and deformation during WEDM experiments on Ti-6Al-4V alloy. The measurement and analysis techniques of the performance responses have been explained in a detailed manner. An in-depth discussion on various wire damages and deformation during the discharge phenomenon has been demonstrated. Moreover, the influence of different process

conditions on wire erosion and on the surface quality achieved by the component has been investigated.

Chapter 6 presents the estimation of a wire surface quality index for the tolerable limit of wire surface erosion using image processing technique. The overall approach of image processing technique has been clearly demonstrated. The utilization of image processing technique to evaluate a wire safety index, which shall establish the tolerance level of wire damages without wire breakage, is elaborated in a comprehensive manner. A relationship between wire wear and product surface quality was also established using the developed technique. A comprehensive discussion on wire breakage due to excessive erosion is also presented in this chapter.

Chapter 7 presents the three-dimensional thermo-mechanical modeling of a zinc-coated brass wire electrode using the finite element method. The model is well validated with experimental data. The temperature and stresses generated in the wire at different sets of process conditions are computed using the developed model. The crater volume produced in the wire is calculated when the temperature exceeds the melting point of the wire material. The wire strength is estimated based on the amount of material removed from the zinc coated brass wire. In the end, parametric studies to investigate the effects of input parameters on the temperature, residual stresses and crater volume generated in the wire are carried out.

Chapter 8 focuses on the measurement and analysis of zinc-coated brass wire erosion and deformation during wire electric discharge machining of Ti-6Al-4V alloy. The overall experimental procedure, experimental setup and methods are similar to as explained in chapter 5. The image processing technique as explained in chapter 6 has been employed to estimate the extent of erosion on the surface of zinc coated brass wires. The relationship between wire wear and workpiece surface roughness is also established. Moreover, the influence of different process conditions on wire erosion and on the surface quality achieved by the component has been investigated.

Chapter 9 summarizes the research contributions of the work and discusses the challenges and future scope of the work.

CHAPTER 2

Literature review

2.0 Scope

This chapter reviews the performance of a wire electrode and various factors associated with wire breakage during machining. It presents a detailed survey on different numerical and experimental studies carried out on the wire tool during WEDM cutting operation. The major causes that lead to wire breakage during the machining process are demonstrated. The influence of the wire electrode on the machining output and the importance of prohibiting the wire breakage phenomenon to achieve good machining precision is explained. Different methodologies to predict and limit the occurrence of wire failure have been comprehensively discussed. The latter section of the chapter discusses certain research gaps related to the concerned area and the research objectives have been derived.

2.1 Causes of wire breakage

The wire tool is an important element of the WEDM setup. Different properties of the wire viz. geometrical properties, heat carrying capacity, thermo-physical properties, wire material etc. significantly affect the efficiency and productivity of the cutting operation. The frequent occurrence of wire rupture, however has tremendously reduced the growth of the manufacturing system.This undesirable situation hampers the overall output of the system causing surface damage to the component, loss of machining time, and resources. Wire failure adversely affects the process productivity and geometrical accuracy of cut parts. There is huge monitory loss for machine downtime during wire breakage. Thus, prediction and prevention of wire breakage is crucial to achieve sustainable and uninterrupted WEDM process. Thus, understanding the causes of wire rupture shall provide certain useful insights to prohibit the occurrence of wire failure.

Figure 2.1 depicts a fishbone diagram showing the critical reasons behind wire failure. During wire EDM process, wire experiences combined thermal and mechanical loads, which decreases its strength and may lead to wire breakage. Apart from this, wire vibration, bowing, the wire lag phenomenon, and various other forces acting on the tool electrode during the discharge phenomenon also contribute to breakage. Research shows that thermal

load is the primary reason behind wire rupture, and the stresses induced due to temperature rise reduce the mechanical strength of the wire, thus making it prone to failure. The wire starts eroding when the temperature gradients exceed the melting point of the wire material. Wire wear reduces the strength and eventually causes the wire to fail, which is a significant disadvantage in the modern manufacturing sector. The wire strength further diminishes due to the thermal and residual stresses originated due to temperature rise during the spark cycles. Figure 2.2 represents the statistics of the research analysis carried out on the various causes of wire failure. The following sections elaborate on each of the wire breakage causes in detail.

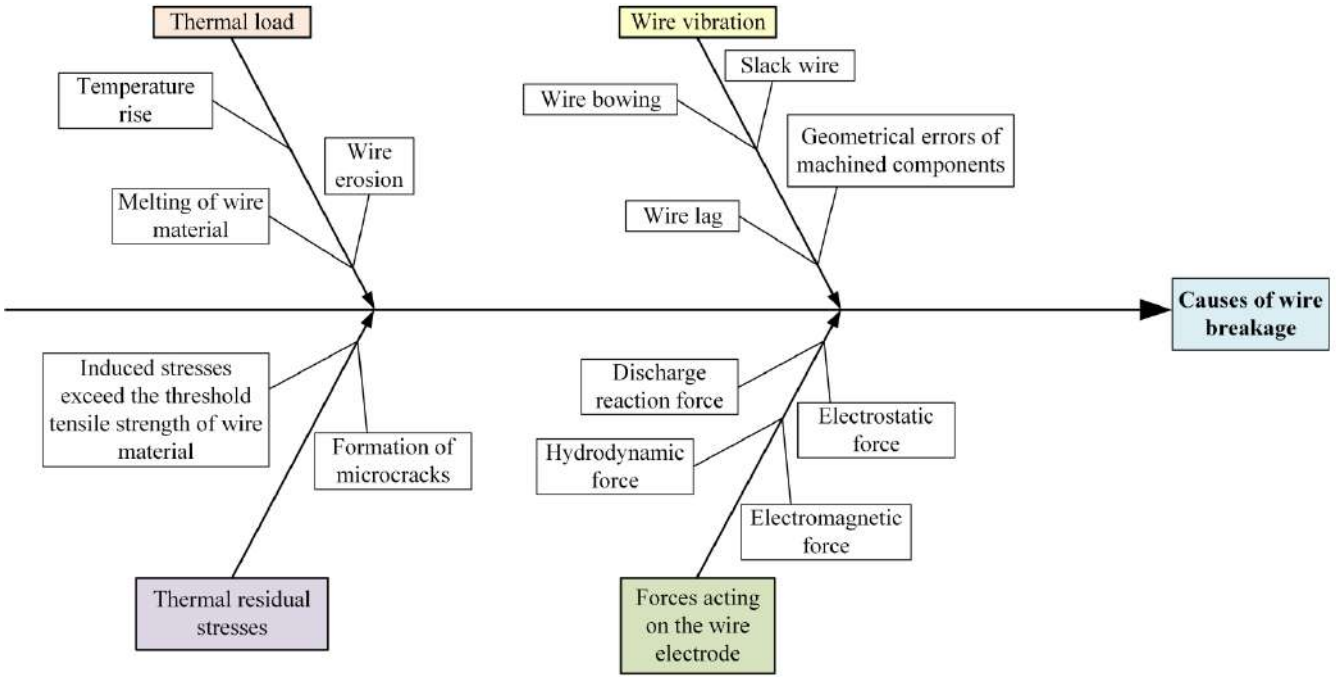

Figure 2.1 A fishbone diagram showing the various causes of wire breakage

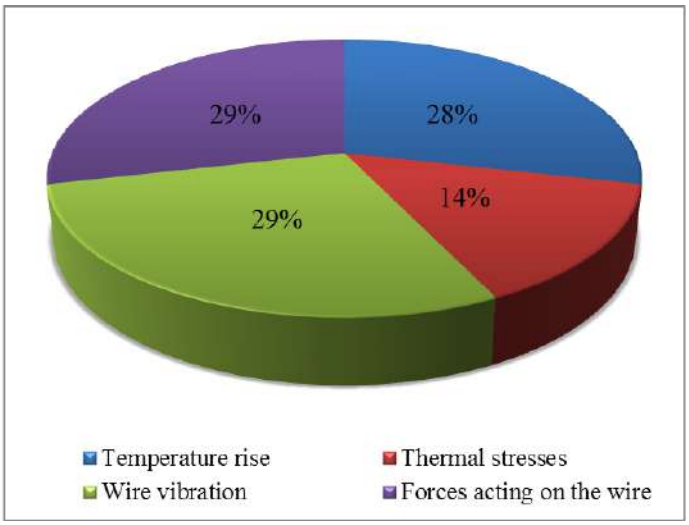

Figure 2.2 Statistical data of the research analysis carried out on the various causes of wire breakage

2.1.1 Thermal loads generated during spark plasma

The wire is subjected to excessive thermal loads due to successive discharges and attains a very high temperature, sometimes exceeding the material's melting point. This causes erosion of the wire material and decreases the cross-sectional area of the electrode, thus diminishing the wire strength. Literature shows that a sharp rise in temperature during the cutting process is the primary factor causing wire breakage.

Researchers have developed numerical models to estimate the temperature rise in the wire electrode during machining. Dekeyser et al. (1985) developed a fundamental thermal model to evaluate the effect of different process conditions on the temperature attained by the wire to predict the wire breakage phenomenon. An analytical solution is compared with a numerical finite difference method, and it was observed that the power dissipation exceeding the normal working conditions is an indicator of wire failure. Similar approaches were adopted by authors (Jennes et al. (1984), Obara (1995)) to predict the temperature contour in the wire and its contribution to wire failure. Figure 2.3 shows the schematic of interaction between the discharge channel, wire, and workpiece during a single discharge.

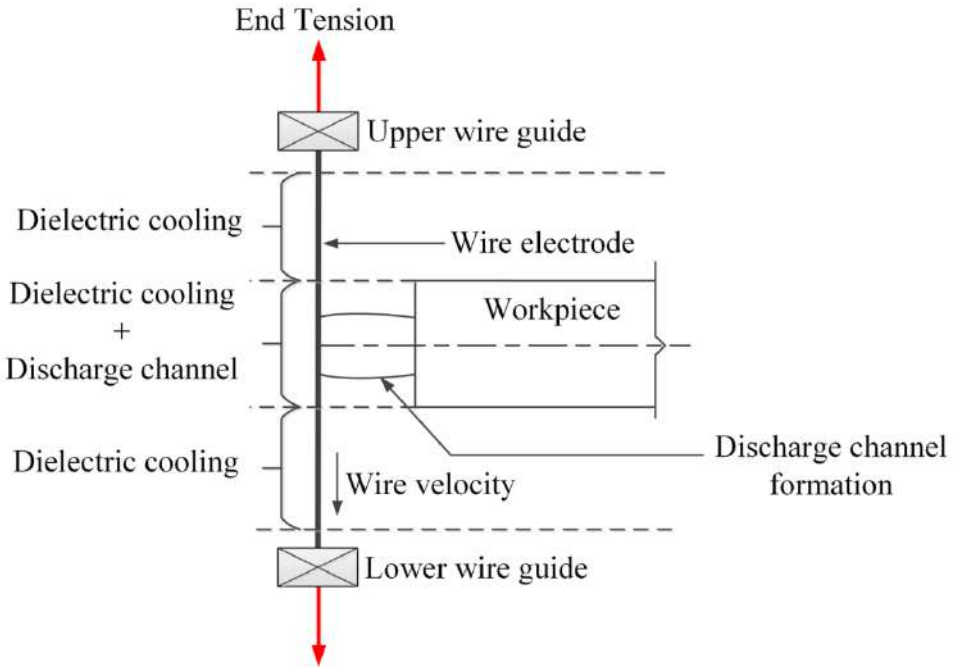

Figure 2.3 Schematic of the interaction between the discharge channel and the wire

It was noted that a sharp rise in temperature with higher input power and reduced diameter of wire increases the probability of failure (Banerjee et al. (1993)). In a similar study, Banerjee et al. (1997) predicted the three-dimensional transient temperature plot and material removed on the wire with the help of an explicit finite difference method. The geometry of interaction between the discharge channel and the wire tool is shown in Figure 2.4. The wire is subjected to heat flux $Q(t)$ for the region A-B i.e. zone I where the discharge channel falls on the wire circumference. The heat transfer analysis is governed by a three-dimensional transient heat conduction equation in cylindrical polar coordinates (r, φ, z) (Banerjee et al. (1997)).

$$\frac{\partial^2 T}{\partial r^2}+\frac{1}{r}\frac{\partial T}{\partial r}+\frac{1}{r^2}\frac{\partial^2 T}{\partial \varphi^2}+\frac{\partial^2 T}{\partial z^2}-n\frac{\partial T}{\partial z}=\frac{1}{\alpha}\frac{\partial T}{\partial t} \tag{2.1}$$

where $n=\dfrac{\rho c v}{k}$.

Assuming semi sine variation of the dissipated power, $Q(t)$ is expressed as

$$Q(t)=\frac{\left[(\pi/2)W_{av}\sin(\pi t/t_{on})\right]}{\pi\left[R(t)\right]^2}. \tag{2.2}$$

The geometry of interaction between the wire geometry and the plasma channel for region A-B (Figure 2.4) is represented by

$$\left(R_w \sin\phi\right)^2 + z_p^2 = \left[R(t)\right]^2 \tag{2.3}$$

where T is the temperature, α is thermal diffusivity (m^2/s), t is time (s), ρ is density of the material (kg/m^3), c is specific heat (J/kg K), v is wire velocity (m/s), k is thermal conductivity (W/mK), $Q(t)$ is the heat flux, W_{av} is the average input power (W), t_{on} is the discharge duration, R is the discharge radius.

For the boundary II region, convection is applied between the wire surface and the dielectric fluid. Results clearly showed that the temperature affected region in the wire shifted in the direction of wire velocity, with increasing pulse duration. The material removal rate (MRR) from the wire surface and the heat-affected zone increase with the increase of discharge power and pulse duration due to the generation of higher temperatures.

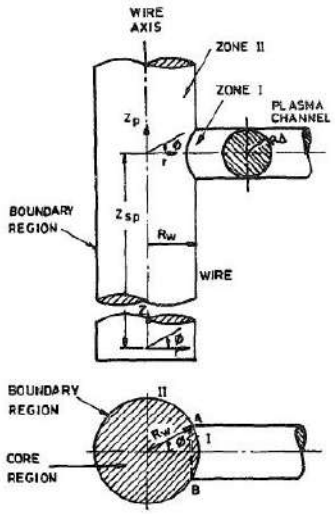

Figure 2.4 Interaction between the plasma channel and the wire during WEDM (Banerjee et al. (1997)) (Reproduced with permission from Elsevier)

Saha et al. (2004) were the first to employ a simple finite element model (FEM) to predict a critical variable for wire breakage. Transient thermal analysis for randomly located multiple discharges on the wire electrode was also reported by Banerjee and Prasad (2010). The effects of process parameters like discharge power input, pulse frequency, duty factor, and wire speed were studied. The predicted values of peak wire temperature suggest the probability of wire rupture risk. The effect of moving wire during the WEDM operation was

incorporated using moving heat source characteristics in a numerical model which was developed for a single pulse (Yang et al. (2012)).

The average temperature rise in the wire electrode was also recorded experimentally which was further used to evaluate the convective heat transfer coefficient during machining (Han et al.(2009)). The temperature attained by the wire is affected by several factors, such as energy density, kerf geometry, and dielectric pressure. Similarly, an attempt was made to measure the temperature rise in the wire electrode by using a two-color pyrometer with an optical fiber (Koyano et al. (2018)).

2.1.2 Thermal residual stresses generated in the wire electrode

The temperature rise during the cutting process generates thermal stresses in the heat-affected region for both the wire and the workpiece. The sudden rise in temperature during the discharge duration and cooling during the discharge off-time generates thermal residual stresses on the electrodes. The induced thermal residual stresses in the wire electrode deteriorate the wire health when the stresses increase above the yield strength of the wire material. The mechanical constraint applied to keep the wire vertically straight controls the deviation but produces plastic strain in the wire which further increases the residual stress formation (Kumar and Bag (2019)). A group of researchers (Saha et al. (2004), Han et al. (2008), Fedorov et al. (2018)) thus thought it important enough to evaluate the impact of residual stresses on the wire failure. The temperature and stress distribution in a microwire after the cutting operation were estimated by a coupled thermo-mechanical model (Han et al. (2008)). Wire tension was optimized and controlled for discharge energy input to improve the machining precision and avoid wire breakage. A 2D model was also developed during a gear cutting process to evaluate the influence of temperature and stresses generated on the wire cross-sectional area (Mohapatra et al. (2018)). The influence of internal thermal stresses generated due to wire thermal expansion and the wire pretension on wire failures was evaluated based on Hooke's law (Fedorov et al. (2018)). The thermal stresses produced in the wire electrode along the radial and longitudinal direction due to temperature rise during the discharge cycles were estimated mathematically using the following equations(Fedorov et al. (2018)).

$$\sigma_{r,T} = \frac{\alpha_e E}{1-\nu}\left(\left[\frac{1}{R_w^{\,2}}\int_0^{R_w} T\,r\,dr - \frac{1}{r^2}\int_0^{r} T\,r\,dr\right]\right) \tag{2.4}$$

$$\sigma_{ax,T} = \frac{\alpha_e E}{1-\nu}\left(\left[\frac{1}{R_w^{\,2}}\int_0^{R_w} T\,r\,dr + \frac{1}{r^2}\int_0^{r} T\,r\,dr - T\right]\right) \tag{2.5}$$

$$\sigma_{ax} = \sigma_{ax,T} + \sigma_{ax,ext}$$

where $\sigma_{r,T}$, $\sigma_{ax,T}$ are the radial and axial stresses originated due to temperature gradients on the wire, α_e is the thermal expansion coefficient (K^{-1}), E is the Young's modulus of the wire material (N/m^2), v is the Poisson's ratio, R_w is the wire radius (μm), T is the temperature (K).

2.1.3 Wire vibration and bowing

The stochastic nature of sparks produced during the discharge phenomenon exerts various forces on the wire electrode, which causes the wire to vibrate and deviate from its vertical position. This deviation of the wire from its straight programmed path is called wire bowing. Wire vibration and bowing result in inaccurate cuts and precision errors in the workpiece. Various attempts have been made till date to model the wire electrode vibration and measure the vibration amplitude. These numerical models are useful tools to understand the wire bowing effect and its connectivity to wire breakage. In the following section, the various causes of wire vibration, bowing, and failure are identified.

The wire electrode can be compared to a vibrating string and the vibration amplitude of the wire in a free environment is reduced to a large extent when immersed in dielectric due to its dampening effect (Dauw et al. (1989)). Arunachalam et al. (1998) pioneered the development of a computational model to evaluate the amount of wire bowing and vibrations induced during the machining process but only in the frontal direction. Figure 2.5 shows the illustration of a wire tool vibration during WEDM. The temperature fields generated on the wire during the cutting operation also have a noteworthy effect on the vibration and stability of the wire (Murphy and Lin (2000)).

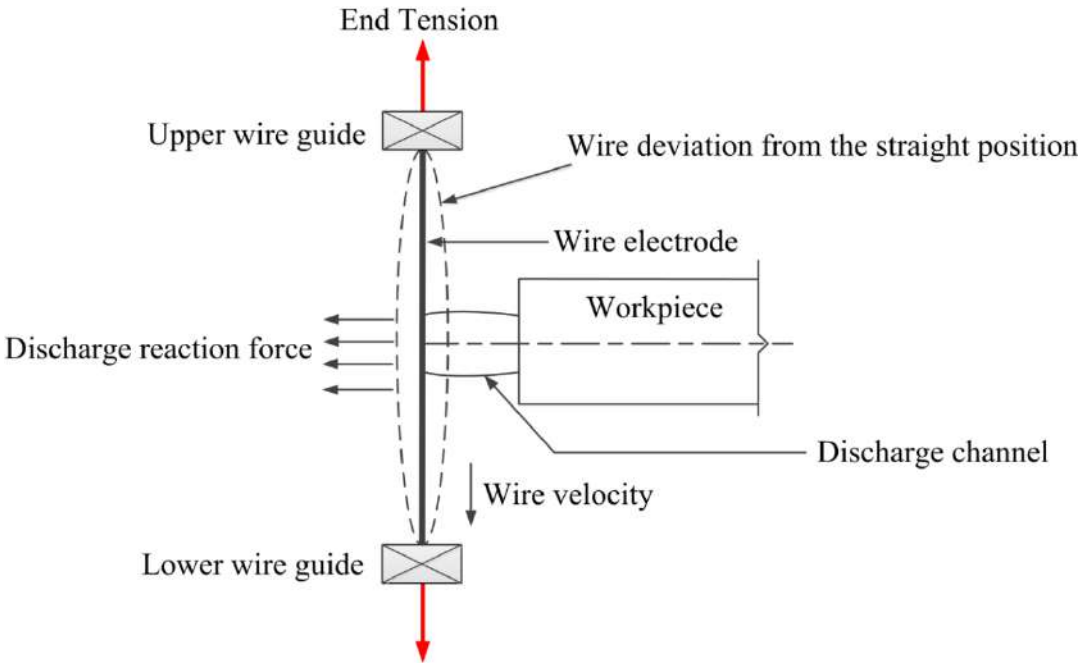

Figure 2.5 Schematic of the wire electrode vibration in the WEDM process

Guo et al. (2003) further extended the study of Arunachalam et al. (1998)to investigate the effects of wire instability on the distribution of the discharge points. During the initial break-in stage, it was observed that accumulation of discharges occurs at distinct regions of the wire, which causes wire failure. It was reported that the vibration amplitude for a particular span of wire under multiple discharge conditions is higher for greater thickness workpieces as compared to that of lesser thickness workpieces (Puri and Bhattacharyya (2003a)).The straight wire configuration is stable at low axial wire transport speed, and the stability of the wire is highly dependent on wire vibration (Lambert and Murphy (2002)). It was also summarized that the amplitude of wire vibration is more in the machining direction as compared to the direction perpendicular to the wire (Kamei et al. (2016)).

Das and Joshi (2010) developed a numerical model by considering the moving heat source characteristics, multiple sparks, and wire vibration to estimate the wear rate of the wire electrode. The authors observed that the wire diameter influences the temperature rise at the periphery. The frequency and amplitude of wire vibration were also analyzed using a multi-physics coupled model by incorporating the thermal, electromagnetic, and physical aspects of modelling (Chen et al. (2015)). It is very essential to minimize the wire deviation caused due to wire vibration to minimize the frequency of wire breakage and to improve

precision machining efficiency. Some practical methods to minimize the wire deviation and inhibit wire failures were proposed by considering the effects of both temperature and wire vibration, such as reducing the wire diameter, reducing the span between the guide wheels, increasing wire tension, and minimizing the discharge energy per single pulse (Zhang et al. (2014)).

2.1.4 Forces acting on the wire electrode

During WEDM operation, various forces act on the wire electrode due to the successive and random spark discharges, flushing of de-ionized water, wire tension, etc. These forces play a vital role in determining the life of the wire. Several authors have designed and developed the EDM setup for optimum functions and maximum stability of the tool electrode, considering the impact of various forces acting on the wire during the discharge phenomenon (Enache and Opran (1993)). The intensity of various forces determines the wire behavior and predicts the likelihood of wire failure. The forces acting on the wire include the pressure from the gas bubbles formed during plasma formation, wire tension, the hydrodynamic forces due to dielectric fluid, the electrostatic forces, and the electro-dynamic forces during the pulsed discharges (Dauw and Beltrami (1994), Kinoshita et al. (1984)). Figure 2.6 illustrates the various forces acting on the wire. The analysis of different force components which cause the wire deformation and wire displacement were carried out by other researchers as well (Mohri et al. (1998), Mori et al. (2016), Herrero et al. (2008)).

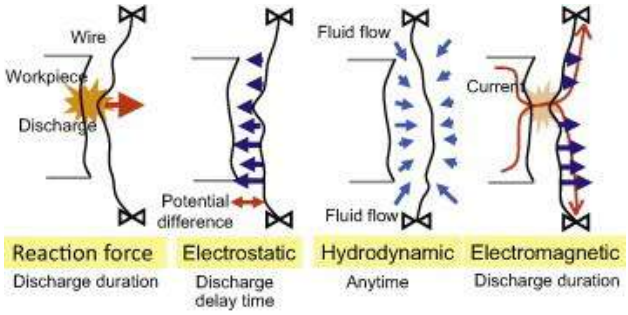

Figure 2.6 Forces acting on wire electrode(Hinduja and Kunieda (2013)**)** (Reproduced with permission from Elsevier)

Tomura and Kunieda (2009) were the pioneers to consider the effect of electromagnetic induction for electromagnetic field analysis of the wire electrode. Electrostatic forces act on the wire during the discharge delay time and an electromagnetic force acts during the

discharge duration. A similar study was established on the electromagnetic forces to analyze the current density and magnetic flux density around the wire and workpiece using the finite element method (Hada and Kunieda (2013)). It is to be noted that the impedances of the wire and the workpiece are dependent on several factors like wire diameter, workpiece height, wire and workpiece materials; which in turn influence the discharge current during spark formation.

The influence of hydrodynamic force on the wire deviation due to jet flushing was investigated by Okada et al. (2015). Accumulation of debris in the kerfs and wire deviation were the reasons responsible for wire breakage. Wire deflection further leads to corner errors as a result of discharge gap, spark angle, and various forces acting on the wire electrode (Abyar et al. (2018)). The forces acting at right angles to the wire movement direction cause the wire deviation errors.

Observations

Reported literature suggested that temperature is the most critical factor for wire failure. Temperature induced residual stresses degrade the wire strength, which increases the probability of wire failure. Microcracks are considered as stress concentrators that propagate into wider and deeper cracks, which finally break the wire. It has been observed that scant studies have been carried out on the influence of thermally generated stresses on the wire health. Apart from these factors, several studies have been reported on wire vibration and wire bowing, which deviate the wire from its straight position resulting in inaccurate cuts. A number of forces act on the wire tool during the discharge phenomenon viz. the discharge reaction force, hydrodynamic force of the dielectric, electrostatic force, electromagnetic force that play an important role in determining the wire life.

2.2 Influence of wire electrode on machining precision and product quality

There have been numerous efforts to improve the product quality and geometrical accuracy of WEDMed components by optimizing the process conditions (Gupta and Jain (2014b), Gupta and Jain (2014b), Puri and Deshpande (2006)). The wire electrode also plays a significant role in deciding the surface quality and geometrical precision of the machined products. The influence of wire electrode and various other processing parameters on

cryogenically treated Ti-6Al-4V alloy material was investigated (Khan et al. (2019)). Pramanik and Basak (2019) observed that higher values of wire tension reduced the fatigue life of WEDMed Ti-6Al-4V alloy and then remained almost constant with a further rise of wire tension. Microstructural characterization of machined workpiece surfaces concluded that wire electrode material diffused into the workpiece, covering almost 90% of the surface with approximately 10-20 μm of melted material thickness (Mouralova et al. (2018)). Unstable machining conditions like high discharge energy, narrow interelectrode gap, and low pulse off-time caused higher contamination of workpiece surface with wire electrode material (Abhilash and Chakradhar (2020a)). Mouralova et al. (2020) made an extensive study on the WEDM of pure molybdenum material and performed defect analysis on the surface and sub-surface layers, morphological characterization, and percentage diffusion of electrode material on the machined surface. Silver-coated brass wire showed better performance in terms of reduced surface roughness (Ra) and minimum wire damage as compared to the conventional brass wire electrode during WEDM of Maraging steel 300 (Sen et al. (2018)).

Several authors have worked to determine optimized wire parameters viz. wire speed, wire tension, wire feed rate on a wide range of materials to achieve favourable machining output without wire breakage (Manjaiah et al. (2014), Owhal et al. (2020)). The vibration of the wire tool is also affected by these wire parameters, which determines the quality and precision of the produced parts (Tang et al. (2019)). Wire tension strongly influences workpiece Ra, MRR, and microhardness of the workpiece but no significant effect on the kerf width of stainless steel material (Chaudhary et al. (2019)). An increased value of wire tension minimizes the corner errors of the workpiece; however very large values of wire tension produced larger angles than desired. The effect of wire tension on the geometrical accuracy of the final component is also dependant on the workpiece thickness (Kirwin et al. (2018)). Banu et al. (2020) employed the one factor at a time (OFAT) approach and design of experiment (DOE) approach for dry micro WEDM operation of SS304 stainless steel and concluded that the wire tension, wire feed, and wire velocity should be kept at an optimized constant value to achieve stable machining without wire ruptures. Increasing wire feed plays a significant role in minimizing geometrical inaccuracies and improving the product surface quality (Gupta and Jain (2014)). On the contrary, it was noted that comparatively lower

values of wire feed rate provided better precision accuracy for thinner workpieces (Kirwin et al. (2018)). A decreasing value of wire feed rate also reduces the spark gap value during WEDM operation (Deshmukh et al. (2019)). Qu et al. (2002) evaluated the effects of wire feed rate and rotational speed to obtain the best surface finish and roundness during cylindrical WEDM process. A particle swarm optimization algorithm was developed to demonstrate the role of wire tension and wire feed rate on the wire wear ratio (Nain et al. (2018a)). It was further found that pulse on-time accelerated the rate of wire erosion during machining. Wire speed plays a very strong role in determining the kerf width (KW) and workpiece Ra of WEDMed components (Sneha et al. (2018)). A wire offset in the range of 0.169–0.173 mm, could further enhance the geometrical precision of the machined components (Farooq et al. (2020)). An effective wire radius compensation methodology was developed to determine the wire location for accurate and precise machining (Lin and Liao (2009)).

The information presented in this section highlights the importance of wire parameters on the machining output. The untimely failure of the wire tool disrupts the machining efficiency and productivity. Thus, the prediction and prevention of wire rupture is a potential research area and needs proper study. The following sections review various methodologies developed to prohibit the occurrence of wire failure and maintain the machining precision of the products.

Observations

The wire electrode is a small but essential element of the WEDM machine. Researchers worldwide have carried out detailed analysis on the influence of wire parameters like wire tension, wire feed, wire geometry and wire material on the machining efficiency and productivity. High values of wire tension minimized the corner errors in the machined components. Studies reported that the role of wire feed on geometrical accuracy and surface quality of the final products depends on the workpiece thickness. Wire speed plays a significant role in determining the extent of erosion undergone by the wire electrode. Sharp temperature gradients generated during the discharge phenomenon cause wire erosion, which degrades the wire strength and diminishes the product quality. Thus, optimal combination of the wire parameters viz. wire tension, wire feed, wire speed needs to be maintained to obtain

the desired machining output without wire breakage. A scant literature is available on the detrimental influence of wire wear on product precision and quality. The damages undergone by the wire tool need to be minimized in order to achieve sustainable and efficient machining.

2.3 Methods to monitor wire health and prevent wire breakage

Prediction and prevention of the wire breakage phenomenon are crucial for efficient and uninterrupted machining operations. Thus, it is of utmost importance to make a comprehensive study of the wire characteristics during and after the machining process. Wire erosion has a detrimental influence on the geometrical accuracy of the WEDMed components. The study of wire morphology along the longitudinal sections and the cross-sections shall give a better insight into the wire erosion mechanism and aid in predicting the wire failure. Another method of monitoring the wire's health is the development of online diagnosing and control systems to detect the unstable machining conditions before the wire rupture. Selection of suitable wire material and improvement in wire properties also play an important role in maintaining the quality and precision of machined products. The following sections discuss the above-mentioned aspects in detail.

2.3.1 Investigation of wire morphology

The study of wire morphology gives an elaborate understanding of the wire erosion mechanism and predicts the behavior of the wire electrode at the time of breakage. Tosun and Cogun (2003) examined the effects of machining parameters on wire erosion and observed that the wire erosion ratio increases with the rise of discharge duration and open gap voltage. The deformation and erosion of wire electrodes during EDM of SiC reinforced Al-based MMCs were also investigated (Pramanik and Basak (2016)). The size of reinforcement particles, pulse duration, and wire tension have a strong influence on the wire erosion rate of MMCs. Figure 2.7 shows the original and deformed oval shapes of the eroded zinc coated brass wire cross-section samples. In a similar study, Pramanik and Basak (2018) observed that rupture incidences of a zinc-coated brass wire were high at lower dielectric pressure and higher wire tension during WEDM of titanium alloy. Figure 2.8explains the morphology of broken wire tips during machining. The cross sections of the wire decrease over a length

before breakage similar to necking; thus causing sharp or blunt broken tips depending on the length of decrease. The broken tips also show melted material sticking on the wire surface. An increase in wire diameter than the original diameter was initially observed followed by reduction in wire diameter as machining proceeds. It was concluded that discharge current, pulse duration, and wire tension strongly affect the wire failure followed by charging time and wire speed (Maher et al. (2017)). Fedorov et al. (2018) classified implicit and explicit wire breakages and further concluded that the Rehbinder effect does not play a significant role in implicit breakages. It was summarized that short circuits were the primary reason for explicit breakages of the wire tool.

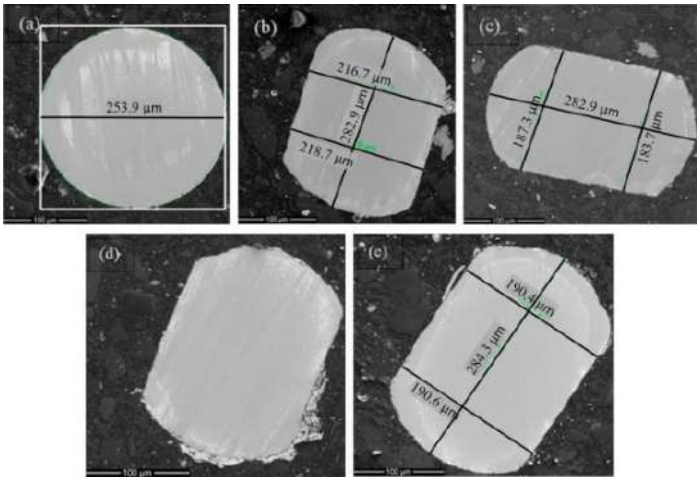

Figure 2.7 (a) Cross-section image of unused wire and (b), (c), (d), (e) Deformation of zinc coated brass wire after WEDM cutting of reinforced MMCs (Pramanik and Basak (2016)) (Reproduced with permission from Elsevier)

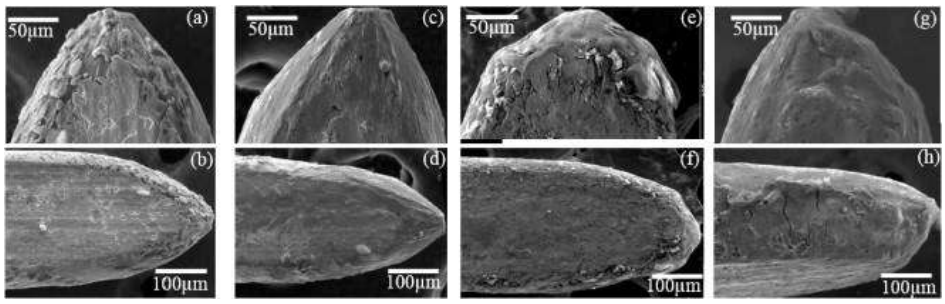

Figure 2.8 Morphology of broken wire tips during WEDM cutting (Pramanik and Basak (2018)) (Reproduced with permission from Elsevier)

2.3.2 Selection of optimum process conditions

Input conditions play a very important role in maintaining the quality and accuracy of the workpiece and the overall productivity of the system. Different methodologies such as ANN, Group Method Data Handling, Taguchi method, genetic algorithm, regression analysis are utilized to optimize WEDM parameters viz. pulse duration, pulse interval, current, flushing rate, bed speed for maximum MRR and minimum tool wear (Gonchikar et al. (2020), Kuruvila and Ravindra (2011)). A high cutting speed without deteriorating the wire electrode health can be achieved by applying high power density discharge pulses and then increasing the pulse density (Luo (1995)). Huang et al. (1999) identified pulse duration and the interelectrode gap as the crucial factors affecting the geometrical accuracy and machining performance due to the wire lag phenomenon. The influence of certain input parameters such as pulse duration, pulse off-time, and peak discharge current during rough cut is considered to be most significant, which causes geometrical error due to wire lag phenomenon (Puri and Bhattacharyya (2003b)). A catalogue could provide a noteworthy contribution in improving the overall productivity of modern manufacturing industries by bridging the gap between the dynamics of wire electrodes and various issues faced during WEDM parameters control (Altpeter and Perez (2004)). The variation of mean gap voltage was monitored during machining of Inconel 718 to predict and limit the frequency of wire breakage at unstable spark gap conditions (Abhilash and Chakradhar (2020a)). Higher wire damages and poor quality of products were obtained at higher variations of mean gap voltage. Jianyong et al. (2018) established a theoretical relationship between the machining time and the real-time wire electrode wear during micro-hole drilling operation of TC4 titanium alloy, TC11 titanium alloy, and GH4169 superalloy. The accumulation of gas bubbles in the interelectrode gap when kept below a threshold limit can reduce the likelihood of wire breakage to a substantial extent (Ly and Sanchez (2020)). The quantity of gas bubbles formed in the discharge zone is evaluated by measuring the impedance of the electrical circuit. An index to monitor wire breakage was also identified by correlating the MRR to the process conditions (Liao et al. (1997)). A support vector machine algorithm and grey relational analysis (GRA) was employed by Nain et al. (2018b) to obtain an optimum range of process conditions for minimum wire wear ratio during WEDM of Udimet-L605. Pulse duration has the highest contribution towards consumption of the wire electrode followed by

pulse off-time and peak current (Deb et al. (2019)). Very low values of pulse interval can cause frequent wire breakage due to insufficient flushing time (Bisaria and Shandilya (2018)). Machining of polyurethane foams resulted in frequent wire breakages due to low electrical conductivity (Azhari et al. (2017)). The sharp concentration of discharges along with high discharge energy and exaggerated pulse frequency were identified to be crucial wire failure indicators (Bergs et al. (2018)).

WEDM also plays an important role in the machining of MMCs for various applications. An increase in the frequency of wire failure was achieved with the increasing percentage contribution of reinforced Al_2O_3 particles in Al_2O_3p/6061Al composites (Yan et al. (2005)). An optimum set of low wire tension, high dielectric flow rate, and high wire velocity values were predicted to minimize wire failures. An increase in wire tool wear and deterioration in workpiece surface quality was observed with the increase in reinforcement particles in MMCs (Naidu et al. (2020)). Rao and Krishna (2013) attempted to improve the overall quality of machining SiC_P reinforced ZC63 MMCs and evaluated the wire wear ratio based on parameters like percentage and volume fraction of reinforced particles, pulse duration, pulse off-time, and wire tension.

Optimum energy utilization is a very crucial factor to achieve sustainable machining. Gamage and Desilva (2016) drew attention to the importance of preventing wire breakages to avoid the various environmental hazards such as energy loss and productivity depletion faced during wire failures. A lower level of discharge voltage and lower wire feed rate is recommended for economical machining (Roy and Narendranath (2018)). Hence, proper selection of input parameters shall be useful in minimizing wire failures.

2.3.3 Online wire monitoring and control systems

There have been numerous efforts in developing online monitoring and diagnosing systems to study the behavior of the wire during machining and to predict the wire rupture phenomenon. Accordingly, many methods were suggested to maintain the process conditions at safe limits to avoid wire failure and enhance the precision efficiency. In the early eighties, Kinoshita et al. (1982) pointed out the importance of wire health, the various reasons behind wire failure, and developed a monitoring system to control the spark frequency. Following the footsteps, Dekeyser et al. (1988) monitored the machining process with a pulse

discriminating system and estimated the probability of wire rupture based on a thermal model to automate the EDM system. An online detection method of spark location was also developed by measuring the ratio of currents supplied through branched wires connected to a tool electrode by maintaining an adequate distance (Kunieda et al. (1990)). Several studies (Yan and Liao (1996), Rajurkar and Wang(1997), Yan and Chien (2007)) have focused on improving the overall performance of a WEDM machine by developing a knowledge-based monitoring and control system that is enabled to give indications regarding faulty operation and wire breakage. Almeida et al. (2021)comprehensively reviewed the servo control strategies for better WEDM operation and concluded that prevention of wire rupture using effective servo control approaches has further research possibilities. A few studies focus on the estimation and prevention of the wire rupture process by developing online monitoring systems that could detect and control the discharge rate at a safe level (Rajurkar et al. (1991), Rajurkar et al. (1994), Rajurkar et al. (1997)). They further developed an adaptive control system to correlate the cutting speed to the discharge rate by measuring the workpiece height with the aid of a non-linear discrete model. The machining rate is kept at an optimum level without risking the wire to frequent breakages. A similar attempt was later carried out to optimize and maintain stable input conditions without wire failure by evaluating the workpiece height using a back propagation neural network-based adaptive control system (Yan and Liao (2001)).The wire deflection caused due to external forces can be monitored online by using an optical sensor to achieve good corner accuracy at high cutting speeds (Beltrami et al. (1996)). An advanced multiple sensors system to detect the generated pulse type and discharge position was developed with the intention of zero defect manufacturing (Caggiano et al. (2016)).

Several studies reported that wire breakage was preceded by a sharp concentration of pulses, resulting in localized temperature rise, thus reducing the mechanical strength of the wire (Shoda et al.(1992)). The yielding of wire material and deformation in the plastic zone are other causes of wire breakage while sharp temperature gradients produced during spark discharges accelerate the failure process (Luo (1999)). A novel self-learning fuzzy controller was developed which increased the pulse-off time to eliminate unstable ignition delays and unhealthy sparks so that the pulsed frequency could be maintained at a constant safe level to prevent wire failure (Yan and Liao (1996)). The wire tension or rigidity should be increased

to reduce the bowing error and corner errors caused due to wire deflection and vibration (Lin et al. (2001)). Huang and Liao (2000) developed an artificial neural network (ANN) integrated expert system (ES) for error detection and maintenance of the system. A geometric path lifting method was also presented (Wang and Ravani (2003))which increases the interelectrode gap to prevent wire breakage during machining corners with very small radii. Sarkar et al. (2011) established a wire lag compensation technique for cylindrical job cutting to modify the programmed path for higher precision efficiency. This method is useful for machining smaller radius jobs where a high level of accuracy is desired. A novel algorithm was developed based on the non-uniform distribution of sparks around the wire, which could identify the geometrical errors in an arced path, wire deflection and the variable spark gap around the wire tool (Abyar et al. (2019)). Based on the proposed model, the machining errors along the arced path were compensated with 84.8 % accuracy.

The development of a closed-loop wire tension control system was useful in deriving dynamic models of the wire feed and tension control device which improved the machining accuracy during WEDM (Yan and Huang (2004)). A closed-loop wire tension control system was further developed to ensure smooth transport system and constant tension value in order to maintain the geometrical accuracy of the machined components (Yan et al. (2004), Yan and Fang (2008)). The developed system further diminishes the probability of wire breakage during wire feeding. A constant wire tension control system was developed based on an improved wire feeding methodology and PID closed-loop control, which improved the product quality, geometrical precision, and control accuracy during machining (Chen et al. (2018a)). A data acquisition system could identify a set of threshold input values related to spark energy, ignition delay time, and discharge current to prevent wire breakage and unstable machining conditions (Cabanes et al. (2008a)). A similar approach was adopted to propose an online surveillance system that could monitor and identify damaged cutting zones and readjust the machining parameters (Cabanes et al. (2008b)). Abhilash and Chakradhar (2020b) predicted and investigated the occurrence of wire breakage by developing an offline three-level classification model with the aid of an ANN model. The model was proved to predict the wire failure with 95 % accuracy.

Okada and his group made some important contributions in monitoring and diagnosing the wire performance during machining. In 2009, Okada et al. (2009) analyzed

the complex fluid flow and debris movement around the wire electrode to ensure stable machining performance without wire failure. The stagnation area with less flow velocity could be observed around the wire under any rate of flushing conditions. A novel method was proposed to measure the distribution of discharge position by analyzing the recorded images of a high-speed video camera during wire movement (Okada et al. (2010)). Figure 2.9 shows the high-speed observation system for a 50 μm diameter tungsten wire with a digital high-speed video camera having a recording speed of 8000 frames per second (fps). A uniform spark distribution was observed at high servo voltage, larger pulse-off time, and low wire velocity. The movements of a tungsten wire electrode were further investigated using a high-speed camera during the fine WEDM process to study the causes of wire breakage (Habib and Okada (2016)). The wire vibration amplitude and machined kerf width reduce with increased values of wire tension and the vibration amplitude parallel to the cutting direction was larger than that of the perpendicular one.

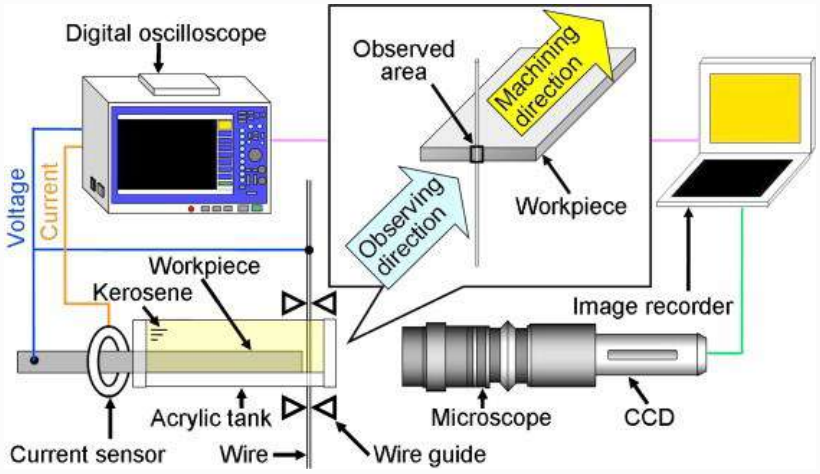

Figure 2.9 High-speed observation system of the wire electrode during WEDM (Okada et al. (2010)) (Reproduced with permission from Elsevier)

2.3.4 Suitable selection of wire material and improvement in wire properties

The wire electrode is a very important accessory of the WEDM setup. The selection of wire material is a very crucial task to obtain the desired operational characteristics. Dauw and Albert (1992) first listed down the necessary characteristics of a wire electrode. The wire should be electrically conductive and possess good mechanical strength. The geometrical properties of the wire (wire shape and size), tensile strength, density, wire elongation,

thermal conductivity, and heat capacity are certain important characteristics of the wire. Figure 2.10 shows the required properties of a wire electrode during WEDM machining. An optimum combination of these properties should be considered during the design and development of wire electrodes to achieve good machining performance and longer wire life. Research has shown that only a few materials are suitable for the wire electrode material which exhibit a good combination of all the desired properties.

Since the first use of commercial WEDM units in 1969, copper was used as the wire electrode (Kapoor et al. (2012)). However copper was not an ideal material for wire due to its low tensile strength. Later, a brass wire was used in the combination of 63–65 % Cu and 35–37 % zinc. The use of brass wire gave better cutting performance and speed as compared to copper wire due to its higher tensile strength (Prohaszka et al. (1997)). However, the addition of zinc to copper decreases the conductivity of the wire electrode considerably. Nowadays, wire made of molybdenum is used in the industrial sector due to its high tensile strength and high melting point (Ezaki et al. (1991)). A suitable yet economical material for wire electrode comprising 0.1-3 % zirconium, 0.5-10 % zinc, and the remaining copper was suggested which enhanced the MRR along with less erosion on the wire electrode surface (Kaneko and Onoue (1984)). With increasing demands of precise manufacturing, coated or stratified wires were developed with excellent sparking abilities. The development of a coated layer of a metal or a metal alloy over the wire core and its advantages were described (Groos et al. (2004)). Fowle (1933) was one of the earliest inventors to patent zinc-coated wires. Zinc-coated brass or zinc-coated copper wires with a coating thickness of about 20-30 μm were developed which improved the cutting speed along with better flushing and debris removal characteristics (Prohaszka et al. (1997)). The zinc coating has a lower vaporization temperature, which acts as a heat sink protecting the core of the wire from thermal shock due to spark discharges. US patent no. 2006/0138091 A1 explains an economical methodology of fabricating zinc-coated wire using a hot-dip galvanizing process (Lee (2006)). Kumar et al. (2018) observed better surface quality and accuracy of WEDMed products with zinc-coated brass wire as compared to uncoated brass wire. The performance of zinc-coated brass wire was also found to be superior in comparison to uncoated brass wire in terms of improved product quality and increased MRR during WEDM of $Ti_{50}Ni_{50-x}Cu_x$ shape memory alloy (Manjaiah et al. (2015)). Maher et al. (2014) also reviewed the evolution of wire tool

electrode and its improvement in terms of wire core material and coating material for better cutting operations. Multi-coated EDM wires were developed to improve the wire life, increase the mechanical strength of the wire tool, eliminate short circuits and lower the cost of production (Groos et al. (2004), Lee(2008)). A composite wire with a core of high tensile strength covered by an insulating layer, a conductive layer, a coating layer covered by a superficial intermediate layer is suitable for low contact resistance and accurate cutting (Kruth et al. (2004)). For WEDM machining of the hard metal workpiece with a binding material, the most suitable wire electrode was chosen as a copper-coated wire with the coating metal which has an electrode potential less than or equal to 0.28 V based on a standard hydrogen electrode (Baumann and Barthel (2002)). A coated wire electrode with two sheath coatings wherein the inner sheath coating comprised of β- brass and outer sheath coating of γ-brass was fabricated for better cutting performance, increased current conductivity, and lesser wear on the wire surface (Groos et al. (2004)). For high accuracy applications, a high tensile strength wire with pearlitic steel comprising of high carbon content as the core material covered by a coating of zinc or zinc alloy was fabricated (Gonnissen et al. (2005)). To improve the machining speed of WEDM operation, a wire with a copper or pinchbeck core with a pinchbeck coating comprising of a sub-layer and a surface layer with fractured structure was used (Blancet al. (2013)).

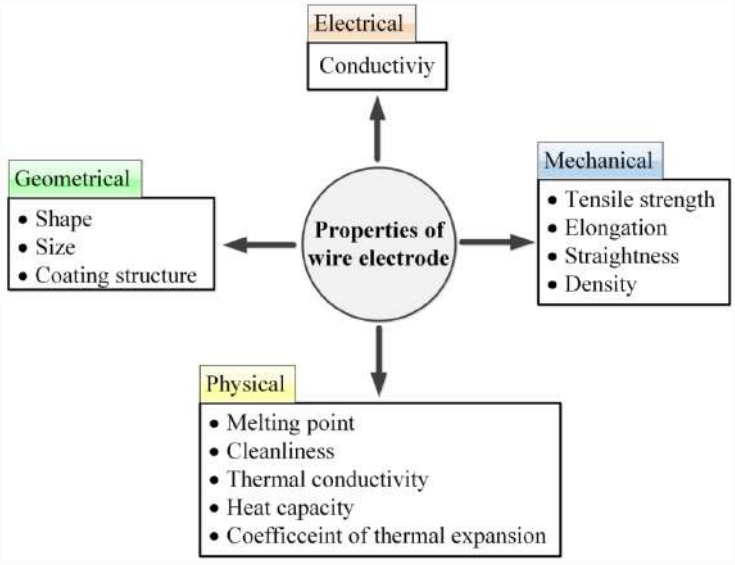

Figure 2.10 Required properties of a wire electrode

Over the years, there were significant improvements in the wire electrode properties to improve the performance characteristics along with longer wire life. An improvement in the machining performance and lower tool wear have been observed by application of low frequency vibration to the workpiece; which facilitates better flushing of debris and reduction of short circuit arcs (Jahan et al. (2010)). Given this, Guo et al. (1997a, 1997b) showed that ultrasonic vibration of the wire electrode also facilitates multiple channel discharges and improves their distribution thus ensuring better surface quality and increased cutting rate. An optimum relationship between the vibration amplitude and input discharge energy was set which further improved the wire health. Further, Zhang et al. (2016) integrated the WEDM technology with both ultrasonic vibration and magnetic field and observed significant improvement in output characteristics, stability of the discharge channel, and better expulsion of debris from the interelectrode gap. Figure 2.11shows the mechanism of applying ultrasonic vibration to the wire tool through a transducer. With the rise in vibration frequency, the wire generates more nodes and antinodes, which increase the fluid pressure variation thus facilitating the better circulation of dielectric fluid and improved debris flushing efficiency. Figure 2.12 shows the schematic of magnetic field-assisted WEDM technology. The magnetic field generates Lorentz force and Ampere force, which combines with the hydrodynamic force, electrostatic force, and electro-dynamic force and creates a force to wash away debris efficiently from the interelectrode gap.

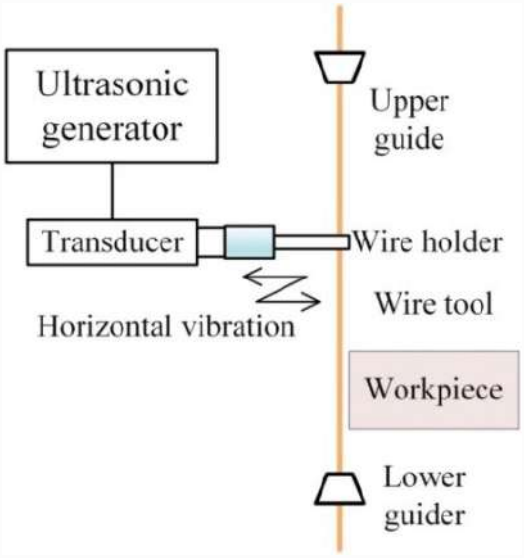

Figure 2.11 Schematic diagram of ultrasonic vibration applied to the wire tool(Zhang et al. (2016)) (Reproduced with permission from Elsevier)

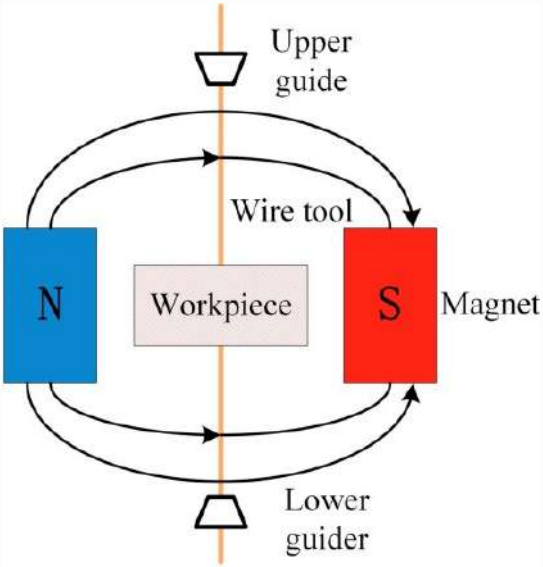

Figure 2.12 Schematic diagram of the magnetic field-assisted WEDM process (Zhang et al. (2016)) (Reproduced with permission from Elsevier)

Hybrid WEDM comprising of both ultrasonic vibration and magnetic field facilitates enhanced machining with high MRR and superior surface quality products along with longer tool life. Low frequency vibrations were applied to the wire electrode to fabricate microstructure grooves on metal surfaces with high precision and low cost (Chu et al. (2019)). A vibration-assisted wire machining setup was also established wherein the wire electrode was equipped with a biaxial sinusoidal vibration source with vibrations of sample amplitude and synchronous waveforms (Hsue (2020)). This vibration-assisted attachment could reduce the probability of wire breakage largely along with maintaining the stability of the WEDM system with improved quality cuts. A traveling wire electrochemical machining method was used for cutting composites and it was observed that the wire wear ratio reduces up to 10 % electrolyte concentration and increases further beyond this concentration (Jain et al. (1991)). In a recent study, the wire erosion was significantly reduced by the wire electrochemical turning (WECT) method by using a continuously running tungsten wire tool and generation of short bipolar pulse current (Han and Kunieda (2021)). Furthermore, the cylindrical acrylic wire guide delivered the best performance due to its electrically non-conductive nature by eliminating guide wear and stray currents in the interelectrode gap.

Yan et al. (2004) successfully utilized thin wires with a diameter of 80 μm, high tensile strength, and melting point. WEDM has shown good potential to fabricate ultra-thin Si wafers as compared to the conventional machining processes (Joshi et al. (2018), Bhartiya et al. (2020)). Ultra-thin foil wire electrodes were utilized for the slicing of SiC ingots into wafers which reduced the wire breakage probability by increasing the tool cross-sectional area (Zhao et al. (2018)). The utility of thin wires with diameters in the range of 20-50 μm during the WEDM process was also demonstrated (Klocke et al. (2004)). The process forces during thin WEDM machining are comparatively larger due to less tension force and less wire weight. A dielectric encased wire tool with its tip stripped was developed for fabrication of holes through EDM (Kumagai et al. (2007). The developed methodology eliminated stray arcs between the wire body and the hole, thus maintaining the wire health as well as the constant dimensions of the machined hole. The exposed wire length is kept constant by maintaining an optimum feed speed, which allows higher cutting speed with minimum wire wear.

The performance of soft wires utilized in taper cutting processes was explained with the aid of FEM by incorporating non-linear characteristics such as contact mechanism, plastic deformation, stress-stiffening, and large displacements (Sanchez et al. (2008)). The results were found to be quite accurate in predicting the angular error in taper cutting operations. Ciwen et al. (2018)further developed ultra-long wire, variable speed WEDM setup with two tensile reels winded to enhance geometrical accuracy and surface quality of the components. The electrostatic induction feeding method facilitates non-contact feeding of current to a micro-wire, which eliminates brush wear and enhances machining accuracy (Yang et al. (2010)). Cryogenically treated wires lead to significant improvement in the electrical conductivity of the tool material and reduce the dimensional deviation of WEDMed components (Singh et al. (2019)). The utilization of a novel wire electrode comprising a continuous wire substrate partially covered with a polymeric substance having thermal decomposition in the range of 100-500˚C could substantially reduce the frequency of wire breakage. The reason behind this is the ability of the polymeric substance to thermally decompose to carbon and combine with the generated gases during WEDM discharges to reduce the oxygen in the interelectrode gap (Inoue (1985)).

In recent years, Zhang et al. (2020) used a novel micro-crack wire electrode which showed significant improvement in machining characteristics along with sustainable manufacturing benefits such as lower energy consumption, less debris pollution, less waste of material resources, decreasing harmful emission, and less frequency of wire breakages. A microcrack wire electrode has the potential to minimize environmental pollution by approximately 23 % as compared to a conventional brass wire electrode. The attachment of debris to the non-smooth surface of the microcrack wire helps in minimizing the occurrence of abnormal discharges and short circuit arcs. This enables better flushing of debris and thus enhances the wire tool life. Some other authors (Yan et al. (2020), Chen et al. (2018b)) also fabricated novel surface microstructure wire electrodes for sustainable production to improve the surface texture of machined products thus enhancing product usability and reliability. Chen et al. (2018b) were successful in minimizing geometrical errors of machined workpieces by approximately 5.53–27.15 % with the use of a novel microstructure wire electrode as compared to a conventional brass electrode.

A brass coated steel wire with track shaped section was effective in achieving less kerf width and minimizing cracks on the machined surface during WEDM slicing of silicon carbide ingot (Kimura et al. (2013)). This novel method of slicing ingots reduced the lateral vibrations of the wire electrode. US patent no. 4,766,280 (Groos(1988)) discusses a methodology of providing projections and recesses on the wire surface by twisting a wire of polygonal cross-section around its axis to obtain better cutting efficiency. A novel methodology was suggested of heating a zinc-coated copper wire in an oxidizing atmosphere to form a zinc copper alloy layer followed by a reduction in diameter to almost its half, which improved the current carrying capacity of the wire without failure (Briffod (1990)). Porous wire electrodes also exhibit better performance in terms of improved cutting speed and longer wire life due to increased surface area of the wire and better flushing conditions (Seong(2001)). A fragmented structure of a brass coating over a brass core wire was used for higher finishing operations in WEDM setup (Ly and Sanchez (2012)).

Observations

Researchers worldwide made several attempts to predict and prevent the wire breakage phenomenon. Limiting the occurrence of wire failure is imperative to achieve sustainable and

uninterrupted machining. Morphological studies of wire electrode and work surface provided a better insight into the wire surface damages and their relation to wire rupture. It was noted that advanced monitoring and control systems help in the efficient supervision of the wire's health and mitigation of wire failure. The development of knowledge-based monitoring systems and advanced control systems could maintain the discharge frequency at a safe level to minimize the frequency of wire breakage. Literature reveals that further study is required to understand the wire erosion and failure mechanism at a deeper level to prevent its occurrence. There is significant research and development scope in improving the areas such as newer and advanced wire materials, minimization of arcing, generation of healthier sparks, multi-physics based modeling of the wire electrode during spark formation to enhance its performance and ensure longer tool life along with better machining productivity. Numerical models are efficient tools and the existing models need to be further evolved in order to have a better comprehension of the wire characteristics during the discharge phenomenon. A wire safety factor could prove to be a useful tool in providing important guidelines to the manufacturers to improve the wire life without compromising the machining rate.

2.4 Discussion

Wire erosion and breakage pose a serious threat to modern manufacturing industries as they cause serious environmental hazards and disrupt the entire production line. Wire breakage affects the environment by increasing energy consumption and machining time. Proper disposal or reusability of used wires is challenging as it increases the risk of environmental contamination. Thus, it is essential to predict and limit the occurrence of wire failure to achieve sustainable and efficient manufacturing.

An extensive amount of research has been reported so far on several causes of wire breakage and different measures to limit its occurrence. Numerical modeling proved to be a useful tool in the prediction of the wire electrode characteristics and identifying the parameters responsible for wire failure. The high amount of temperature generated during the discharge phenomenon causes material erosion from the wire tool which degrades the wire strength. The intense temperature generated at spark plasma primarily affects the wire's health. The temperature generated further induces thermal stresses in the heated and nearby region of both the wire electrode and workpiece. It was noted that significant studies have

been reported on the stresses induced on workpiece surfaces during WEDM process, however, scant work is available on the stresses induced on wire electrode surfaces. Moreover, the numerical models presented in the existing literature have primarily focussed only on the influence of temperature on the wire health. The existing models make several simplifying assumptions and use a lot of empirical data. There is a dire need to have a dedicated model of wire electrode to predict and mitigate the frequency of wire failure along with efficient machining. A wire safety index can be recommended depending on the wire material, workpiece material, and process conditions that should be maintained throughout the machining to prevent wire failure. The estimation of a wire safety factor could prove to be a useful tool to the manufacturers to achieve uninterrupted machining.

Over the years, numerous researchers have focussed their attention on optimizing the WEDM performance by studying the workpiece morpholgy and performance parameters. The influence of process conditions in achieving the desired efficiency and machining rate is thoroughly studied. However, limited studies have been conducted so far which explains in detail the nature and intensity of wire erosion during machining (Pramanik and Basak (2016), Pramanik and Basak (2018)). A comprehensive analysis of the wire wear and its deformation mechanism, morphology study of the eroded wire samples is very crucial in restricting wire failure and enhancing the overall efficiency of the operation. The damages undergone by the wire also have a notable effect on the surface quality achieved by the workpiece during machining. The effects of different wire parameters viz. wire velocity, wire feed, wire tension on the output performance have been investigated by many researchers. The existing literature, however, has shown very little knowledge on the influence of wire erosion on the surface roughnessof the workpiece. Thus, it is of utmost importance to analyze the wire erosion and investigate its detrimental influence on workpiece surface quality to achieve uninterrupted and efficient machining. Moreover, to the best knowledge of the authors, scant literature is reported on molybdenum and coated wires that are extensively used in WEDM machines.

The damages undergone by the wire tool deteriorate the wire health as well as diminish the product quality. The wire wear cannot be eliminated completely but can be minimized to achieve the desired machining efficiency without wire failure. Very scant information is reported on the tolerance level of damages on the wire surface in order to

minimize the wire failure. The estimation of a wire quality index could provide a threshold limit to the extent of wire erosion and aid in improving the wire life. Thus, the established methodologies in the present work can act as a predictive tool for manufacturers in selection of safe machining conditions to minimize the wear erosion rate and wire failure probability.

2.5 Research objectives

The literature survey presented above shows that an extensive amount of research has been carried out on different aspects of WEDM viz. machining of advanced materials like tool steel, composites, titanium, Inconel; optimization of process conditions to achieve maximum material removal rate and minimum surface roughness; wire health monitoring etc. Different types of materials are used for the wire tool in WEDM machines viz. brass, copper, tungsten, molybdenum, coated wires etc. It was further noted that fewer studies have been carried out on the wire electrode as compared to the workpiece during WEDM. Based on the research gaps identified during the literature review on various aspects of the wire electrode, the objectives of the present research work have been derived. The overall objective of the present work is to improve the performance of WEDM process by carrying out systematic experimental and numerical investigations into the wire health and timely prediction and prevention of wire breakage to achieve uninterrupted and efficient machining. To achieve this, the following sub-objectives have been noted down.

- To study the thermo-mechanical behaviour of wire electrode for a wide range of process parameters by using finite element (FE) simulations. It is envisaged that by using the developed method, one can easily predict the deterioration of wire electrode, which will ensure uninterrupted and efficient wire electric discharge machining operation.
- To estimate the wire strength and evaluate a wire safety factor based on the temperature and residual stresses induced during wire electric discharge machining. The wire safey factor shall provide useful guidelines to modern day manufacturerers to optimize the machining in order to prevent wire failure and achieve sustainable machining.
- To carry out systematic and extensive experimental investigations into the wire erosion and deformation during wire electric discharge machining. An in-depth understanding of the wire erosion mechanism shall give a proper insight into the wire breakage phenomenon; thus predicting and preventing untimely wire failure.

- To study the influence of process parameters viz. discharge voltage, discharge current, pulse duration, pulse off-time, and wire velocity on the wire health parameters and also the workpiece surface quality.

- To evaluate the intensity of damages undergone by the wire electrode by determining a wire surface quality index for the tolerable limit of surface erosion with the aid of image processing technique. The evaluation of a wire safety index may provide useful insights into sustainable and economical machining in modern industrial practice. A comprehensive analysis of the wire eroded samples is crucial in restricting wire failure and enhancing the overall efficiency of the operation.
- To establish a relationship between the wire damages and the surface quality achieved by the WEDMed work part. A deeper understanding of this relationship can be useful in achieving desired product quality.

To achieve the research objectives, the overall thesis work has been carried out in five different modules. Figure 2.13 gives an overview of the research work carried out. The various stages of the work are as follows.

Module1: An extensive literature study has been carried on WEDM machining and the importance of wire electrode during the cutting process. Various methods to monitor the wire health and prevention measures to limit the occurrence of wire failure have been explored. Based on the literature survey carried out, the research gaps have been identified and the research objectives have been set.

Module 2: A three-dimensional thermo-mechanical finite element model of the molybdenum wire electrode is developed to determine the strength of the wire during the machining process. The coupled thermo-mechanical model analyzes both the temperature and stress distributions at the end of a pulse cycle. The temperature profile obtained and residual stresses retained on the wire electrode after a single pulse cycle determine the reduction in strength of the wire and predict the probability of wire breakage for a particular process set. The strength of the wire tool is estimated based on the results predicted by the developed finite element model. A wire safety index is evaluated by comparing the maximum value of stresses induced to the yield stress of the material. It is envisaged that by using the developed method, one can easily predict and limit the occurrence of wire failure.

Module 3: This section reports an extensive experimental investigation on the measurement and analysis of molybdenum wire erosion and deformation after WEDM of Ti-6Al-4V alloy at varying input levels viz. discharge voltage, discharge current, pulse duration, pulse off-time, and wire speed. The various forms of wire damages and deformation during the cutting operation were critically analyzed. A wire surface quality index for the tolerable limit of wire surface erosion was estimated using the image processing technique.

Module 4: A three-dimensional thermo-mechanical finite element model of a zinc-coated brass wire electrode is developed to determine the strength of the wire during the machining process. The coupled thermo-mechanical model analyzes both the temperature and stress distributions at the end of a pulse cycle. The crater volume obtained on the wire after a single pulse was also computed numerically when the generated temperature exceeds the melting point of the wire material.The wire strength is estimated based on the amount of material removed from the wire during the spark discharges.

Module 5: An extensive experimental analysis was carried out to have a deeper understanding of the damages undergone by a zinc-coated brass wire during WEDM of Ti-6Al-4V alloy. The cross-section samples of the eroded wires were also examined to observe some major changes in wire shape during the spark discharges. A wire surface quality index for the tolerable limit of wire surface erosion was also estimated using the image processing technique.

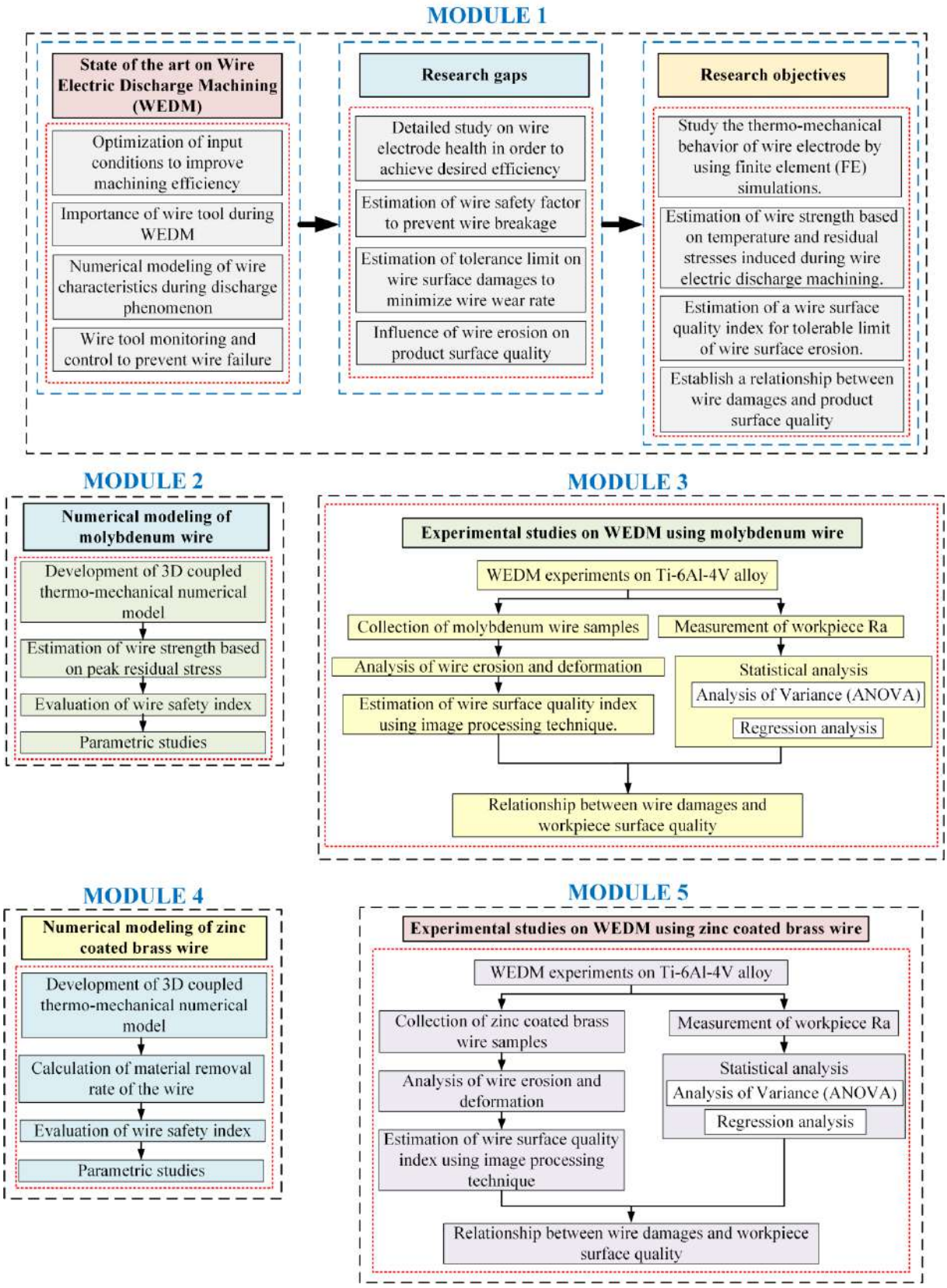

Figure 2.13 Overview of the present research work

CHAPTER 3

Three-dimensional thermo-mechanical analysis of molybdenum wire electrode during wire EDM process

3.0 Scope

This chapter presents the development of a three-dimensional thermo-mechanical finite element model (FEM) of a molybdenum wire electrode during wire electric discharge machining (WEDM) process. The need to carry out the thermo-mechanical analysis of the wire tool is explained. The overview of the process model development using FEM is presented. The numerical model is presented in detail, in terms of its governing equations, assumptions, boundary conditions, heat flux model, material properties and solution methodology. The mesh discretization is optimized for better convergence of results in optimum time. The finite element model is validated with published results and experimental data. In the end, a case study on the numerical simulation of the thermo-mechanical characteristics of the wire electrode, which computes the temperature and stresses generated in the wire is presented. The chapter is summarized with conclusions.

3.1 The need

Frequent breakages of wire electrode during WEDM adversely affect the productivity and surface quality of the finished products. Uncontrolled thermal loads and large thermal stresses generated during the discharge phenomenon reduce the strength of the wire, which eventually leads to wire rupture. This adversely affects the process productivity and geometrical accuracy of cut parts. Spark discharges produce intense temperatures for very short periods of time, which induce thermal stresses in the heated and nearby region of both the wire electrode and workpiece. Thermal residual stresses retained in the wire can cause the formation of microcracks, voids and pits, which increase the probability of wire rupture. It is essential to predict and prevent the wire breakage phenomenon for better machining productivity. Thus, the development of a numerical model shall provide useful information in estimating the wire strength based on the temperature and stresses generated in the wire electrode.

Several studies have been reported to predict the temperature generated in both the electrodes during EDM and WEDM cutting operation (Dekeyser et al. (1985a), Joshi and Pande (2010), Banerjee et al. (1993), Banerjee and Prasad (2010)). Moreover, literature survey showed that significant studies have been reported on the stresses induced on workpiece surfaces during the spark discharges (Yadav et al. (2002), Ekmekci et al. (2006),Zhang et al. (2018), Pramanik and Basak (2019)); however, a scant work is available on the stresses induced on the wire electrode surface (Saha et al. (2004),Fedorov et al. (2018)). The strength of the wire electrode is dependent upon the temperature and thermal residual stresses generated in the wire during the discharge phenomenon. Thus, a need was identified to predict the thermo-mechanical characteristics of the wire during the cutting operation to predict and limit the occurrence of wire failure.

In view of this, in this work, a three-dimensional nonlinear transient thermo-mechanical model for a molybdenum wire used during WEDM has been developed to compute the temperature and the induced stresses in the wire. The computational ability of the developed model has been verified by conducting systematic experiments. The model eliminates the need for costly, time-consuming and tedious experiments. It is envisaged that by using the developed method, one can easily predict the deterioration of wire electrode, which will ensure uninterrupted and efficient wire electric discharge machining operation. The details of the developed numerical model are presented in the following sections.

3.2 Generation of spark plasma on the wire surface

In EDM, a potential difference is applied between the tool and workpiece. When a pulse of DC electricity is delivered to the tool electrode and workpiece, there is a continuous flow of electrons and ions between the cathode and anode. An intense electrical field is created at the point where surface irregularities provide the narrowest gap. As a result of this field, naturally occurring microscopic contaminants suspended in the dielectric fluid begin to migrate and concentrate at the strongest point in this field. Simultaneously, negatively charged particles (electrons) break loose from the cathode surface and move towards the anode surface under the influence of the electric field forces. The wire acts as the cathode during the WEDM process. During the movement of electrons and ions in the interelectrode gap, the electrons collide with the neutral molecules of the dielectric. In this process,

electrons are also liberated from these neutral molecules of dielectric, resulting in still more ionization. The ionization soon becomes so intense that a very narrow channel of continuous conductivity is established. Figure 3. depicts the generation of plasma in the interelectrode gap. Here, F_a, F_c and F_d represent the fraction of energy absorbed by the anode, cathode and dielectric respectively. Q_a and Q_c denote the heat flux at the anode and cathode respectively. R_a and R_c are the radii of the plasma channel (R_p) at the anode and cathode respectively. In this channel, there is a continuous flow of considerable number of electrons towards the anode and that of ions towards the cathode (Jain(2004)). At approximately the midpoint of the electrical pulse, the power supply decreases the voltage delivered to the gap but raises the current. Current flows through the gap only during the pulse on time. This has the effect of increasing both the temperature and pressure in the spark channel. Such intense localized heat flux leads to an extreme instantaneous confined rise in temperature, which would be more than 10,000^{o}C. The extremely high temperature of the spark melts and vaporizes material from the surfaces of both the wire electrode and workpiece. The gaseous by-products of vaporization form a bubble, which rapidly expands outward from the spark channel. The bubble collapses as soon as the discharge stops. This creates a shock wave front and the violent rush of dielectric fluid into the machining zone flushes away the molten material forming small craters in both the wire electrode and workpiece.

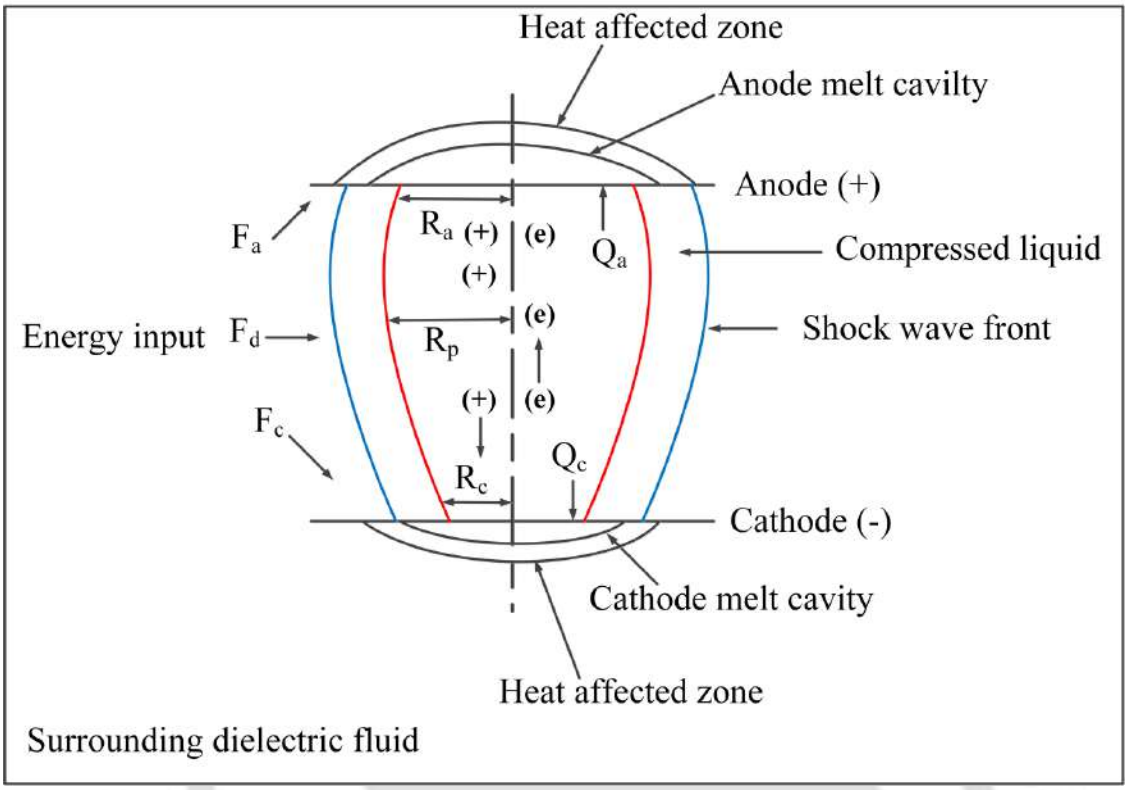

Figure 3.1 Generation of spark plasma between the wire electrode and workpiece

3.3 Thermo-mechanical modeling of the wire tool

To predict and prevent the wire breakage phenomenon, it is imperative to understand the thermo-mechanical behavior of the wire at different process conditions during the discharge phenomenon. Thus, a numerical model has been developed which shall pave the way to estimate the wire strength based on the temperature generated and the residual stresses induced in the wire. Figure 3.2 shows the schematic of the wire tool for the development of the coupled thermo-mechanical model of the wire electrode during the machining process. Heat flux is assumed to be distributed over boundary region 1, where the discharge channel interacts between the wire tool and workpiece. In the remaining portion of the wire periphery, i.e. boundary 2, convection is applied as the boundary condition. End tension is applied at both ends of the wire. This model shall be useful to estimate the total thermal load in the wire and evaluate the effects that lead to wire breakage by determining the stresses induced due to sparks during the operation.

The model development primarily consists of the following steps.

- Development of geometric model of the wire tool.

- Applying material properties – thermal and mechanical.
- Define the governing equations and boundary conditions.
- Define the spark radius equation and the Gaussian heat flux model.
- Solve the problem using finite element based software ABAQUS^{TM} in transient mode.
- Determination of temperature, thermal stresses and residual stresses induced in the wire during the discharge phenomenon at different levels of process conditions.
- Validation of the developed model with published results and experimental data.

The above mentioned steps are discussed in detail in the following sections.

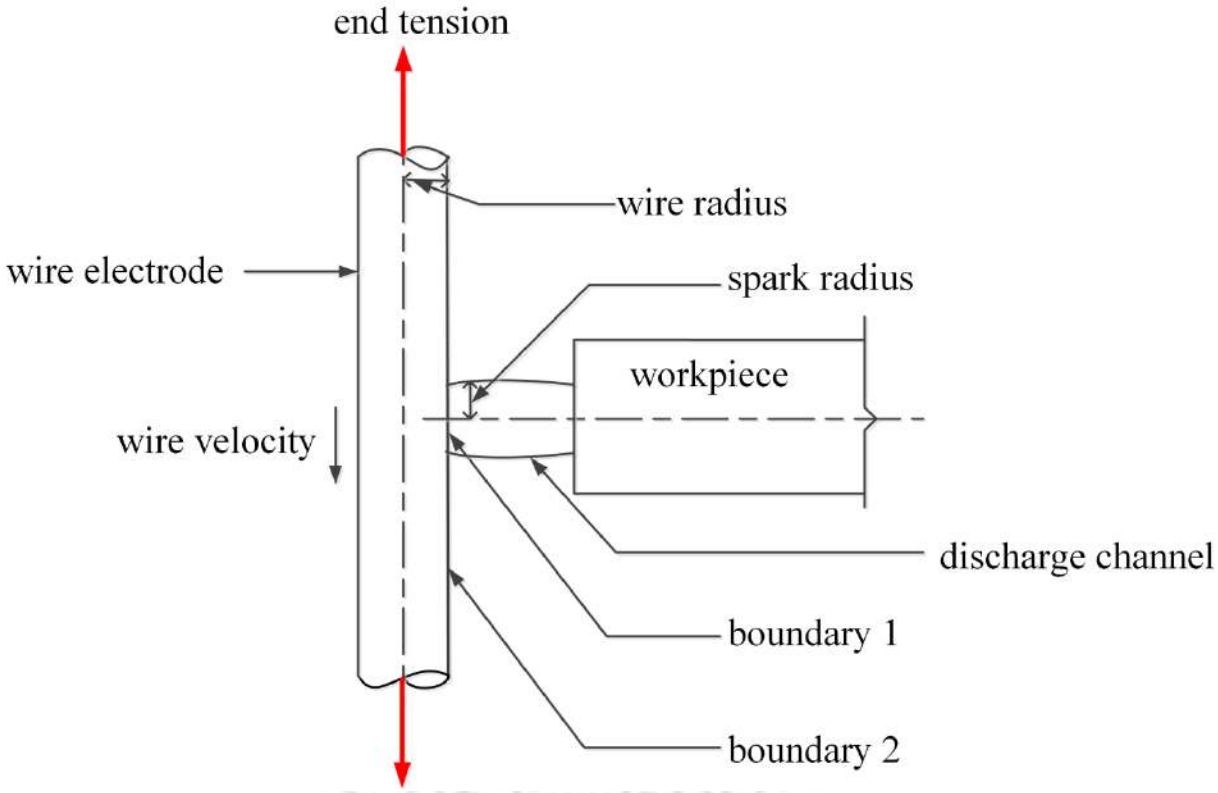

Figure 3.2 Schematic of wire electrode-spark-workpiece arrangement during WEDM machining

3.3.1 Assumptions

The development of the numerical model involves complex interactions between the discharge channel, wire tool and the workpiece. Hence, the following assumptions were considered to simplify the model.

- The material of the wire is homogeneous and isotropic.

- The material properties of the wire are temperature dependent.
- Heat flux is assumed to be Gaussian distributed.
- A fraction of total heat dissipated by the spark is only absorbed by the wire electrode. The rest of the energy is absorbed by the workpiece and lost into the dielectric.
- Joule heating and cross vibration effects of the wire are neglected.
- The wire is initially considered to be free of residual stresses.
- von-Mises criterion is used for the plastic yielding.

3.3.2 Governing equation and boundary conditions

A. Thermal analysis

Governing equation

Heat flow through the wire is governed by a three-dimensional transient heat conduction equation given by the partial differential equation in cylindrical polar coordinates (Carslaw and Jaeger, (1959)).

$$\frac{\partial^2 T}{\partial r^2} + \frac{1}{r}\frac{\partial T}{\partial r} + \frac{1}{r^2}\frac{\partial^2 T}{\partial \varphi^2} + \frac{\partial^2 T}{\partial z^2} - n\frac{\partial T}{\partial z} = \frac{1}{\alpha}\frac{\partial T}{\partial t} \qquad (3.1)$$

where T is the temperature, α is thermal diffusivity (m^2/s), t is time (s) and $n = \rho cv/k$ where ρ is density of the material (kg/m^3), c is specific heat (J/kg K), v is wire velocity (m/s) and k is thermal conductivity (W/mK).

Boundary conditions

The heat flux is assumed to be distributed over boundary 1 (Figure 3.2). On the remaining portion of the wire (boundary 2), convection between the wire surface and the dielectric is considered as the boundary condition. Mathematically, these boundary conditions can be described as follows:

For boundary region 1:

$$k\frac{\partial T}{\partial r} = Q(r) \quad \text{for } r = R_w \qquad (3.2a)$$

where $Q(r)$ is the heat flux applied and R_w is the radius of the wire.

For boundary region 2:

$$k \frac{\partial T}{\partial r} = h\,\theta \quad \text{for } r = R_w \tag{3.2b}$$

where h is the convective heat transfer coefficient (W/m^{2}K).

The initial temperature of the wire at time t = 0 is assumed to be at room temperature of 300 K.

Spark radius

For a single pulse discharge process in wire EDM, it is very difficult to measure the spark radius experimentally due to very short duration of the pulses (in the range of microseconds). A number of researches have been reported to determine the spark radius during a single discharge. DiBitonto et al. (1989) approximated spark as a point for cathode erosion and calculated the plasma radius, R_a at anode erosion(Patel et al. (1989)) as a function of time, which is given as

$$R_a = k' t^{n'} \tag{3.3}$$

where *n'* and *k'* were considered to have values of 0.75 and 0.788e-6 respectively, based on experimental results.

Pandey and Jilani (1986) suggested an equation for the discharge radius, R in the EDM process based on the boiling point temperature T_b of work material, energy density E_0 and thermal diffusivity α of workpiece material. The equation has limited applicability for steel-copper pair, given as

$$T_b = \frac{E_0 r}{K \pi^{0.5}} \tan^{-1}\left[\frac{4\alpha t}{r^2}\right]^{0.5} \tag{3.4}$$

A semi-empirical equation of spark radius, R (μm) termed as "equivalent heat input radius" was derived by Ikai and Hashiguchi (1995) as a function of discharge current, I (A) and pulse on-time, t_{on} (μs), given as

$$R = (2.04 \times 10^{-3})\, I^{0.43}\, t_{on}{}^{0.44}\ (\mu m) \tag{3.5}$$

In the present numerical model, this approach (Equation 3.5) has been used to calculate the spark radius as it gives more realistic results compared to the above mentioned approaches.

Heat flux on the wire electrode

Different approaches of heat flux were used by several researchers in the numerical modeling of electrical discharge machining process. Literature suggests that two forms of heat input sources have been considered in the thermal models developed initially viz. point heat source (DiBitonto et al. (1989)) and uniformly distributed heat flux (Beck (1981), Jilani and Pandey (1982), Pandey and Jilani (1986)). However, these assumptions were found to be not realistic in nature. In this work, the approach of Gaussian distribution of heat flux as suggested by Patel et al. (1989) is used because the results predicted were in higher agreement with the experimentally obtained values. The Gaussian heat flux equation is,

$$Q(r) = \frac{4.57\, F_c\, V\, I}{\pi R^2} \exp\left(-4.5\, \frac{r^2}{R^2}\right) \tag{3.6}$$

where F_c is the fraction of total EDM spark power going to the wire electrode (cathode); V is discharge voltage (V); I is discharge current (A) and R is spark radius (μm). The energy distribution factor (F_c) is a critical factor in the heat flux equation because it gives the fraction of total energy absorbed by the wire electrode during the discharge phenomenon. The discharge energy is distributed between the wire electrode and workpiece, while the rest of the heat is lost into the dielectric. Researchers employed various values of F_c in the literature. Previous reports suggested that 50-60 % of the total heat generated during spark discharges is absorbed by the cathode and anode (Yeo et al. (2008)). However, this assumption was not able to produce realistic results when compared to the experimental data. DiBitonto et al. (1989) collected data over a long period at various process conditions. Comparing the analytical and experimental data, it was recommended that the energy distribution factor for cathode should be chosen as 0.183 for better agreement between the analytical and experimental results. In the present model, we have chosen this value of energy distribution factor, F_c to calculate the heat flux and to estimate the temperature increment on the wire as the wire acts as the cathode for a wire EDM process.

Incorporation of the concept of moving heat source

The wire is constantly moving during the WEDM cutting operation. The effect of moving wire tool is incorporated in the numerical model by using the concept of moving heat source characteristics, which gives a more realistic approach to the model. The temperature

distribution in the wire is evaluated at the end of a single pulse by using moving heat source characteristics in the developed model. The wire moves at a constant velocity during the discharge phenomenon. Thus, the Gaussian heat flux is assumed to move along the length of wire at a constant velocity, which gives the temperature generated at the end of a single pulse. For a single pulse cycle, the wire moves a distance (L), which is given by

$$L = v\,(t_{on} + t_{off}) \tag{3.7}$$

It is assumed that the Gaussian heat flux traverses a distance over the wire surface that is traveled by the wire during a single pulse at a constant velocity. Thus, the Gaussian heat flux moves a distance L over the wire surface during a single discharge cycle. The incorporation of moving heat source characteristics gives a realistic approach to the process model. In the present model, a user subroutine DFLUX has been written and employed in ABAQUS^{TM} to incorporate the effect of moving wire electrode during wire EDM machining. The DFLUX subroutine is provided in Appendix A3.

Convective heat transfer coefficient

The heat transfer phenomenon in wire EDM process is quite complex; therefore, estimating the convective heat transfer coefficient (h) experimentally is quite complicated. The convective heat transfer coefficient is assumed to have a constant value of 10,000 W/m^{2}K referring to Dekeyser et al. (1985b). Banerjee et al. (1993) has also used this value of h and the results were quite satisfactory.

B. Mechanical analysis

The temperature distribution from the thermal analysis was given as input to the mechanical analysis. The structural analysis was carried out to calculate the stresses induced in the wire due to the sparks produced during machining.

Governing equations

The thermo-elasto-plastic material model is based on the von-Mises yield criterion. Basically, two sets of equations govern the analysis, which are the equilibrium equations and

the constitutive equations (Nart and Celik (2013)). Equations of equilibrium can be given as

$$\sigma_{ij} + \rho b_i = 0, \qquad \sigma_{ij} = \sigma_{ji} \tag{3.8}$$

where σ_{ij} is the stress tensor and b_i is the body force vector. Consequently, constitutive equations for the thermo-elasto-plastic model are considered. Stress-strain relations can be given as

$$[d\sigma] = ([D^e] + [D^p])\,[d\varepsilon] + [K^{th}]\,dT \tag{3.9}$$

where $[D_e]$ is the elastic stiffness matrix, $[D_p]$ is the plastic stiffness matrix, $[K_{th}]$ is the thermal stiffness matrix, $d\sigma$, $d\varepsilon$, and dT are the stress, strain, and temperature increments, respectively. Thermal expansion caused due to the sparks during wire EDM process induces thermal stresses in the irradiated region. These stresses lead to elastic and plastic strains in the material.

Elastic strains are calculated through isotropic Hook's, law and yielding is determined by using von-Mises criterion as

$$\frac{1}{2}\left[(\sigma_1 - \sigma_2)^2 + (\sigma_2 - \sigma_3)^2 + (\sigma_1 - \sigma_3)^2\right] = \sigma_y^2 \tag{3.10}$$

where σ_y is the yield stress and σ_1, σ_2 and σ_3 are x, y and z components of the stresses, respectively. Von-Mises criterion is used for plastic yielding of the wire material since it is suitable for ductile materials.

To avoid the rigid body movement, both ends of the wire were pinned with zero displacement boundary conditions. The surface of the wire was free of any mechanical boundary conditions. End tension of 14 N was applied at both ends of the wire as shown in Figure 3.2.

3.3.3 Solution methodology

The governing equations along with the boundary conditions are solved by using finite element method (FEM) to predict the thermo-mechanical characteristics of the wire during the cutting operation. FEM is a numerical technique to obtain an approximate solution to a class of problems governed by partial differential equations and a set of boundary conditions. The FEM technique converts the partial differential equation into a set of algebraic equations, which can be easily solved by using suitable approximations for the variables over the elements (Dixit (2009)). The model geometry is divided into small elements forming a mesh.

Each element is characterized by a set of points called nodes. The algebraic equations are obtained for each of the elements in the mesh. The solution to a FEM problem is obtained in the form of values of field variables at the nodes such as temperature, stress, strain, displacements etc.

The FEM model of the wire tool during spark discharges gives the values of temperature and stresses generated in the wire during the discharge phenomenon. The coupled thermo-mechanical analysis has been carried out as it gives a more realistic approach compared to the sequential thermo-mechanical analysis. In a coupled thermal-stress analysis, both the temperature and stresses are dependent on each other and computed simultaneously. On the other hand, in sequential thermal stress analysis, the computation of the stress field is dependent on the temperature field, but the temperature field can be computed independently without any knowledge of the stress response.

3.4 Finite element formulation

The following steps constitute a FEM problem: (a) pre-processing, (b) obtaining elemental equations, (c) assembly, (d) application of boundary conditions, (e) solution and (f) post-processing (Dixit (2009)). The details of finite element formulation are discussed below.

3.4.1 Continuum discretization

In FEM, the model geometry considered for analysis is discretized into a finite number of small elements. The elements can be of different shapes and are characterized by some points called nodes. This entire process of discretizing the process model into small elements is called mesh generation. It is to be noted that the same meshing is used for both the thermal and stress analysis. In the present work, a 3D eight-node brick element is used. Hexahedral (brick) elements are suitable for three-dimensional analysis as it gives better convergence of results at minimum cost.

The eight noded hexahedral element or brick element has eight corner nodes with isoparametric coordinates given by ξ, η, ζ. The Lagrange shape function can be written as(Alavala (2010)):

$$N_i = \frac{1}{8}\left(1+\xi_i\,\xi\right)\left(1+\eta_i\,\eta\right)\left(1+\zeta_i\,\zeta\right) \qquad i=1,\ldots,8 \tag{3.11}$$

where (ξ_i, η_i, ζ_i) represent the coordinates of node *i* of the element in the natural coordinate system.(Figure 3.3)

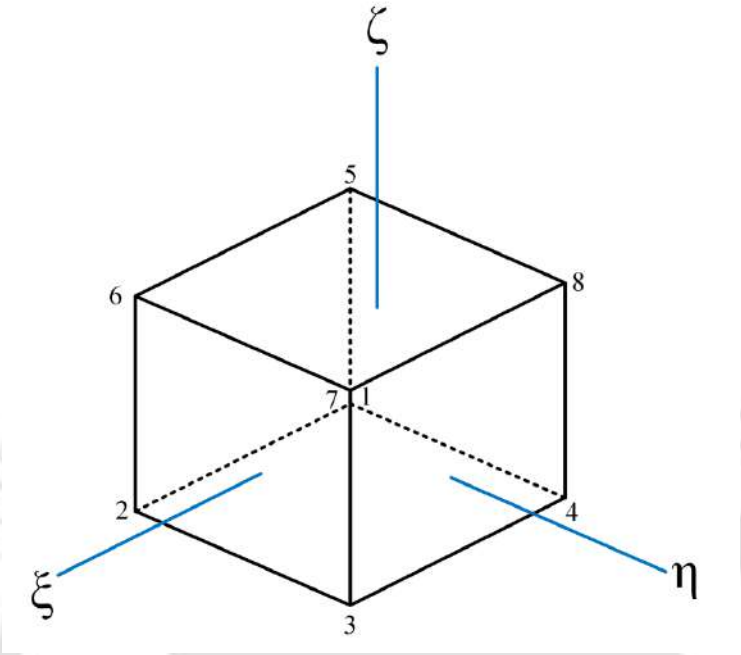

Figure 3.3 Eight-node hexahedral element

$$
\begin{aligned}
N_1 &= \frac{1}{8}(1-\xi)(1-\eta)(1-\zeta)\\
N_2 &= \frac{1}{8}(1+\xi)(1-\eta)(1-\zeta)\\
N_3 &= \frac{1}{8}(1+\xi)(1+\eta)(1-\zeta)\\
N_4 &= \frac{1}{8}(1-\xi)(1+\eta)(1-\zeta)\\
N_5 &= \frac{1}{8}(1-\xi)(1-\eta)(1+\zeta)\\
N_6 &= \frac{1}{8}(1+\xi)(1-\eta)(1+\zeta)\\
N_7 &= \frac{1}{8}(1+\xi)(1+\eta)(1+\zeta)\\
N_8 &= \frac{1}{8}(1+\xi)(1+\eta)(1-\zeta)
\end{aligned}
\qquad (3.12)
$$

3.4.2 Thermal analysis

In thermal analysis, the field variable is temperature, which is approximated within the element using its nodal temperatures,

$$T=[N]\{T_e\} \tag{3.13}$$

$$T_{,x}=[N_{,x}]\{T_e\}=[B]\{T_e\} \tag{3.14}$$

where $[N]$ is the shape function matrix, $\{T_e\}$ is the element nodal temperature matrix, $[B]$ is the geometry matrix, and the subscript x denotes differentiation with respect to x.

The above equations are solved using FEM and expressed in matrix form as

$$[C]\{T\}+[K]\{T\}=\{Q\} \tag{3.15}$$

where $\{Q\}$ is the heat flux matrix, $[C]$ and $[K]$ are the global heat capacity matrix and the global conductivity matrix respectively, expressed as

$$[C]=\int_V \rho c[N][N]^T\, dV \tag{3.16}$$

$$[K]=\int_V k[B][B]^T\, dV \tag{3.17}$$

3.4.3 Mechanical analysis

The nodal temperatures computed in the thermal analysis are given as input to each incremental time step for the generation of stress field. Stress and strain are related by the constitutive matrix $[D]$ in the following form

$$\sigma=D\varepsilon \tag{3.18}$$

D is the constitutive matrix given by

$$D=\frac{E}{(1+\nu)(1-2\nu)}\begin{bmatrix} 1-\nu & \nu & \nu & 0 & 0 & 0 \\ \nu & 1-\nu & \nu & 0 & 0 & 0 \\ \nu & \nu & 1-\nu & 0 & 0 & 0 \\ 0 & 0 & 0 & 0.5-\nu & 0 & 0 \\ 0 & 0 & 0 & 0 & 0.5-\nu & 0 \\ 0 & 0 & 0 & 0 & 0 & 0.5-\nu \end{bmatrix} \tag{3.19}$$

The total strain can be calculated as a sum of elastic, plastic and thermal strains, given as

$$\varepsilon_{total}=\varepsilon_{elastic}+\varepsilon_{plastic}+\varepsilon_{thermal} \tag{3.20}$$

and the stress is represented as

$$[\sigma]=\begin{bmatrix}\sigma_1\\ \sigma_2\\ \sigma_3\\ \sigma_{12}\\ \sigma_{23}\\ \sigma_{13}\end{bmatrix} \tag{3.21}$$

The displacement field $\{u\}$ is represented by

$$\{u\}=[N]\{d\} \tag{3.22}$$

where $\{u\} = [u\ v\ w]^T$ and $\{d\}$ is the nodal displacement degree of freedom of an element.

Strains are determined by the relation

$$\{\varepsilon\}=[B]\{d\} \tag{3.23}$$

and

$$[B]=[\partial][N] \tag{3.24}$$

In coupled thermo-mechanical analysis, both the temperature and stress are computed simultaneously.

3.5 Computation of temperature and stresses generated in the wire using the developed model

3.5.1 Material properties

A molybdenum wire (0.18 mm diameter) which is generally used in commercial WEDM machines is considered for analysis in the present model. The temperature dependent properties of molybdenum are shown in Figures 3.4 and 3.5. Table 3.1 lists some of the general properties of molybdenum.

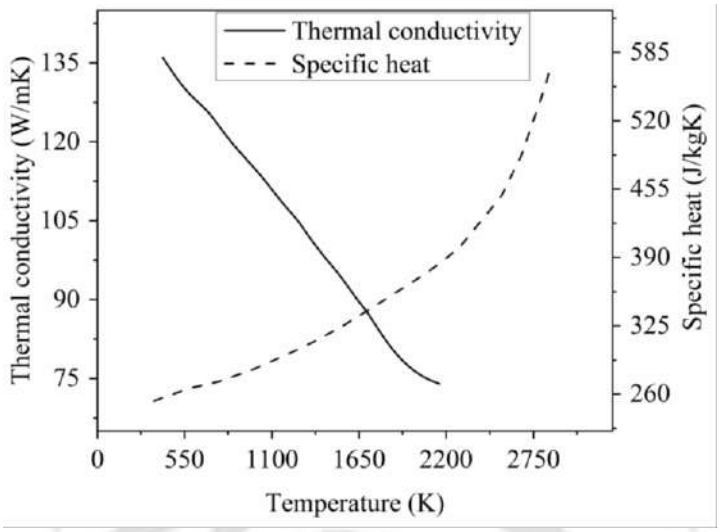

Figure 3.4 Temperature dependent thermal conductivity(Tietz and Wilson (1961)) and specific heat (Taylor and Finch(1964)) of molybdenum

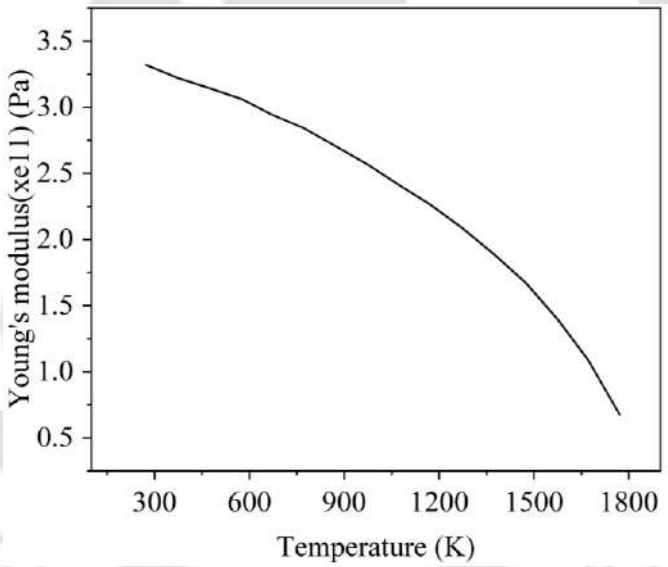

Figure 3.5 Temperature dependent Young's modulus of molybdenum(Zhang et al. (2014))

Table 3.1 Thermal and physical properties of molybdenum(Zhang et al. (2014))

Property	Value
Density(kg/m^3)	10200
Poisson's ratio	0.3
Coefficient of thermal expansion (μm/m-ºC)	4.6
Melting point (K)	2896

Tensile testing of molybdenum wire

The yield strength and tensile strength of the wire were determined by performing a tensile test of a fresh molybdenum wire. The tensile testing of the wire was carried out on a micro-tensile machine by Deben (Deben micro test MT10081), shown in Figure 3.6. The micro tensile machine had an upper limit of up to 5 kN tensile load and maintained the crosshead speed at 0.2mm/min. The tensile testing was carried out under ambient conditions. The data from the tensile test was collected and converted into stress-strain values. The stress-strain behavior of the molybdenum wire was studied to determine the yield strength and ultimate strength of the wire. Figure 3.7 shows the stress-strain behavior of the wire during the tensile testing. The yield point of the molybdenum wire was determined to be about 600 MPa and the ultimate strength at around 1472 MPa. These values of yield stress and strain were taken from the graph to be incorporated into the numerical model.

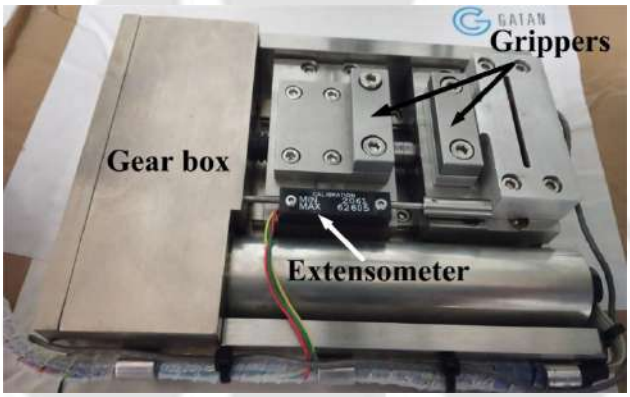

Figure 3.6 Micro tensile testing machine

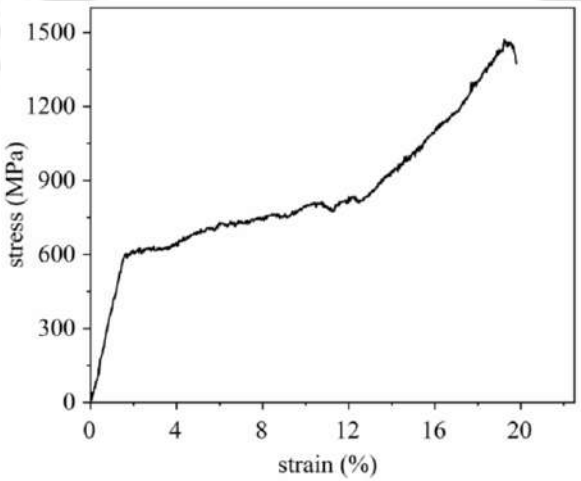

Figure 3.7 Stress vs. strain graph of a molybdenum wire

3.5.2 Process parameters used for the model

In the present model, four input parameters, viz. discharge voltage, discharge current, pulse on-time and pulse off-time were varied at different levels. The process parameters have been selected by performing extensive preliminary experiments. The trade literature and research articles have been duly referred to choose the ranges of the process parameters. The levels chosen for each process parameter are listed in Table 3.2.

Table 3.2 Process parameters and their levels

Factors	Level 1	Level 2	Level 3
Discharge voltage (V)	60	85	-
Discharge current (A)	4	6	8
Pulse on-time (μs)	4	8	16
Pulse off-time (μs)	2	4	6

The wire velocity (v) was kept constant at 6 m/s in the present model.

3.5.3 Overview of the process model development

Figure 3.8 shows the schematic representation of the thermo-mechanical analysis that was carried out to compute the thermal residual stresses. A three-dimensional coupled thermo-mechanical model was developed for the wire electrode. In the present study, the temperature is first evaluated during the thermal analysis and based on the temperature distributions obtained, the stresses on the wire are calculated after a single pulse at different process conditions. This model shall pave the way to estimate the total thermal load in the wire and evaluate the effects that lead to wire breakage by determining the stresses induced due to sparks during the operation.

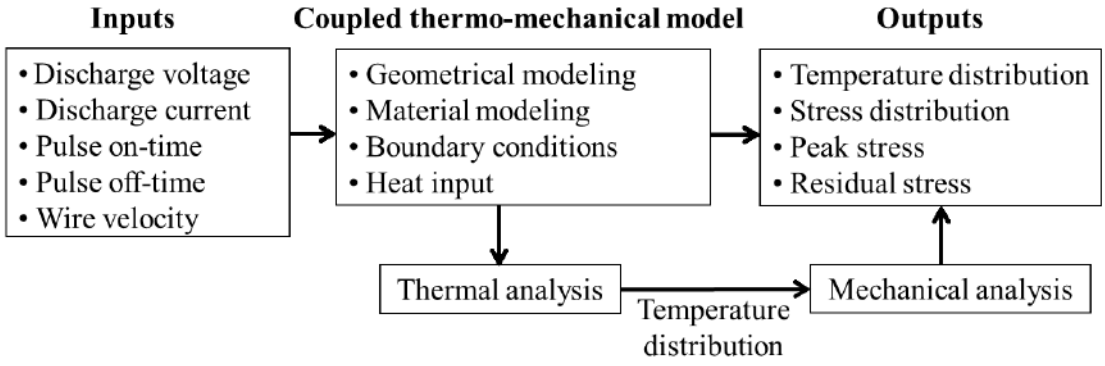

Figure 3.8 Schematic representation of thermo-mechanical analysis

3.5.4 Finite element meshing of the wire geometry

The process model along with the boundary conditions was solved in transient mode by using ABAQUS™, a commercial FEM solver. The wire geometry is discretized with eight-node hexahedral elements C3D8T. The elements 'C3D8T' are especially suitable for coupled thermo-structural analysis. Figure 3.9 shows the meshed model of the wire electrode along with the incorporated boundary conditions. Mesh optimization was performed for better convergence of results in optimum time. The overall mesh size was kept at 30 µm for the wire model. The heated and nearby region was discretized using finer mesh size to get better accuracy of results. The mesh sensitivity analysis was carried out for a single process condition at discharge voltage (V) = 60 V, discharge current (I) = 6 A, pulse on-time (t_{on}) = 16 µs, pulse off-time (t_{off}) = 6 µs, wire velocity (v) = 6m/s. The heated region was discretized with a fine mesh of various sizes, shown in Table 3.3. It was observed that the smallest change in temperature occurs when the fine mesh size changes from 10 µm to 8 µm as compared to the other cases. Thus, the element of 8 µm size was selected as the optimum fine mesh size for the heated region to achieve better results. The moving heat source concept was used in the model to incorporate the effect of moving wire during the wire EDM machining process. The Gaussian heat flux moving at a constant velocity over the wire surface was employed using a user subroutine DFLUX. The subroutine is included in Appendix A3. The FORTRAN code was written to define the input process conditions during a single discharge phenomenon during wire EDM cutting. The movement of Gaussian heat flux over the wire surface is shown in Figure 3.9. The transient heat transfer problem was solved by applying

the heat flux at the spark location and adopting an automatic time step increment. Convection heat transfer is applied over the wire surface as shown in Figure 3.9.

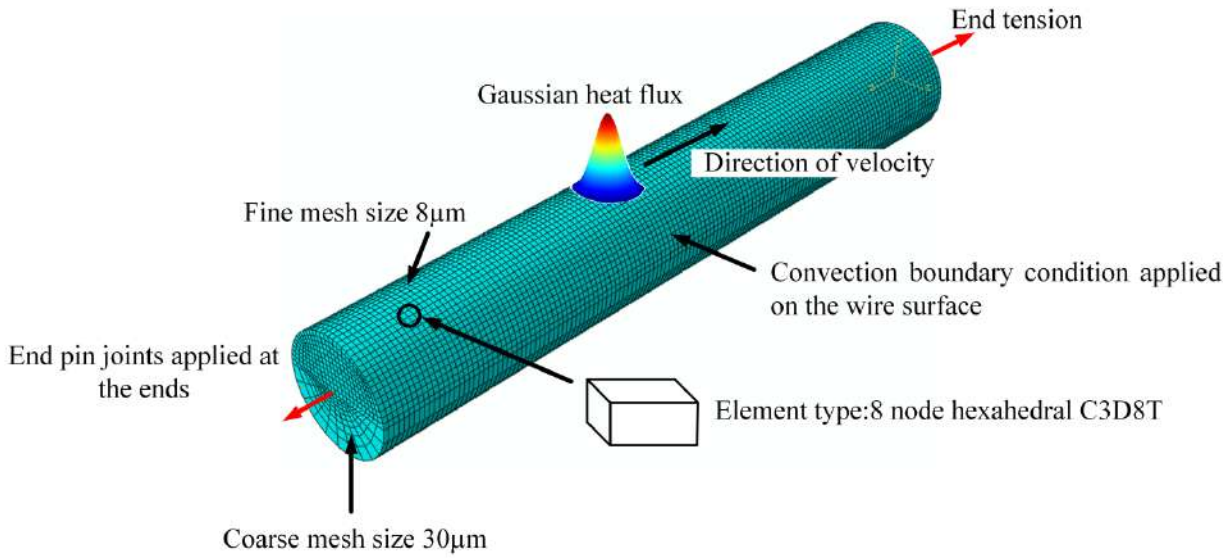

Figure 3.9 Mesh model of wire electrode

Table 3.3 Mesh sensitivity analysis for the fine mesh in the heated region

Serial no.	Mesh size (µm)	Temperature output (K)	Change in temperature (%)	CPU time (hrs.)
1	25	664.3	-	0.15
2	20	517.4	22.11	0.26
3	15	500.6	3.24	1.79
4	10	470	6.11	5.92
5	**8**	**460.7**	**1.97**	**8.92**

3.6 A case study on the temperature and residual stresses generated in the wire

After the development of the numerical model, simulation was carried out for a typical process condition to compute the temperature generated in the wire and the residual stresses induced in the wire. In order to study the effects of various process parameters on the temperature obtained and the stresses generated in the wire electrode during the machining process, eighteen cases have been considered as suggested by the Taguchi L18 array. The effects of different input parameters on the temperature and stresses induced in the wire have

been discussed in detail in the next chapter. Figure 3.10 shows the temperature profile at the end of a single pulse cycle for a typical process condition: discharge voltage (V) = 60V, discharge current (I) =6 A, pulse on-time (t_{on}) =16µs, pulse off-time (t_{off}) = 6 µs. The temperature profile takes the shape of an ellipse due to the moving heat source characteristics of Gaussian heat flux. It is observed that as the heat source moves along the wire axis, the temperature keeps on increasing during the pulse on-time and starts cooling during the pulse off-time. The peak temperature is obtained at the end of the discharge duration. The increase in temperature generates thermal stresses in the irradiated and nearby region. After the cooling effect in a single pulse, the stresses retained in the wire are the residual stresses induced. Figure 3.11 shows the stress contour induced on the wire surface during the discharge phenomenon for the same process condition. The thermal residual stresses retained in the wire weakens the wire strength which, might eventually cause wire failure. This model was developed to investigate and analyze the contribution of the thermally generated stresses to wire failure. The variation of equivalent thermal residual stresses along the wire axis at the end of a single pulse is depicted in Figure 3.12. When the induced thermal residual stresses exceed the yield strength of the wire material, the deformation of the wire goes into the plastic zone, which degrades the wire strength further. Plastic strains are induced in the wire. The wire breaks off when the ultimate tensile strength of wire is reached.

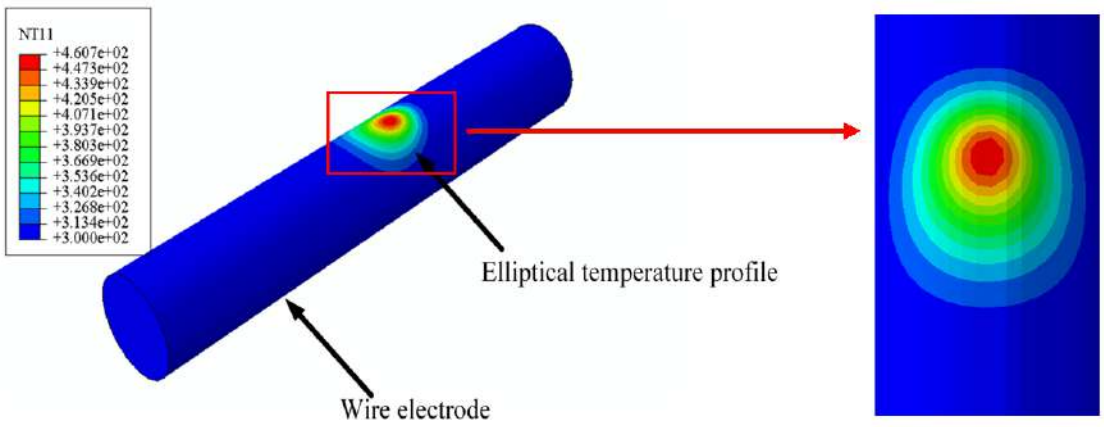

Figure 3.10 Elliptical temperature profile after a single pulse

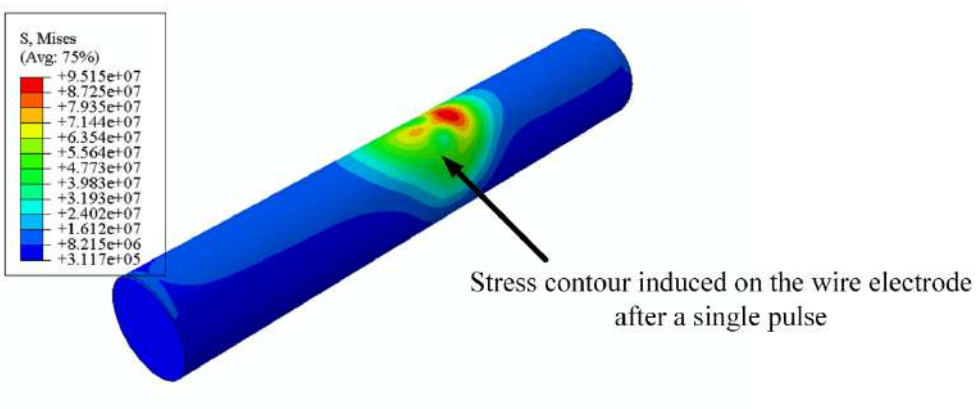

Figure 3.11 Stress contour on the wire electrode

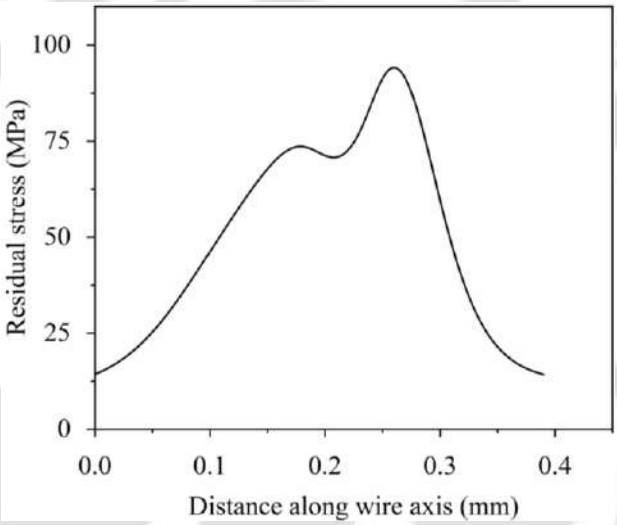

Figure 3.12 Variation of equivalent residual stresses along the wire axis (V = 60 V, I = 6 A, t_{on}= 16 µs, t_{off}= 6 µs)

3.7 Validation of the developed numerical model

The results predicted by the present numerical model viz. temperature and residual stress were compared with published results and in house experimental results. It is challenging to experimentally record the temperature rise in the wire at a particular location since the wire is continuously moving and immersed in the dielectric. Thus, the peak temperature predicted by our model is compared with that of theoretical published results initially. However, the peak residual stress at the end of a single pulse predicted by our model is validated using in house experimental results.

3.7.1 Validation of temperature using published data

The peak temperature obtained in the wire after a single discharge predicted by our model was compared with published theoretical results by adopting the same process conditions reported by Zhang et al. (2014) and Chen et al. (2015). Table 3.4 shows the comparison of peak temperature predicted by our numerical model and the reported theoretical model results (Zhang et al. (2014), Chen et al. (2015)). The comparisons revealed that the peak temperature predicted by our numerical model was well in agreement with the results reported in the literature. Gaussian distribution of heat flux, pulse on-time dependent spark radius equation and the moving heat source were considered in our numerical model, which made the developed model of wire electric discharge machining process more realistic. However, constant joule heat source has been used by Zhang et al. (2014), which might be the reason behind the errors in the comparison of results.

Table 3.4 Comparison of the predicted results: Peak temperature

Published reports	Discharge voltage (V)	Discharge current (A)	Pulse on-time (µs)	Pulse off-time (µs)	Wire velocity (m/s)	Our numerical model(K)	Published data(K)	Absolute deviation (%)
Zhang et al., 2014	100	5	50	250	10	660.9	683	3.23
Chen et al., 2015	40	10	25	10	2	390	360	8.33

3.7.2 Experimental validation of residual stresses using X-ray diffraction technique

To establish the validity of the proposed numerical model, the model results were validated with experimental data. Tensile residual stresses were obtained on the wire surface in a small region surrounding the spark, which is in accordance with previous literature (Guu et al. (2003), Ekmekci et al. (2006), García Navas et al. (2008)). These residual stresses retained in the wire are the result of non-uniform temperature distributions during the heating and cooling cycles of the discharge. The maximum value of residual stresses induced in the wire electrode predicted numerically was compared with the residual stress values measured experimentally by X-ray diffraction (XRD) technique.

Experiments were conducted on a wire electric discharge machine (MAKE JK MACHINES, MODEL ECO32). Wire EDM machining was performed on Ti-6Al-4V alloy with molybdenum wire (0.18 mm diameter) at different process conditions. Wire samples were collected after each experiment set just after the spark discharges were produced between the wire and workpiece, as it is not practically possible to achieve a single spark during the machining process. The WEDM setup was stopped as soon as the sparks were generated to collect the wire samples for further examination. The collected wire sample was tested for stress measurement using the XRD technique. Due to the small size of the wire (diameter 0.18 mm), the exact location of the wire where the X-ray falls cannot be precisely determined; thus, the peak values of equivalent residual stresses predicted by the model are validated with the experimental data.

X-ray residual stress method of determination measures the strain, ε of a sample by using the distance between crystallographic planes, d as a strain gauge and the residual stress producing the strain is calculated, assuming a linear elastic distortion of the crystal lattice. When a beam of X-ray with a specific wavelength, λ falls on the surface of a sample, the scattered radiation undergoes interference according to Bragg's law, which governs the X-ray diffraction theory. Bragg's law is given by:

$$n\lambda = 2d\sin\theta \tag{3.25}$$

where n is an integer denoting the order of diffraction and θ is the diffraction angle (Prevey(1986)). The d spacing in a specimen changes if residual stresses are present in the sample. The strain producing the shift in d spacing is calculated and converted to stress values using Hooke's law. The most commonly used method for XRD residual stress determination is the $sin^2\ \psi$ method, assuming a biaxial stress state on the sample surface. Figure 3.13 represents the schematic of residual stress measurement by XRD technique for a plane (hkl) tilted by ψ and rotated by ϕ. XRD measurements for evaluating the residual stresses are made by fixing a diffraction angle, 2θ and scans are made at different psi tilts. For higher precision of XRD stress measurement results, the Bragg peak angle is generally kept at an angle higher than 120º.

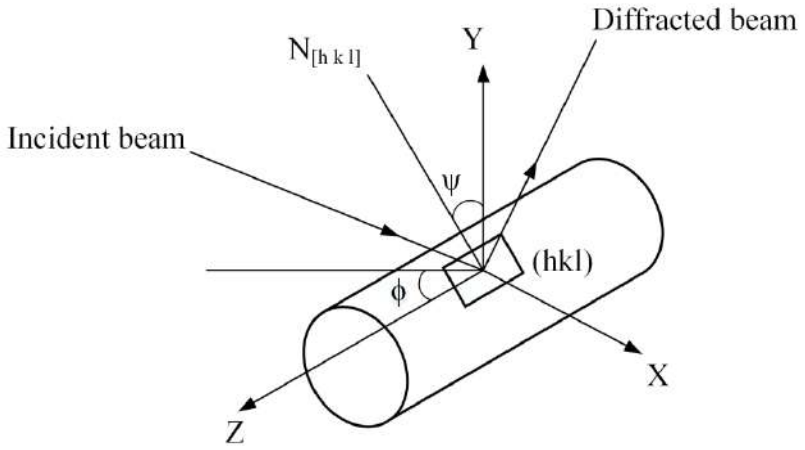

Figure 3.13 Schematic of XRD for residual stress measurement

The inter-planar spacing of a material that is free from strain will produce a characteristic diffraction pattern for that material. When a material is strained, elongations and contractions are produced within the crystal lattice, which change the inter-planar spacing of the (hkl) lattice planes. This induced change in d will cause a shift in the diffraction pattern. By precise measurement of this shift, the change in the inter-planar spacing can be evaluated and thus the strain within the material deduced.

If $d_{\varphi\psi}$ is the spacing between the lattice planes measured in the direction defined by φ and ψ, the strain can be expressed in terms of changes in the spacing of the crystal lattice as

$$\varepsilon_{\phi\psi} = \frac{\Delta d}{d_0} = \frac{d_{\phi\psi} - d_0}{d_0} \tag{3.26}$$

The x-ray penetration is extremely shallow (< 10 μm), thus a condition of plane-stress is assumed to exist in the diffracting surface layer. The stress distribution is then described by principal stresses σ_{11}, and σ_{22} in the plane of the surface, with no stress acting perpendicular to the free surface. The normal component σ_{33} and the shear stresses $\sigma_{13} = \sigma_{31}$ and $\sigma_{23} = \sigma_{32}$ acting out of the plane of the sample surface are zero. The strain in the sample surface at an angle φ from the principal stress σ_{11} is then given by (Prevey (1986)):

$$\varepsilon_{\phi\psi} = \frac{1+\nu}{E}\,\sigma_{\phi}\,\sin^2\psi - \frac{\nu}{E}\,(\sigma_{11} + \sigma_{22}) \tag{3.27}$$

Combining equations3.26 and 3.27,

$$\frac{d_{\phi\psi} - d_0}{d_0} = \frac{1+\nu}{E}\sigma_\phi \sin^2\psi - \frac{\nu}{E}(\sigma_{11} + \sigma_{22})$$

$$\Rightarrow d_{\phi\psi} = \left(\frac{1+\nu}{E}\right)\sigma_\phi d_0 \sin^2\psi - \frac{\nu}{E} d_0(\sigma_{11} + \sigma_{22}) + d_0 \quad (3.28)$$

where $d_{\phi\psi}$ is the lattice spacing of (hkl) planes tilted by ψ and rotated by ϕ; $\varepsilon_{\varphi\psi}$ is the strain measured in the direction defined by the angles ϕ, ψ; σ_φ is the stress component along ϕ direction; d_0 is the unstressed d spacing; E is the Young's modulus of the sample; ν is the Poisson's ratio; $\sigma_{11}$and σ_{22} are the principal biaxial stress components.

For an isotropic material, if the sample has a biaxial stress state, then the residual stress is calculated from equation 3.28 (Fitzpatrick et al., 2005).

The slope of the plot is

$$\frac{\partial d_{\phi\psi}}{\partial \sin^2\psi} = \left(\frac{1+\nu}{E}\right)\sigma_\phi d_0$$

$$\therefore m = \left(\frac{1+\nu}{E}\right)\sigma_\phi d_0$$

$$\sigma_\phi = \frac{m}{d_0}\left(\frac{E}{1+\nu}\right) \quad (3.29)$$

Equation 3.29 is used to calculate the value of residual stresses present on the surface of a sample.

The intercept of the plot of d vs. $sin^2\psi$ at $sin^2\psi = 0$ ($\psi = 0$) is

$$d_{\phi 0} = 0 - \frac{\nu}{E} d_0(\sigma_1 + \sigma_2) + d_0$$

$$d_{\phi 0} = d_0 - \frac{\nu}{E} d_0(\sigma_1 + \sigma_2)$$

$$d_{\phi 0} = d_0\left[1 - \frac{\nu}{E}(\sigma_1 + \sigma_2)\right] \quad (3.30)$$

In the present method of residual stress determination, the d spacing calculated at ψ = 0 is substituted for the unstressed d spacing, d_0.This assumption introduces a minimal error (less than 0.1%) of the Poisson's ratio contraction caused by the principal stresses (Fitzpatrick et al., 2005).

The XRD measurement method was used to measure the residual stresses on the wire electrode after machining at different process conditions using an XRD facility (MAKE:

Rigaku, MODEL: Smart Lab) with CuKα source having a wavelength of 1.54 A˚, working at 45V and 200mA. The sample is rotated through a series of angles, ψ (keeping 2θ constant and $\phi = 0$ constant). The d spacing in the wire will slightly shift due to the residual stresses present in the specimen.

The (hkl) plane (321) was selected for molybdenum for the residual stress measurement with Bragg peak angle 132.6. A higher Bragg peak angle is chosen for better accuracy of the results. The Bragg peak (2θ) was converted to d values and plotted against $sin^2\psi$ values to calculate the slope of the plot. The value of slope obtained was substituted in Equation 3.29 to obtain the value of residual stresses. The wire sample with the process set (V = 60 V, I = 4 A, t_{on} = 8µs, t_{off} =4 µs) was collected after machining, and a small wire specimen was tested for residual stress using the XRD machine. Five angles of ψ (keeping 2θ = 132.6 constant) were varied and the corresponding d values were obtained. The intensity vs. 2θ plot for different ψ values is shown in Figure 3.14. The d vs. $sin^2\psi$ values are shown in Table 3.5, which are plotted to obtain the slope.

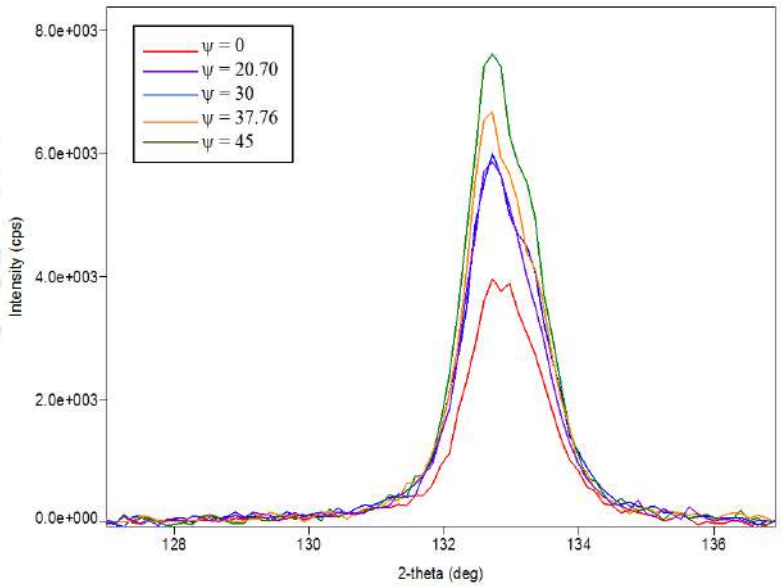

Figure 3.14 Intensity vs. 2θ graph for plane (321) of molybdenum

Table 3.5 d vs. $sin^2\psi$ data from XRD results

2θ	d	$sin^2\psi$
132.68	0.84098	0
132.71	0.84090	0.1249

132.654	0.84107	0.25
132.662	0.84105	0.37499
132.65	0.84108	0.5

The slope of d vs. $sin^2\psi$ plot from the data in Table 3.5 is calculated as 0.000280032. The residual stress generated on the wire electrode surface by substituting the value of slope in Equation 3.29 is obtained as 80.68 MPa.

The numerically predicted value of equivalent peak residual stress (von-Mises residual stress) at the end of a single pulse for this process set is computed as 81.74 MPa which is quite in agreement with the experimental value (80.684 MPa) of residual stress measured by XRD. The calculated error is around 1.31 %, which is very well acceptable. The comparison of residual stresses induced on the wire electrode at different process conditions predicted numerically and experimentally using XRD results has been shown in Table 3.6. Figure 3.15 also shows the comparison results of residual stresses on the wire electrode between our numerical model and experimental results.

Table 3.6 Comparison of numerical vs. experimental results of residual stresses induced on the wire electrode

Serial no.	Discharge voltage (V)	Discharge current (A)	Pulse on-time (µs)	Pulse off-time (µs)	Numerical value of Peak residual stress (MPa)	Experimental residual stress value (MPa)	Absolute deviation (%)
1	60	4	8	4	81.74	80.68	1.31
2	85	4	16	4	135.7	145.31	6.62
3	85	6	16	2	492.5	452.3	8.88
4	60	4	16	6	65.31	73.75	11.44
5	60	6	16	6	95.15	117.57	19.06

Average deviation 9.46%

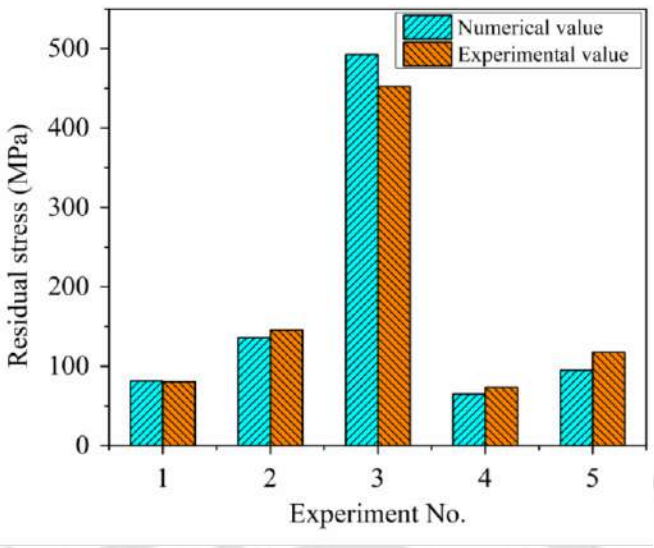

Figure 3.15 Comparison of residual stresses between the model and experimental data

Table 3.6 shows that the predicted values of residual stresses and the experimental XRD results are well matching which establishes the validity of the proposed model. It has been observed that in most cases, our model predicts lower values of residual stresses than the experimentally determined values at the end of a pulse cycle because the numerical model predicts the stress values for a single discharge, whereas multiple discharges occur in real conditions. The exact position of the wire where the X-ray falls cannot be determined precisely which could be one of the reasons for the deviation between the numerical and experimental results. Moreover, misalignment and positioning errors might also cause some error during the XRD measurements.

3.8 Summary

This chapter presented in detail, the development of a three-dimensional numerical model to predict the thermo-mechanical characteristics of the wire electrode during the spark discharges. The transient model for the wire tool was developed using finite element method to predict the temperature and stresses generated in the wire. The governing equations and boundary conditions employed in the FEM model have been explained in detail. An empirical spark radius equation dependent on current and pulse duration has been utilized. Gaussian distribution of heat flux with moving characteristics was incorporated in the model. Time dependent material properties have been used for better accurate results. Mesh

sensitivity analysis was carried out for better convergence of results in an optimum time frame. A case study was carried out to predict the temperature distribution and stress contour produced on the wire surface after a single pulse. It was observed that as the heat source moves along the wire axis, the temperature keeps on increasing during the pulse on-time and starts cooling during the pulse off-time. The thermally induced stresses in the wire weaken the wire strength. The results predicted by the developed model were validated using published data and experimental results. The peak values of residual stresses were determined using X-ray diffraction technique and the results were found to be in close approximation with the numerically computed values.

The next chapter presents a methodology to estimate the wire strength based on the results computed by the developed finite element model in order to predict and limit the occurrence of wire failure. The temperature and stresses generated in the wire during the discharge phenomenon are critical factors responsible for wire breakage. The strength of the wire electrode depends upon the thermal residual stresses induced in the wire during the cutting operation.Thus, it was thought to be worthy of developing a wire safety index based on the temperature and thermal residual stresses generated on the wire electrode surface.

CHAPTER 4

Estimation of wire strength based on residual stresses induced and parametric studies

4.0 Scope

This chapter presents the estimation of the strength of a molybdenum wire based on thermally generated residual stresses induced in the wire electrode during the pulsed discharges. The need to calculate a wire safety index for sustainable and uninterrupted WEDM process is explained. The stresses are computed from the developed numerical model presented in chapter 3. The overall approach to estimate the wire strength during the cutting operation is described in detail. The methodology to estimate a wire safety factor based on the results predicted by the finite element model is described. The peak residual stresses generated in the wire are compared to the yield stress of the wire material in order to estimate the reduction in wire strength during spark discharges. The chapter is summarized with conclusions.

4.1 The need

The wire electrode is a very crucial element of the WEDM process. During the machining operation, the wire is subjected to combined thermal and mechanical loads. The wire surface exposes to high temperature and stresses. When the temperature exceeds the melting point of wire material, wire erosion occurs. Sharp temperature gradients result in the generation of thermal stresses in the wire. The stresses that retain in the wire after the cooling cycle are termed as thermal residual stresses. The strength of wire electrode is dependent upon the amount of material eroded from the wire and thermal residual stresses originated in the wire during the discharge phenomenon. These temperature induced stresses are one of the primary factors responsible for wire breakage. The wire strength degardes due to induction of thermal stresses which may lead to catastrophic failure of the wire.

The literature reports limited studies on the influence of thermal stresses on the wire strength (Saha et al. (2004), Fedorov et al. (2018)). Very scant studies have been reported on erosion and strength of molybdenum wire during machining. In view of this, determination of a safety factor for molybdenum wire electrode could be useful in estimation of wire

strength and prediction of wire failure. In the present work, a wire safety index is determined based on thermal residual stresses induced in the molybdenum wire during the machining operation. These stresses are computed by using the three-dimensional thermo-mechanical finite element model of the wire electrode that has been presented in chapter 3. The evaluation of a wire safety index may provide useful insights into sustainable and economical machining without wire breakage in modern industrial practice.

4.2 Overall approach for the estimation of wire strength during wire EDM process

Figure 4.1 shows the overall approach of the estimation of wire strength based on thermal residual stresses induced during the WEDM process. The developed coupled thermo-mechanical model presented in chapter 3 analyzes both the temperature and stress distributions at the end of a pulse cycle. The temperature obtained and residual stresses retained on the wire electrode after a single pulse cycle determine the reduction in strength of the wire and predict the probability of wire breakage for a particular process set. It was observed that the temperatures generated in the molybdenum wire were below the melting point of molybdenum for a single spark cycle. Thus, a wire safety index is evaluated by comparing the maximum value of stresses induced to the yield stress of the wire material. Formation of microcracks on the wire surface were considered as indicators of wire rupture based on which a threshold value of thermally induced stresses in the wire was estimated to ensure safe machining without wire failure. The process conditions where thermal residual stresses exceed the unsafe limit need to be avoided in order to prevent wire rupture. It is envisaged that by using the developed method, one can easily predict the deterioration of wire electrode, which will ensure uninterrupted and efficient wire electric discharge machining operation. Finally, parametric studies were also performed to assess the effects of process conditions on the temperature and stresses induced in the wire.

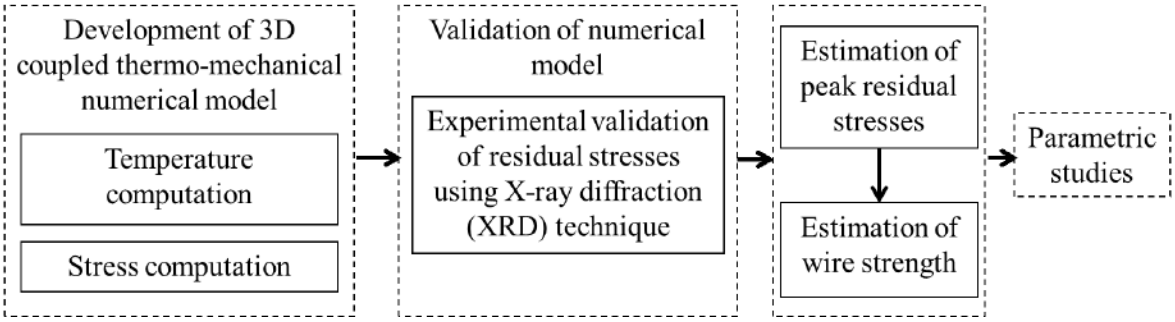

Figure 4.1 Overall approach of estimation of wire strength

4.3 Computation of peak residual stresses induced in the wire electrode

The sparks produced in the interelectrode gap between the wire tool and workpiece produces huge amount of temperature and stresses in both the wire tool and workpiece. After the cooling cycle in pulsed discharges, some stresses retain in the wire tool as the residual thermal stresses. The magnitude of stresses induced in the wire depends upon the wire material properties viz. yield strength, ultimate tensile strength, young's modulus, plastic strain of the wire material and on the process conditions used. The stresses induced in the wire were determined from the developed finite element model (refer chapter 3). In the developed finite element model, temperature and thermal residual stresses were predicted at various levels of machining conditions viz. discharge voltage, discharge current, pulse on-time, pulse off-time and wire velocity. Figure 4.2 shows the stress contour developed on the wire surface after a single discharge phenomenon for the process set: V = 85 V, I = 6 A, t_{on} = 16 µs, t_{off} = 2 µs. The peak residual stress was computed as 492.5 MPa on the wire surface. The numerical model was validated with experimental data obtained from X-ray diffraction technique, as explained in chapter 3. The developed model was simulated at 18 process conditions according to Taguchi L18 array and the temperature and stresses generated in the wire were noted down as shown in Table 4.1. It was noted that for a molybdenum wire, the temperature predicted at the end of the pulse duration was below the melting point (2896 K) of the wire material. Thus, no material erosion was observed for a single pulse. However, the stresses predicted in the molybdenum wire tool were observed to exceed the yield strength and tensile strength of the wire at certain process sets. Thus, the wire safety factor was determined based on the residual stresses induced during the spark discharges.

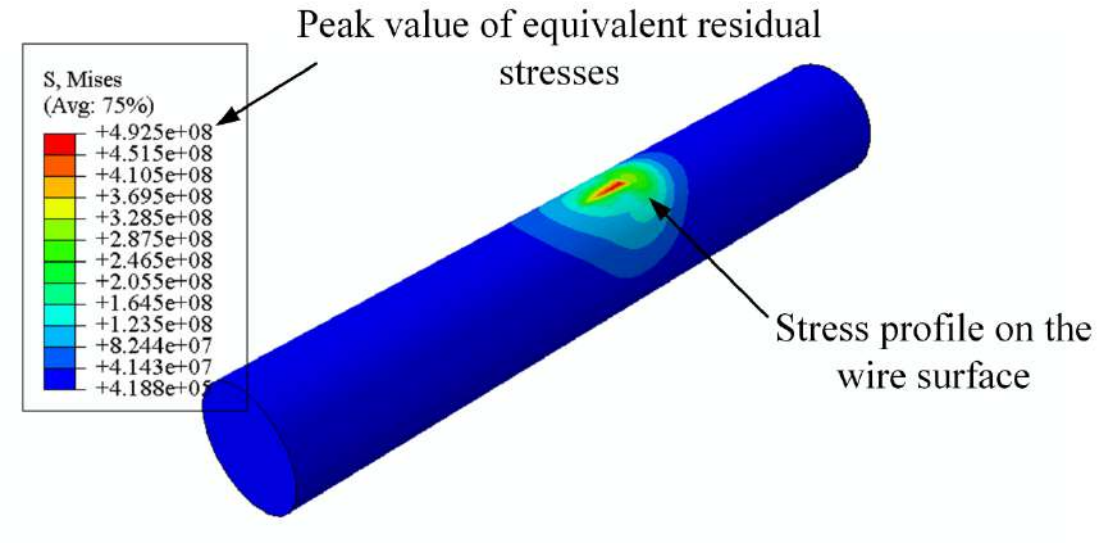

Figure 4.2 Stress contour on the wire surface for process set: $V = 85$ V, $I = 6$ A, $t_{on} = 16$ µs, $t_{off} = 2$ µs

Table 4.1 Values of temperatures and residual stresses computed on the wire electrode at different process sets by thermo-mechanical numerical model

Serial No.	Discharge voltage (V)	Discharge current (A)	Pulse on-time (µs)	Pulse off-time (µs)	Temperature at the end of t_{off} (K)	Peak residual stress (MPa)
1	60	4	4	2	720.3	217.5
2	60	4	8	4	453.7	81.74
3	60	4	16	6	408.2	65.31
4	60	6	4	2	918	462.9
5	60	6	8	4	531.7	281
6	60	6	16	6	460.7	95.15
7	60	8	4	4	585.9	1017
8	60	8	8	6	492.4	784.2
9	60	8	16	2	803.7	299.7
10	85	4	4	6	406.7	727.4
11	85	4	8	2	877.3	436.5
12	85	4	16	4	529.6	135.7
13	85	6	4	4	652.5	1327
14	85	6	8	6	514.4	1105
15	85	6	16	2	911.5	492.5

16	85	8	4	6	532.2	1482
17	85	8	8	2	1433	976.7
18	85	8	16	4	768	757.4

The values of peak residual stresses shown in Table 4.1 are the peak values of equivalent residual stresses or von-Mises stresses induced in the wire. It was observed that for some process conditions, the residual stresses exceeded the yield strength of the molybdenum wire material (600 MPa). The wire strength starts reducing as the stresses induced exceed the yield strength of the wire material i.e. the wire starts deforming, which indicates the onset of wire failure.

4.4 Estimation of wire safety index based on residual stresses

The maximum computed values of residual stresses obtained were compared with the yield stress of molybdenum wire (600 MPa) and the reduction in strength of the wire was determined by calculating a ratio (X) of peak stress value to the yield stress value. The equivalent peak residual stress values induced in the wire electrode and their corresponding values of X at various process conditions are listed in Table 4.2. If the value of X is less than 1, the peak residual stress in the wire is below the yield point of the wire material and the wire is considered within the safe limit. If the value of peak stress achieved by the wire exceeds the yield point, the wire strength starts deteriorating and finally ruptures when the equivalent stress exceeds the failure point of the wire material. The ultimate strength of the molybdenum wire was experimentally determined and found as 1472 MPa, which gives the X value as 2.45. Thus when the ratio, X goes beyond the value of 2.45, the maximum stress values achieved by the wire exceeds the ultimate strength of the wire, which indicates a high probability of wire failure. This suggests to avoid the use of corresponding process condition. The ratio X can be used as an index in determining the strength of the wire based on the residual stresses induced during the discharge phenomenon. The developed numerical model can thus be useful in predicting and preventing the wire breakage phenomenon.

Table 4.2 Residual stresses* induced in the wire and the corresponding values of X at different process sets

Serial No.	Discharge voltage (V)	Discharge current (A)	Pulse on-time (µs)	Pulse off-time (µs)	Residual stresses* (MPa)	$\frac{\text{Residual stress}}{\text{Yield stress}}$ (X)
1	60	4	4	2	217.5	0.36
2	60	4	8	4	81.74	0.14
3	60	4	16	6	65.31	0.11
4	60	6	4	2	462.9	0.77
5	60	6	8	4	281	0.47
6	60	6	16	6	95.15	0.16
7	60	8	4	4	1017	1.70
8	60	8	8	6	784.2	1.31
9	60	8	16	2	299.7	0.50
10	85	4	4	6	727.4	1.21
11	85	4	8	2	436.5	0.73
12	85	4	16	4	135.7	0.23
13	85	6	4	4	1327	2.21
14	85	6	8	6	1105	1.84
15	85	6	16	2	492.5	0.82
16	85	8	4	6	1482	2.47
17	**85**	**8**	**8**	**2**	**976.7**	**1.63**
18	85	8	16	4	757.4	1.26

*These values are the peak residual stresses induced in the wire

It was observed that the maximum value of residual stresses induced in the wire during certain machining conditions exceeds the yield point of the molybdenum wire (600 MPa). This causes a reduction in strength of the wire, which contributes to wire breakage due to temperature rise and stresses induced due to sparks. If the peak value of equivalent residual stresses exceeds the yield point of the wire only at a particular node of the developed numerical model, instantaneous rupture of the wire shall not occur. However, eventually when nodes over a large area exceed the yield point of the wire material, the breakage of wire may occur.

In order to determine the threshold value of wire strength above which the wire is considered to be unsafe due to high value of thermally induced stresses during the machining process, WEDM experiments were conducted on Ti-6Al-4V alloy with molybdenum wire (0.18 mm diameter) at different process conditions. Wire samples were collected for each experiment just after the sparks were produced between the wire and workpiece. The WEDM machine tool was not equipped with the facility to generate a single spark. The morphology of the machined wire samples were investigated with the help of field emission scanning electron microscope (FESEM). Figure 4.3 shows some collected FESEM wire images at different process parameters. It was observed that for the process condition of V = 85 V, I = 8 A, t_{on} = 8 µs, t_{off} = 2 µs in Table 4.2, a small micro crack was observed on the wire surface which has been shown in Figure 4.4.

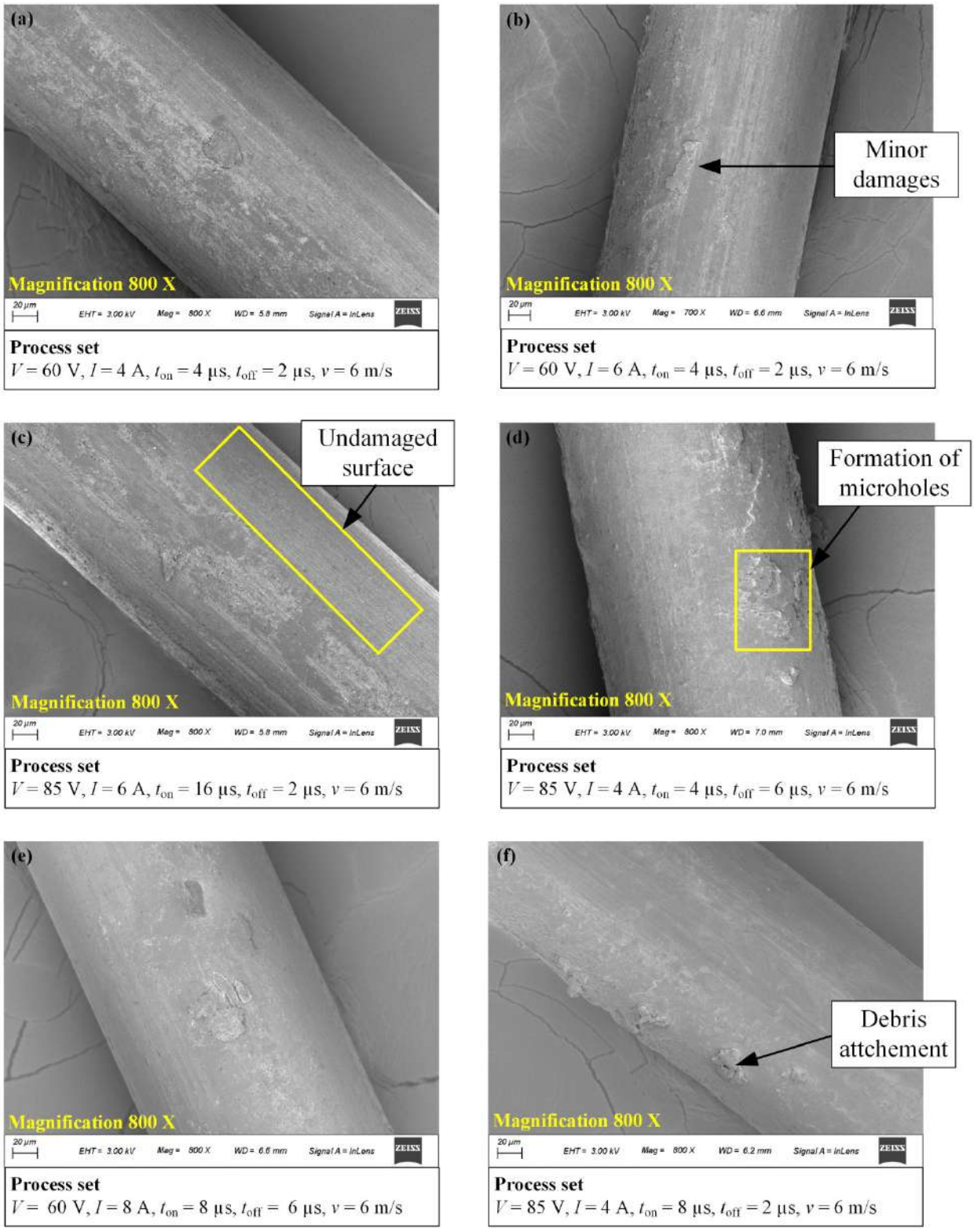

Figure 4.3 FESEM wire images at different sets of process parameters.

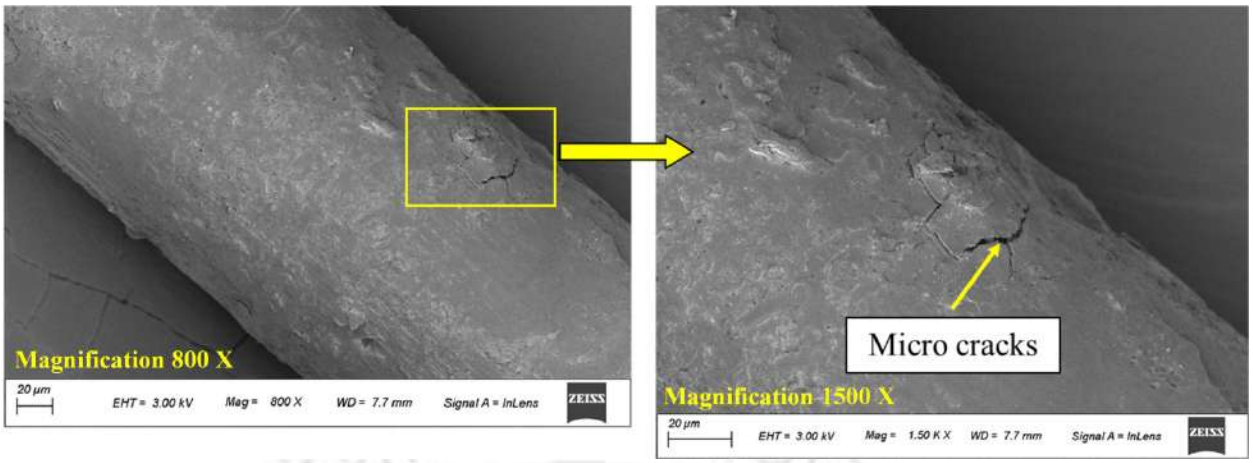

Figure 4.4 FESEM image of machined wire sample during WEDM at process condition : $V = 85$ V, $I = 8$ A, $t_{on} = 8$ µs, $t_{off} = 2$ µs, $v = 6$ m/s

The reason for micro cracks on the wire surface is the thermally induced stresses due to steep temperature gradients generated during the discharge phenomenon. High tensile residual stresses retained in the wire electrode due to rapid heating and cooling of wire surface initiate micro cracks. This might eventually cause propagation of deeper cracks leading to catastrophic failure of the wire. The corresponding X value (1.63) for this process set is considered as the threshold value beyond which the wire strength is not considered within the safe limit. Formation of microcracks on the wire surface is considered as an indicator of wire breakage to estimate the threshold value of wire strength beyond which the wire is considered to be unsafe for machining. Figure 4.5 depicts the approach for prediction and prohibition of wire breakage during WEDM operation based on the developed methodology. Residual stresses higher than the threshold limit might not cause instantaneous tool rupture but definitely increases the likelihood of failure.

The process conditions where the value of X is less than the threshold value are considered safe for the wire during machining as the thermally induced stresses are within the safe limits. However, when the peak values of equivalent residual stresses are very high, i.e., the values of X cross the safe boundary, the probability of wire rupture increases and measures are to be taken to prevent the wire failure and ensure better machining productivity. Thus, the developed numerical model can be used as a predictive tool in determining the wire strength based on the residual stresses induced in the wire electrode during the machining process.

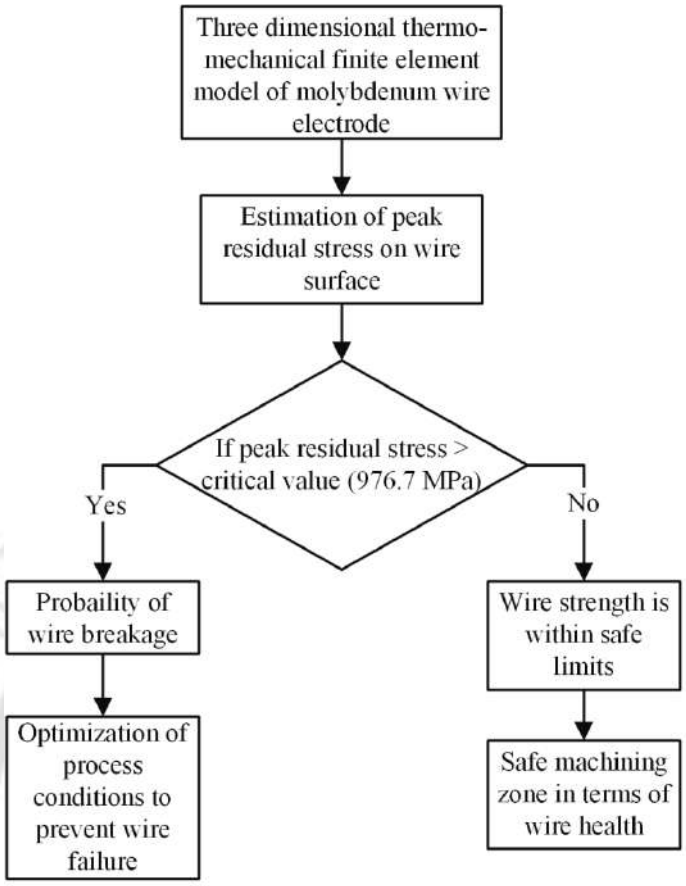

Figure 4.5 Approach for prediction and prohibition of wire failure

4.5 Parametric studies using the developed numerical model

Parametric studies were performed to investigate the effects of process parameters on the temperature obtained and the residual stresses induced in the wire during the discharge phenomenon.

4.5.1 Effects of process parameters on temperature generated in the wire

Figure 4.6 shows the effect of discharge voltage on temperature distribution with respect to time. It is observed that the temperature on the wire increases during the pulse on-time and reaches its peak at the end of the discharge duration. The temperature starts decreasing during the pulse off-time when no heat flux is applied. The temperature increases with an increase in discharge voltage due to increase in input power. The discharge energy increases with increase in discharge voltage, which causes rise in temperature in the wire tool. The peak temperature observes a sharp increase with increase in voltage.

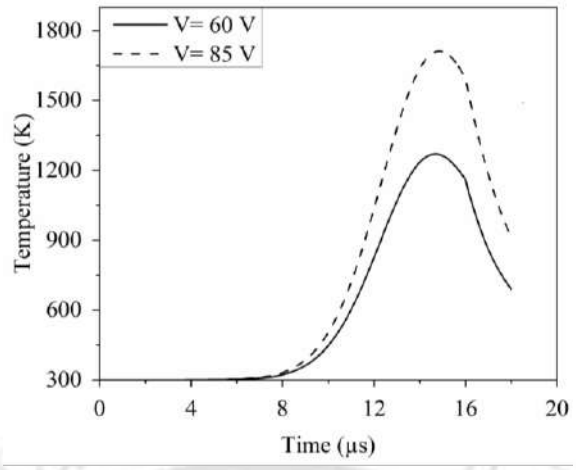

Figure 4.6 Effect of discharge voltage on temperature distribution (I = 6 A, t_{on} = 16 μs, t_{off} = 2 μs)

Figure 4.7 depicts that the temperature generated in the wire also observes an increasing trend with increasing discharge current. The temperature increases during the discharge duration and attains its peak at the end of pulse on-time (4 μs). The temperature starts decreasing gradually during the pulse off-time. The peak temperature obtained in the wire electrode after a single discharge increases with an increase in voltage and current due to the increase of input power. Increasing voltage and current increases the discharge energy in the interelectrode gap, which generates larger temperature gradients.

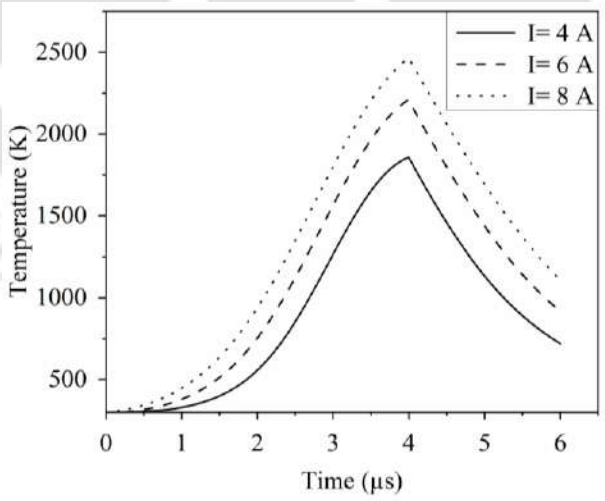

Figure 4.7 Effect of discharge current on temperature distribution (V = 60 V, t_{on} = 4 μs, t_{off} = 2 μs)

Figure 4.8 shows the effect of pulse on-time on the temperature achieved by the wire during a single discharge phenomenon, respectively. The peak temperature obtained in the wire electrode after a single discharge decreases with an increase in pulse on-time. This may be because the spark radius over which the heat flux is applied increases with an increase in pulse on-time (Equation 3.5); thus, the heat is dissipated over a larger area of the wire surface, thus reducing the peak temperature obtained in the wire. However, the thermally affected region increases with the increase in pulse on-time.

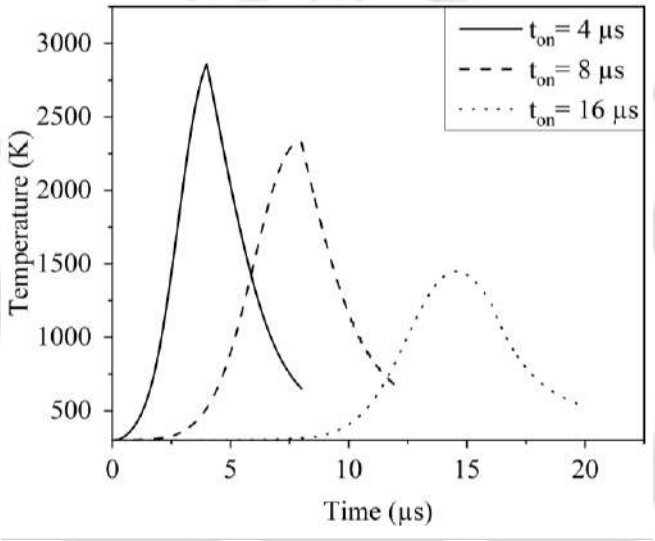

Figure 4.8 Effect of pulse on-time on temperature distribution (V = 85 V, I = 6 A, t_{off} = 4 µs)

The concept of moving heat source was incorporated in the model to consider the effect of wire velocity on the temperature profile obtained on the wire electrode. Figure 4.9 shows the effect of wire velocity on the temperature obtained by the wire. It is observed that the temperature on the wire decreases with the increase in wire velocity as the Gaussian heat flux traverses the wire surface at a higher speed. At lower wire velocities, the Gaussian heat source travels over the wire surface slowly causing localized temperature rise and increasing the peak temperature obtained by the wire. Lower wire speeds also cause localized material ablation from the wire surface. The peak temperature drops distinctively along with the increasing of wire velocity.

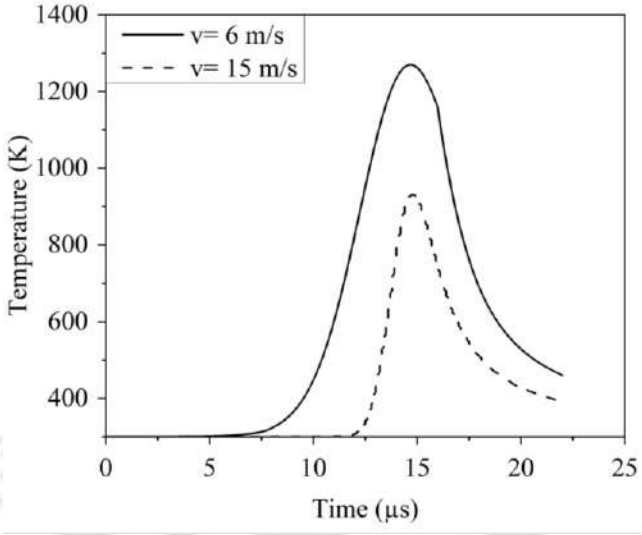

Figure 4.9 Effect of wire velocity on temperature distribution
(V = 60 V, I = 6 A, t_{on} = 16 μs, t_{off} = 6 μs)

4.5.2 Effects of process parameters on residual stresses induced in the wire

The residual stress distribution at the end of a pulse cycle along the wire axis was also plotted to study the effects of process conditions on the stresses retained in the wire. Figures 4.10 and 4.11 show the effect of voltage and current on the equivalent residual stress distribution obtained along the wire axis.

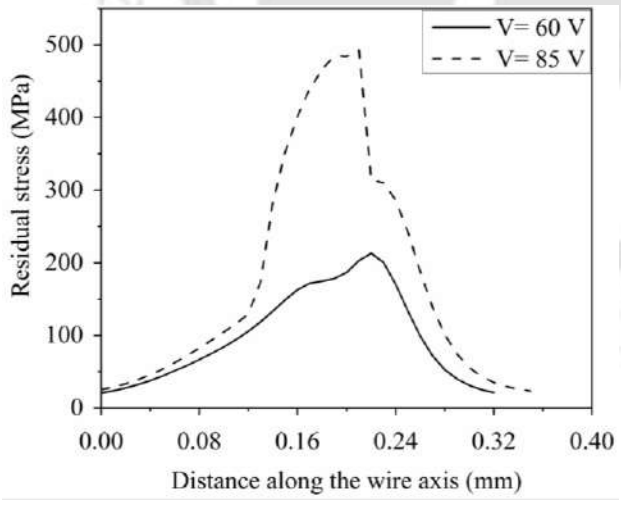

Figure 4.10 Effect of discharge voltage on residual stress distribution
(I = 6 A, t_{on} = 16 μs, t_{off} = 2 μs)

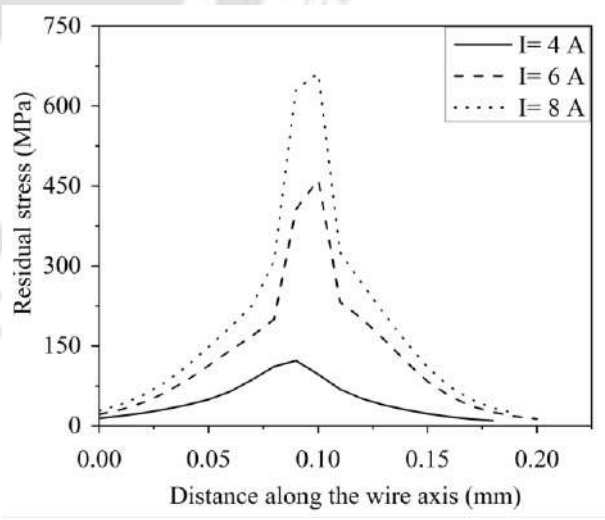

Figure 4.11 Effect of discharge current on residual stress distribution
(V = 60 V, t_{on} = 4 μs, t_{off} = 2 μs)

It was observed that residual stresses on the wire electrode increase with an increase in voltage and current due to an increase in input power. The equivalent residual stresses along the wire axis first increases and decreases during the cooling period. These stresses are produced on the wire surface. Residual stresses are also generated beneath the wire surface and in certain cases obtain a peak value underneath the surface. The peak value of residual stresses also increases distinctively with input power as an increase in peak temperature causes an increase in thermal stresses in the heated region. Higher input current might cause the formation of deeper cracks in the wire thus reducing the strength of the wire and increasing the probability for wire breakage. Further, it can be observed from Figures 4.10 and 4.11 that the residual stress profile is independent of the input power.

4.6 Summary

In this chapter, a simple and novel method has been developed, which computes the wire safety index based on the residual stresses generated on the molybdenum wire electrode surface. The merit of the developed method lies in the use of a three-dimensional thermo-mechanical nonlinear numerical model to compute the wire strength based on the stresses generated during machining.

If the equivalent residual stresses produced in the wire during the discharge phenomenon is well below the yield strength of the wire, the wire is said to be within the safe limit. As the residual stress values cross the yield point, the strength of the wire starts deteriorating which is harmful to the health of the wire. Experimental studies found that the microcracks initiate on the surface, when the peak residual stress achieved by the molybdenum wire exceeds the value of 976.7 MPa. The corresponding X value of 1.63 can be considered as a critical value to determine the safe zone of machining in terms of wire health. Overall, it can be concluded that the proposed methodology to compute the wire safety index eliminates the need of costly, time-consuming and tedious experiments. By using the developed method, one can easily predict the deterioration of wire electrode, which will ensure uninterrupted and efficient wire electric discharge machining operation. The thermo mechanical analysis also showed that the peak temperature and the peak value of residual stresses achieved by the wire increase with voltage and current levels. However,

peak temperature decreases with the increase in pulse on-time but increases the thermally affected region.

Successive and random multiple discharges during WEDM operation cause wire erosion due to excessive material ablation from the wire surface. The following chapter presents a comprehensive experimental analysis on the erosion and deformation of a molybdenum wire tool during metal cutting operation. It is imperative to have a deeper understanding of the wire erosion and breakage phenomenon in order to predict and prevent wire failure. The eroded wire samples are collected after WEDM machining of Ti-6Al-4V alloy and analyzed carefully for wire damages, which have been illustrated in the next chapter.

CHAPTER 5

Experimental measurement and analysis of molybdenum wire erosion and deformation during wire electric discharge machining of Ti-6Al-4V alloy

5.0 Scope

This chapter presents a detailed experimental investigation of wire erosion and deformation during WEDM experiments on Ti-6Al-4V alloy. Firstly, the need to investigate the wire damages during spark discharges in order to achieve improved wire health is presented. The overall experimental procedure is elaborated followed by experimental setup and methods. The measurement and analysis techniques of the performance responses have been explained in a detailed manner. An in-depth discussion on various wire damages and deformation during the discharge phenomenon has been demonstrated. Moreover, the influence of different process conditions on wire erosion and on the surface quality achieved by the component has been investigated. Finally, the chapter is summarized with conclusions.

5.1 The need

Sharp temperature gradients produced during the WEDM discharge phenomenon cause material removal from both the wire electrode and workpiece. Although material removal from the workpiece is desirable to achieve the required shape and contour, wire erosion and damage are detrimental to the overall machining process. With growing demands of manufacturing sector, wire wear and breakage act as major challenges during WEDM cutting. Wire wear reduces the wire strength and eventually causes the wire to fail, which is a major limitation of wire EDM. This undesirable situation hampers the overall output of the system causing surface damage to the component, increase in energy consumption, loss of machining time, and resources. Several factors, including the machining conditions, wire material properties, and wire geometry, influence the wire wear and damage. Temperature rise during the repetitive spark discharges is the most critical factor responsible for wire erosion and failure (Dekeyser et al. (1988)). The wire starts eroding when the temperature gradients exceed the melting point of the wire material. The damages undergone by the wire also have a notable effect on the surface quality achieved by the workpiece during machining. Thus, it is of utmost importance to analyze the wire erosion and investigate its

detrimental influence on workpiece surface quality in order to achieve uninterrupted and efficient machining.

An in-depth understanding of the wire erosion mechanism shall give a proper insight into the wire breakage phenomenon; thus predicting and preventing untimely wire failure. Although the monitoring systems and numerical models presented in chapter 2 are quite useful in the prediction of wire behavior, however, limited studies have been conducted so far which explains the erosion and failure mechanism of the wire electrode during machining (Pramanik and Basak (2016), Pramanik and Basak (2018)). Thus, this chapter reports an extensive experimental investigation on the erosion and damages of the molybdenum wire electrode after WEDM of industrially important Ti-6Al-4V alloy. Moreover, the existing literature reports suggest that the morphology of molybdenum wire used in WEDM machines has not been studied earlier. The findings presented in this chapter extend the existing area of knowledge in this field and aid in achieving stable machining without wire breakage.

5.2 Overall experimental methodology

Figure 5.1 represents the overall experimental methodology, measurement and analysis process that was followed during the current study. The present work mainly focuses on analyzing the erosion and damages undergone by the wire electrode during WEDM process and its influence on workpiece surface quality in order to overcome the drawbacks of wire wear and failure. The detrimental influence of wire wear on workpiece surface roughness is explained in detail in the next chapter. A series of WEDM experiments of Ti-6Al-4V alloy was carried out on the wire EDM machine (MAKE JK MACHINES, MODEL EC032). Ti-6Al-4V or Titanium Grade 5 alloy is an important industrial metal. It has excellent strength, high resistance to corrosion and fatigue, and large strength to mass ratio. Molybdenum wire (99 % purity) with a diameter of 0.18 mm is considered as the tool electrode. The machining parameters were chosen based on previous literature and after carrying out trial experiments based on the facilities available in the workshop. The levels of input parameters used are presented in Table 5.1. A total of 36 experiments according to the Taguchi L36 array were carried out and each experiment was repeated thrice. Corner cutting experiments were performed on a 60 × 60 × 12 mm^3 Ti-6Al-4V plate and wire samples were collected after every three cuts for a single process set. The measurement of deformed wire cross section

diameters and analysis of wire surface damages after the cutting operation were performed with the help of optical microscope, Field emission scanning electron microscope (FESEM) and Energy-Dispersive X-ray spectroscopy system (EDX). The eroded wire samples were further examined to evaluate the effects of different machining parameters on wire wear and damages. The surface roughness values (*Ra*) of machined samples were measured using a non-contact optical profilometer. The influence of machining conditions on workpiece *Ra* was evaluated using analysis of variance (ANOVA) technique.

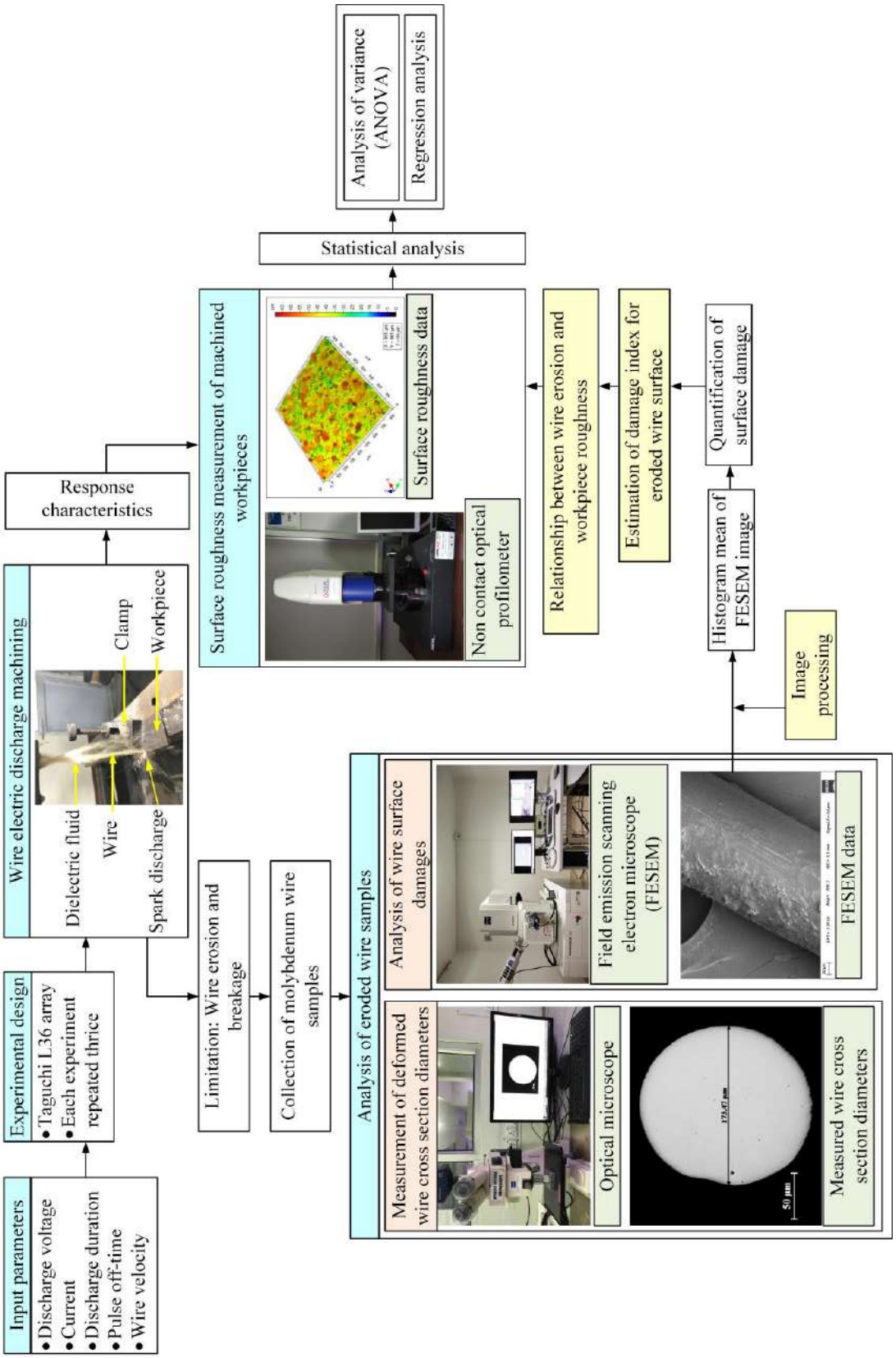

Figure 5.1 Overall measurement and analysis methodology

Table 5.1 Selected levels of input parameters

Parameters	Level 1	Level 2	Level 3
Discharge voltage (V)	60	85	-
Discharge current (A)	4	6	8
Pulse on-time (μs)	4	8	16
Pulse off-time (μs)	2	4	6
Wire velocity (m/s)	3	6	9

5.3 Experimental setup and methods

This section describes the experimental setup used to carry out the WEDM experiments and the measurement techniques used to study the damages on the wire surface. The surface roughness of the workpiece samples were also measured using an optical profilometer. Each of the methods has been explained below in a detailed manner.

5.3.1 Wire electric discharge machining (WEDM) setup

WEDM experiments on Ti-6Al-4V alloy were carried out by using a wire EDM machine (MAKE JK MACHINES, MODEL EC032). The photograph of the experimental setup is shown in Figure 5.2. Deionized water is used as the dielectric fluid during the experiments. The specifications of the WEDM setup are listed in Appendix A5.1.

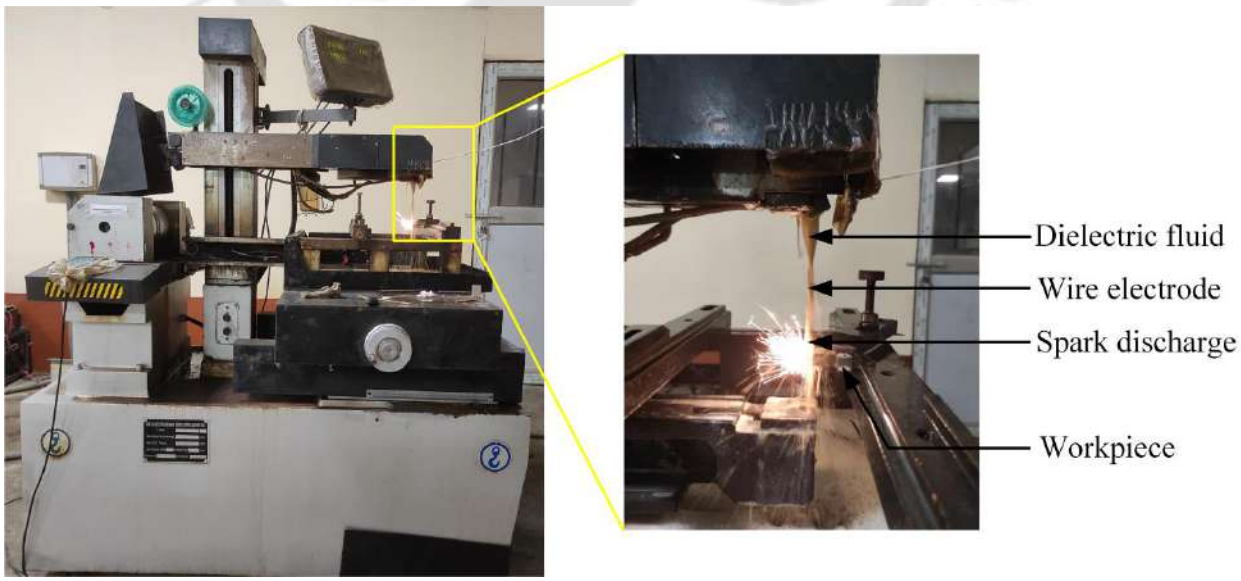

Figure 5.2 Wire electric discharge machine

5.3.2 Analysis of wire wear using field emission scanning electron microscope (FESEM)

The surface damages of eroded wires were examined with the help of field emission scanning electron microscope (FESEM) integrated with energy-dispersive X-ray spectroscopy system (EDX). Figure 5.3 shows the methodology of FESEM analysis. FESEM uses a focused beam of electrons to generate an image or to analyze the specimen. Eroded wire sections were collected after every experiment and prepared for FESEM analysis. In the first stage, the samples were made conductive for current for the FESEM analysis. For this purpose, the wire samples were coated with a thin layer of gold of thickness in the range of 1.5 – 3.0 nm. The coating thickness depends on type of sample (organic, conducting etc.) used. The sample was fixed to a stub of size 10 mm using carbon tape for continuous conduction of electrons. The samples were single coated for 60 s duration. The images were obtained using SmartSEM software.

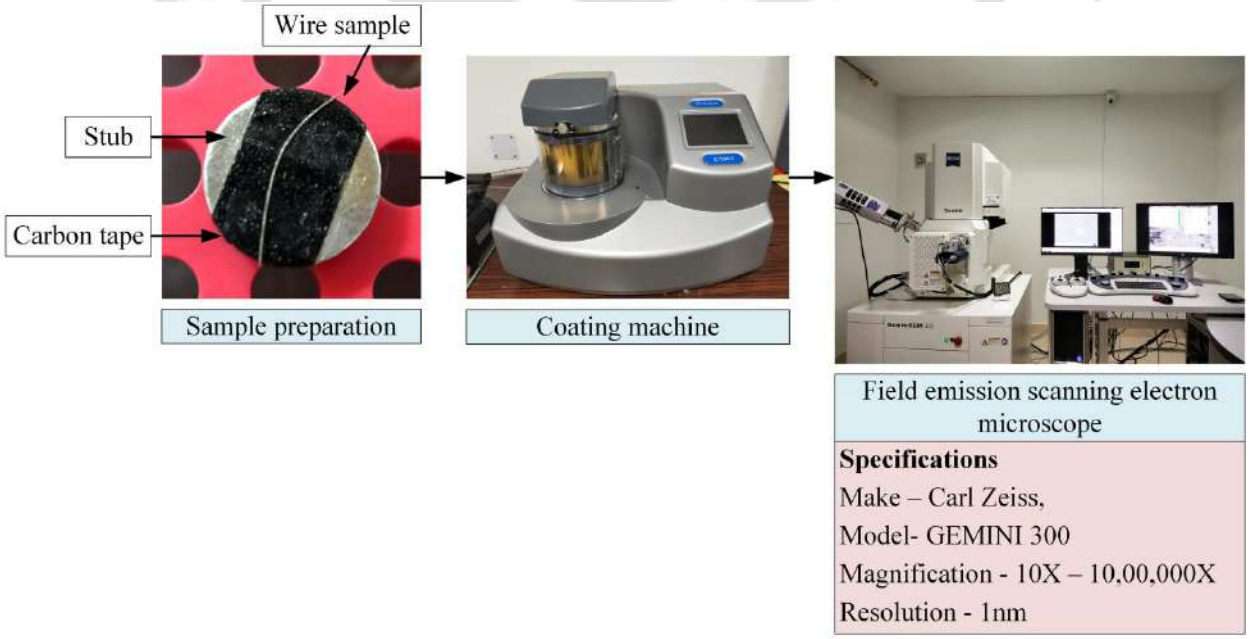

Figure 5.3 Analysis of wire surface erosion using field emission scanning electron microscope (FESEM)

5.3.3 Analysis of wire deformation using optical microscope

Wire samples were collected after every experimental set and cross-section samples of the wire were prepared using a standard method. The measurement procedure comprises of vertically mounting the wire samples in resin, and then polishing on emery papers with sizes

P220, P400, P800, P1000, P1500, P2000 and P2500 in a polishing machine. It is followed by final polishing of the samples on a velvet cloth with 0.3 μm size alumina solution. The wire cross-sections were mirror polished and observed under the optical microscope to determine the change in wire shape and size after the cutting process. Figure 5.4 shows the step-by-step measurement methodology of analyzing the wire cross sections after the machining process. Etching of the wire cross section samples was performed to observe the grain structure of the molybdenum wire material. Etching of the polished wire samples was performed with standard Murakami reagent for molybdenum (1 g KOH: 1g $K_3Fe(CN)_6$: 10 ml H_2O). The sample was swabbed with the etchant using a cotton bud and the etching time was kept at 5 seconds.

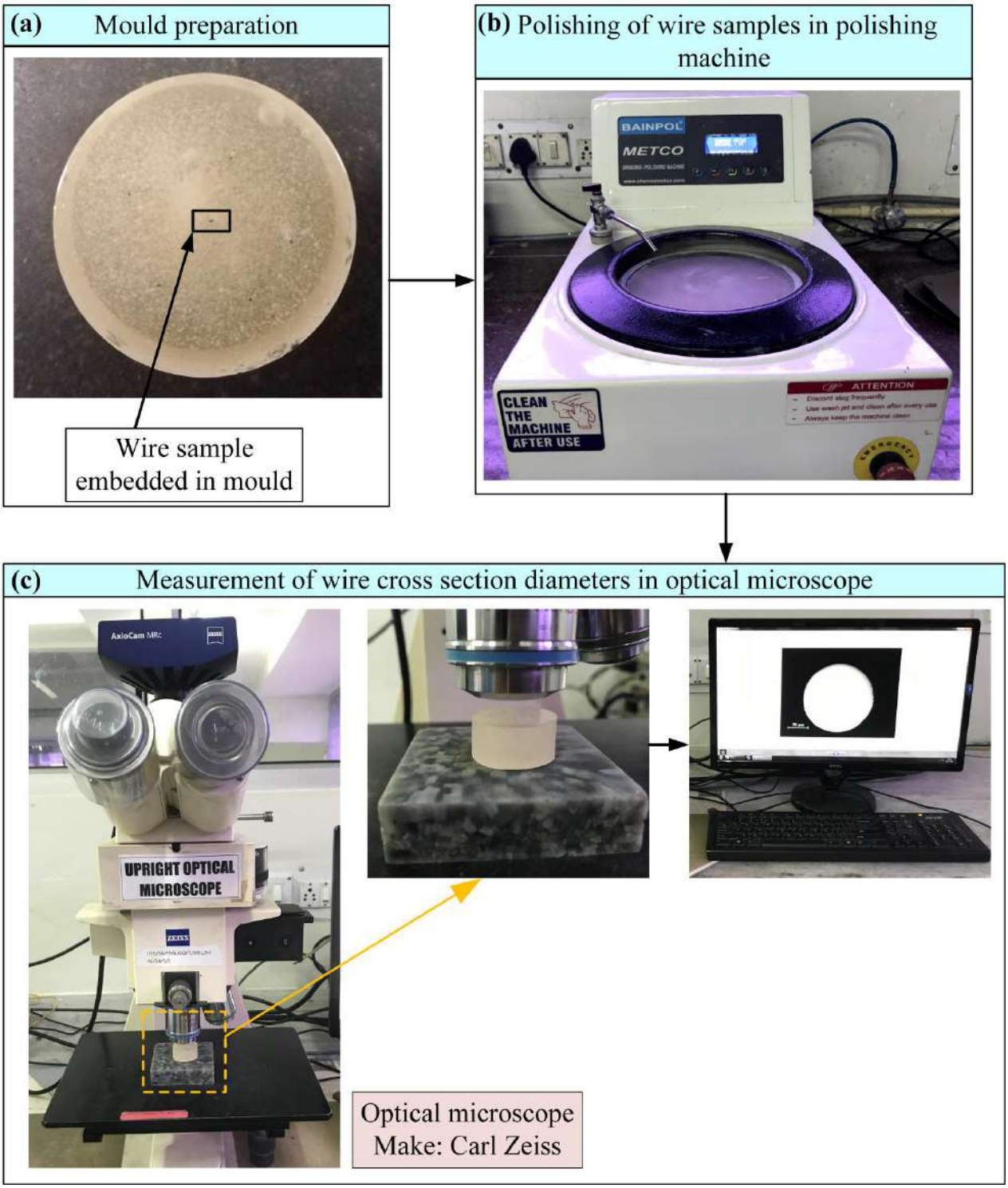

Figure 5.4 Measurement methodology of deformed wire cross section diameters

5.3.4 Measurement of workpiece surface roughness using optical profilometer

The surface *Ra* of machined components after every single cut was measured using a non-contact optical profilometer. Figure 5.5 depicts the measurement methodology of *Ra* of machined components using the optical profilometer. It is a non-contact type, high precision white light interference microscope with an objective lens of 20X magnification and focal distance of 4.7 mm. The head of the profilometer consisting the objective lens was moved along the z-axis until the light is focused on the workpiece surface. The *Ra* values were obtained using the 3-D analysis software TalyMap. Surface roughness measurements were carried out at five different locations for a single workpiece, and the average value was considered for further analysis.

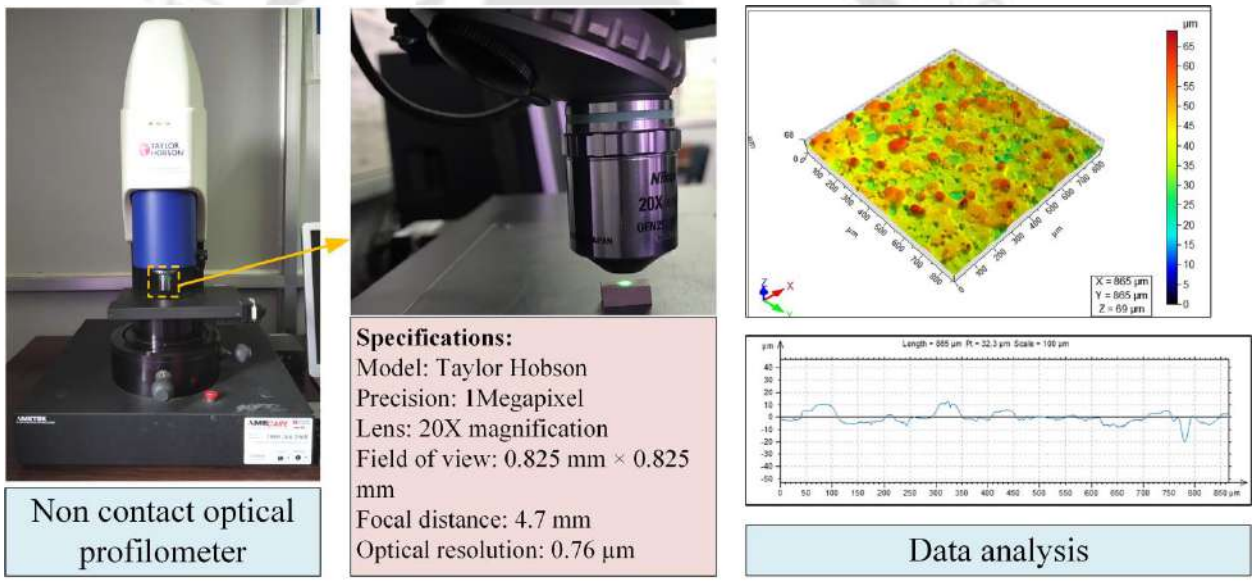

Figure 5.5 Measurement methodology of surface roughness of machined components

5.4 Measurement and analysis of experimental results

5.4.1 Study of erosion on the molybdenum wire surface

Figure 5.6 shows the FESEM image of an unused molybdenum wire before machining. EDX analysis (Figure 5.7a) and elemental mapping (Figure 5.7 (b–g)) of an eroded wire sample show that workpiece material also adheres to the wire surface. This is because of the spattering of molten workpiece material on the wire surface due to extreme temperature rise. The mapping scan analysis of the eroded wire sample shows the distribution of parent wire

material and attached workpiece material on the wire surface during machining. EDX analysis further shows the presence of carbon (C) in the spectra, which is due to the use of carbon tape during the preparation of samples for the analysis.

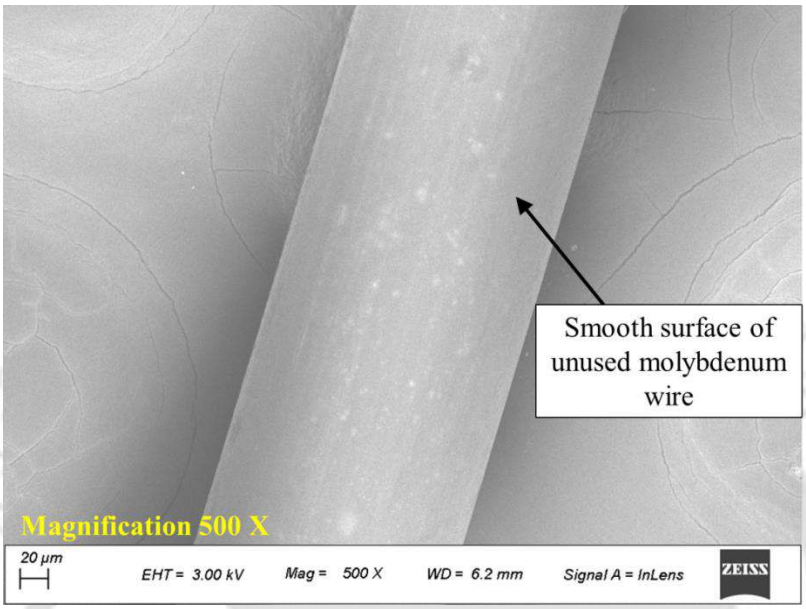

Figure 5.6 FESEM image of unused molybdenum wire

An increase in wire temperature, interaction with the dielectric, generation of debris in the machining zone, and the formation of undesired sparks degrade the surface integrity of the wire. The machining debris is attached to the wire surface due to insufficient flushing time and improper flushing pressure (Figures 5.8a, 5.8b). It decreases the interelectrode gap, which may cause undesired arc formation resulting in abrupt temperature rise. Thus, the wire gets subjected to violent thermal shock leading to surface degradation in the form of craters, pits, microholes, and microcracks. In certain conditions, the material eroded during the discharge duration is resolidified and redeposited on the wire surface due to sudden cooling by the continuously flowing dielectric and insufficient flushing pressure (Figure 5.8c). At lower pulse off-times, when the discharges occur at short intervals, the accumulated debris is not washed away due to insufficient flushing time. Instead, the melted material forms a pool of resolidified material and deposits on the wire surface. In certain regions, the splashing of the melted material on the wire surface was also observed, as shown in Figures 5.8d, 5.8e.

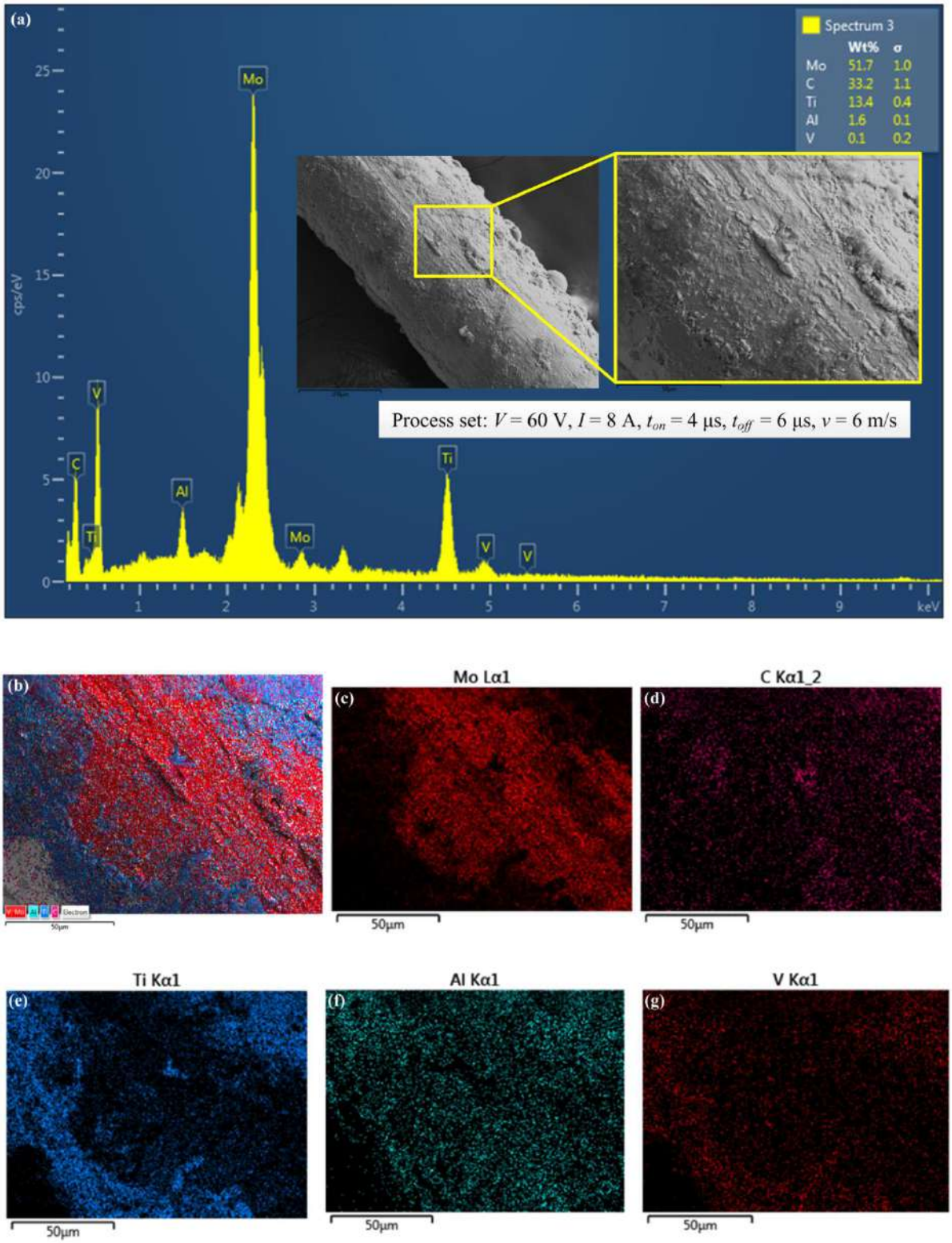

Figure 5.7 (a) EDX analysis and (b), (c), (d), (e), (f), (g) Elemental mapping of an eroded wire sample for the process set: $V = 60$ V, $I = 8$ A, $t_{on} = 4$ µs, $t_{off} = 6$ µs, $v = 6$ m/s

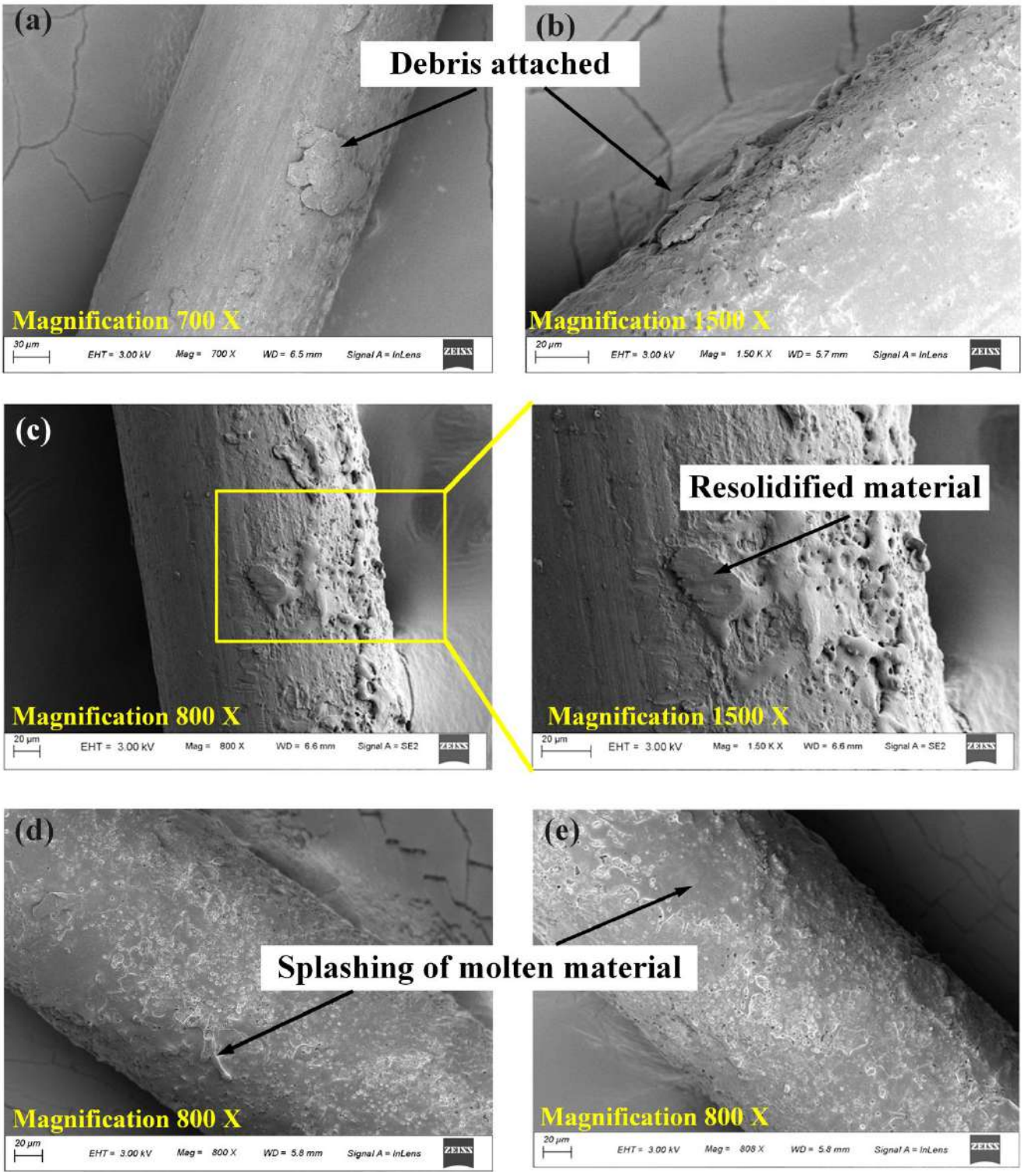

Figure 5.8 (a), (b) sticking of debris, (c) resolidified material and (d), (e) splashing of molten material on eroded wire surfaces

5.4.2 Measurement of deformed wire cross section diameters

The optical images of the cross-sections of unused molybdenum wire before and after the etching process are obtained. The unused wire is circular with a diameter of approximately 180 μm (Figure 5.9a). A uniform grain structure with very minute grains was observed after etching the polished wire sample, which appears to be a result of the wire drawing process during wire manufacturing (Figure 5.9b). The cross-sections of the eroded wire samples were prepared at various sections along the wire length and examined under the optical microscope to investigate the deterioration in wire form as the machining proceeds. Figures 5.9 (c–h) shows the cross sections of eroded wire samples at different sections for the process condition: V = 85 V, I = 4 A, t_{on} = 16 μs, t_{off} = 4 μs, v = 6 m/s. It was observed that the wire cross section loses its circularity and undergoes deformation during machining in two major steps, (i) an increase in wire diameter on one side at initial stage of machining and, (ii) decrease in wire diameter than the original diameter on both sides of the wire cross section as the machining proceeds. The wire suffers severe plastic degradation because of the steep temperature slope generated during the discharge phenomenon. The reason behind the change in wire shape can be attributed to a combined effect of (a) temperature rise, (b) plastic deformation when stresses originated crosses the yield point of the wire material, (c) mechanical tension applied to the wire to keep it vertically straight and (d) continuous movement of the wire electrode. This causes geometrical inaccuracy and precision error of the machined components. It further diminishes the surface quality and integrity of the products.

Minor deformation of the wire periphery starts at the initiation of sparks due to sudden temperature rise and thermal shock. As the complete diameter of the wire is inside the generated slot, sparks occur from all the sides pressing the wire as it traverses forward through the workpiece. The majority of wire damage takes place in this region, and the wire loses its original circular shape. At this stage, the wire diameter increases than the original diameter on one side and decreases on the other side (Figures 5.9c and 5.9d). Temperature rise during machining has a direct effect on the crystal structure of molybdenum, making the pattern of arrangement of atoms more regular. It reduces the number of grain boundaries, thus making the material more soft and malleable. The malleability of the molybdenum wire increases with temperature, which causes the material to flow downward, thus increasing the

diameter of the wire. The wire diameter also increases due to the sticking of debris onto the wire surface caused due to inefficient flushing and spattering of molten material. As the wire proceeds further along the feed direction, a steady decrease of wire diameter was observed due to the melting and vaporization of wire material above the melting point (Figure 5.9e). The diameters on both sides of the wire cross-sections are found to be unequal and become smaller than the original one (Figures 5.9f, 5.9g, 5.9h). It reduces the overall cross-sectional area of the wire, thus increasing the stress in the wire cross-section. Temperature rise further causes the generation of thermal stresses in the wire electrode, which diminishes its strength.

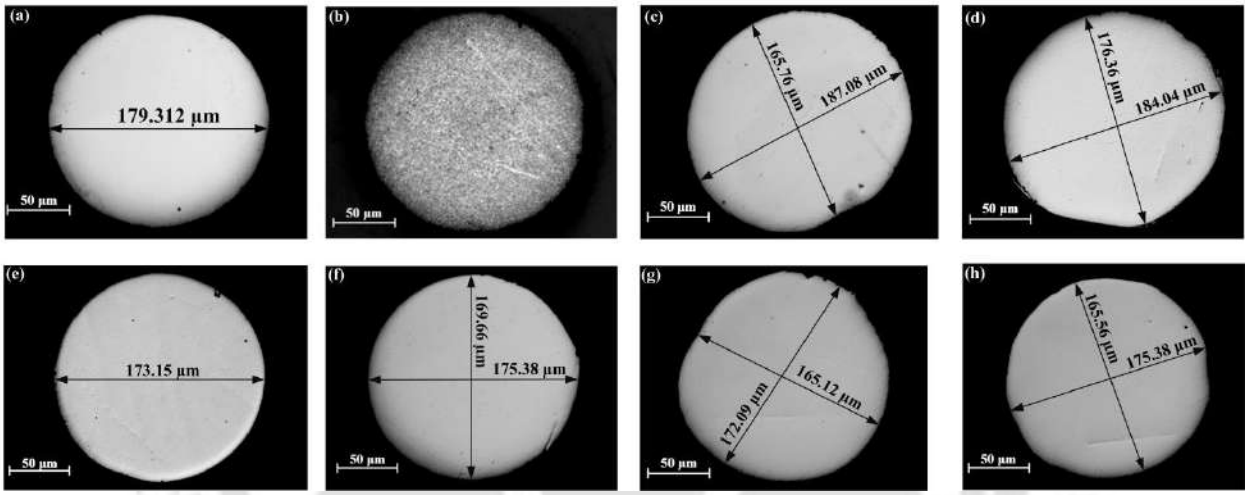

Figure 5.9 (a) unetched and (b) etched cross-sections of unused molybdenum wire, (c), (d), (e), (f), (g), (h) Deformed wire cross-sections with unequal diameters for the process set: $V = 85$ V, $I = 4$ A, $t_{on} = 16$ µs, $t_{off} = 4$ µs, $v = 6$ m/s

5.4.3 Measurement and analysis of surface roughness of machined workpieces

The surface roughness of the workpiece samples were measured using a non-contact optical profilometer. Three samples were cut for every process set and the *Ra* value was evaluated for every single workpiece. The measurements were carried out at five different locations for a single sample and the average value was considered for further analysis as listed in Table 5.2. Here, Ra_1, Ra_2 and Ra_3 indicate the surface roughness after 1st cut, 2nd cut and 3rd cut respectively. The blank spaces in the table indicate wire breakage.

Table 5.2 Surface roughness values (*Ra*) of workpieces measured after the experimental sets

Serial no.	Discharge voltage (V)	Discharge current (A)	Pulse on-time (µs)	Pulse off-time (µs)	Wire speed (m/s)	Surface roughness (µm)			
						Ra_1	Ra_2	Ra_3	Avg.
1	60	4	4	2	3	2.25	2.49	2.88	2.54
2	60	6	8	4	6	2.01	2.23	2.81	2.35
3	60	8	16	6	9	2.11	2.24	2.79	2.38
4	60	4	4	2	6	1.88	2.01	2.53	2.14
5	60	6	8	4	9	1.97	2.2	2.64	2.27
6	60	8	16	6	3	2.61	2.75	3.1	2.82
7	60	4	8	6	3	2.18	2.33	2.9	2.47
8	60	6	16	2	6	2.62	2.77	3.07	2.82
9	60	8	4	4	9	1.94	2.15	2.54	2.21
10	60	4	16	4	3	2.6	2.7	3.13	2.81
11	60	6	4	6	6	1.9	2.05	2.56	2.17
12	60	8	8	2	9	2.27	2.5	3.15	2.64
13	60	6	16	2	9	2.24	2.45	2.9	2.53
14	60	8	4	4	3	2.49	2.66	3.07	2.74
15	60	4	8	6	6	1.83	1.98	2.37	2.06
16	60	6	16	4	3	2.67	2.87	3.07	2.87
17	60	8	4	6	6	1.98	2.2	2.63	2.27
18	60	4	8	2	9	1.87	2.22	2.24	2.11
19	85	6	4	6	9	1.93	2.26	2.41	2.2
20	85	8	8	2	3	2.83	2.98	3.37	3.06
21	85	4	16	4	6	2.18	2.31	2.86	2.45
22	85	6	8	6	9	1.86	1.99	2.48	2.11
23	85	8	16	2	3	3.11	3.23	-	3.17
24	85	4	4	4	6	1.89	2.23	2.3	2.14
25	85	8	8	2	6	2.79	2.91	3.09	2.93

26	85	4	16	4	9	1.97	2.19	2.5	2.22
27	85	6	4	6	3	2.23	2.34	2.93	2.5
28	85	8	8	4	6	2.76	-	-	2.76
29	85	4	16	6	9	1.9	2.19	2.45	2.18
30	85	6	4	2	3	2.79	2.91	3.09	2.93
31	85	8	16	6	6	2.36	2.5	3.21	2.69
32	85	4	4	2	9	1.76	1.89	2.41	2.02
33	85	6	8	4	3	2.39	2.89	2.91	2.73
34	85	8	4	4	9	2.17	2.49	2.69	2.45
35	85	4	8	6	3	2.23	2.5	2.86	2.53
36	85	6	16	2	6	2.78	2.9	3.11	2.93

The experimentally obtained results are analyzed using response surface methodology (RSM) which is a well-known mathematical and statistical procedure to correlate input parameters with the response variables. Analysis of variance (ANOVA) was performed to analyze the contribution of each factor and the interaction terms on the selected response variable, i.e. *Ra* of the workpiece. This was followed by a quadratic regression analysis equation depending on the significant factors, which could predict the surface *Ra* value at any set of process conditions. The important statistical terms in ANOVA analysis are described as follows.

- ***F* value**: The *F* value is used to determine whether the test is statistically significant. Statistically significant results mean that the results likely did not occur by chance.
- ***P* value**: The *P* value determines whether a parameter's effect is significant or not. Usually, a significance level of 0.05 is considered for ANOVA analysis. If the *P* value is less than 0.05, then the source parameter is considered to have a significant effect on the response variable. If the *P* value is greater than 0.05, then the parameter is deemed insignificant.
- $\boldsymbol{R^2}$: R^2 is called the coefficient of determination. R^2 is a statistical measure that gives the variation of a dependent variable based on the independent variable(s) in a regression model. The value of R^2 ranges from 0 to 1 and are commonly denoted in percentages from 0 to 100 %. The predicted model is considered significant if the R^2 value is greater than 75 %. The *adjusted*-R^2 compares the descriptive power of regression models that

include several independent variables. Every term added to a model increases R^2 and never decreases it. Thus, the *adjusted*-R^2 compensates for the addition of new independent variables and only increases if the new term enhances the model more than what would be obtained by probability. Another term used in ANOVA is the *predicted*-R^2. It decides how well the model can predict response variables for any new observation.

Table 5.3 shows the ANOVA table with surface *Ra* as the response characteristic using backward elimination. The columns in the table indicate the source parameters, the degrees of freedom (DF), adjusted sum of squares (Adj SS), adjusted mean sum of squares (Adj MS), F value (Adj MS/ MS error) and Probability (P) value. The interaction terms in table 5.3 represent the significant terms that affect the response variable (workpiece *Ra*) variation. For solving real life complex problems, second order models are generally used. They are flexible and can estimate the coefficients easily by the method of least squares. The insignificant terms were eliminated by backward elimination procedure. The source parameters and their interaction terms whose P value are less than 0.05 have a noteworthy impact on the response variable. It was observed from Table 5.3 that current and pulse duration have the most noted contribution towards the response variable variation. The insignificant terms were eliminated by backward elimination procedure.

The combined effect of the terms $t_{on} \cdot t_{on}$, $t_{off} \cdot t_{off}$, $v \cdot v$, $I \cdot t_{on}$, $I \cdot t_{off}$, $I \cdot v$, $t_{on} \cdot t_{off}$ depicted important contribution. Pulse off-time (t_{off}) has no significant contribution towards *Ra* values. The quadratic effect of t_{off} was found to be significant; thus the linear term was also considered in the ANOVA table. R^2 is the coefficient of determination and gives a measure of the closeness of the experimentally obtained values to the fitted regression line. The R^2, *adjusted*-R^2 and *predicted*-R^2 values for the *Ra* values were found to be 0.9810, 0.9711 and 0.9559 respectively. The predicted model is considered to be sensitive if R^2 is greater than 0.75. It is further observed that the predicted R^2 is in close agreement with adjusted R^2, which indicates that the model is able to predict a new response for any observation with 95.59 % variability.

Table 5.3 ANOVA table for surface roughness after backward elimination

Source	DF	Adj SS	Adj MS	F-Value	P-Value
V (V)	1	0.17943	0.17943	62.05	0.000
I (A)	1	1.11447	1.11447	385.44	0.000
t_{on} (μs)	1	1.47138	1.47138	508.87	0.000
t_{off} (μs)	1	0.01213	0.01213	4.19	0.052
v (m/s)	1	0.44010	0.44010	152.21	0.000
t_{on} (μs) · t_{on} (μs)	1	0.01949	0.01949	6.74	0.016
t_{off} (μs) · t_{off} (μs)	1	0.01186	0.01186	4.10	0.05
v (m/s) · v (m/s)	1	0.02234	0.02234	7.73	0.011
I (A) · t_{on} (μs)	1	0.02374	0.02374	8.21	0.009
I (A) · t_{off} (μs)	1	0.01244	0.01244	4.30	0.049
I (A) · v (m/s)	1	0.10945	0.10945	37.85	0.000
t_{on} (μs) · t_{off} (μs)	1	0.01787	0.01787	6.18	0.021
Error	23	0.06650	0.00289		
Total	35	3.50110			

The correlation between the significant input factors and their quadratic factors with the response variable (Ra) was obtained using a polynomial equation after discarding the non-significant terms. The regression equation derived for Ra in terms of linear and interaction factor is as follows.

$$Ra = 2.499 + 0.006231\,V + 0.0212\,I + 0.0988\,t_{on} - 0.1324\,t_{off} - 0.2505\,v - 0.001888\,t_{on}\cdot t_{on} + 0.01136\,t_{off}\cdot t_{off} + 0.00608\,v\cdot v - 0.00418\,I\cdot t_{on} + 0.01015\,I\cdot t_{off} + 0.01492\,I\cdot v - 0.00309\,t_{on}\cdot t_{off} \quad (5.1)$$

5.5 Parametric studies

5.5.1 Effects of process parameters on wire surface wear

At higher discharge energy settings, the erosive nature of the sparks causes the formation of craters, microholes, globules, and pits on the wire surface. Successive and random discharges raise the temperature as high as 10000º C or more due to the high plasma energy of the spark, which removes material from both the electrodes. The discharge energy increases along with

increasing voltage, current and discharge duration causing critical damage on the wire surface. The damages on the wire surface are minor at low levels of current due to low discharge energy (Figure 5.10a). At higher current levels, craters approximately of the size of 20 µm are formed on the wire surface (Figure 5.10b). It was further noted that wire wear occurs at about half of the wire circumference. Longer pulse duration produces heat flux for a longer time causing severe erosion from the wire electrode due to excessive temperature rise. The thermally affected region due to spark formation is more significant at higher pulse durations, as shown in Figure 5.11c. It increases the generation of debris and unwanted arcs in the machining zone, which degrades wire quality and increases the probability of wire failure. During the spark discharge duration, the dielectric fluid vaporizes and forms a high-pressure bubble. The bubble suddenly collapses as the pulse energy ends. The dielectric flushes the molten material from the machining zone. However, due to inefficient flushing at lower pulse off-times, all the melted debris is not washed away and resolidifies on the wire surface. During this process, some gas bubbles are entrapped in the resolidified region, causing the formation of microholes or micro pits on the wire surface (Figure 5.12).

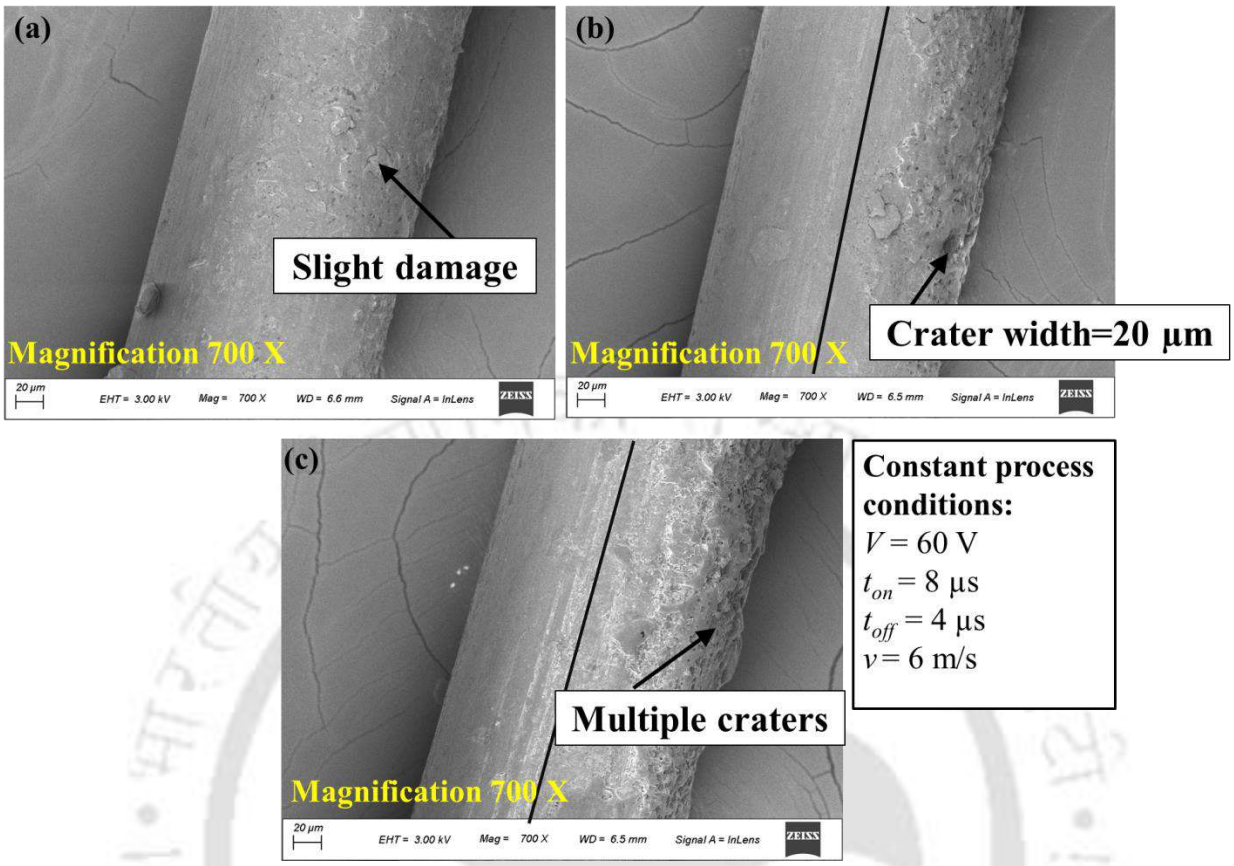

Figure 5.10 FESEM wire images after WEDM of Ti-6Al-4V at varying current settings: (a) 4 A, (b) 6A, (c) 8 A

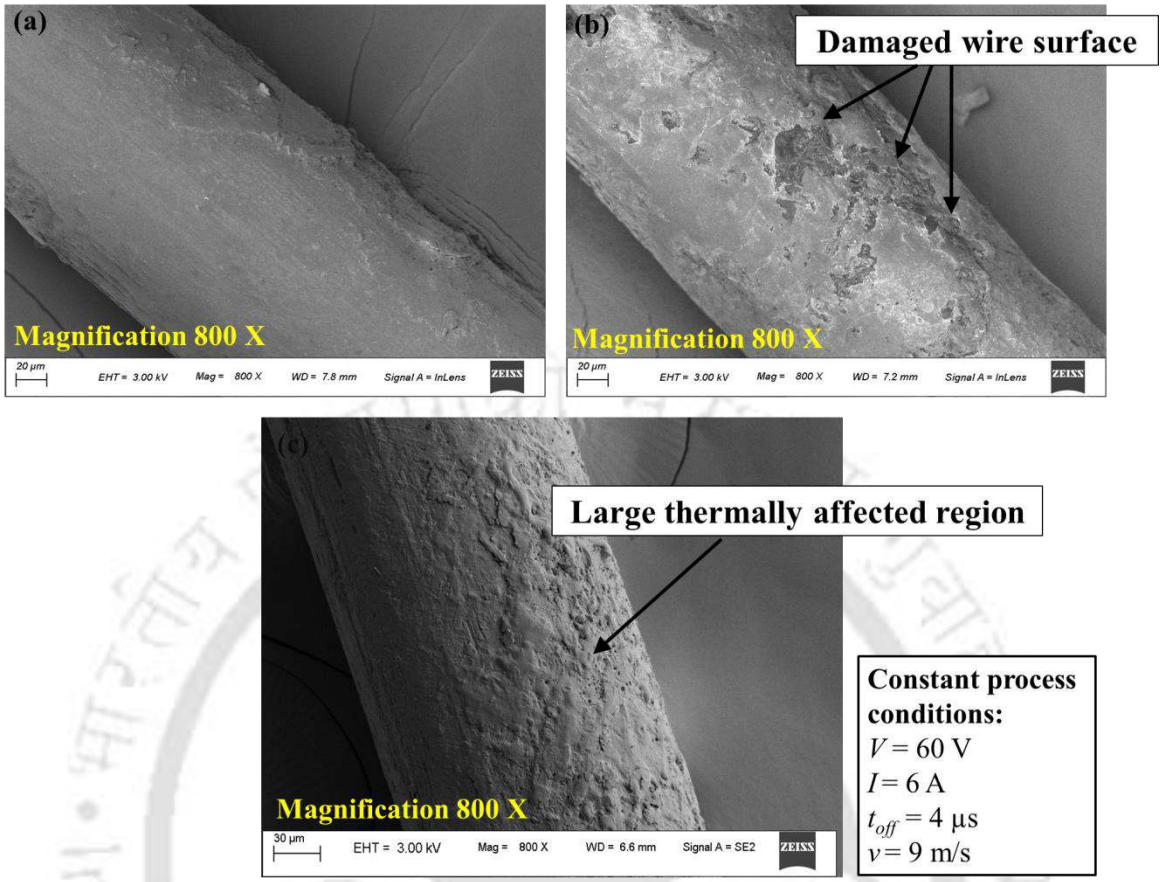

Figure 5.11 FESEM wire images after WEDM of Ti-6Al-4V at varying discharge durations: (a) 4 µs, (b) 8 µs, (c) 16 µs

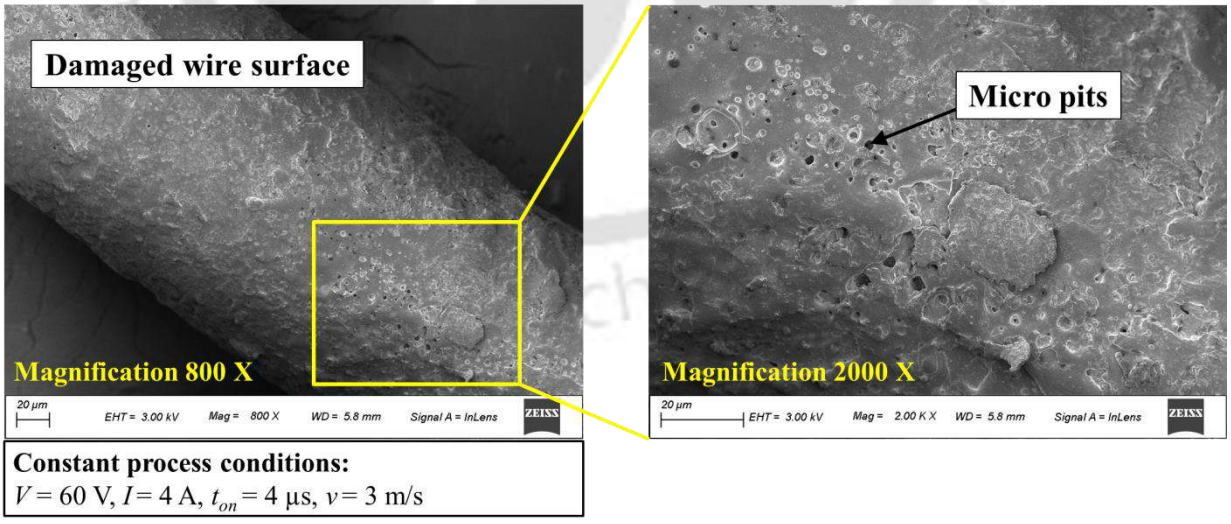

Figure 5.12 FESEM wire images after WEDM of Ti-6Al-4V at low pulse off-time of 2 µs

The wire speed also plays a crucial role in determining the nature and intensity of wire surface wear. When the wire speed is quite low, there is a localized temperature rise because the heat flux traverses over the wire surface at a low velocity. As a result, localized material ablation takes place, causing the formation of deep and large craters (Figure 5.13a). At higher wire speed, the wire quickly traverses the workpiece getting less time to form deep craters on the wire surface (Figure 5.13b). Thus, the wire wear at higher speed is less intense as compared to that of lesser wire velocity.

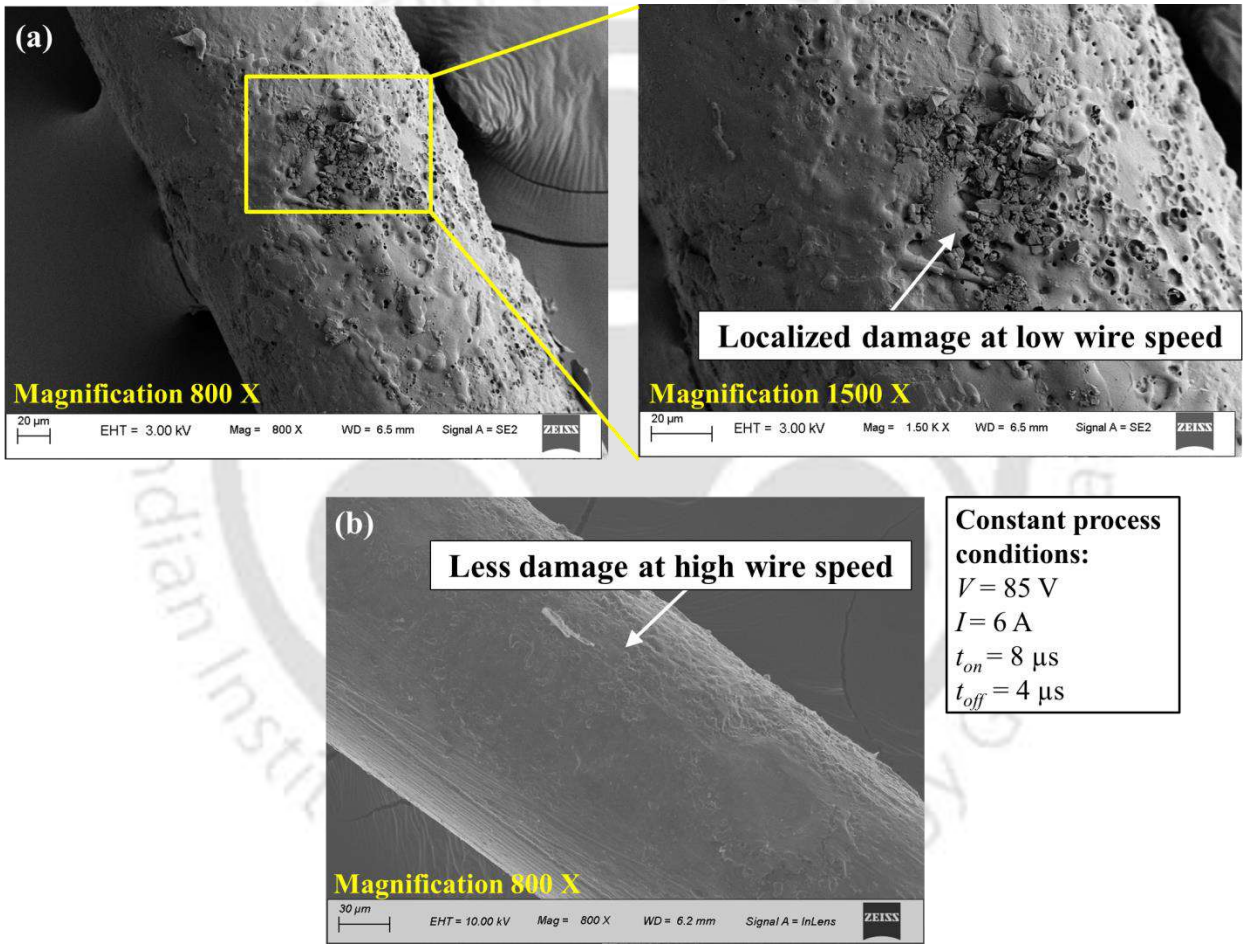

Figure 5.13 FESEM wire images after WEDM of Ti-6Al-4V at varying wire speeds: (a) 3 m/s, (b) 9 m/s

5.5.2 Effects of process parameters on workpiece surface roughness

The contribution of various input parameters viz. discharge voltage, discharge current, pulse on-time, pulse off-time and wire velocity on the response variable i.e workpiece *Ra* was

evaluated using the ANOVA analysis. Figure 5.14 shows the interaction plots of workpiece surface response variation with respect to the significant interaction terms $\left(I \cdot t_{on},\ I \cdot t_{off},\ I \cdot v,\ t_{on} \cdot t_{off}\right)$ which are obtained from Table 5.3. It is noted that *Ra* value rises with an increase in voltage and current due to a rise in discharge energy. Higher spark energy causes deep and wide craters on the workpiece surface, thus increasing the surface *Ra* with successive discharges. Discharges with similar nature form overlapping craters on the irradiated region. Longer pulse durations increase the thermally affected area causing higher material erosion. Pulse off-time has no significant effect on *Ra*, as shown from the ANOVA analysis (Table 5.3). However, a slight decrease in *Ra* values were observed with increasing pulse off-time. The decrease in the pulse off-time leads to an increase of the duty factor. This factor allows the formation of smaller and fewer gas bubbles containing lesser energy. When the discharge stops, these small gas bubbles will collapse which result in finer craters, thus decreasing the surface *Ra* of the machined surface. Also, it has been observed from Figure 5.14 that with an increase in wire velocity, the workpiece surface quality improves. This is because with an increase in wire speed, the heat flux moves over the wire surface at a higher speed, thus providing very less time for temperature rise on the wire surface as well as on the workpiece surface. Less temperature rise causes less material melting and eventually causes lesser damage on the machined surface, which reduces the surface roughness. Higher values of wire speed further causes less localized damage on the workpiece surface instead forming micro craters over a larger surface thus improving the surface finish.

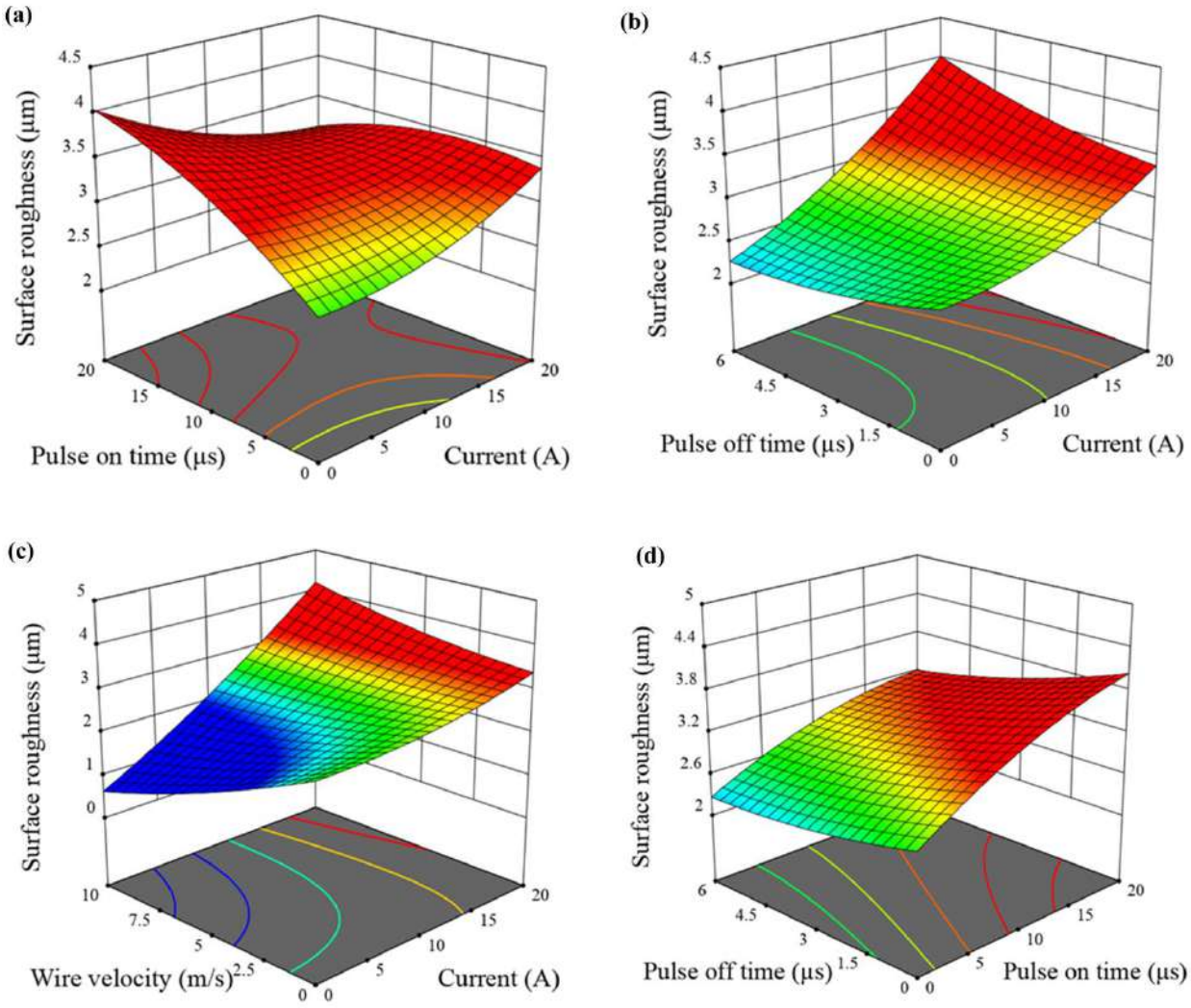

Figure 5.14 Analysis plots for surface roughness: (a) interaction of current and pulse on-time, (b) interaction of current and pulse off-time, (c) interaction of current and wire velocity, (d) interaction of pulse on-time and pulse off-time

5.6 Summary

This chapter reported an extensive experimental investigation on the measurement and analysis of molybdenum wire degradation and wear during WEDM of Ti-6Al-4V alloy. The existing literature reports scant analysis on the study of molybdenum wire electrode, which is extensively used in modern WEDM machines. A total of 36 WEDM experiments were carried out on Ti-6Al-4V alloy to investigate the influence of different process conditions viz. discharge voltage, discharge current, pulse on-time, pulse off-time and wire speed on the wire erosion and also on the surface quality achieved by the component. ANOVA analysis and regression analysis were carried out to study the effects of process parameters and their

interaction terms on the workpiece *Ra*. The following are the significant conclusions drawn from the current study:

- The wire surface undergoes severe degradation during WEDM pulse discharges in the form of craters, microholes, pits and cracks. Insufficient flushing time and improper flushing pressure causes inefficient flushing of debris; thus causing the machining debris to get attached onto the wire surface. The melted material sometimes gets resolidified and redeposited on the wire surface due to lack of sufficient flushing time. This reduces the spark gap thus causing undesired arc formation and exposing the wire to violent spark formation and thermal shock. Excessive wire erosion degrades the wire strength finally causing the failure of wire. Thus, it is essential to optimize the process conditions such that the damages on the wire surface are minimized in order to limit the occurrence of wire failure.
- The original circular cross-section of the wire continually changes its shape during the cutting operation. The wire deformation caused during metal cutting operation results in geometrical errors in machined components. During machining, the wire diameter initially increases on one side than the original diameter. As the wire traverses forward along the feed direction, the wire diameter then gradually becomes smaller than the original one.
- The intensity of wire surface erosion is controlled by the levels of process conditions used. It was clearly observed from the collected wire images that deep and wide craters were formed on the wire surface at higher levels of current. Higher pulse duration increases the thermally affected region in the wire. The reason behind this is because the wire surface is exposed to spark discharges for a longer duration at higher pulse on-times; thus subjecting the wire surface to more heat and severe surface degradation. At lower pulse off-times, microholes or micropits were observed on the wire surface due to inefficient debris removal mechanism.
- The effects of various input conditions showed that current and pulse on-time have the most considerable contribution towards workpiece *Ra* variation. Higher spark energy causes deep and wide craters on the workpiece surface, thus increasing the surface *Ra* with successive discharges. Pulse off-time has no significant contribution towards the surface quality achieved by the product. The workpiece surface quality was also observed

to be deteriorated at lower values of wire speed due to localized material ablation from the surface.

The detrimental influence of wire wear on the product surface quality is discussed in detail in the next chapter. The intensity of wire surface erosion at varying input levels is quantified using image processing technique and a tolerance limit is set for the extent of erosion undergone by the wire surface. The nature of wire breakage due to excessive erosion is also illustrated in the following chapter.

CHAPTER 6

Wire surface quality index for wire surface erosion using image processing technique

6.0 Scope

This chapter presents the estimation of a wire surface quality index for the tolerable limit of wire surface erosion using image processing technique. The need to evaluate the intensity of wire surface damages has been explained. The overall approach of image processing technique has been demonstrated. Wire samples were collected after WEDM experiments as explained in chapter 5 and the collected FESEM images were analyzed. The eroded wire surfaces reported damages in the form of craters, globules, microholes. The utilization of image processing technique to evaluate a wire safety index which shall establish the tolerance level of wire damages without wire breakage is elaborated. A relationship between wire wear and product surface quality was also established using the developed technique. A comprehensive discussion on wire breakage due to excessive erosion is also presented in this chapter. Finally, the chapter is summarized with conclusions.

6.1 The need

Wire erosion and breakage are major drawbacks in modern manufacturing industries as it impede the overall production rate in the system. Excessive temperature produced during the WEDM sparks causes melting and material removal from both the wire tool and workpiece. Material removal from the wire causes wire to erode off which degrades its strength extensively. Wire wear also deteriorates product quality and precision accuracy of final WEDMed components. Wire erosion cannot be entirely eliminated but it can be minimized by taking suitable precautions while machining and optimizing the process parameters. The intensity of damages on the wire surface depends largely on the selected sets of input parameters. Thus, we found it worthy enough to estimate a wire surface quality index to estimate the extent of erosion on the wire surface. The estimation of the wire surface quality index would provide some useful guidelines in calculating a threshold limit beyond which the damages are critical and prone to failure. The relationship between wire wear and product surface quality can also be established using the developed methodology.

Although the monitoring systems and numerical models presented in the existing reports are quite useful in the prediction of wire behavior, however, limited studies have been conducted so far which explains in detail the nature and intensity of wire erosion during machining (Pramanik and Basak (2016), Pramanik and Basak (2018)). A comprehensive analysis of the wire eroded samples to estimate a tolerable limit for wire surface erosion is very crucial in restricting wire failure and enhancing the overall efficiency of the operation.

Surface roughness (*Ra*) is a fundamental output characteristic of WEDMed components. Several WEDM studies have focused on the modeling and optimization of process conditions to obtain the desired product surface quality (Singh and Misra (2019), Mahapatra and Patnaik (2007), Roy and Narendranath (2018), Kavimani et al. (2019), Lalwani et al. (2020)). The existing literature, however, provides limited knowledge on the influence of wire erosion on the workpiece *Ra* values obtained. Thus, it is essential to have an in-depth knowledge of the physical mechanism of wire wear in order to evaluate its detrimental influence on the product surface quality. The proposed methodology can throw some light in establishing a relationship between wire wear and workpiece surface roughness. A deeper understanding of this relationship can be very useful in minimizing wire erosion and achieving desired product quality. Thus, the findings presented in this chapter extend the existing area of knowledge in this field and give better insights to understand the wire erosion mechanism and achieve stable machining without wire breakage.

6.2 Overall methodology of image processing technique

Image processing is a method to convert an image to a digital aspect and perform some operations on it, in order to get an enhanced image or to extract some useful information from it.

Nowadays, image processing is one of the fastest growing technologies, which has extensive applications in medical industry, astronomy, industrial robotics, and remote sensing by satellites.

The image processing technique comprises of the following steps: (a) importing the image via an image acquisition software; (b) analyzing the image; (c) obtaining the output. There are two methods used for image processing viz. analogue and digital image processing. Analogue image processing is used for the hard copies like printouts and photographs.

Digital image processing is used to manipulate the digital images using computers. The processing of digital images can be divided into several classes: image enhancement, image restoration, image analysis, and image compression. Image processing has been developed in response to three major problems concerned to pictures: (Petrou and Petrou (2010))

- Picture digitisation and coding to facilitate transmission, printing and storage of pictures
- Picture enhancement and restoration
- Picture segmentation and description as an early stage to Machine Vision

A digital image can be represented by a two-dimensional matrix where every element is given by a mathematical function f (x, y) where x and y represent the horizontal and vertical space coordinates respectively. The dimensions of the image is the dimensions of this two dimensional array. Each element of the array is called pixel or pel, derived from the term "picture element". Pixel is the basic building element of a digital image. A digital gray scale image in a computer is represented by pixels matrix. The pixel intensity defines the light intensity of the image at a particular location. The value of f (x, y) at any point in the image is given by the pixel intensity at that location. The pixel values of a gray image are usually represented with an 8 bit number; thus the pixel intensity value ranges from 0–255 (2^8-1). The value 0 indicates a completely dark (black) image and the value 255 indicates a completely light (white) image.

A digital image is represented in matrix form as

$$f(x,y)=\begin{bmatrix} f(1,1) & f(1,2) & . & . & . & f(1,N) \\ f(2,1) & f(2,2) & . & . & . & f(2,N) \\ . & . & & & & . \\ . & . & & & & . \\ . & . & & & & . \\ f(M,1) & f(M,2) & . & . & . & f(M,N) \end{bmatrix} \tag{6.1}$$

The right side of this equation represents an image in digital form.

6.3 Estimation of a wire surface quality index for the intensity of wire surface erosion using image processing technique

Extensive amount of erosion causes wire failure, which is one of the major drawbacks in the manufacturing sector. Thus, an attempt was made to determine a surface quality index of the

eroded wires in order to estimate the intensity of wire surface damages and identify a tolerable limit of wire wear to avoid wire failure. The developed methodology shall be useful in establishing a relationship between the wire damages and surface roughness of the machined components. A wire surface quality index was determined from the FESEM images of the wire electrode by plotting an image histogram using the image processing technique. A histogram in image processing is a graphical plot, which denotes the frequency of different pixel intensities. An image histogram is a gray-scale value distribution showing the frequency of occurrence of each gray-level value. It is a graphical representation of the tonal distribution in a digital image. It plots the number of pixels for each tonal value. Histograms have many uses in image processing like image analysis, image brightness, adjusting contrast of an image, image equalization, thresholding and computer vision. The horizontal axis of the histogram plot represents the tonal variations, while the vertical axis represents the total number of pixels in that particular tone. The pixel intensity values ranges from 0–255 in the horizontal axis for an 8-bit grayscale image. An image is scanned and a running count of the number of pixels found at each intensity value is kept. This then constructs a suitable histogram for the image. The histogram of a dark image will have most of its data points towards left and centre of the graph. On the other hand, a bright image will have its data points towards right and centre of the graph.

Figure 6.1 depicts the flowchart for estimating the wire surface quality index using the image processing technique. A series of WEDM experiments was carried out on the wire EDM machine (MAKE JK MACHINES, MODEL EC032) with Ti-6Al-4V alloy as the workpiece material and molybdenum wire tool. A total of 36 experiments according to the Taguchi L36 array were carried out and every single set was repeated thrice as explained in chapter 5. Corner cutting experiments were performed on a 60 × 60 × 12 mm^3 Ti-6Al-4V plate and wire samples were collected after every three cuts for a single process set. The collected wire samples were examined in FESEM. A histogram was plotted for the FESEM wire images to observe the change in pixel intensity at different locations using the ImageJ software. The region with damages or craters on the wire surface will denote a different pixel intensity and thus can be distinguished from a surface with lesser wear. Thus, an image histogram plot can be considered as a useful tool to estimate the intensity of wire erosion

during the cutting operation. A particular area of the wire sample was considered for analysis keeping the pixel count constant.

Figure 6.2a shows the wire sample for process set: V = 60 V, I = 4 A, t_{on} = 8 µs, t_{off} = 6 µs, v = 6 m/s; and the histogram of the considered region was plotted (Figure 6.2b). The histogram mean value was evaluated as 176.53. A similar technique was applied to Figure 6.2c, which showed critical and substantial amount of wear. The corresponding histogram mean was found to be lower (127.45) i.e. the histogram is shifted towards the darker side. The reason behind this is because the light intensity reduces in the region where the damage occurs, thus the pixel intensity reduces and the histogram shifts towards the darker side. This shifting of image histogram towards the darker side for wire surfaces with critical damages can be considered as the verification of the image processing technique. It has been observed that an image with a substantial amount of damage on the wire surface will produce a lower mean value of histogram. Damages in the form of craters or pits on the wire surface reduce the light intensity in that particular area which shifts the histogram to the left (darker) side. This lowers the histogram mean value. Thus, the mean value of the plotted histogram can be considered as a wire surface quality index to denote the extent and intensity of erosion undergone by the electrode. Lower mean values of wire image histogram denote a lower surface quality of the wire samples.

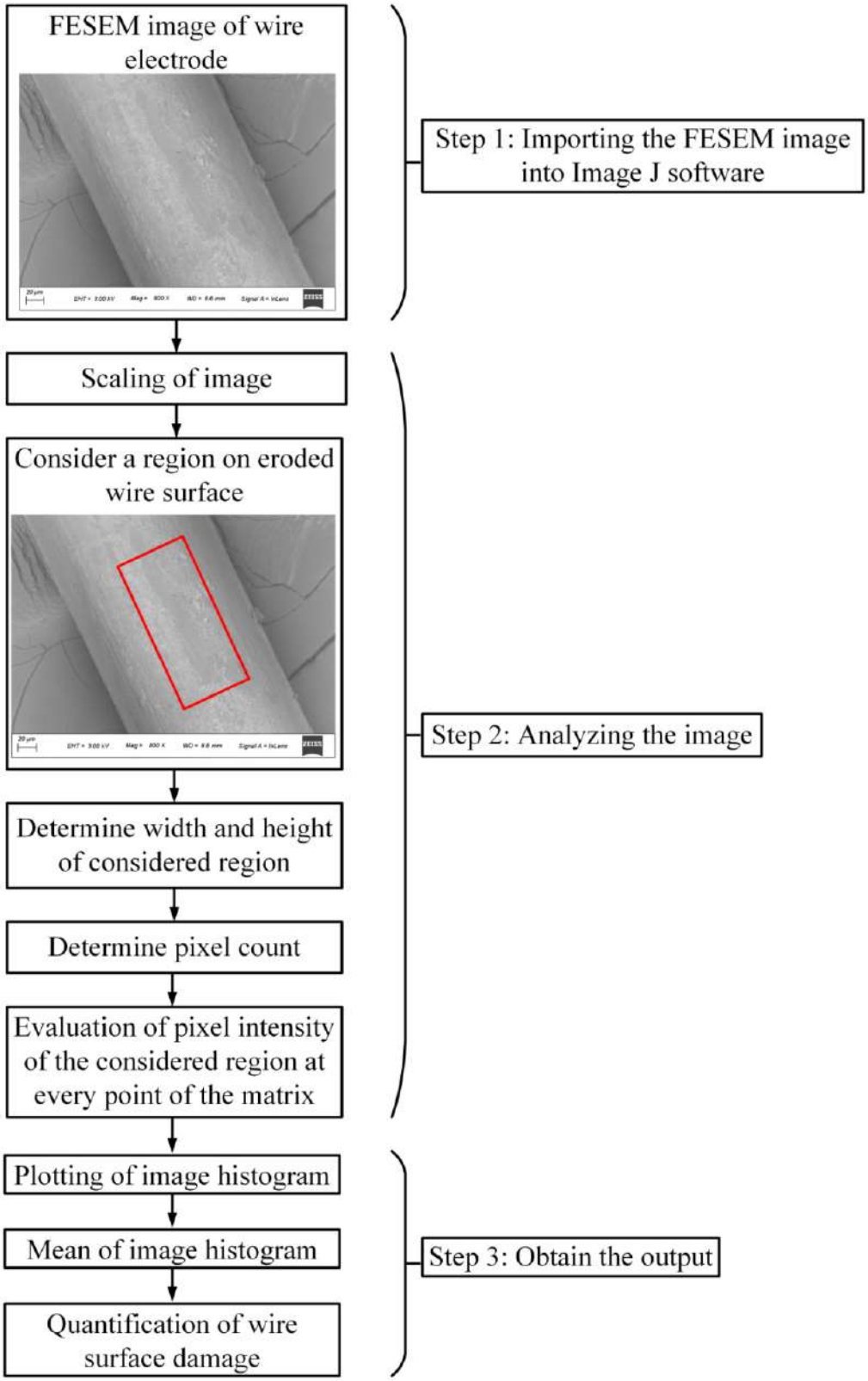

Figure 6.1 Flowchart to estimate the wire surface quality index for an eroded wire surface

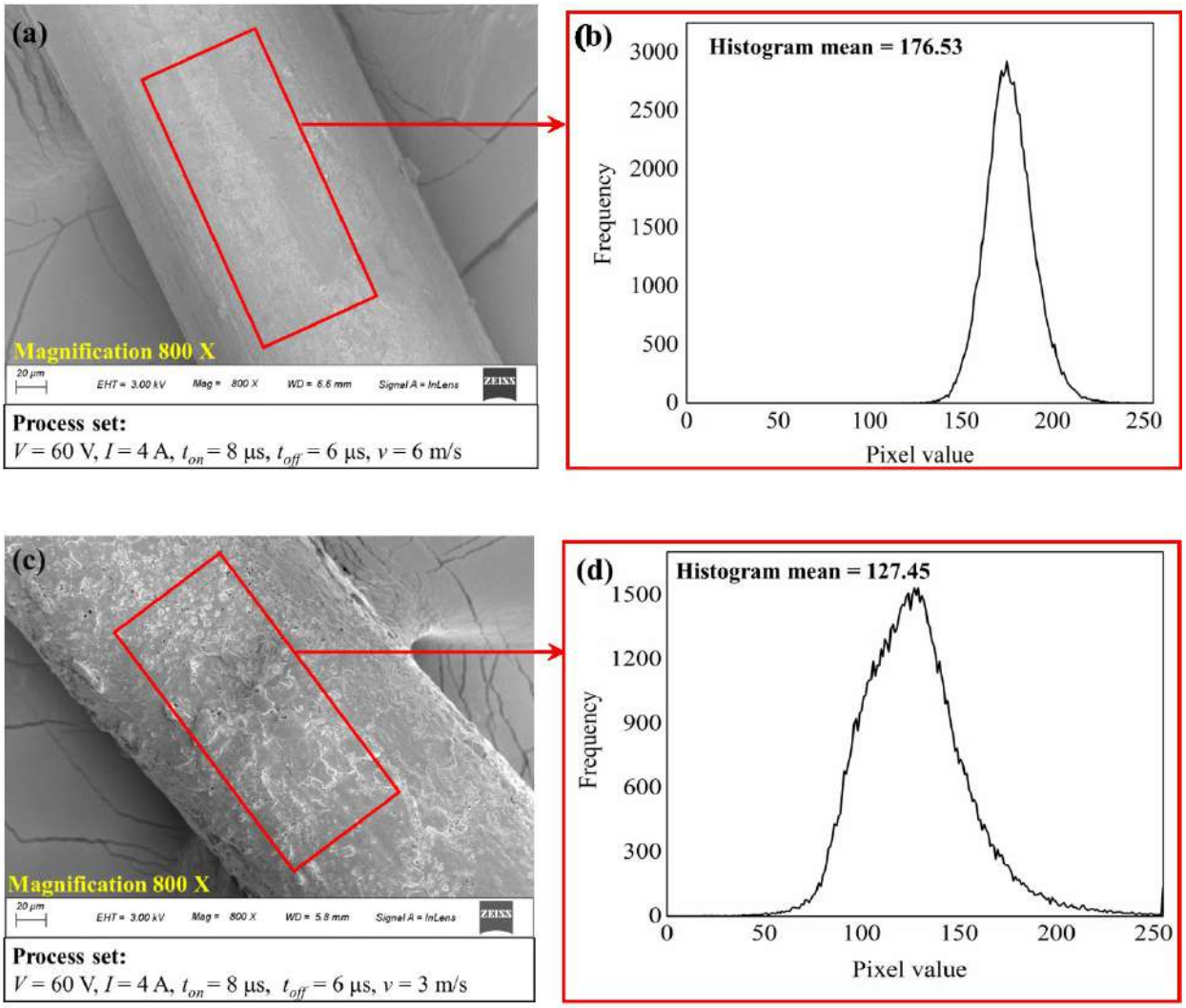

Figure 6.2 Analysis of eroded wire samples using image processing technique (a), (c) FESEM wire images after WEDM of Ti-6Al-4V and (b), (d) histogram plots of eroded wire surfaces at the chosen parameter sets.

Table 6.1 shows the histogram mean values of the FESEM wire images collected at different sets of process conditions. FESEM images were analysed at 36 different sets as discussed in chapter 5. A lower histogram mean value denotes larger intensity of wear on the wire surface. This developed methodology can be useful in understanding the detrimental influence of wire erosion on product surface quality, which is explained in the next section.

Table 6.1 Histogram mean values of wire samples at different process conditions

Serial no.	Discharge voltage (V)	Discharge current (A)	Pulse on-time (µs)	Pulse off-time (µs)	Wire speed (m/s)	Histogram mean
1	60	4	4	2	3	124.1
2	60	6	8	4	6	145.26
3	60	8	16	6	9	143.89
4	60	4	4	2	6	164.01
5	60	6	8	4	9	146.21
6	60	8	16	6	3	108.3
7	60	4	8	6	3	127.45
8	60	6	16	2	6	108.11
9	60	8	4	4	9	150.06
10	60	4	16	4	3	108.77
11	60	6	4	6	6	157.79
12	60	8	8	2	9	123.85
13	60	6	16	2	9	126.31
14	60	8	4	4	3	113.83
15	60	4	8	6	6	176.53
16	60	6	16	4	3	106.96
17	60	8	4	6	6	146.87
18	60	4	8	2	9	170.01
19	85	6	4	6	9	150.26
20	85	8	8	2	3	104.97
21	85	4	16	4	6	129.88
22	85	6	8	6	9	170.05
23	85	8	16	2	3	104.35
24	85	4	4	4	6	164.57
25	85	8	8	2	6	105.44
26	85	4	16	4	9	148.44
27	85	6	4	6	3	127

28	85	8	8	4	6	110.33
29	85	4	16	6	9	157.02
30	85	6	4	2	3	105.67
31	85	8	16	6	6	122.17
32	85	4	4	2	9	180.45
33	85	6	8	4	3	116.79
34	85	8	4	4	9	130.59
35	85	4	8	6	3	126.04
36	85	6	16	2	6	105.28

6.4 Relationship between wire erosion and workpiece surface quality

A desired surface quality of the WEDMed products with minimal damages on the wire surface, avoiding wire failure, is vital for the process efficiency of the system. Wire erosion and damages have a detrimental effect on the surface quality of machined components. The histogram means of the wire images at certain input conditions have been listed in Table 6.2 along with the corresponding workpiece *Ra* values. It has been observed that as the histogram mean decreases, the corresponding *Ra* value for the workpiece increases. Thus, it can be inferred that as the intensity of wear increases, the surface quality of the workpiece also deteriorates. Hence, the histogram mean can be used as an indicative tool to establish a correlation between the intensity of damages undergone by the wire surface and the surface quality of the products. It was further observed that for the process set: V = 85 V, I = 8 A, t_{on} = 16 µs, t_{off} = 6 µs and v = 6 m/s; the wire erodes largely forming deep and wide craters on the surface and the corresponding *Ra* value (2.69 µm) is also degrading. Thus, the corresponding histogram mean value (122.17) provides a tolerable limit below which the damages undergone by the wire electrode are critical and unsafe for machining in terms of wire strength and surface quality of the machined products. Figure 6.3 shows the FESEM wire image at the process set: V = 85 V, I = 6 A, t_{on} = 8 µs, t_{off} = 4 µs and v = 3 m/s, which has a lower mean value (116.79) than the threshold limit (122.17). The figure depicts a damaged wire surface with large craters and pits, which lowers the pixel intensity values of the image and thus yields a lower histogram mean value. At further lower mean values, wire breakage was observed for the corresponding process conditions (Table 6.2). Hence, the

proposed methodology shall provide useful guidelines to correlate the wire surface erosion with the product surface quality in order to uplift the machining efficiency.

Table 6.2 Histogram mean values of the wire samples and workpiece *Ra* values at different input parameters

Discharge voltage (V)	Discharge Current (A)	Pulse duration (µs)	Pulse off-time (µs)	Wire speed (m/s)	Histogram mean	Workpiece *Ra* (µm)
60	4	8	6	6	176.53	2.06
60	6	4	6	6	157.79	2.17
60	6	8	4	6	145.26	2.35
60	4	8	6	3	127.45	2.47
85	8	16	6	6	122.17	2.69
85	6	8	4	3	116.79	2.73
85	8	8	4	6	110.33	2.76*
85	8	16	2	3	104.35	3.17*

* Wire breakage

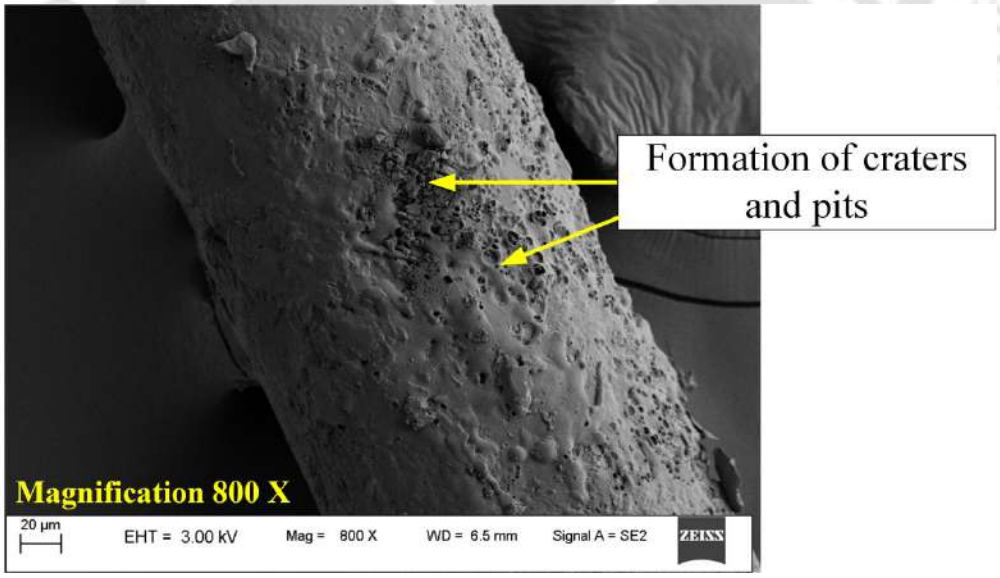

Figure 6.3 FESEM wire sample for the process set**:** V = 85 V, I = 6 A, t_{on} = 8 µs, t_{off} = 4 µs, v = 3 m/s

It was further observed from Table 5.2 of chapter 5 that the average *Ra* value gradually increases from the 1st cut to 3rd cut under the same machining condition. Figure 6.4 depicts the influence of wire wear on workpiece *Ra* at different energy settings (Low = 0.00096 J, Medium = 0.00288 J, High = 0.01088 J). The *Ra* value increases with a rise in discharge energy as higher material erosion occurs at higher discharge energy settings, which deteriorates the workpiece surface quality. The *Ra* value was further observed to increase by approximately 25–35 % from the 1st cut to 3rd cut. For set 1 of Table 5.2, the *Ra* value at 1st cut (2.25 µm) increases by 28 % upto the *Ra* value at 3rd cut (2.88 µm) for the same process set. For set 17, the Ra value increases substantially by 32 % from the 1st cut to 3rd cut and so on. The reason behind this can be attributed to the fact that as the fresh molybdenum wire starts entering the workpiece, the surface finish of the component is at its best as the wire surface damages are at its primary stage. As the machining proceeds further for the second and third cut, the wire erodes to a substantial extent because of the violent and erosive nature of successive random discharges during the spark cycles. The wire health deteriorates continuously due to the formation of several craters, pits, and debris generation in the discharge zone. The eroded and uneven wire surface further diminishes the surface quality and integrity of the WEDMed product. Thus, apart from the influence of process conditions on response characteristics, the wire surface wear plays a crucial role in determining the surface quality and precision of the cut.

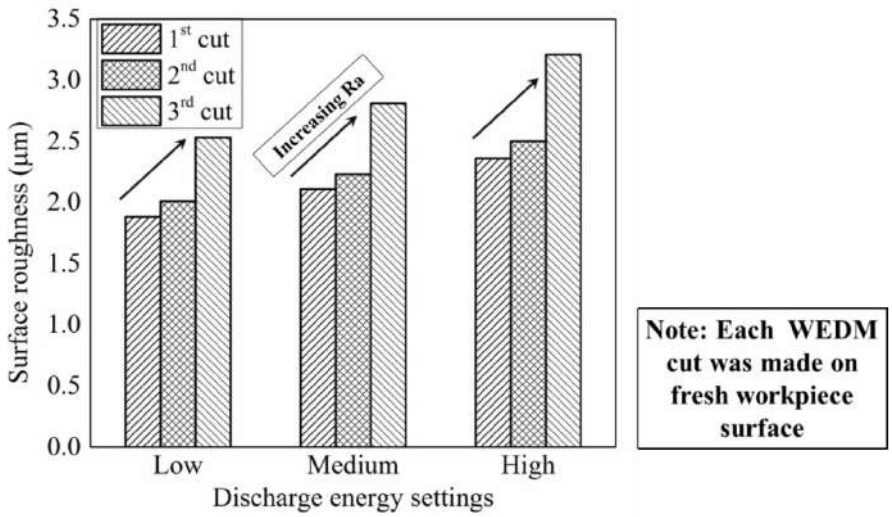

Figure 6.4 Effect of wire wear on workpiece surface roughness at different discharge energy settings

6.5 Wire breakage and its relationship with wire wear

Wire wear and breakage are major concerns during the WEDM process, which impede the overall chain of production in the system. Estimation of wire rupture probability and its prohibition is thus very essential to achieve overall efficiency in production. Understanding the morphology of broken wire samples shall give a better approach to the relationship between wire wear and wire failure. Figure 6.5 shows the broken wire tip morphology for process set: $V = 85$ V, $I = 8$ A, $t_{on} = 8$ µs, $t_{off} = 4$ µs, $v = 6$ m/s.

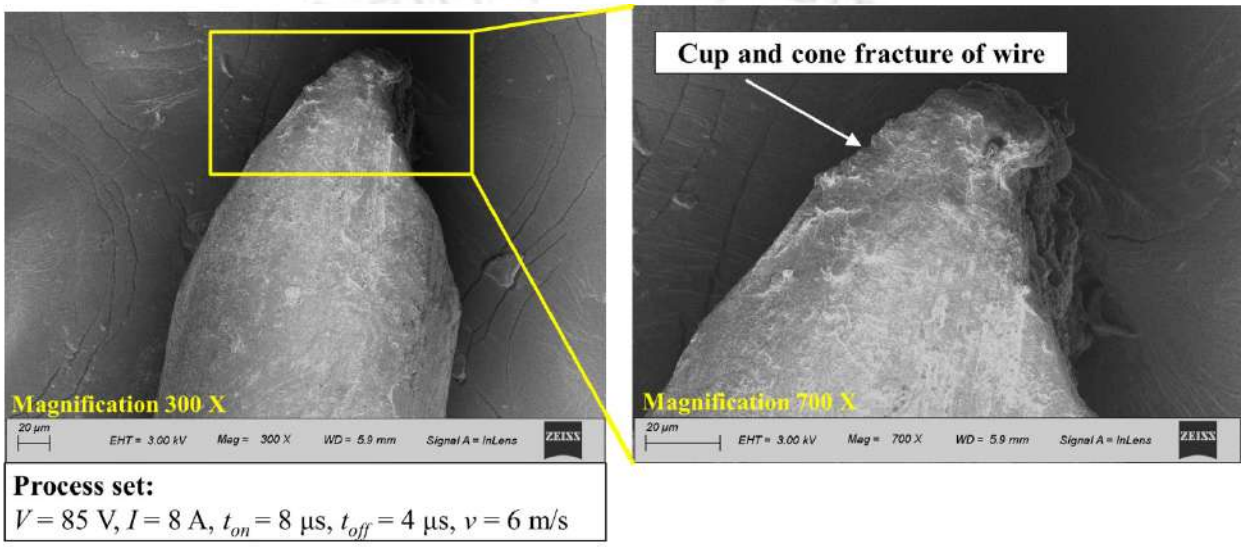

Figure 6.5 Broken wire tip at the chosen parameter set

It can be observed from Figure 6.5 that the wire experiences necking before failure, which is characteristic of the ductile behaviour of materials. The wire diameter near the broken tip reduces and exhibits cup-cone like fracture. Molybdenum has a body-centred cubic structure and becomes ductile at higher temperatures, which are obtained during the discharge cycle. The yield strength of material also reduces at a higher temperature, and the fracture of material becomes ductile. A moderately sharp tip with symmetric material erosion is observed from both sides of the broken wire tip. Excessive temperature rise above the melting point during the spark pulses is the primary factor responsible for wire wear and failure during the cutting operation.

Wire breakages were observed at higher discharge energy settings, lower values of pulse off-time and lower values of wire speed due to generation of a huge amount of

temperature at these conditions. Erosion of wire material due to melting and vaporisation and the violent nature of unwanted arc formation weaken the wire, which increases the threat of wire failure. Sharp temperature gradients also generate thermally induced stresses on the wire electrode that decline its strength and initiate microcracks on the surface. Microcracks are considered as stress concentrators that indicate the onset of wire breakage. They propagate into deep and broader cracks as the wire strength diminish, finally causing the failure of the wire.

6.6 Summary

The present work proposes a methodology to estimate the intensity of wire surface erosion in order to estimate a threshold limit of wire damages. The importance of the work lies in the estimation of a wire surface quality index for the tolerable limit of wire surface erosion using image processing technique. Further, the interrelationship between wire wear and the achieved workpiece surface quality was also established using this methodology. The following are the significant conclusions drawn from the current study:

- A wire surface quality index was proposed using image processing technique to estimate the extent of erosion undergone by the wire surface. The mean value of an image histogram of the eroded wire samples was used as an indicator in determining a tolerance for wire wear below which the wire is highly prone to breakage and also deteriorates the workpiece surface quality.
- A histogram mean of 122.17 was observed to be the threshold limit below which the damages on the wire surface are critical thus increasing the probability of wire failure. Wire surfaces with lower histogram mean values than the tolerable limit were observed to have extensive damages on the surfaces or experience failure.
- The wire surface quality index for the molybdenum wire decreases as the intensity of wire surface erosion increases.
- The developed technique was useful in establishing a relationship between the wire wear and the product surface quality. It was observed that as the wire surface quality index decreases, the workpiece *Ra* value increases.
- Wire wear has shown a detrimental effect on the surface roughness of WEDMed components and deteriorate the surface quality by approximately 25–35 %.

- Wire rupture occurs due to a reduction in wire strength when excessive erosion degrades the integrity of the wire surface and the thermal residual stresses induced during the temperature rise exceed the threshold strength of molybdenum wire material. The wire experiences necking before failure due to the transition of molybdenum material from brittle to ductile behaviour at higher temperatures, which are achieved during the discharge phenomenon.
- Wire failure incidents were observed at higher discharge energy settings and low level of wire speed. Low wire speed causes localized damages on the surface and produces more debris, which can easily break the wire.

After carrying out detailed analysis on the molybdenum wire tool, a need was identified to investigate the characteristics and health of coated wires, which are extensively used in WEDM machines. Numerical and experimental investigations were carried out on a zinc coated brass wire in order to have a deeper understanding of the effect of a coating material over the wire core, which are presented in the next two chapters.

CHAPTER 7

Development of a three-dimensional thermo-mechanical model of a zinc-coated brass wire during WEDM process

7.0 Scope

This chapter presents the development of a three-dimensional thermo-mechanical finite element model (FEM) of a zinc coated brass wire electrode. The need to carry out the thermo-mechanical analysis of the coated wire tool is explained. The overview of the process model development using FEM is presented. The numerical model is presented in details, in terms of its governing equations, assumptions, boundary conditions, heat flux model, material properties and solution methodology. The FEM model is well validated with experimental data. The temperature and stresses generated in the wire at different sets of process conditions are computed using the developed model. The crater volume produced in the wire is calculated when the temperature exceeds the melting point of the wire material. The wire strength is estimated based on the amount of material removed from the zinc coated brass wire. In the end, parametric studies to investigate the effects of input parameters on the temperature, residual stresses and crater volume generated in the wire are carried out. The chapter is summarized with conclusions.

7.1 The need

With increasing demands of higher machining efficiency and productivity, coated or stratified wires were developed with excellent sparking abilities. Coated wires are extensively used in WEDM setups due to its low cost and improved properties as compared to uncoated wires. The development of a coated layer of a metal or a metal alloy over the wire core and its advantages were described by Groos et al. (2004). Zinc-coated brass or zinc-coated copper wires with a coating thickness of about 10-20 μm were developed which improved the cutting speed along with better flushing and debris removal characteristics (Prohaszka et al. (1997)). The zinc coating has a lower vaporization temperature, which acts as a heat sink protecting the core of the wire from thermal shock due to spark discharges. The performance of zinc-coated brass wire was also found to be superior in comparison to

uncoated brass wire in terms of improved product quality and increased MRR (Kumar et al. (2018), Manjaiah et al. (2015)).

As discussed in the previous chapters, frequent breakages of wire electrode during WEDM adversely affect the productivity and surface quality of the finished products. Prediction and prevention of wire breakage phenomenon are crucial in order to achieve sustainable and efficient machining. Numerical models prove to be useful tools to understand the characteristics of the wire tool during the spark discharges. Literature survey suggests that no such numerical model has been developed for coated wires. Thus, it was thought worthy enough to develop a three-dimensional thermo-mechanical model for a zinc coated brass wire in order to predict and limit the occurrence of wire failure. The developed model was aimed to predict the temperature and the induced stresses in the wire. The amount of material eroded from the wire surface was also computed when the induced temperature exceeds the melting point of the wire material. It is envisaged that by using the developed method, one can easily predict the deterioration of wire electrode, which will ensure uninterrupted and efficient wire electric discharge machining operation. The details of the developed numerical model are presented in the following sections.

7.2 Development of numerical model for computation of temperature and stresses generated in the wire

7.2.1 Governing equations and boundary conditions

The step-by-step development of the three-dimensional coupled thermo-mechanical model of the zinc coated brass wire is the same as for the molybdenum wire, which is explained in detail in chapter 3. The governing equations, boundary conditions, and the heat flux equation employed in the numerical model have been depicted in Table 7.1.

Table 7.1 Governing equations and boundary conditions incorporated in the model

Governing equations	**Thermal analysis** $\frac{\partial^2 T}{\partial r^2} + \frac{1}{r}\frac{\partial T}{\partial r} + \frac{1}{r^2}\frac{\partial^2 T}{\partial \varphi^2} + \frac{\partial^2 T}{\partial z^2} - n\frac{\partial T}{\partial z} = \frac{1}{\alpha}\frac{\partial T}{\partial t}$	(7.1)
	Mechanical analysis Equilibrium equations $\sigma_{ij} + \rho b_i = 0, \qquad \sigma_{ij} = \sigma_{ji}$	(7.2)
	Constitutive equation $[d\sigma] = ([D^e] + [D^p])[d\varepsilon] + [K^{th}]dT$	(7.3)
	von-Mises criterion $\frac{1}{2}[(\sigma_1 - \sigma_2)^2 + (\sigma_2 - \sigma_3)^2 + (\sigma_1 - \sigma_3)^2] = \sigma_y^2$	(7.4)
Boundary conditions	**Thermal analysis** $k\frac{\partial T}{\partial r} = Q(r) \quad \text{for } r = R_w$	(7.5a)
	$k\frac{\partial T}{\partial r} = h\,\theta \quad \text{for } r = R_w$	(7.5b)
	Mechanical analysis Pin end joints were applied at both ends of the wire to avoid movement. The wire surface was applied with no mechanical constraints.	
Spark radius	$R = (2.04\times10^{-3})\, I^{0.43}\, t_{on}^{\ 0.44}\ (\mu m)$	(7.6)
Heat flux on the wire electrode	$Q(r) = \frac{4.57\, F_c\, V\, I}{\pi R^2}\exp\left(-4.5\,\frac{r^2}{R^2}\right)$ $F_c = 0.183$	(7.7)
Convective heat transfer coefficient	h = 10,000 W/m^{2}K	
Initial temperature	300 K	

7.2.2 Material properties

In the developed thermo-mechanical finite element model, temperature dependent material properties have been considered for both the brass core and the outer zinc coating. The general properties of brass and zinc have been listed in Table 7.2. The thermal and mechanical properties of zinc and brass are shown in Figures 7.1–7.5, according to Table 7.3.

Table 7.2 General properties of zinc and brass

Property	Values for zinc coating	Values for brass core
Density(kg/m^3)	7130	8800
Poisson's ratio	0.245	0.331
Coefficient of thermal expansion (μm/m-ºC)	34	18
Melting point (K)	693	1203

Table 7.3 Thermal and physical properties of zinc and brass

Property	Figure nos. for zinc coating	Figure nos. for brass core
Thermal conductivity (W/mK)	7.1	7.3
Specific heat (J/kgK)	7.1	7.3
Stress-strain curve	7.2	7.4
Young's modulus	–*	7.5

* The Young's modulus of zinc is taken at a constant value of 7x10^{10} Pa.

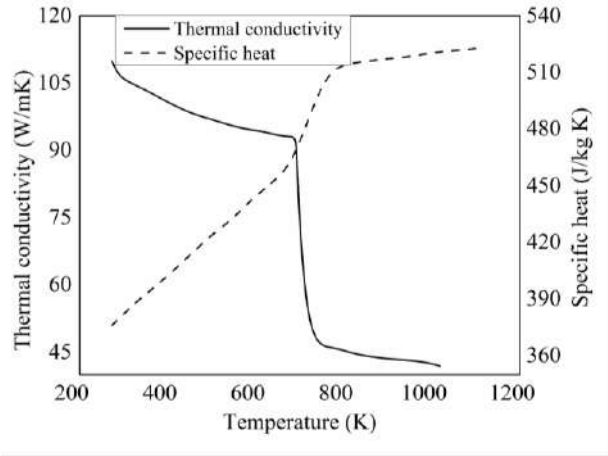

Figure 7.1 Thermal conductivity (Powell and Childs (1973)) and specific heat (Valencia and Quested (2008)) of zinc

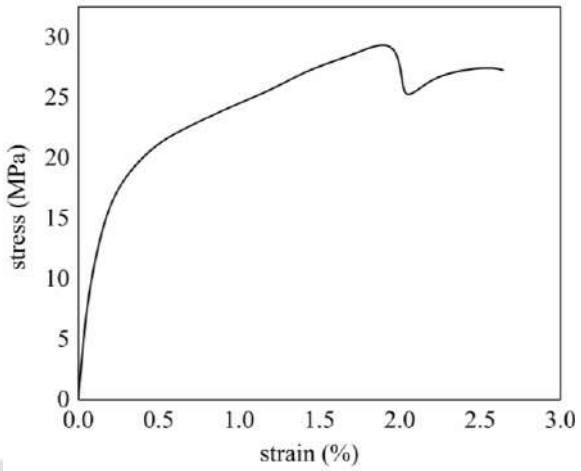

Figure 7.2 Stress strain curve of zinc (Liu et al. (2016))

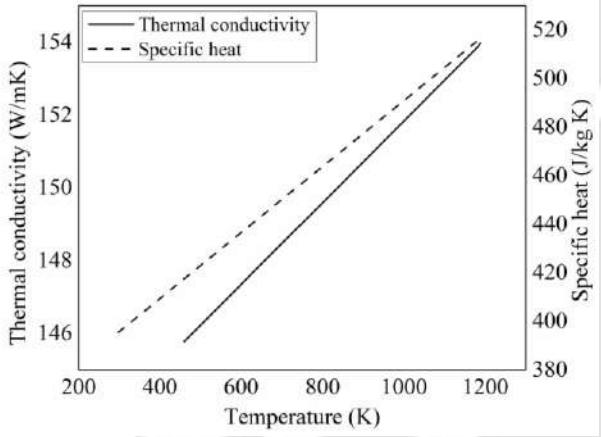

Figure 7.3 Thermal conductivity and specific heat of brass (Valencia and Quested (2008))

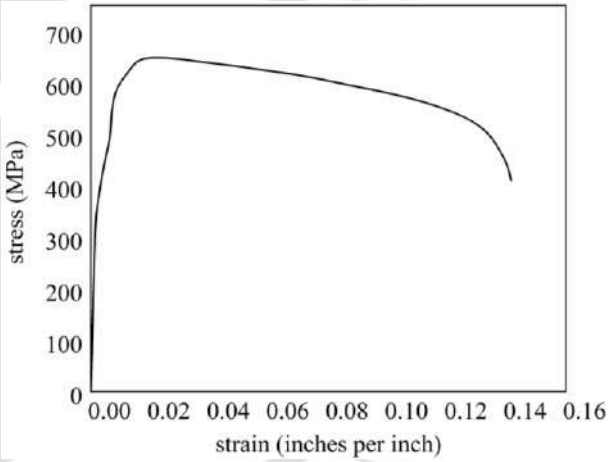

Figure 7.4 Stress strain curve of brass (Reed and Mikesell (1967))

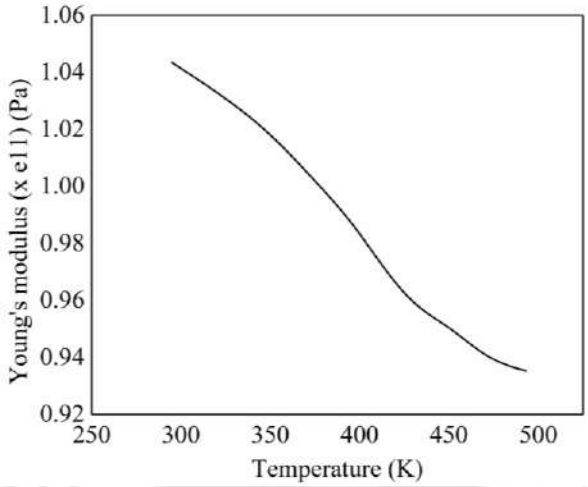

Figure 7.5 Young's modulus of brass (Reed and Mikesell (1967))

7.2.3 Process parameters used for the model

In the present model, four input parameters viz. discharge voltage, discharge current, pulse on-time and pulse off-time were varied at different levels. The process parameters have been selected based on the facilities available in our workshop. The levels of these input parameters have been kept at the same levels as for the molybdenum wire in order to compare the behaviour of both types of wires. The levels chosen for each process parameters are shown in Table 7.4.

Table 7.4 Process parameters and their levels

Factors	Level 1	Level 2	Level 3
Discharge voltage (V)	60	85	-
Discharge current (A)	4	6	8
Pulse on-time (μs)	4	8	16
Pulse off-time (μs)	2	4	6

The wire velocity (v) was kept constant at 6 m/s in the present model.

7.2.4 Overview of the process model development

A three-dimensional coupled thermo-mechanical model was developed for the zinc coated brass wire electrode in a similar manner as discussed in chapter 3 (Figure 3.8). Four input parameters viz. discharge voltage, discharge current, pulse on-time and pulse off-time were

given as input to the model, which predicts the temperature generated in the wire. Based on the temperature distribution, the stress distribution in the wire tool at the end of the pulse is predicted.

In the present model, a zinc coated brass wire with 250 µm diameter is considered for analysis. An outer zinc coating of 10 µm thickness over a brass core is considered as the model geometry (Figure 7.6). Figure 7.7 shows the process model of the zinc coated brass wire with the incorporated boundary conditions. The outer coated layer of zinc over the brass core was modelled using tie constraints in ABAQUS^{TM}. Heat flux is applied at the spark location and the rest of the wire surface is applied with convection boundary condition. Both ends of the wire are hinged with pin joints and end tension is applied at both ends of the wire.

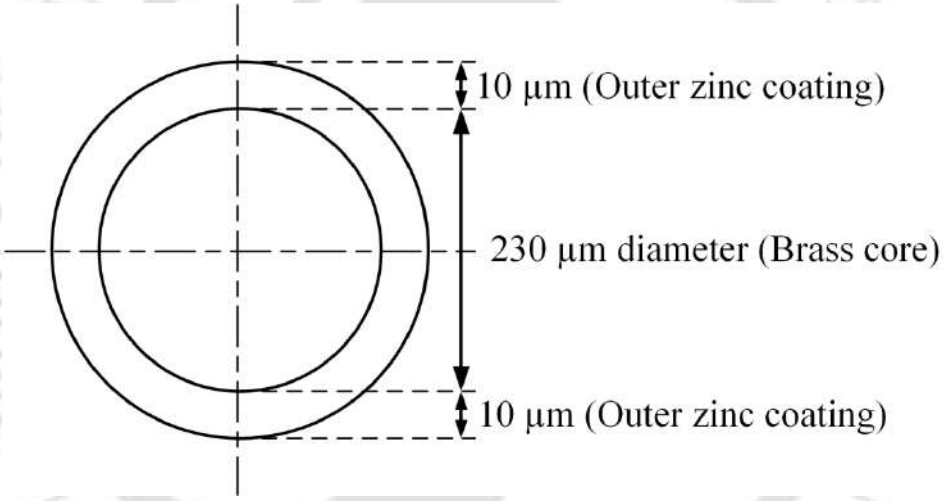

Figure 7.6 Cross-sectional view of the zinc coated brass wire model geometry

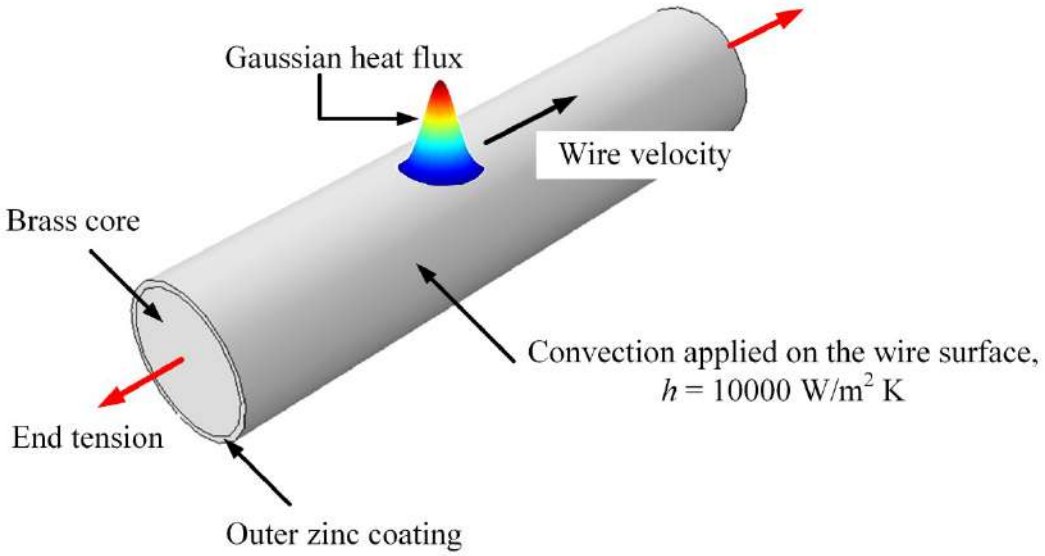

Figure 7.7 Process model geometry of the zinc coated brass wire

7.2.5 Finite element meshing of the wire geometry

The process model along with the boundary conditions was solved by using ABAQUS^{TM}, a commercial FEM solver in transient mode. The wire geometry is discretized with eight-node hexahedral elements C3D8T. The meshed geometry of the coated wire is shown in Figure 7.8. The mesh was refined in the region where the heat flux is applied. The rest of the wire geometry was discretized with coarse mesh to reduce the computational time. Mesh optimization was performed for better convergence of results in optimum time. The overall mesh size was kept at 30 µm for the wire model. The heated and nearby regions were discretized using finer mesh size to get better accuracy of results. The mesh sensitivity analysis was carried out for a single process condition at discharge voltage (V) = 60 V, discharge current (I) = 6 A, pulse on-time (t_{on}) = 16 µs, pulse off-time (t_{off}) = 6 µs, wire velocity (v) = 6m/s. The heated region was discretized with a fine mesh of various sizes, which have been shown in Table 7.5. It was observed that the smallest change in temperature (0.099 %) occurs when the fine mesh size changes from 10 µm to 8 µm as compared to the other cases. Thus, the element of 8 µm size was selected as the optimum fine mesh size for the heated region to achieve better results. The moving heat source concept was used in the model to incorporate the effect of moving wire during the wire EDM machining process. The Gaussian heat flux moving at a constant velocity over the wire surface was employed using a

user subroutine DFLUX of ABAQUS^{TM}. The transient heat transfer problem was solved by applying the heat flux at the location of spark and adopting an automatic time step increment. Convection heat transfer is applied over the wire surface. The model was developed considering the automatic time step increment and the maximum allowable temperature change per increment was set to 10.

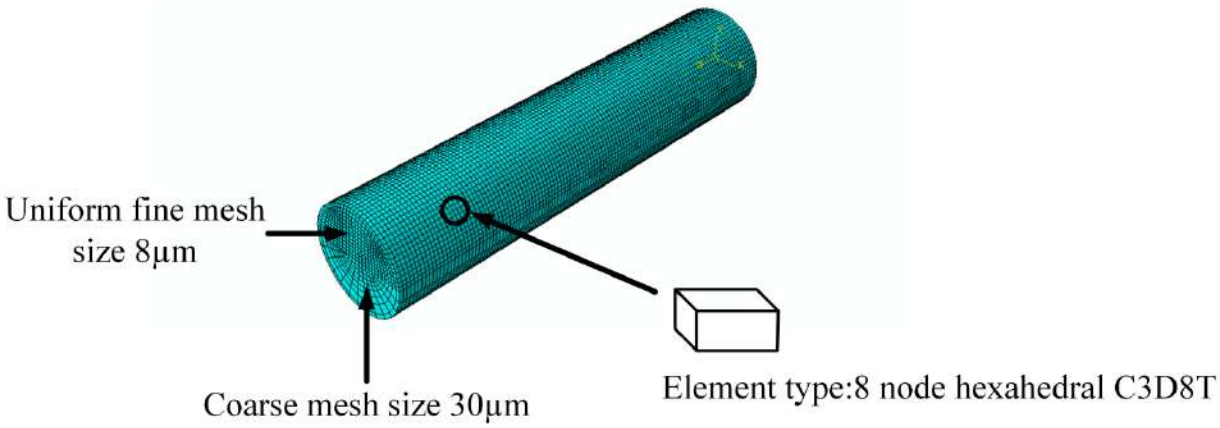

Figure 7.8 Mesh model of the wire electrode

Table 7.5 Mesh sensitivity analysis for the fine mesh in the heated region

Serial no.	Mesh size (μm)	Temperature output (K)	Change in temperature (%)	CPU time (hrs.)
1	25	721	-	1.308
2	20	636.1	11.77	1.682
3	15	556.7	12.48	1.97
4	10	503.1	9.62	3.76
5	**8**	**503.6**	**0.099**	**7.38**

7.3 Computation of temperature and stresses generated in the wire

After the development of the numerical model, simulation was carried out for a typical process condition to compute the temperature generated in the wire and the residual stresses induced in the wire. In order to study the effects of various process parameters on the temperature obtained and the stresses generated in the wire electrode during the machining process, eighteen cases have been considered as suggested by the Taguchi L18 array. The

effects of different input parameters on the temperature and stresses induced in the wire have been discussed in detail in the latter section. Figure 7.9 shows the temperature profile at the end of a single pulse cycle for a typical process condition: discharge voltage (V) = 60 V, discharge current (I) = 4 A, pulse on-time (t_{on}) = 16 µs, pulse off-time (t_{off}) = 6 µs. The temperature profile takes the shape of an ellipse due to the moving heat source characteristics of Gaussian heat flux. It is observed that as the heat source moves along the wire axis, the temperature keeps on increasing during the pulse on-time and starts cooling during the pulse off-time. The peak temperature is obtained at the end of the discharge duration. The increase in temperature generates thermal stresses in the irradiated and nearby region. After the cooling effect in a single pulse, the stresses that retain in the wire are the residual stresses induced. Figure 7.10 shows the stress contour induced on the wire surface during the discharge phenomenon for the same process condition. An enlarged sectional view of the wire shows that the peak value of equivalent residual stress is obtained at a certain depth below the wire surface. Figure 7.11 shows the variation of equivalent residual stresses along the depth of the wire. It is observed that the peak value of residual stresses is obtained at a certain depth below the surface and not on the top surface of the wire. Table 7.6 depicts the peak temperatures and peak values of thermal residual stresses generated in the wire at different combinations of machining parameters.

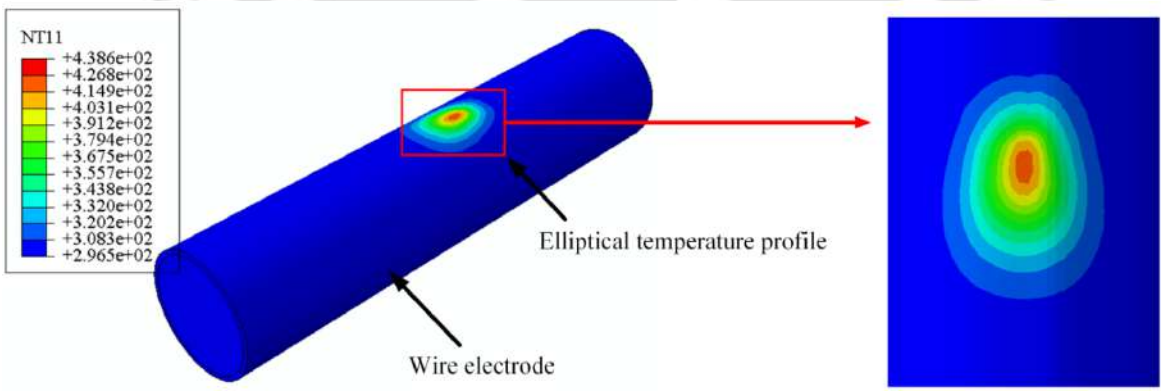

Figure 7.9 Elliptical temperature profile on the wire after a single pulse

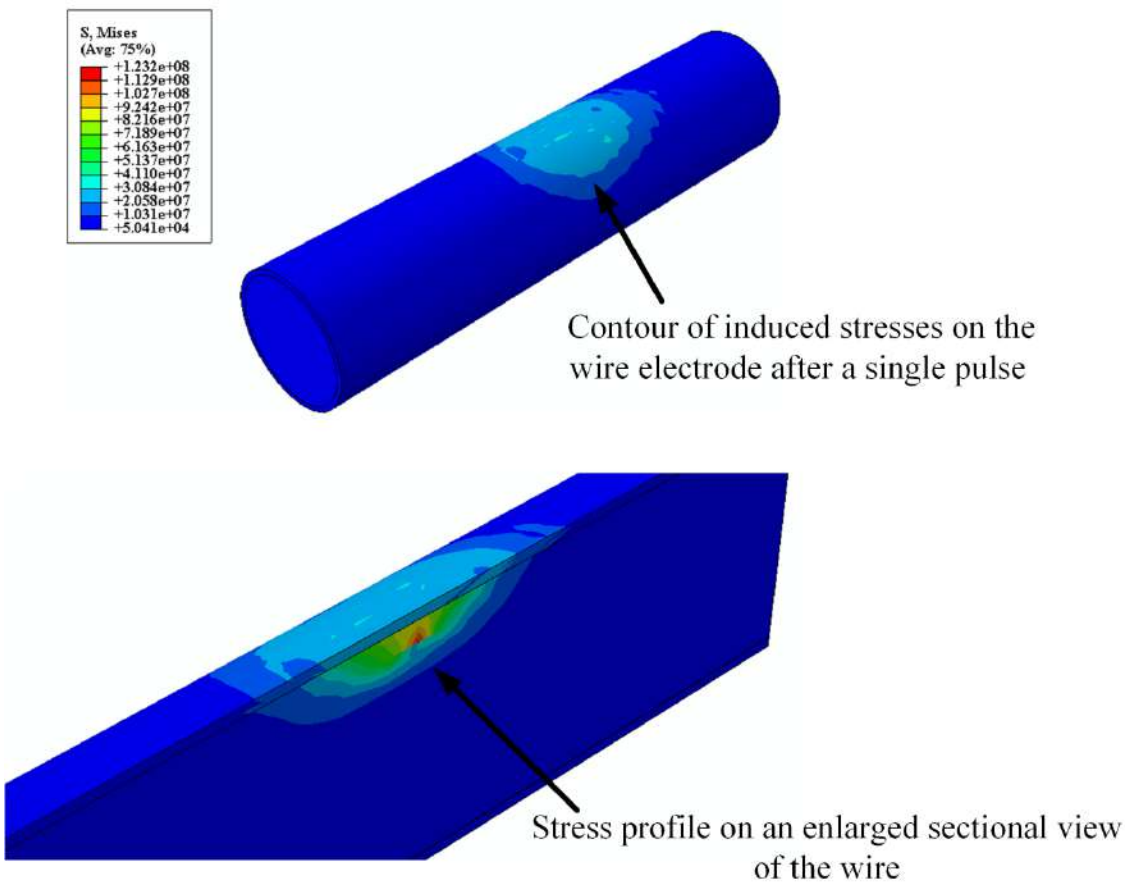

Figure 7.10 Stress contour on the wire electrode

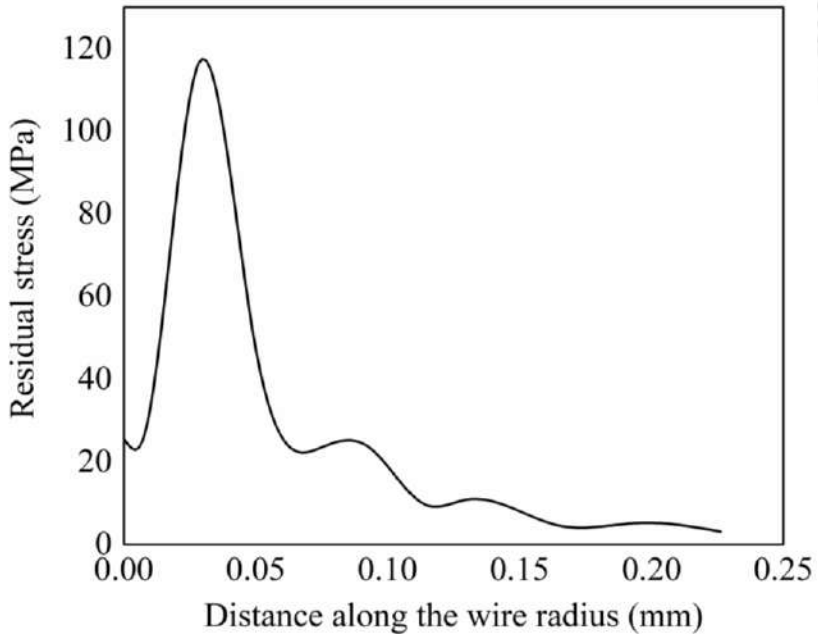

Figure 7.11 Variation of residual stress along the wire depth direction

Table 7.6 Values of temperatures obtained and residual stresses on the wire electrode at different process sets

Serial No.	Discharge voltage (V)	Discharge current (A)	Pulse on-time (µs)	Pulse off-time (µs)	Temperature at the end of t_{off} (K)	Peak temperature at the end of t_{on} (K)	Peak residual stress (MPa)
1	60	4	4	2	978.5	1873	76.09
2	60	4	8	4	483.3	1603	122.6
3	60	4	16	6	438.6	996.5	123.2
4	60	6	4	2	1382	2560	141.1
5	60	6	8	4	653.6	1883	179.5
6	60	6	16	6	503.6	1245	177.2
7	60	8	4	4	997.4	3062	174.5
8	60	8	8	6	584.3	2161	193.7
9	60	8	16	2	948.2	1446	298.6
10	85	4	4	6	500.2	2569	109.6
11	85	4	8	2	1089	2109	194.4
12	85	4	16	4	564.6	1404	210.1
13	85	6	4	4	1120	3572	185.4
14	85	6	8	6	644.6	2610	209.5
15	85	6	16	2	1089	1700	325.4
16	85	8	4	6	897.2	4292	210
17	85	8	8	2	1799	2975	332.9
18	85	8	16	4	993.7	2147	351

7.4 Computation of crater volume generated in the wire

The developed numerical model records the peak temperature obtained on the wire surface after every process set. The wire material starts melting and vaporizing when the temperature exceeds the melting point of the wire material. Material removal from the wire causes wire erosion, which degrades the wire strength and increases the probability of wire rupture. In the present work, the peak temperature at the end of discharge duration is recorded after every pulse, which is used to calculate the crater volume generated in the wire. The crater width

and the crater depth are computed numerically at the end of pulse on-time for every process set when the temperature exceeds the melting point of wire material. Figures 7.12 and 7.13 depict the crater width and crater depth on the wire computed numerically after a single pulse for the process set: V = 85 V, I = 8 A, t_{on} = 16 µs, t_{off} = 4 µs. The temperature generated during the discharge is plotted along the longitudinal axis of the wire. The crater width is determined by calculating the distance where the temperature exceeds the melting point of the outer zinc coating. For calculating the crater depth, the temperature is plotted along the wire radius and the distance was calculated where the temperature exceeds the melting point of brass.

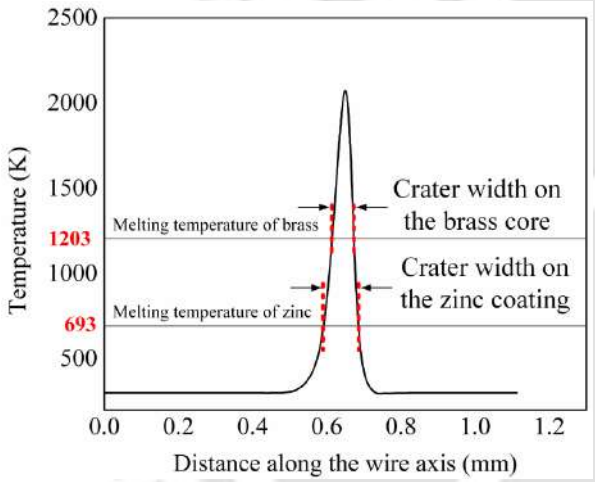

Figure 7.12 Numerically computed crater width on the wire for process set: V = 85 V, I = 8 A, t_{on} = 16 µs, t_{off} = 4µs

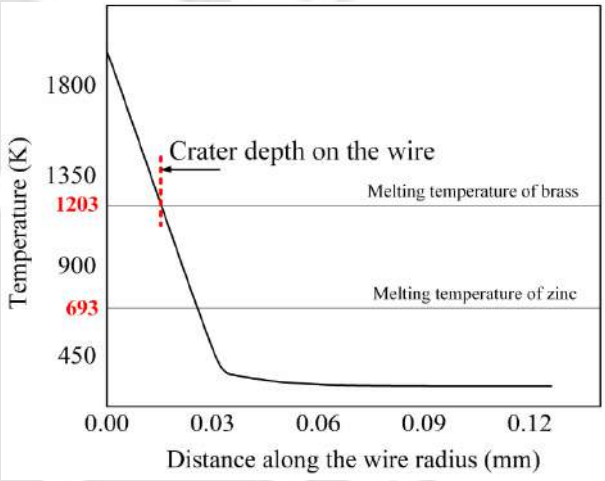

Figure 7.13 Numerically computed crater depth on the wire for process set: V = 85 V, I = 8 A, t_{on} = 16 µs, t_{off} = 4µs

The crater volume V_c (µm^3) generated on the wire electrode after a single discharge is calculated as (Chen et al. (2018))

$$V_c = \frac{1}{2}\pi R_c^2 D_c \tag{7.8}$$

where R_c is the radius of discharge crater (µm) and D_c is the depth of discharge crater (µm).

7.5 Experimental validation of the developed numerical model

7.5.1 Validation of crater volume generated in the wire

For validation of the developed model on the zinc-coated brass wire, the volume of material removed per discharge cycle obtained numerically was compared to the experimentally obtained values. WEDM experiments were performed on the WEDM machine (MAKE JK MACHINES, MODEL EC032) with Ti-6Al-4V as the workpiece. Zinc coated brass wire with 0.25 mm diameter was used as the wire tool electrode. To measure the experimental values of crater volume on the wire, wire samples were collected after each experiment set just after the spark discharges were generated in the interelectrode gap. The cross-section samples of the wire were then prepared by vertically mounting the samples in resin. The samples were polished with emery papers of grit sizes ranging from 200–2500, followed by final polishing on velvet cloth with diamond paste. After the final polishing, the images of the wire cross-section were captured using an optical microscope and the cross-sectional area of the eroded wire samples was evaluated using IMAGEJ software. The optical image of the wire cross section for the process set V = 60 V, I = 6 A, t_{on} = 8 µs, t_{off} = 4 µs is shown in Figure 7.14. The calculated cross sectional area (A_c) of the eroded wire sample measured using IMAGEJ software is 48368.273 µm^2. The amount of material removed from the wire cross section (A_{rem}) can be calculated by subtracting the eroded cross-sectional area from the original cross-sectional area (Equation 7.9). The amount of material removed from the wire cross-section (A_{rem}) multiplied by the distance travelled by the wire during the pulse on-time (L_{on}) is assumed to give the experimental crater volume ((V_c)$_{exp}$) obtained on the wire (Equation 7.11).

$$\text{Original cross-sectional area}\left(A_0\right)=\pi R_0^2=\pi\left(125\,\mu\text{m}^2\right)=49087.38\,\mu\text{m}^2$$

$$\begin{aligned}\text{Amount of material removed from the wire cross-section}\left(A_{rem}\right)&=A_0-A_c\\&=\left(49087.38-48368.27\right)\mu\text{m}^2\\&=719.11\,\mu\text{m}^2\end{aligned}\quad(7.9)$$

$$\begin{aligned}\text{Distance travelled by the wire in a single pulse on-time}\left(L_{on}\right)&=v\cdot t_{on}\\&=6\,\text{m/s}\times 8\times10^{-6}\,\text{s}\\&=48\,\mu\text{m}\end{aligned}\quad(7.10)$$

Experimentally obtained crater volume on the wire $(V_c)_{\exp} = A_{rem} \cdot L_{on}$

$$= 719.11 \times 48\,\mu m^3 \quad (7.11)$$
$$= 34517.28\,\mu m^3$$

The experimental crater volume for this corresponding process set is 34517.28 μm^3, which is in close agreement with the numerically computed value (36475.796 μm^3) with an absolute deviation of 5.67 %. Table 7.7 shows the comparison between the numerically computed V_c values and the experimentally obtained V_c values on the wire at different sets of machining parameters. The average deviation is 7.25 %, which proves the validity of the developed model.

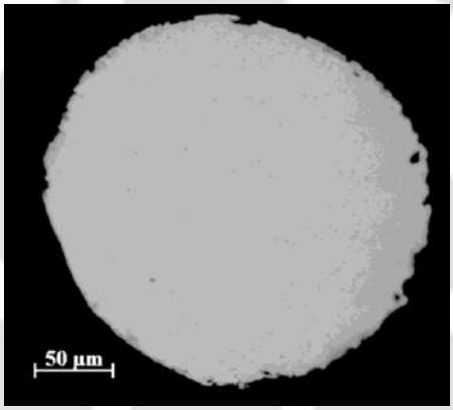

Figure 7.14 Wire cross-sectional image for the process set:
V = 60 V, I = 6 A, t_{on} = 8 µs, t_{off} = 4µs

Table 7.7 Comparison between numerically computed and experimentally obtained crater volumes on the wire

Serial no.	Discharge voltage (V)	Discharge current (A)	Pulse duration (µs)	Pulse off-time (µs)	Numerical crater volume on the wire (μm^3)	Experimental crater volume on the wire (μm^3)	Absolute deviation (%)
1	60	6	8	4	36475.79	34517.28	5.67
2	85	8	4	6	37326.37	37625.81	0.79
3	60	8	8	6	51866.57	58439.62	11.24
4	85	4	4	6	18544.43	17258.57	7.45
5	85	8	16	4	51375.25	57799.48	11.11

Average deviation 7.25 %

7.6 Estimation of a wire safety factor for the zinc coated brass wire

It was observed from the developed model that the residual stresses induced in the zinc coated brass wire is well below the yield point of brass (400 MPa); however, the induced stresses exceed the yield strength of the outer zinc coating. Since the zinc layer is just an outer coating of a few microns over the brass core, thus exceeding the yield strength of zinc will not actually hinder the strength of the wire. Hence, the stresses induced during a single pulse in the zinc coated brass wire do not induce the probability of failure as the residual stresses are well within the safety limit of the wire. It was however observed that the temperature generated in the zinc coated brass wire exceeds the melting point of zinc (693 K) and brass (1203 K), which causes wire erosion and degrades the wire strength. Wire breakages were also observed at certain process sets. Thus, the strength of the zinc coated brass wire was estimated based on the amount of material eroded from the wire surface.

The numerically computed crater width and crater depth generated in the wire during the single spark phenomenon were used to determine the crater volume. Table 7.8 shows the crater width, crater depth and crater volume at different sets of machining parameters. Wire samples were collected after every process set just after the spark was produced in the interelectrode gap. The collected wire samples were carefully examined using FESEM. It was observed that the wire experienced breakage at certain process sets almost instantaneously as the sparks were produced. Figure 7.15 shows the broken wire tip for the process set: V = 60 V, I = 8 A, t_{on} = 8 µs, t_{off} = 6 µs. The numerically computed crater volume for the corresponding process set is 51866.57 µm^3. The broken wire samples were examined carefully and it was noted that wire breakages were observed for the input conditions where the crater volume exceeded the value of 51866.57 µm^3. Thus, this value of V_c can be considered as unsafe for machining in terms of wire health. Therefore, it can be inferred that the crater volume value of 51375.25 µm^3, (lower than 51866.57 µm^3) for the process set: V = 85 V, I = 8 A, t_{on} = 16 µs, t_{off} = 4 µs, can be considered as the threshold value of crater volume (V_c) without wire failure. Material removal from the wire tool diminishes the wire strength and it breaks off when the wire erosion exceeds the safety limit.

Table 7.8 Numerically computed crater volumes in the wire at different process sets

Serial No.	Discharge voltage (V)	Discharge current (A)	Pulse on-time (µs)	Pulse off-time (µs)	Crater width (µm)	Crater depth (µm)	Numerically computed crater volume (μm^3)
1	60	4	4	2	35.72	21.37	10704.31
2	60	4	8	4	37.89	22.6	12734.95
3	60	4	16	6	40.49	10	6437.34
4	60	6	4	2	41.6	30.31	20590.08
5	60	6	8	4	53.31	32.7	36475.79
6	60	6	16	6	62.34	10	15256.08
7	60	8	4	4	46.20	34.10	28572.36
8	60	8	8	6	60.67	35.90	**51866.57***
9	60	8	16	2	75.17	10	22176.55
10	85	4	4	6	39.45	30.36	18544.43
11	85	4	8	2	53.16	31.24	34640.99
12	85	4	16	4	62.4	10	15283.01
13	85	6	4	4	45.87	36.8	30387.02
14	85	6	8	6	61.82	38.75	**58138.09***
15	85	6	16	2	79.9	11.31	28329.71
16	85	8	4	6	49.07	39.5	37326.37
17	85	8	8	2	65.29	41.5	**69433.29***
18	85	8	16	4	92.40	15.33	51375.25

*Wire breakage

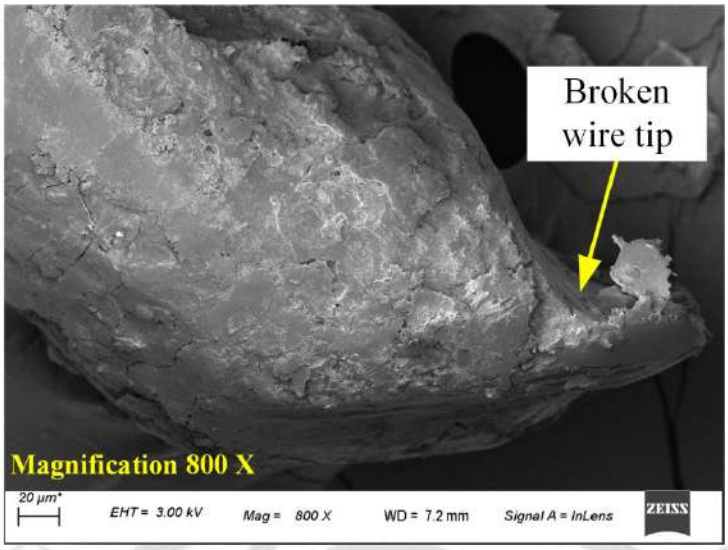

Figure 7.15 Broken wire tip for the process set: $V = 60$ V, $I = 8$ A, $t_{on} = 8$ µs, $t_{off} = 6$ µs

7.7 Parametric studies

The effects of various process conditions on the temperature obtained and the residual stresses originated in the zinc coated brass wire during a single pulse cycle were studied. The influence of input parameters on the crater volume generated in the wire was also investigated. Parametric studies shall provide suitable knowledge to optimize the input parameters in order to predict and restrict the wire failure process.

7.7.1 Effects of process parameters on temperature generated in the wire

Figures 7.16 – 7.19 show the effects of process parameters on the temperature obtained in the wire. The peak temperature in the wire increases with an increase in voltage and current due to an increase in discharge energy. Higher discharge energy produces more heat, which also increases the material removed from the wire surface when the temperature exceeds the melting point of the wire material. However, the peak temperature was observed to have a decreasing trend when the pulse on-time increases. At larger values of pulse on-time, the spark radius increases (Equation 7.6) which distributes the heat over a larger wire surface. This causes heat conduction over a larger area thus reducing the peak temperature obtained in the wire. However, the thermally affected region increases with the increase in pulse on-time.

Wire velocity also plays an important role in determining the peak temperature attained by the wire. At higher wire velocities, the peak temperature attained by the wire

decreases as the wire surface gets very little time to attain high temperatures. At lower wire velocities, the heat flux traverses over the wire surface at very low speed thus causing an increase in peak temperature and localized material ablation.

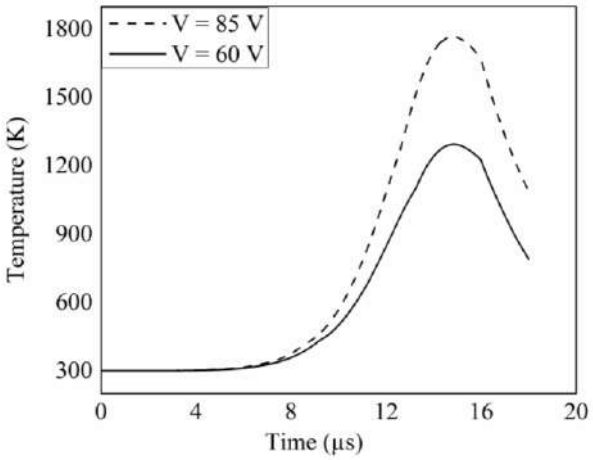

Figure 7.16 Effect of discharge voltage on temperature distribution (I = 6 A, t_{on} = 16 μs, t_{off} = 2 μs)

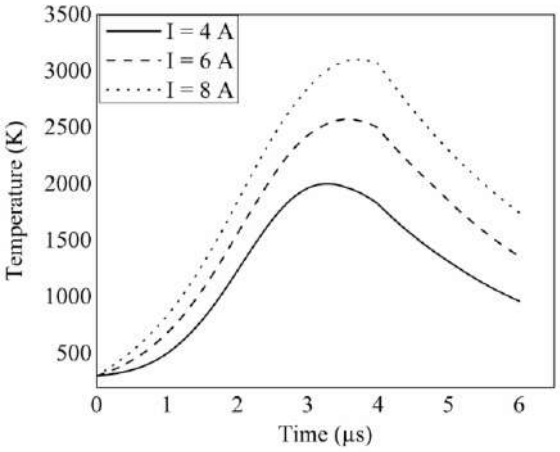

Figure 7.17 Effect of discharge current on temperature distribution (V = 60 V, t_{on} = 4 μs, t_{off} = 2 μs)

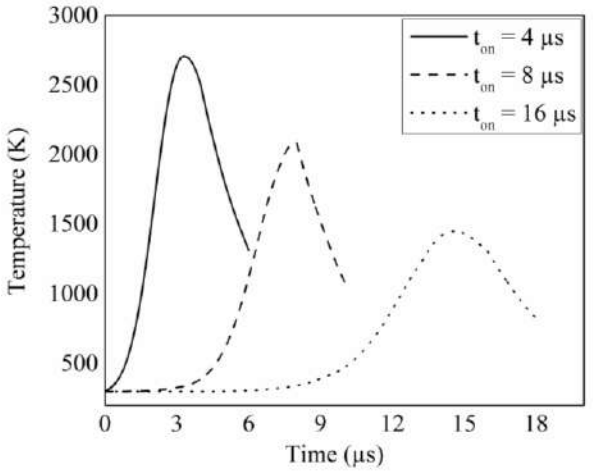

Figure 7.18 Effect of pulse on-time on temperature distribution (V = 85 V, I = 6 A, t_{off} = 4 μs)

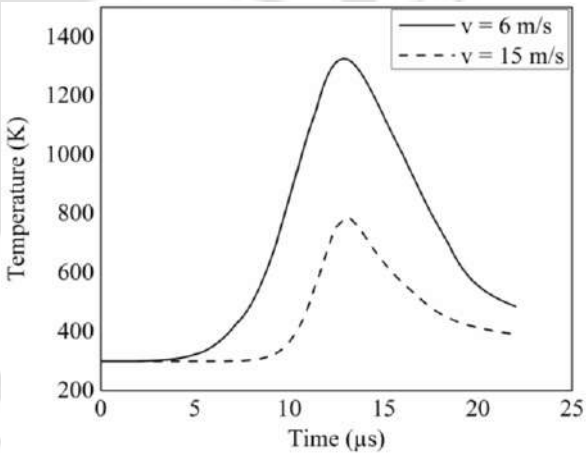

Figure 7.19 Effect of wire velocity on temperature distribution (V = 60 V, I = 6 A, t_{on} = 16 μs, t_{off} = 6 μs)

7.7.2 Effects of process parameters on residual stresses generated in the wire

The influence of process parameters on the residual stress distribution in the wire was investigated. It was observed from Figures 7.20 and 7.21 that the peak residual stresses in the

wire observed an increasing trend with increasing discharge voltage and discharge current due to increasing discharge energy. The equivalent residual stresses along the wire axis first increases and then decreases during the cooling period. Increase in discharge energy increases the temperature produced in the wire, which produces higher thermally induced stresses in the wire. The peak value of residual stresses also increases distinctively with input power as an increase in peak temperature causes an increase in thermal stresses in the heated region. Further, it can be observed from Figures 7.20 and 7.21 that the residual stress profile is independent of the input power. These stresses are produced on the wire surface. It was noted that for the zinc coated brass wire, the peak residual stresses was observed not on the surface but at a certain depth beneath the surface.

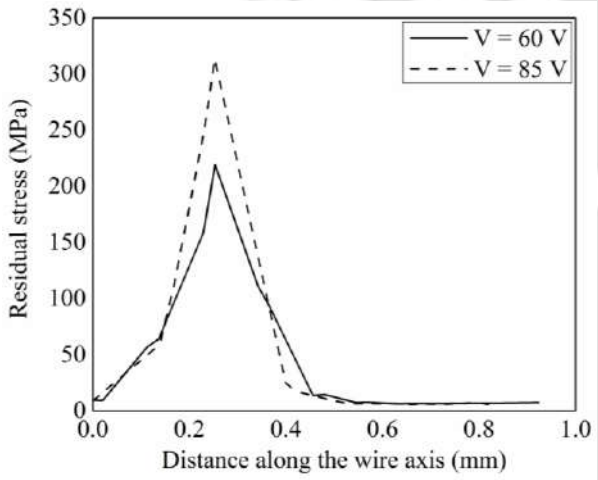

Figure 7.20 Effect of discharge voltage on residual stress distribution
(I = 6 A, t_{on} = 16 µs, t_{off} = 2 µs)

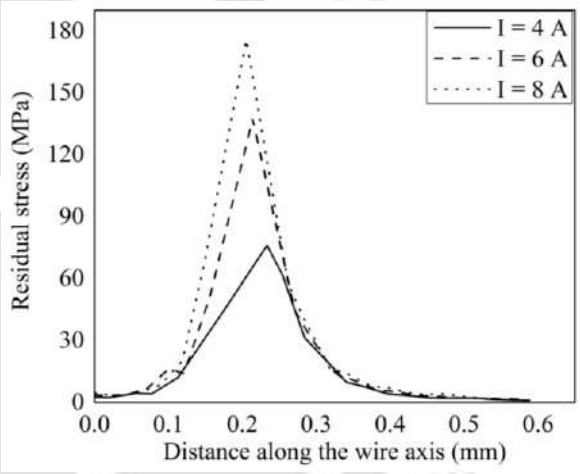

Figure 7.21 Effect of discharge current on residual stress distribution
(V = 60 V, t_{on} = 4 µs, t_{off} = 2 µs)

7.7.3 Effects of process parameters on material removed from the wire

High temperature gradients produced during WEDM cutting operation removes material from the wire tool. Excessive wire wear is detrimental to wire health and wire life. Thus, the effects of machining parameters on the amount of material removed from the wire have been studied in this section. Optimization of the input parameters is essential in order to minimize the amount of material eroded from the wire surface and prohibit the wire failure. It was observed that with increasing discharge voltage and discharge current, the crater width and crater depth increases due to increase in discharge energy (Figures 7.22, 7.23, 7.25 and 7.26). Higher discharge energy increases the temperature obtained and causes higher material

erosion from the wire surface. The heat flux increases at higher values of voltage and current, which causes higher temperature generation and hence higher erosion from the wire tool. Accordingly, the crater volume also observed an increasing trend with increasing discharge voltage and discharge current (Figures 7.24 and 7.27).

It was however noted from Figure 7.23 that there was a negligible change in crater depth at lower levels of current. The probable reason behind this is that at lower current values, the heat conduction along the depth direction is less due to less discharge energy, thus producing insignificant changes in crater depth. The crater depth showed a significant increase with voltage at higher current levels. It was further observed from Figure 7.23 that at lower levels of voltage, the crater depth remains almost constant irrespective of current when the pulse on-time was kept at a constant level of 16 µs. However, the crater depth varies largely with current at higher values of discharge voltage. The reason behind this can be attributed to the fact that at lower voltage levels, the discharge energy is low which results in less conduction of heat along the radial direction of the wire. On the contrary, it was observed from Figure 7.26 that the crater depth increases gradually with current at low voltage levels (V = 60 V), when the pulse duration is kept at a low level (t_{on} = 4 µs). The reason behind this is because at larger values of pulse on-time, the heat conduction along the depth direction decreases due to increase in spark radius. The heat flux intensity decreases, which further decreases the change in crater depth.

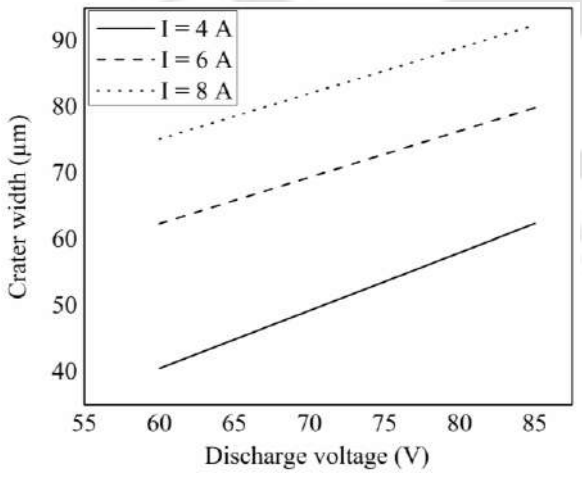

Figure 7.22 Effect of discharge voltage on crater width generated in the wire (constant parameter: t_{on} = 16 µs)

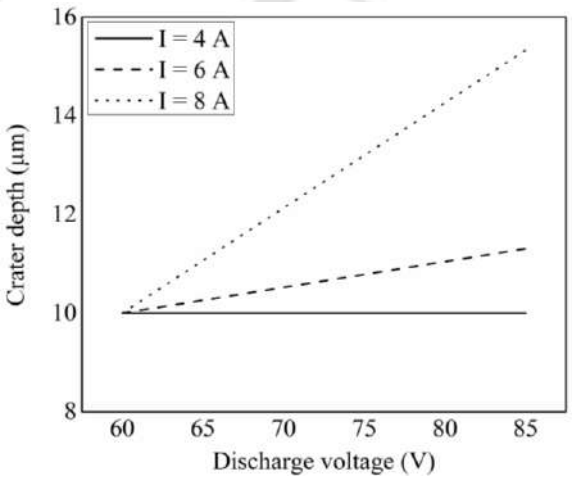

Figure 7.23 Effect of discharge voltage on crater depth generated in the wire (constant parameter: t_{on} = 16 µs)

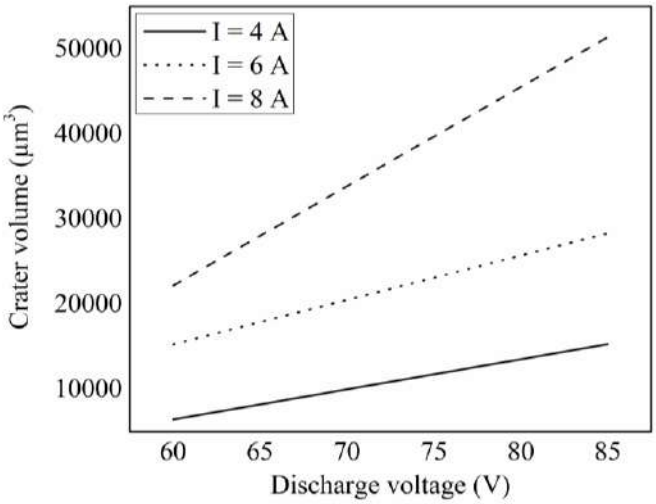

Figure 7.24 Effect of discharge voltage on crater volume generated in the wire (constant parameter: t_{on} = 16 μs)

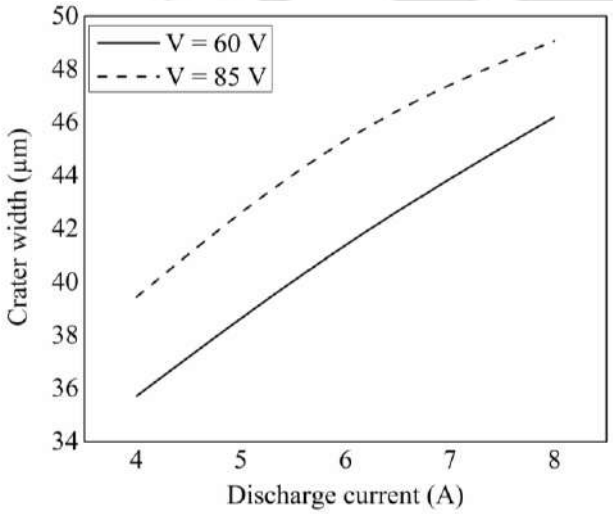

Figure 7.25 Effect of discharge current on crater width generated in the wire (constant parameter: t_{on} = 4 μs)

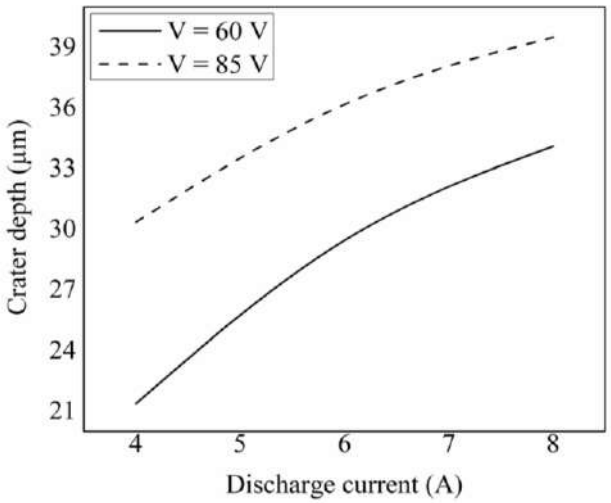

Figure 7.26 Effect of discharge current on crater depth generated in the wire (constant parameter: t_{on} = 4 μs)

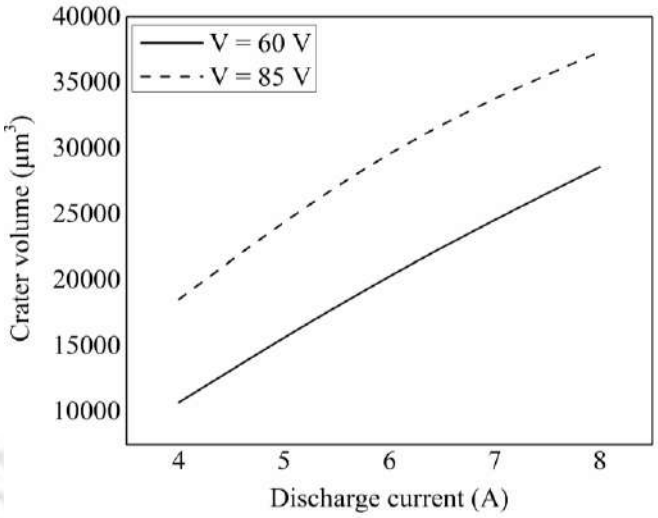

Figure 7.27 Effect of discharge current on crater volume generated in the wire (constant parameter: t_{on} = 4 μs)

With increasing pulse duration, the crater width increases (Figure 7.28). This is because, the spark radius increases at larger values of pulse duration, which increases the width of the thermal affected region and hence increases the crater width. However, with increasing pulse on-time, it was observed that the crater depth first observed a slightly increasing trend and then starts decreasing (Figure 7.29). It may be due to the fact that, as the discharge duration increases, the heat flux intensity decreases due to larger spark radius. This reduces the heat conduction along the depth direction resulting in lesser crater depth at higher pulse on-times. As a result of this, crater volume (V_c) on the wire first increases with increases in pulse duration and then decreases at further higher values of pulse on-times (Figure 7.30). Moreover, at higher values of pulse duration, the molten material of the wire may get resolidified within the discharge time and redeposit on the wire surface which further decreases the crater depth.

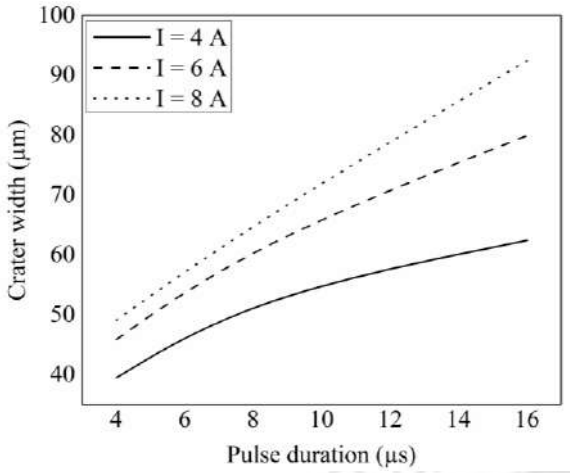

Figure 7.28 Effect of pulse duration on crater width generated in the wire (constant parameter: 85 V)

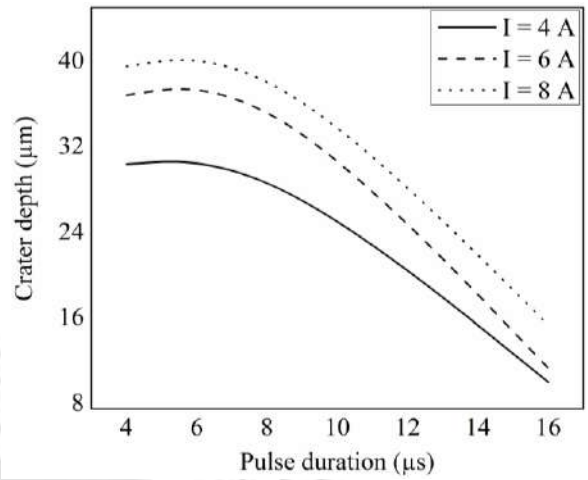

Figure 7.29 Effect of pulse duration on crater depth generated in the wire (constant parameter: 85 V)

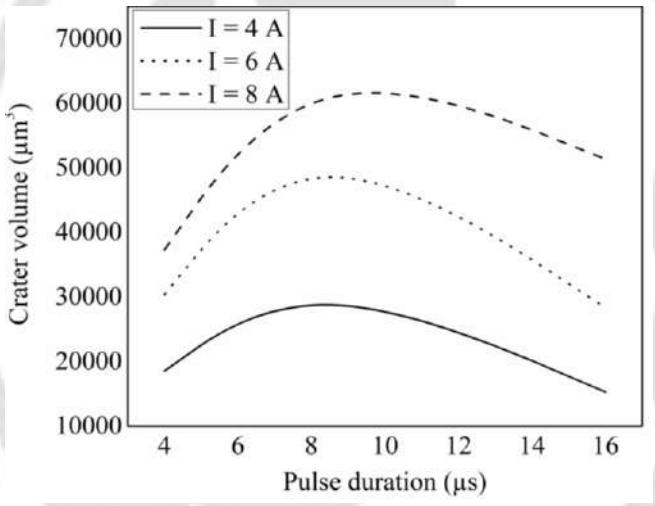

Figure 7.30 Effect of pulse duration on crater volume generated in the wire (constant parameter: 85 V)

7.8 Comparison between molybdenum wire and zinc coated brass wire

The three-dimensional thermo-mechanical finite element models have been developed for both the molybdenum wire (refer chapter 3) and zinc coated brass wire. It has been observed that the characteristics of both the wires are quite different in terms of temperature and stresses generated during machining. The numerical model predicted that the temperatures generated in the molybdenum wire were lower than the melting point of molybdenum (2896 K) during a single discharge phenomenon. Thus, material erosion does not occur during a single pulse for the molybdenum wire. However, it was noted that the stresses induced in the

molybdenum wire exceeded the yield strength of the wire material (600 MPa). Thus, the strength of the molybdenum wire was estimated based on the amount of stresses induced in the wire. A residual stress value of 976.7 MPa on the molybdenum wire was found to be the threshold value beyond which the wire strength degrades and becomes prone to failure. On the contrary, the characteristics of the zinc coated brass wire were observed to be different from the molybdenum wire based on the results predicted from the developed model. Material erosion from the zinc coated brass wire was observed due to the lower melting point of zinc (693 K) and brass (1203 K) as compared to molybdenum (2896 K). The zinc coating wears off faster, thus acting as a protective layer over the brass core. However, the residual stresses induced in the zinc coated brass wire were found to be within the safe limits during a single spark cycle i.e. below the yield strength of the brass core. The strength of the zinc coated brass wire was thus estimated based on the amount of material removed from the wire. A crater volume value of 51375.25 μm^3 was considered as the threshold value of crater volume (V_c) without wire failure. Thus, it can be inferred that the strength of the wire electrode during machining depends on the wire material and its thermo mechanical characteristics.

7.9 Summary

This chapter presented in detail, the development of a three-dimensional numerical model to predict the thermo-mechanical characteristics of the zinc coated brass wire electrode during the spark discharges. The transient model for the wire tool was developed using finite element method to predict the temperature and stresses generated in the coated wire. The model was developed in a similar manner as for the molybdenum wire electrode. An empirical spark radius equation dependent on current and pulse on-time has been utilized. Gaussian distribution of heat flux with moving characteristics was incorporated in the model, which makes the model more realistic. The results predicted by the developed model were validated using experimental results. The crater volumes generated in the wire were validated experimentally by collecting the eroded wire samples and examination of the wire cross-sections in an optical microscope. The temperature and stresses generated in the wire during the discharge phenomenon are critical factors responsible for wire breakage.

It was observed that for the zinc coated brass wire, the residual stresses induced in the wire are below the yield strength of the wire core material brass. Thus, the stresses induced are within the safe limits and do not initiate failure. However, it was noted that temperature produced in the wire exceeds the melting point of the core material brass (1203 K). This causes wire erosion which degrades the wire strength. The wire strength was estimated based on the crater volume generated in the wire. It was observed that when the crater volume exceeded the value of 51375.25 μm^3, the wire experiences failure. Thus, this value of crater volume can be considered as the threshold value above which the wire is highly prone to breakage. Hence, the corresponding process conditions must be avoided to achieve uninterrupted machining.

By using the developed method, one can easily predict the deterioration of wire electrode, which will ensure uninterrupted and efficient wire electric discharge machining operation. The thermo physical analysis also showed that the peak temperature and the peak value of residual stresses achieved by the wire increase with voltage and current levels. However, peak temperature decreases with the increase in pulse on-time but increases the thermally affected region. The crater volume observed an increasing trend with increasing voltage and current due to increase of input power. The crater volume, however, initially increases with pulse duration and gradually starts decreasing at higher values of pulse on-time. The reason behind this is because at higher values of pulse duration, the heat conduction decreases along the depth direction which reduces the crater depth, resulting in a decrease of crater volume.

The following chapter presents a comprehensive experimental analysis on the erosion and deformation of a zinc coated brass wire tool during metal cutting operation. It is imperative to have a deeper understanding of the wire erosion and breakage phenomenon in order to predict and prevent wire failure. The eroded wire samples are collected after WEDM machining of Ti-6Al-4V alloy and analyzed carefully for wire damages, which have been illustrated in the next chapter.

CHAPTER 8

Experimental analysis on the erosion and deformation of zinc-coated brass wire during WEDM of Ti-6Al-4V alloy

8.0 Scope

This chapter presents a detailed experimental investigation of the erosion and deformation of a zinc coated brass wire during WEDM experiments on Ti-6Al-4V alloy. Firstly, the need to investigate the damages of coated wires during spark discharges is presented. The measurement and analysis of various wire damages and deformation during the WEDM cutting operation have been illustrated. The image processing technique as explained in chapter 6 has been employed to estimate the extent of erosion on the surface of zinc coated brass wires. The relationship between wire wear and workpiece surface roughness is also established. Moreover, the influence of different process conditions on wire erosion and on the surface quality achieved by the component has been investigated. Finally, the chapter is summarized with conclusions.

8.1 The need

With the advent of modern manufacturing technologies, coated or stratified wires are extensively used in WEDM setups. Over the years, coated wires have shown better sparking abilities as compared to uncoated cores. As already mentioned in chapter 7, zinc coated brass wires are widely used in industries due to their improved cutting speed. Moreover, zinc coated brass wires are economical as compared to the molybdenum wires. Literature reveals that scant work has been reported on erosion analysis of coated wires (Pramanik and Basak (2016), Pramanik and Basak (2018)). Thus, a need was identified to study the damages and deformation undergone by the zinc coated brass wire during WEDM process. An in-depth understanding of the wire erosion mechanism shall give a proper insight into the wire breakage phenomenon; thus predicting and preventing untimely wire failure. The role of the coating material over the brass core also needs further understanding. In order to expand the usability of coated wires, it is crucial to broaden the existing knowledge on the characteristics of zinc coated wires. Therefore, a better understanding of the zinc coated brass wire erosion

mechanism is vital to predict the probability of wire failure and uplift the machining precision.

8.2 Experimental setup and methods

The experimental methodology, setup used to perform the WEDM experiments and the measurement techniques employed to characterize the damages on the wire surface are the same as explained in sections 5.2 and 5.3 of chapter 5. WEDM experiments on Ti-6Al-4V alloy were performed on a wire EDM machine (MAKE JK MACHINES, MODEL EC032) available at central workshop, IIT Guwahati. The surface damages of eroded wires were examined with the help of field emission scanning electron microscope (FESEM) integrated with energy-dispersive X-ray spectroscopy system (EDX). The wire cross-sections were then mirror polished and observed under the optical microscope to determine the change in wire shape and size after the cutting process. The surface roughness of the workpiece samples were also measured using an optical profilometer.

8.3 Measurement and analysis of experimental results

8.3.1 Study of erosion on the zinc coated brass wire surface

Figure 8.1 shows the FESEM image of an unused zinc coated brass wire surface prior to machining. EDX analysis (Figure 8.2a) and elemental mapping (Figure 8.2 (b–h)) of an eroded wire sample shows that workpiece material adheres to the wire surface. It is because of the spattering of molten workpiece material on the wire surface due to extreme temperature rise. The mapping scan analysis of the eroded wire sample shows the distribution of parent wire material and attached workpiece material on the wire surface during machining. EDX analysis further shows the presence of carbon (C) in the spectra, which is due to the use of carbon tape during the preparation of samples for the analysis.

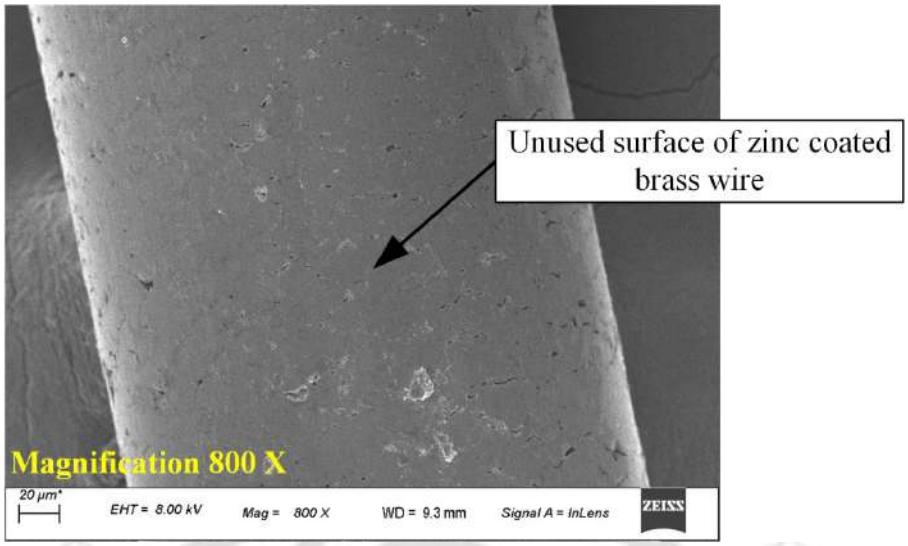

Figure 8.1 FESEM image of unused zinc coated brass wire

Figure 8.3 shows various forms of damages undergone by the zinc coated brass wire surface. The FESEM images of the collected wire samples show that the wire has severe degradation in the form of craters, pits, microholes, cracks, debris attachment, material deposition etc., which is harmful for the overall wire health. The nature and intensity of wire wear is dependent on several factors like process parameters, wire material and workpiece material. In case of zinc coated brass wires, the outer coating layer of zinc wears off faster due to its low melting point (693 K). The zinc coating provides a protection to the brass core against thermal shock as brass has a higher melting point (1203 K). Successive and random spark discharges generate huge amount of temperature, which erodes material from the zinc coating and brass core of the wire. Wire wear reduces the wire strength thus increasing the probability of wire failure.

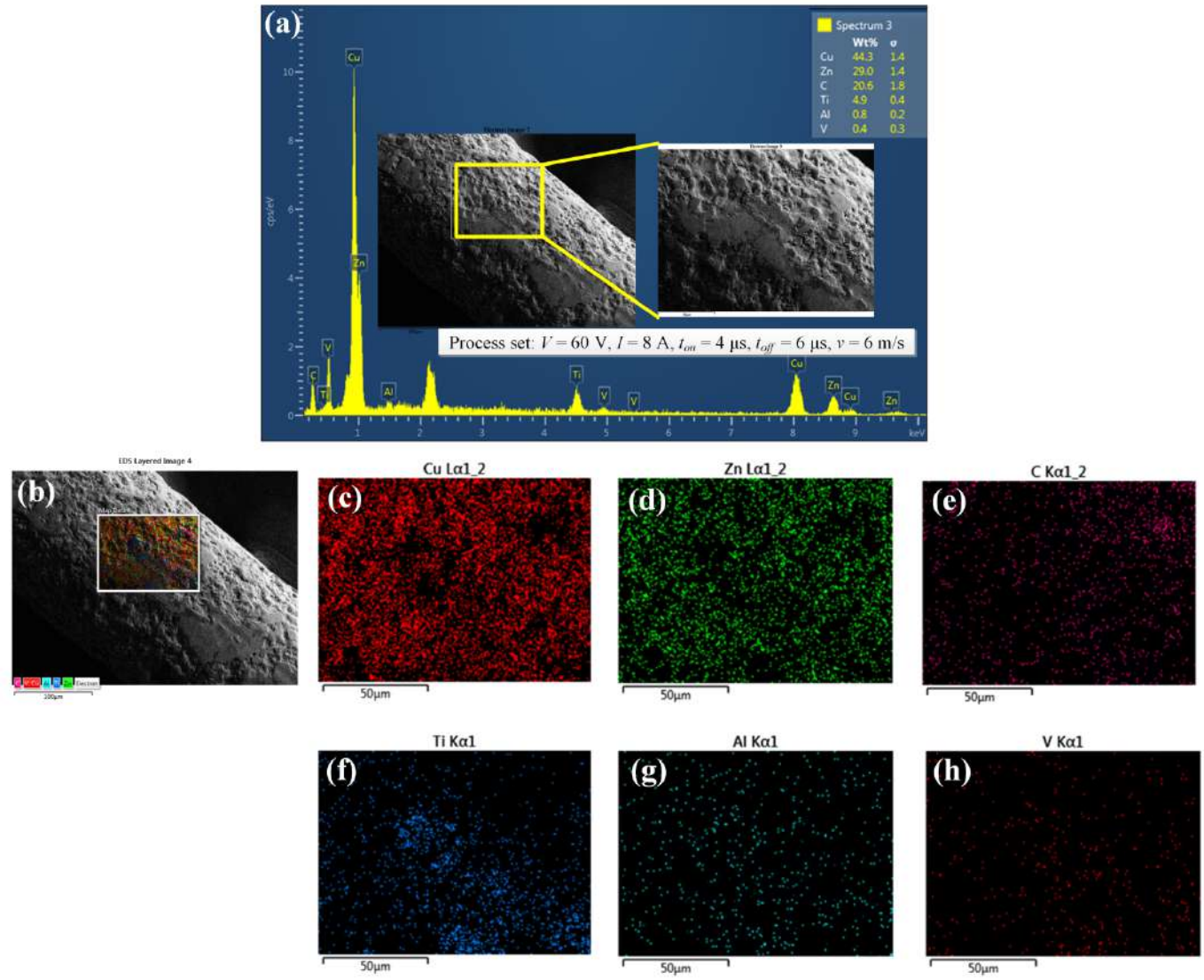

Figure 8.2 (a) EDX analysis and (b), (c), (d), (e), (f), (g) elemental mapping of an eroded wire sample for the process set: $V = 60$ V, $I = 8$ A, $t_{on} = 4$ µs, $t_{off} = 6$ µs, $v = 6$ m/s

The degradation of wire surface during machining and its primary causes have already been explained in chapter 5. An increase in wire temperature, interaction with the dielectric, generation of debris in the machining zone, and the formation of undesired sparks degrade the surface integrity of the wire. The FESEM images collected of the eroded samples of zinc coated brass wires show that the intensity of damages are severe as compared to molybdenum wire. The outer zinc coating starts eroding first and when the temperature generated exceeds the melting point of brass, severe erosion of the core material vitiate the wire strength. Figure 8.3b shows localized material ablation from the wire surface. Such

excessive wear hampers the surface integrity of the wire, which further diminishes the product quality and precision. Attachment of debris on the wire surface due to insufficient cooling time and less dielectric pressure reduces the interelectrode gap between the wire tool and workpiece (Figure 8.3c). This gives rise to undesired arc formation thus subjecting the wire surface to sudden thermal shocks, which deteriorate the wire surface quality. Insufficient cooling time also causes the resolidification and redeposition of molten material on the wire surface, which traps some gas bubbles in the resolidified region. These trapped bubbles cause the formation of microholes or micropits on the wire surface (Figure 8.3d). Visual observation of the FESEM images of eroded wire samples show that the damages undergone by the zinc coated brass wire are much severe than the molybdenum wire for the same set of process conditions. The reason behind this is that the melting point of molybdenum (2896 K) is higher than the melting point of zinc (693 K) and brass (1203 K). Sharp peaks in temperature during the discharge phenomenon originate residual thermal stresses on the wire surface. The concentration of stresses on the wire surface cause the initiation of microcracks on the wire surface (Figure 8.3e) which propagates into deeper and wider cracks (Figure 8.3f) finally causing wire rupture.

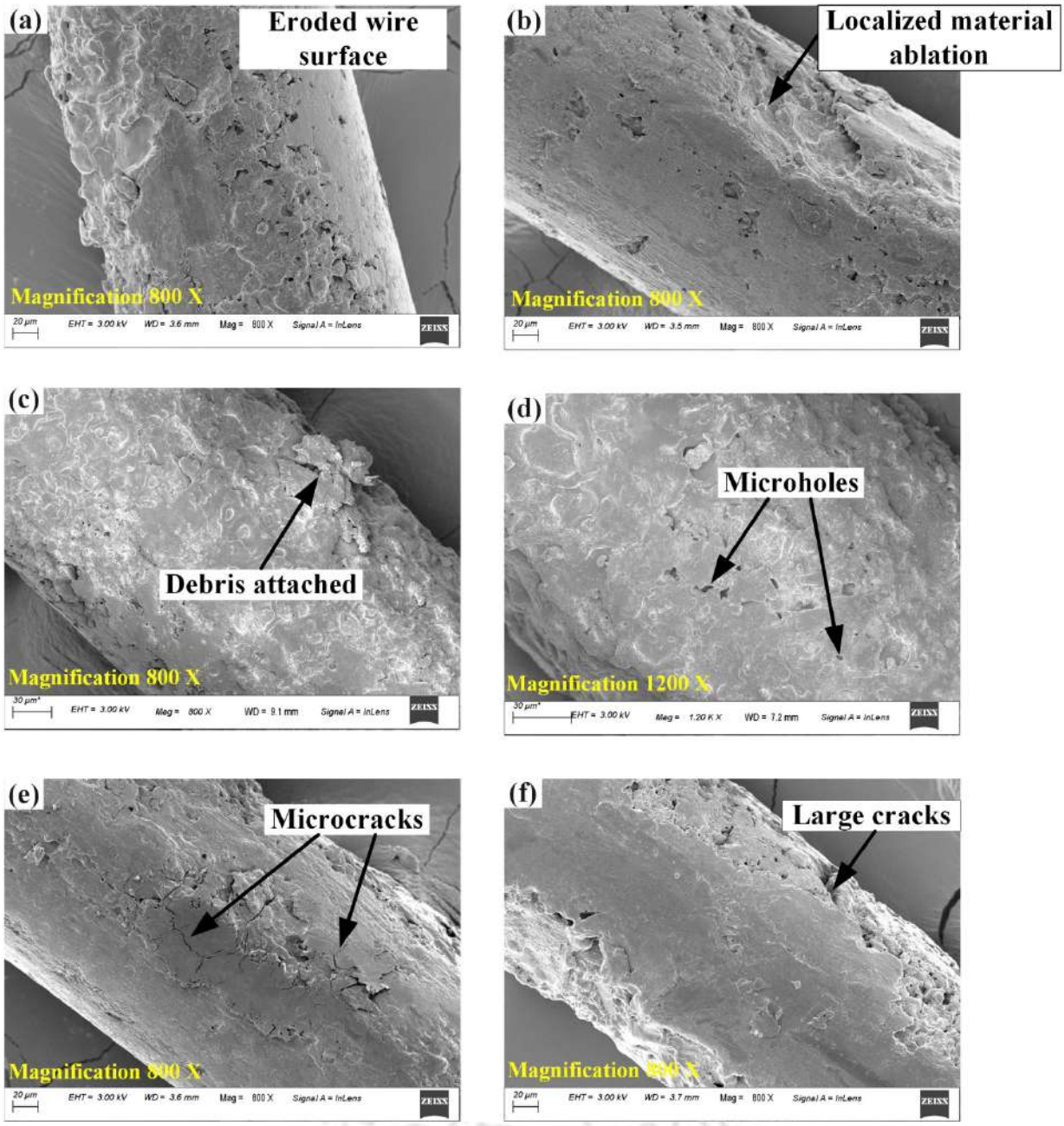

Figure 8.3 (b) localized material ablation, (c) attachment of debris, (d) formation of microholes, and (e), (f) formation of cracks on the wire surface

8.3.2 Measurement of deformed wire cross section diameters

The optical images of the cross-sections of unused zinc coated brass wire before and after the etching process are obtained. The unused wire is circular with a diameter of approximately 250 μm (Figure 8.4a). The etching of the coated wire was carried out using the reagent recommended by Beckert and Klemm (1984), with the following composition: 5 g of $FeCl_3$

and 100 cm^3 of 10% hydrochloric acid. A uniform grain structure with very minute grains was observed after etching of polished wire sample, which appears to be a result of the wire drawing process (Figure 8.4b). The etched wire sample shows the outer zinc coating on the wire periphery. The cross-sections of the eroded wire samples were prepared at various sections along the wire length and examined under optical microscope to investigate the deterioration in wire form as the machining proceeds. Figure 8.4 (c–h) shows the cross sections of eroded wire samples at different sections for the process condition: V = 85 V, I = 4 A, t_{on} = 16 µs, t_{off} = 4 µs, v = 6 m/s. It was observed that the wire cross section loses its circularity and undergoes deformation during machining in two major steps, (i) an increase in wire diameter on one side at initial stage of machining and, (ii) decrease in wire diameter than the original diameter on both sides of the wire cross section as the machining proceeds. The wire suffers severe plastic degradation because of steep temperature slope generated during the discharge phenomenon. The zinc coating wears off quickly as the discharge occurs during the metal cutting operation. After the outer layer of zinc wears off, the inner brass core starts eroding which degrades the wire strength. As the induced stresses in the wire exceed the yield stress of the wire material, the wire deformation starts in the plastic zone, which causes the distortion of the original circular shape of the wire cross-section. Wire deformation causes geometrical error of machined components and diminishes the surface quality of machined surface. The reason behind the change in wire shape can be attributed to a combined effect of (a) temperature rise, (b) plastic deformation when stresses originated crosses the yield point of the wire material, (c) mechanical tension applied to the wire to keep it vertically straight and (d) continuous movement of the wire electrode.

The pattern of deformation of the zinc coated brass wire is similar as compared to the molybdenum wire. In the initial stage of machining, the wire diameter increases than the original diameter on one side and decreases on the other side (Figure 8.4c and 8.4d). As the wire proceeds further along the feed direction, a steady decrease of wire diameter was observed due to the melting and vaporization of wire material above the melting point. The diameters on both sides of the wire cross-sections are found to be unequal and become smaller than the original one (Figure 8.4e, 8.4f, 8.4g, 8.4h). The overall cross-sectional area of the wire is reduced, thus increasing the stress in the wire cross-section.

The deformation of the molybdenum wire due to violent spark discharges during the metal cutting operation of Ti-6Al-4V alloy has been illustrated in chapter 5. The changes in wire diameter and the wire distortion in case of zinc coated brass wire are more critical as compared to the molybdenum wire. This is because molybdenum has a higher tensile strength as compared to brass. Higher tensile strength and yield strength of the wire material is beneficial to reduce the deformation of the moving wire tool during the discharge process.

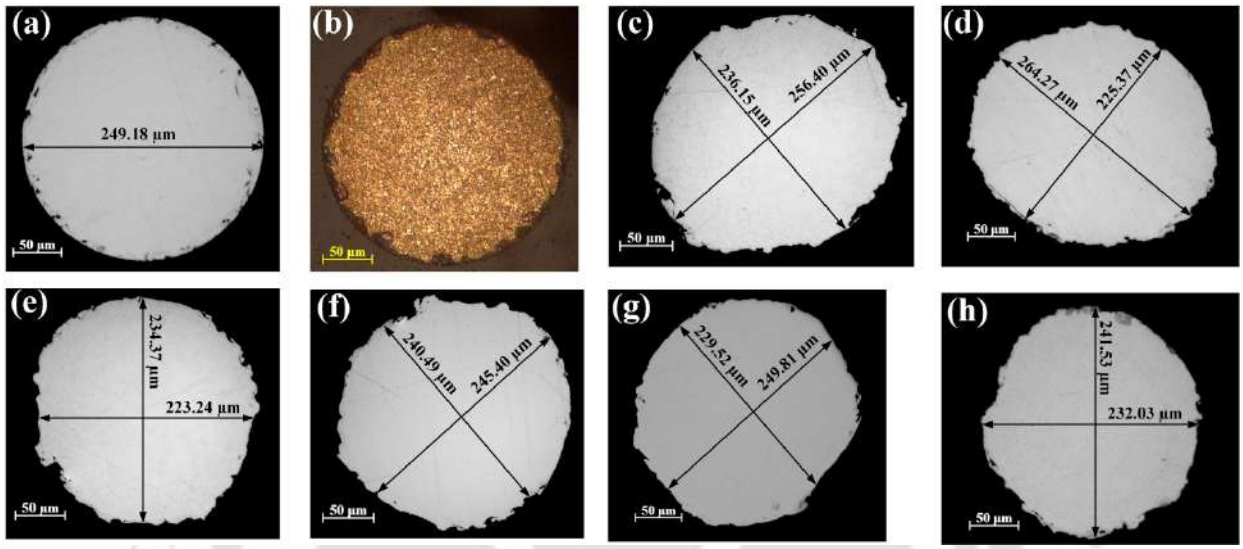

Figure 8.4 (a) unetched and (b) etched cross-sections of unused zinc coated brass wire, (c), (d), (e), (f), (g), (h) deformed wire cross-sections with unequal diameters for the process set: $V = 85$ V, $I = 4$ A, $t_{on} = 16$ µs, $t_{off} = 4$ µs, $v = 6$ m/s

8.3.3 Measurement and analysis of surface roughness of machined workpieces

The surface roughness of the workpiece samples were measured using a non-contact optical profilometer. Three samples were cut for every process set and the *Ra* value was determined for every single workpiece. The measurements were carried out at five different locations for a single sample and the average value was considered for further analysis. The results are listed in Table 8.1. Here, Ra_1, Ra_2 and Ra_3 indicate the surface roughness after 1st cut, 2nd cut and 3rd cut respectively. The blank spaces in the table indicate wire breakage.

Table 8.1 Average workpiece surface roughness values (*Ra*) of the experimental sets

Serial no.	Discharge voltage (V)	Discharge current (A)	Pulse on-time (µs)	Pulse off-time (µs)	Wire speed (m/s)	Surface roughness (µm)			
						Ra_1	Ra_2	Ra_3	Avg.
1	60	4	4	2	3	2.79	2.84	2.89	2.84
2	60	6	8	4	6	2.54	2.62	3.39	2.85
3	60	8	16	6	9	2.98	3.08	3.21	3.09
4	60	4	4	2	6	2.41	2.53	2.74	2.56
5	60	6	8	4	9	2.41	2.59	3.07	2.69
6	60	8	16	6	3	2.99	3.26	3.95	3.4
7	60	4	8	6	3	2.77	2.94	3.08	2.93
8	60	6	16	2	6	2.99	3	3.04	3.01
9	60	8	4	4	9	2.64	2.77	3.53	2.98
10	60	4	16	4	3	2.85	3.05	3.64	3.18
11	60	6	4	6	6	2.22	2.39	2.8	2.47
12	60	8	8	2	9	2.85	3.04	3.26	3.05
13	60	6	16	2	9	2.75	2.83	2.97	2.85
14	60	8	4	4	3	2.94	3.14	3.55	3.21
15	60	4	8	6	6	2.44	2.61	3.17	2.74
16	60	6	16	4	3	3.01	3.14	3.27	3.14
17	60	8	4	6	6	2.81	2.96	3.44	3.07
18	60	4	8	2	9	2.26	2.34	2.45	2.35
19	85	6	4	6	9	2.51	2.59	2.67	2.59
20	85	8	8	2	3	3.67	–	–	3.67*
21	85	4	16	4	6	2.75	2.89	3.27	2.97
22	85	6	8	6	9	2.69	2.75	3.08	2.84
23	85	8	16	2	3	3.54	–	–	3.54*
24	85	4	4	4	6	2.51	2.56	2.7	2.59
25	85	8	8	2	6	3.12	3.27	3.78	3.39
26	85	4	16	4	9	2.74	2.9	3.27	2.97

27	85	6	4	6	3	2.73	2.89	3.26	2.96
28	85	8	8	4	6	3.18	3.50	–	3.34*
29	85	4	16	6	9	2.64	2.88	3.12	2.88
30	85	6	4	2	3	2.95	3.09	3.56	3.2
31	85	8	16	6	6	3.21	3.25	3.32	3.26
32	85	4	4	2	9	2.48	2.55	2.68	2.57
33	85	6	8	4	3	2.99	3.57	–	3.28*
34	85	8	4	4	9	2.76	2.91	3.6	3.09
35	85	4	8	6	3	2.84	3.1	3.39	3.11
36	85	6	16	2	6	3.05	3.15	3.34	3.18

*Wire breakage

The experimentally obtained results were analyzed using response surface methodology (RSM) which is a well-known mathematical and statistical procedure to correlate input parameters with the response variables. Analysis of variance (ANOVA) was performed to analyze the contribution of each factor and the interaction terms on the selected response variable, i.e. *Ra* of the workpiece. This was followed by a quadratic regression analysis equation depending on the significant factors, which could predict the surface *Ra* value at any set of process conditions. The RSM methodology and ANOVA technique have been clearly explained in chapter 5. Table 8.2 shows the ANOVA table with surface *Ra* as the response characteristic using backward elimination. The combined effect of the terms $I \cdot I, t_{on} \cdot t_{on}, I \cdot t_{on}, I \cdot v, t_{on} \cdot t_{off}$ depicted important contribution. The R^2, *adjusted*-R^2 and *predicted*-R^2 values for the *Ra* values were found to be 0.9723, 0.9652 and 0.9507 respectively. It was observed that the predicted R^2 is in close agreement with adjusted R^2, which indicates that the model is able to predict a new response for any observation with 95.07 % variability.

Table 8.2 ANOVA table for surface roughness after backward elimination

Source	DF	Adj SS	Adj MS	F-Value	P-Value
Model	10	3.15229	0.31523	57.72	0
Linear	5	2.94438	0.58888	107.82	0
V (V)	1	0.28275	0.28275	51.77	0
I (A)	1	1.17445	1.17445	215.03	0
t_{on} (μs)	1	0.52376	0.52376	95.9	0
t_{off} (μs)	1	0.03085	0.03085	5.65	0.025
v (m/s)	1	0.92808	0.92808	169.92	0
I (A) · I (A)	1	0.04284	0.04284	7.84	0.01
t_{on} *(μs)*· t_{on} (μs)	1	0.04444	0.04444	8.14	0.009
I (A) · t_{on} (μs)	1	0.0923	0.0923	16.9	0
I (A) · v (m/s)	1	0.0317	0.0317	5.8	0.024
t_{on} (μs) · t_{off} (μs)	1	0.0271	0.0271	4.96	0.035
Error	25	0.13654	0.00546		
Total	35	3.28883			

The correlation between the significant input factors and their quadratic factors with the response variable (*Ra*) was obtained using a polynomial equation after discarding the non-significant terms. The regression equation derived for *Ra* in terms of linear and interaction factor is as follows.

$$Ra = 2.602 + 0.00735V - 0.1199I + 0.0963t_{on} - 0.0583t_{off} - 0.1142v + 0.02087I \cdot I - 0.002376t_{on} \cdot t_{on} - 0.00663I \cdot t_{on} + 0.00791I \cdot v + 0.00399t_{on} \cdot t_{off} \quad (8.1)$$

8.4 Estimation of a wire surface quality index for zinc-coated brass wire

A surface quality index was determined for the zinc coated brass wire surface to estimate the intensity of damages on eroded wire surfaces. The image processing technique was utilized to calculate the histogram mean of FESEM images of eroded wire samples. The methodology of image processing technique has been demonstrated in chapter 6 in detail. A histogram was plotted for the FESEM wire images to observe the change in pixel intensity at different locations using the ImageJ software.

Figure 8.5a shows the wire sample for process set: V = 60 V, I = 4 A, t_{on} = 8 µs, t_{off} = 6 µs, v = 6 m/s; and the histogram of the considered region was plotted (Figure 8.5b). The histogram mean value was evaluated as 164.98. A similar technique was applied to Figure 8.5c, which showed critical and substantial amount of wear. The corresponding histogram mean was found to be lower (118.99) i.e. the histogram is shifted towards the darker side. This is because the light intensity reduces in the region where the damage occurs, thus the pixel intensity reduces and the histogram shifts towards the darker side. It has been noted in chapter 6 that an image with a substantial amount of damage on the wire surface will produce a lower mean value of histogram. Lower mean values of wire image histogram denote a lower surface quality of the wire samples.

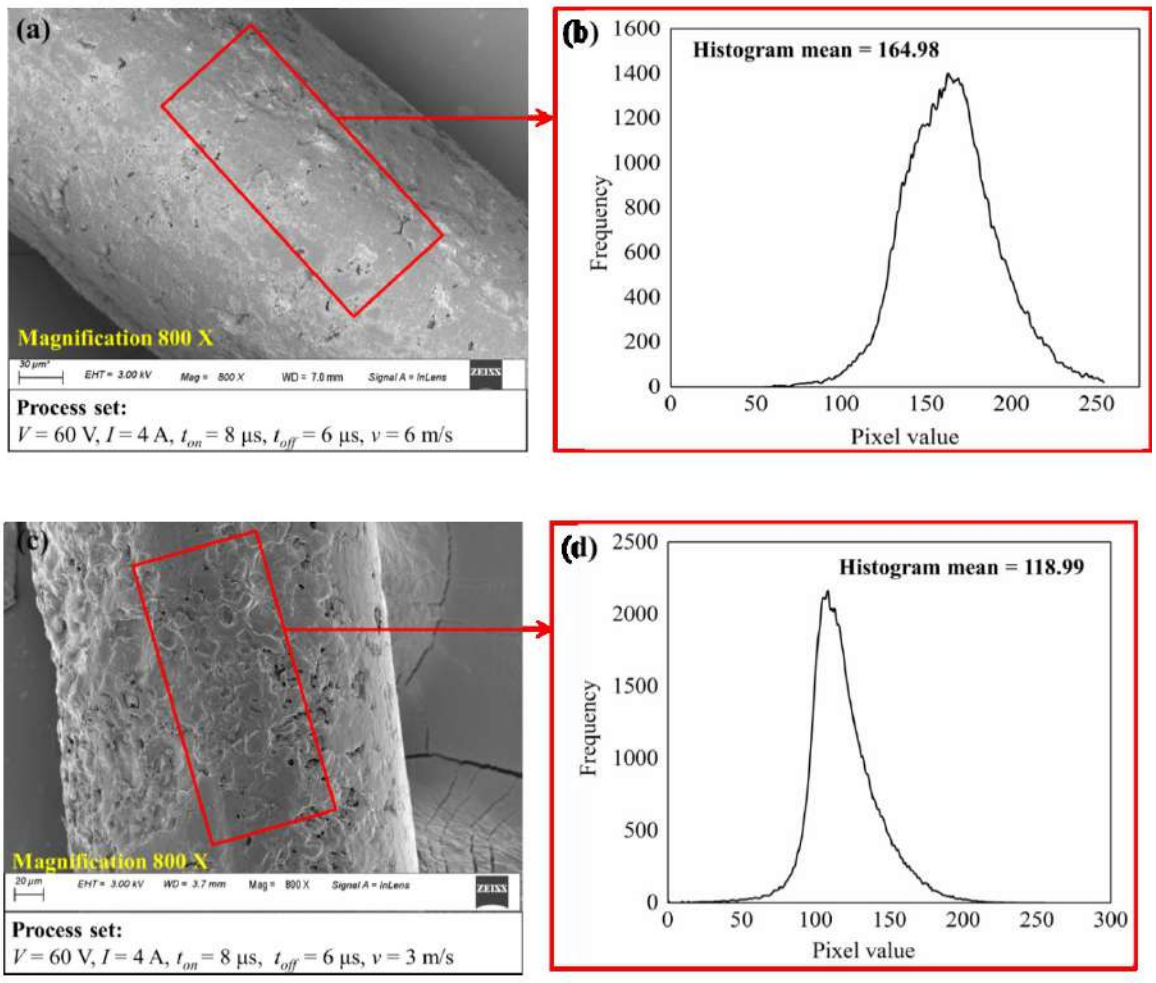

Figure 8.5 Analysis of eroded wire samples using image processing technique (a), (c) FESEM wire images after WEDM of Ti-6Al-4V and (b), (d) histogram plots of eroded wire surfaces at the chosen parameter sets.

8.5 Relationship between wire erosion and workpiece surface quality

The histogram mean evaluated using image processing technique proved to be an useful tool in establishing a relationship between wire wear and the surface roughness achieved by the workpiece, which has been explained in chapter 6. Table 8.3 depicts the histogram mean values and average surface roughness values of the workpiece at varying sets of process conditions. For the zinc coated brass wire too, it was clearly observed that the histogram mean values of the wire images decrease as the workpiece *Ra* values keep on increasing. Decreasing values of histogram mean denote higher intensity of wire surface erosion. This clearly indicates that the product surface quality degrades with wire wear.

Wire breakages were observed at certain sets of process parameters as shown in Table 8.3. Wire failure occurs due to excessive erosion from the wire surface, which degrades the wire strength enormously. It was observed in chapter 7 that the zinc coated brass wire experiences failure when the crater volume generated in the wire exceeds a certain threshold value. Excessive rise in temperature during the multiple spark discharges also generates stresses in the wire, which may be another reason of wire rupture. It was further observed from Table 8.3 that at histogram mean values lower than 117.02, wire breakages were observed. The corresponding *Ra* values also followed an increasing trend as the histogram mean value decreases. Thus, the histogram mean value of 117.02 can be considered as the threshold value below which there is a high probability of wire failure. Figure 8.6 shows a broken wire sample for the process set: V = 85 V, I = 8 A, t_{on} = 8 µs, t_{off} = 4 µs, v = 6 m/s. Understanding the morphology of broken wire samples gives a better approach to the relationship between wire wear and wire failure. It can be observed from Figure 8.6 that the wire experiences necking before failure, which is characteristic of the ductile behavior of materials. The wire diameter near the broken tip reduces and exhibits cup-cone like fracture. The yield strength of material also reduces at a higher temperature, and the fracture of material becomes ductile. A sharp tip with unsymmetrical material erosion is observed from both sides of the broken wire tip.

Table 8.3 Histogram mean values of the wire samples and workpiece *Ra* values at different input parameters

Discharge voltage (V)	Discharge Current (A)	Pulse on-time (µs)	Pulse off-time (µs)	Wire speed (m/s)	Histogram mean	Workpiece *Ra* (µm)
60	4	8	6	6	164.98	2.74
60	6	8	4	6	133.52	2.85
60	4	8	6	3	118.99	2.93
85	8	16	6	6	117.02	3.26
85	6	8	4	3	107.75	3.28*
85	8	8	4	6	103.19	3.34*
85	8	16	2	3	100.98	3.54*
85	8	8	2	3	100.01	3.67*

* Wire breakage

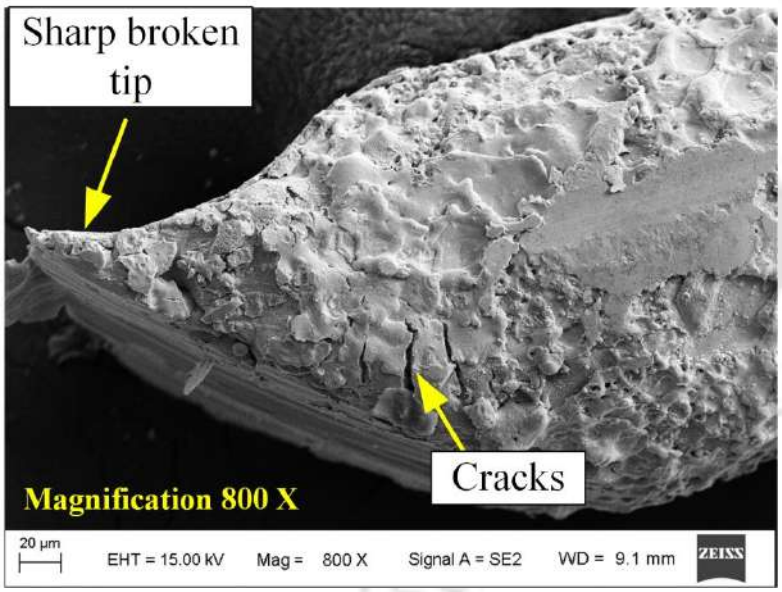

Figure 8.6 Broken wire tip for the process set: $V = 85$ V, $I = 8$ A, $t_{on} = 8$ µs, $t_{off} = 4$ µs, $v = 6$ m/s

It was further observed from Table 8.1 that the average *Ra* value gradually increases from the 1st cut to 3rd cut under the same machining condition. This trend was also observed in case of the molybdenum wire as shown in chapter 6. Figure 8.7 depicts the influence of wire wear on

workpiece *Ra* at different energy settings (Low = 0.00096 J, Medium = 0.00288 J, High = 0.01088 J). The *Ra* value increases with a rise in discharge energy as higher material erosion occurs at higher discharge energy settings, which deteriorates the workpiece surface quality. The reason behind this can be attributed to the fact that as the fresh zinc coated brass wire enters the workpiece, the surface finish of the component is at its best as the wire surface damages are at its primary stage. As the machining proceeds further for the second and third cut, the wire erodes to a substantial extent because of the violent and erosive nature of successive random discharges during the spark cycles. The wire health deteriorates continuously due to the formation of several craters, pits, and debris generation in the discharge zone. The eroded and uneven wire surface further diminishes the surface quality and integrity of the WEDMed product.

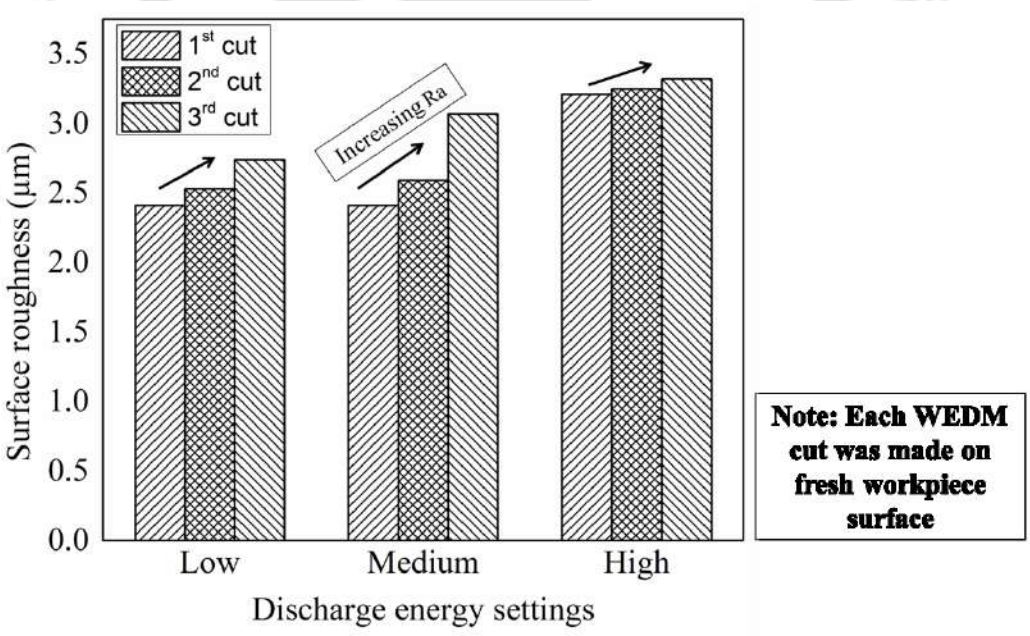

Figure 8.7 Effect of wire wear on workpiece surface roughness at different discharge energy settings

8.6 Parametric studies

8.6.1 Effects of process parameters on wire surface wear

Successive and random discharges during WEDM raise the temperature as high as 10000 °C or more due to the high plasma energy of the spark, which removes material from both the electrodes. The discharge energy increases along with increasing voltage and current causing

critical damage on the wire surface. The damages on the wire surface are minor at low levels of current due to low discharge energy (Figure 8.8a). At higher current levels, deep and wide craters are formed on the wire surface (Figure 8.8c). It was observed that the surface integrity of the wire deteriorates at higher levels of current due to generation of higher temperatures.

Longer pulse duration produces heat flux for a longer time causing severe erosion from the wire electrode due to excessive temperature rise. The thermally affected region due to spark formation is more significant at higher pulse on-time (8 μs), as shown in Figure 8.9b. It increases the generation of debris and unwanted arcs in the machining zone, which degrades the wire surface quality and increases the probability of wire failure.

The wire speed also plays a crucial role in determining the nature and intensity of wire surface wear. When the wire speed is quite low, there is a localized temperature rise because the heat flux traverses over the wire surface at a low velocity. As a result, localized material ablation takes place, causing the formation of deep craters in a particular region of the wire surface (Figure 8.10a). At higher wire speed, the wire quickly traverses the workpiece getting less time to form deep craters on the wire surface (Figure 8.10b). Thus, the wire wear at higher speed is less intense as compared to that of lesser wire velocity.

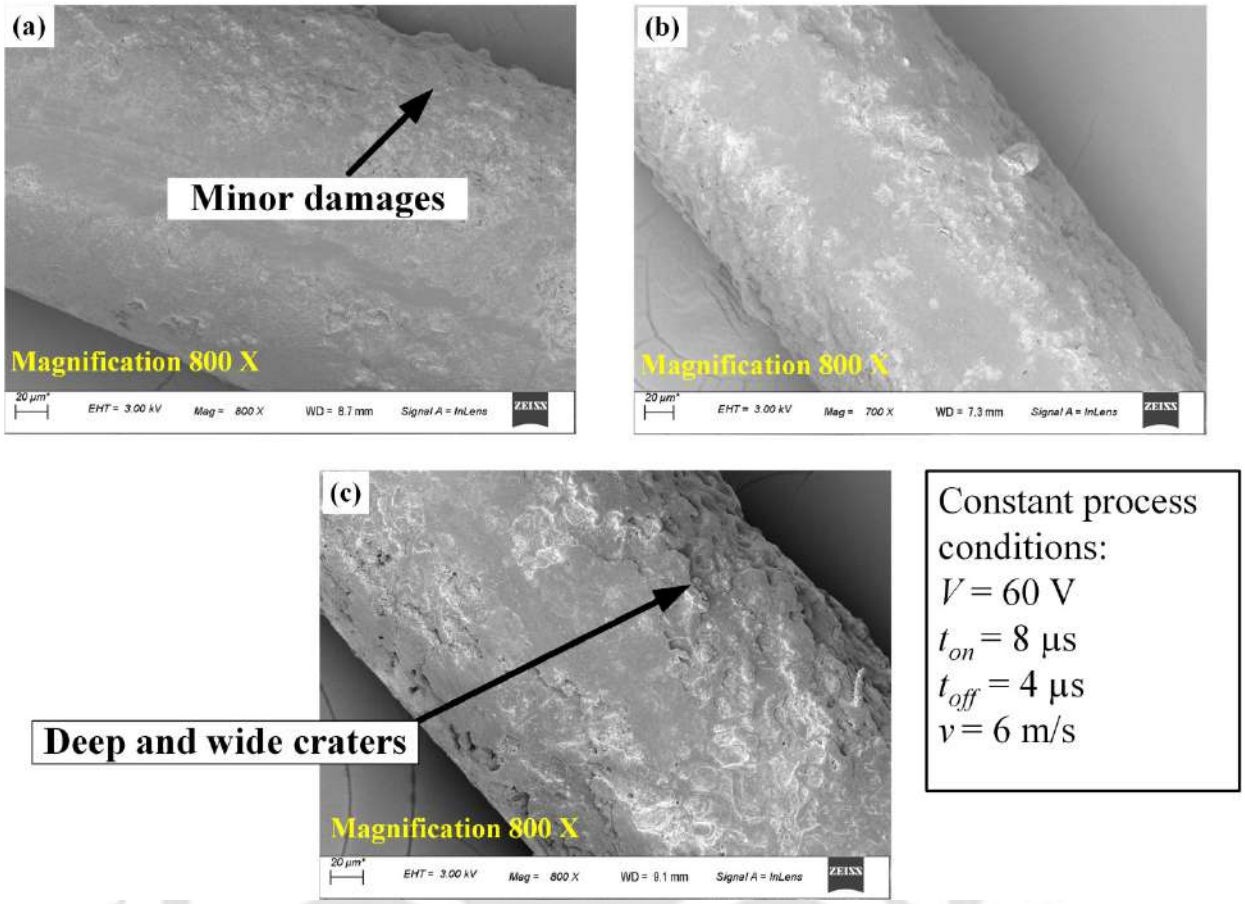

Figure 8.8 FESEM wire image after WEDM of Ti-6Al-4V at varying currents: (a) 4 A, (b) 6A, (c) 8 A

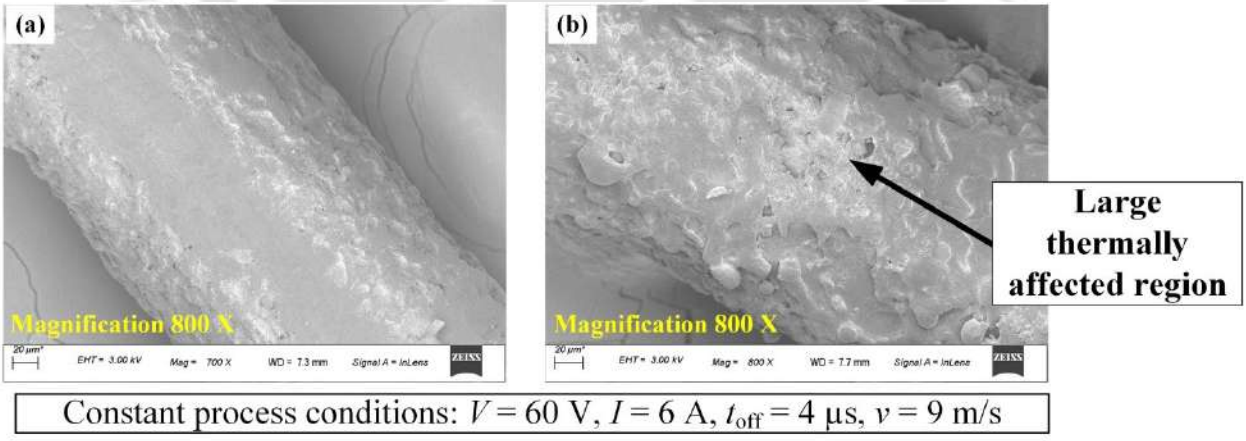

Figure 8.9 FESEM wire image after WEDM of Ti-6Al-4V at varying discharge durations: (a) 4 µs, (b) 8 µs

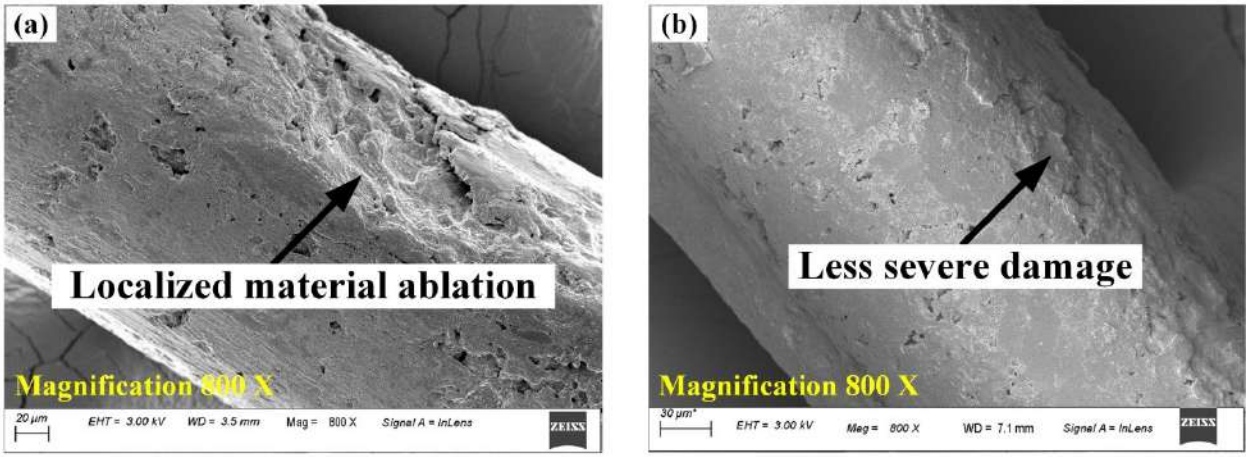

Figure 8.10 FESEM wire image after WEDM of Ti-6Al-4V at varying wire speeds: (a) 3 m/s, (b) 9 m/s

8.6.2 Effects of process parameters on workpiece surface roughness

The contribution of various input parameters viz. discharge voltage, discharge current, pulse on-time, pulse off-time and wire velocity on the response variable i.e workpiece *Ra* was evaluated using the ANOVA analysis. It was observed from Table 8.2 that all the considered input parameters have significant influence on the response variable variation. Figure 8.11 shows the interaction plots of workpiece surface response variation with respect to the significant interaction terms $\left(I \cdot t_{on},\ I \cdot v,\ t_{on} \cdot t_{off}\right)$. It is noted that *Ra* value rises with an increase in voltage and current due to a rise in discharge energy. Higher spark energy causes deep and wide craters on the workpiece surface, thus increasing the surface *Ra* with successive discharges. Discharges with similar nature form overlapping craters on the irradiated region. A slight decrease in *Ra* values were observed with increasing pulse off-time. The decrease in the pulse off-time leads to an increase of the duty factor. This factor allows the formation of smaller and fewer gas bubbles containing lesser energy. When the discharge stops, these small gas bubbles will collapse which result in finer craters, thus decreasing the surface *Ra* of the machined surface. Also, it has been observed from Figure 8.11 that with an increase in wire velocity, the workpiece surface quality improves. This is because with an increase in wire speed, the heat flux moves at a higher speed, thus providing very less time for temperature rise on the wire surface as well as on the workpiece surface.

Less temperature rise causes less material melting and eventually causes lesser damage on the machined surface, which reduces the surface roughness. Higher values of wire speed further causes less localized damage on the workpiece surface instead forming micro craters over a larger surface thus improving the surface finish.

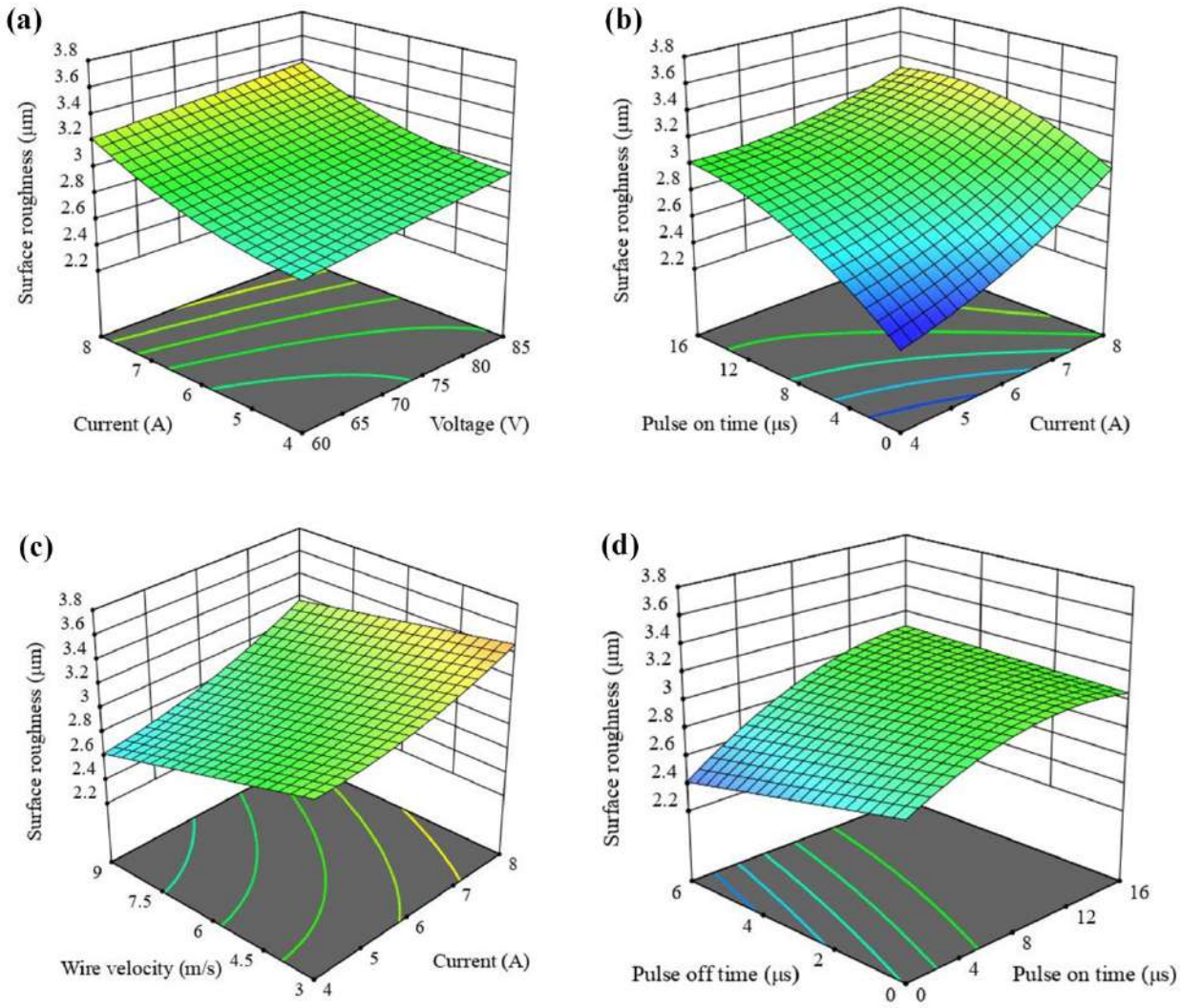

Figure 8.11 Analysis plots for surface roughness: (a) interaction of voltage and current, (b) interaction of current and pulse on-time, (c) interaction of current and wire velocity, (d) interaction of pulse on-time and pulse off-time

8.7 Comparison between molybdenum wire and zinc coated brass wire

Extensive experimental investigations were carried out for both the molybdenum wire and zinc coated brass wire to understand the wire erosion mechanism and minimize the frequency of wire failure. FESEM images were collected to carefully examine the damages undergone

by both the types of wire surfaces. Visual observation of the images showed that the zinc coated brass wire suffered severe damages as compared to the molybdenum wire. The reason behind this is because the melting point of zinc (693 K) and brass (1203 K) are lower than the melting point of molybdenum (2896 K). The zinc coating initially acts as a protection to the brass core against the violent spark discharges. The outer coating finally wears off and erosion starts occurring from the brass core, which degrades the wire strength. A wire surface quality index for the eroded wire samples was evaluated to quantify the extent of erosion undergone by the wire tool. It was noted that for the same set of process conditions, the histogram mean values for the zinc coated brass wire were lower as compared to the values of molybdenum wire. This indicates that the intensity of erosion for the coated wire is critical as compared to the molybdenum wire. The zinc coated brass wire has lower tensile strength, which further causes higher deformation than the molybdenum wire. The workpiece *Ra* values were found to be higher while machining with the coated wire in comparison to the molybdenum wire. Thus, apart from the process conditions used, the wire material also plays an important role in determining the surface quality of the machined components. Therefore, the performance of the molybdenum wire can be considered better in terms of wire health and workpiece surface quality. The disadvantage associated with molybdenum wire is its high cost and hence industries may prefer zinc-coated brass wire for bulk machining of products and rough cutting operations for a set of optimized process conditions.

8.8 Summary

This chapter reported an extensive experimental investigation on the measurement and analysis of zinc coated brass wire degradation and wear during WEDM of Ti-6Al-4V alloy. A total of 36 WEDM experiments were carried out on Ti-6Al-4V alloy to investigate the influence of different process conditions viz. discharge voltage, discharge current, pulse on-time, pulse off-time and wire speed on the wire erosion and also on the surface quality achieved by the component. ANOVA analysis and regression analysis were carried out to study the effects of process parameters and their interaction terms on the workpiece *Ra*. The intensity of damages on the wire surface was quantified using image processing technique. Further, the interrelationship between wire wear and the achieved workpiece surface quality

was also established using this methodology.The following are the significant conclusions drawn from the current study:

- The wire surface undergoes severe degradation during WEDM pulse discharges in the form of craters, microholes, pits and cracks. Insufficient flushing time and improper flushing pressure causes inefficient flushing of debris. This results in sticking of debris onto the wire surface. The melted material sometimes resolidifies and redeposits on the wire surface due to lack of sufficient flushing time. This reduces the spark gap thus causing undesired arc formation and exposing the wire to violent spark formation and thermal shock. Excessive wire erosion degrades the wire strength finally causing the failure of wire. Thus, it is essential to optimize the process conditions such that the damages on the wire surface are minimized to limit the occurrence of wire failure.
- The original circular cross-section of the wire continually changes its shape during the cutting operation. The wire deformation caused during metal cutting operation results into geometrical errors in the machined components. During machining, the wire diameter initially increases on one side than the original diameter. As the wire traverses forward along the feed direction, the wire diameter then gradually becomes smaller than the original one.
- It was observed from the collected wire images that deep and wide craters were formed on the wire surface at higher levels of current. Higher pulse on-time (8 μs) increases the thermally affected region in the wire. This is because the wire surface is exposed to spark discharges for a longer duration at higher pulse on-times. Localized material ablation was observed on the wire surface at lower wire velocities because the heat flux traverses over the wire surface at lower speeds thus giving rise to higher temperatures.
- The effects of various input conditions showed that discharge voltage, discharge current, pulse duration, pulse off-time and wire velocity have significant contribution towards workpiece *Ra* variation. Higher spark energy causes wide craters on the workpiece surface, thus increasing the surface *Ra* with successive discharges. The workpiece surface quality was also observed to be deteriorated at lower values of wire speed due to localized material ablation from the surface.
- A wire surface quality index was proposed using image processing technique to estimate the extent of erosion undergone by the wire surface. The mean value of an image

histogram of the eroded wire samples was used as an indicator in determining a tolerance for wire wear below which the wire is highly prone to breakage and also deteriorates the workpiece surface quality. A histogram mean of 117.02 for the zinc coated brass wire was observed to be the threshold limit below which wire breakages were observed.

- The wire surface quality index for the zinc coated brass wire decreases as the intensity of wire surface erosion increases.
- The developed technique was found to be useful in establishing a relationship between the wire wear and the product surface quality. It was observed that as the wire surface quality index decreases, the workpiece *Ra* value increases.
- Wire rupture occurs due to a reduction in wire strength when excessive erosion degrades the integrity of the wire surface and the thermal residual stresses induced during the temperature rise exceed the threshold strength of the wire material. The wire experiences necking before failure and sharp broken tips with unsymmetrical breakage on both sides of the zinc coated brass wire were observed.
- Wire failure incidents were observed at higher discharge energy settings and low level of wire speed. Low wire speed causes localized damages on the surface and produces more debris, which can easily break the wire.

CHAPTER 9

Conclusions

9.0 Overview

The work presented in this thesis primarily focuses on predicting the wire characteristics during the discharge phenomenon to mitigate the frequency of wire failure. Timely prediction and prevention of wire breakage is imperative to achieve sustainable and efficient machining. In this research study, two types of wires viz. molybdenum wire and zinc coated brass wire have been considered for analysis. Both these types of wires are extensively used in manufacturing industries, hence it is envisaged that the research work carried out shall provide useful guidelines in improving the wire life and achieving the desired machining efficiency. The work reported herein was carried out in the following stages:

- Development of a three-dimensional thermo-mechanical finite element model of a molybdenum wire during WEDM process and estimation of wire strength, followed by experimental validation of the developed model.
- Experimental measurement and analysis of molybdenum wire erosion and deformation during wire electric discharge machining of Ti-6Al-4V alloy.
- Estimation of a wire surface quality index to establish a threshold limit of surface damages undergone by the wire tool.
- Development of a three-dimensional thermo-mechanical finite element model of a zinc coated brass wire during WEDM process and estimation of wire strength, followed by experimental validation of the developed model.
- Experimental measurement and analysis of zinc coated brass wire erosion and deformation during wire electric discharge machining of Ti-6Al-4V alloy, followed by estimation of the wire surface quality index.

9.1 Conclusions and research contributions

Specific contributions of the research work are presented below.

9.1.1 Three-dimensional thermo-mechanical model of a molybdenum wire during WEDM process and estimation of wire strength

- A realistic three-dimensional numerical model was developed to predict the thermo-mechanical characteristics of the wire electrode during the spark discharges. A case study was carried out to predict the temperature distribution and stress contour produced on the wire surface after a single pulse. It was observed that as the heat source moves along the wire axis, the temperature keeps on increasing during the pulse on-time and starts cooling during the pulse off-time. The thermally induced stresses in the wire weaken the wire strength. The peak temperature predicted numerically was validated using published results as it is very difficult to experimentally obtain the temperature generated during the discharge process. The peak values of residual stresses were validated using X-ray diffraction technique and the results were found to be in close approximation with the numerically computed values with an average error of 9.46 %.
- The strength of the molybdenum wire electrode depends upon the thermal residual stresses induced in the wire during the cutting operation. A simple and novel method has been developed, which computes the wire safety index based on the residual stresses generated on the wire electrode surface. The merit of this work lies in the use of a three-dimensional thermo-mechanical nonlinear numerical model to compute the wire strength based on the stresses generated during machining. The stresses were compared to the yield strength of the molybdenum wire material to estimate the reduction in wire strength during the discharge phenomenon.
- If the equivalent residual stresses produced in the wire during the discharge phenomenon is well below the yield strength of the wire, the wire is said to be within the safe limit. As the residual stress values cross the yield point, the strength of the wire starts deteriorating which is harmful to the health of the wire. Experimental studies found that the microcracks initiate on the surface, when the peak residual stress achieved by the molybdenum wire exceeds the value of 976.7 MPa. The corresponding X value of 1.63 can be considered as a critical value to determine the safe zone of machining in terms of

wire health. Overall, it can be concluded that the proposed methodology to compute the wire safety index eliminates the need of costly, time-consuming and tedious experiments.

- The thermo mechanical analysis also showed that the peak temperature and the peak value of residual stresses achieved by the wire increase with voltage and current levels. However, peak temperature decreases with the increase in pulse on-time but increases the thermally affected region.

9.1.2 Experimental analysis of molybdenum wire erosion and deformation during WEDM of Ti-6Al-4V alloy and estimation of wire surface quality index

- The wire surface undergoes severe degradation during WEDM pulse discharges in the form of craters, microholes, pits and cracks. Insufficient flushing time and improper flushing pressure causes inefficient flushing of debris; thus causing the machining debris to get attached onto the wire surface. The melted material sometimes gets resolidified and redeposited on the wire surface due to lack of sufficient flushing time. This reduces the spark gap thus causing undesired arc formation and exposing the wire to violent spark formation and thermal shock. Excessive wire erosion degrades the wire strength finally causing the failure of wire. Thus, it is essential to optimize the process conditions such that the damages on the wire surface are minimized in order to limit the occurrence of wire failure.
- The original circular cross-section of the wire continually changes its shape during the cutting operation. The wire deformation caused during metal cutting operation causes geometrical errors in machined components. During machining, the wire diameter initially increases on one side than the original diameter. As the wire traverses forward along the feed direction, the wire diameter then gradually becomes smaller than the original one.
- The intensity of wire surface erosion is controlled by the levels of process conditions used. It was clearly observed from the collected wire images that deep and wide craters were formed on the wire surface at higher levels of current. Higher pulse duration (8 μs) increases the thermally affected region in the wire. At lower pulse off-times (2 μs), microholes or micropits were observed on the wire surface due to inefficient debris

removal mechanism. Lower values of wire velocity (3 m/s) cause localized and critical material ablation from the wire surface due to higher temperatures obtained.

- The effects of various input conditions showed that current and pulse duration have the most considerable contribution towards workpiece *Ra* variation. Higher spark energy causes deep and wide craters on the workpiece surface, thus increasing the surface *Ra* with successive discharges. Pulse off-time has no significant contribution towards the surface quality achieved by the product. The workpiece surface quality was also observed to be deteriorated at lower values of wire speed (3 m/s) due to localized material ablation from the surface.
- The mean value of an image histogram of the eroded wire samples was used as an indicator in determining a tolerance for wire wear below which the wire is highly prone to breakage and also deteriorates the workpiece surface quality. The wire surface quality index for the molybdenum wire decreases as the intensity of wire surface erosion increases.
- A histogram mean of 122.17 was observed to be the threshold limit below which the damages on the wire surface are critical thus increasing the probability of wire failure. Wire surfaces with lower histogram mean values than the tolerable limit were observed to have extensive damages on the surfaces or experience failure.
- Further, the interrelationship between wire wear and the achieved workpiece surface quality was also established using the developed methodology. It was observed that as the wire surface quality index decreases, the workpiece *Ra* value increases.
- Wire wear has shown a detrimental effect on the surface roughness of WEDMed components and deteriorate the surface quality by approximately 25-35 %.
- Wire rupture occurs due to a reduction in wire strength when excessive erosion degrades the integrity of the wire surface and the thermal residual stresses induced during the temperature rise exceed the threshold strength of molybdenum wire material. The wire experiences necking before failure due to the transition of molybdenum material from brittle to ductile behaviour at higher temperatures, which are achieved during the discharge phenomenon.

9.1.3 Three-dimensional thermo-mechanical model of a zinc-coated brass wire during WEDM process and estimation of wire strength

- A three-dimensional numerical model was developed to predict the thermo-mechanical characteristics of the zinc coated brass wire electrode during the spark discharges. The results predicted by the developed model were validated using experimental results. The crater volumes generated in the wire were validated experimentally by collecting the eroded wire samples and examination of the wire cross-sections in an optical microscope. The numerically computed values of crater volume in the wire were found to be in close approximation with the experimental crater volumes with an absolute deviation of 7.25 %.
- The behavior of the zinc coated brass wire was found to be quite different as compared to the molybdenum wire characteristics. It was observed that for the zinc coated brass wire, the residual stresses induced in the wire are below the yield strength of the wire core material brass. Thus, the stresses induced are within the safe limits and do not initiate failure. However, it was noted that temperature produced in the wire exceeds the melting point of the outer zinc coating (693 K) and the core material brass (1203 K). This causes wire erosion, which degrades the wire strength.
- The wire strength was estimated based on the crater volume generated in the wire. It was observed that when the crater volume exceeded the value of 51375.25 μm^3, the wire experiences failure. Thus, this value of crater volume can be considered as the threshold value above which the wire is highly prone to breakage. Hence, the corresponding process conditions must be avoided to achieve uninterrupted machining. By using the developed method, one can easily predict the deterioration of wire electrode, which will ensure uninterrupted and efficient WEDM operation.
- The thermo physical analysis also showed that the peak temperature and the peak value of residual stresses achieved by the wire increase with voltage and current levels. However, peak temperature decreases with the increase in pulse on-time but increases the thermally affected region. The crater volume observed an increasing trend with increasing voltage and current due to increase of input power. The crater volume, however, initially increases with pulse duration and gradually starts decreasing at higher values of pulse on-time.

9.1.4 Experimental analysis on the erosion and deformation of zinc-coated brass wire during WEDM of Ti-6Al-4V alloy and estimation of wire surface quality index

- The wire surface undergoes severe degradation during WEDM pulse discharges in the form of craters, microholes, pits and cracks. Insufficient flushing time and improper flushing pressure cause inefficient flushing of debris; thus causing the machining debris to get attached onto the wire surface. The melted material sometimes gets resolidified and redeposited on the wire surface due to lack of sufficient flushing time. This reduces the spark gap thus causing undesired arc formation and exposing the wire to violent spark formation and thermal shock. Excessive wire erosion degrades the wire strength finally causing the failure of wire. The intensity of damages on the zinc coated brass wire was observed to be severe as compared to the molybdenum wire.
- The original circular cross-section of the wire continually changes its shape during the cutting operation. The wire deformation caused during metal cutting operation causes geometrical errors in machined components. During machining, the wire diameter initially increases on one side than the original diameter. As the wire traverses forward along the feed direction, the wire diameter then gradually becomes smaller than the original one.
- It was clearly observed from the collected wire images that deep and wide craters were formed on the wire surface at higher levels of current (8 A). Higher pulse duration (8 μs) increases the thermally affected region in the wire. Localized material ablation was observed on the wire surface at lower wire velocities of 3 m/s because the heat flux traverses over the wire surface at lower speeds thus giving rise to higher temperatures.
- The effects of various input conditions showed that discharge voltage, discharge current, pulse duration, pulse off-time and wire velocity have significant contribution towards workpiece *Ra* variation. Higher spark energy causes wide craters on the workpiece surface, thus increasing the surface *Ra* with successive discharges. The workpiece surface quality was also observed to be deteriorated at lower values of wire speed due to localized material ablation from the surface.

- The wire surface quality index for the zinc coated brass wire decreases as the intensity of wire surface erosion increases. A histogram mean of 117.02 for the zinc coated brass wire was observed to be the threshold limit below which wire breakages were observed.
- The image histogram mean values were found to be lower for the zinc coated brass wire as compared to the molybdenum wire for the same sets of process conditions. This indicates that the intensity of wire surface erosion is more critical for the zinc coated brass wire.
- The developed technique was useful in establishing a relationship between the wire wear and the product surface quality. It was observed that as the wire surface quality index decreases, the workpiece *Ra* value increases. This indicates that the workpiece surface quality deteriorates as the wire erosion intensity increases.
- Wire rupture occurs due to a reduction in wire strength when excessive erosion degrades the integrity of the wire surface and the thermal residual stresses induced during the temperature rise exceed the threshold strength of the wire material. The wire experiences necking before failure and sharp broken tips with unsymmetrical breakage on both sides of the zinc coated brass wire were observed.

9.2 Scope for future work

The present research work can be extended on the following fronts.

- Limited research has been carried out on the static deflection of the wire i.e. the wire lag phenomenon, which is an important factor to be considered for precision machining. The wire lag phenomenon causes inaccurate cuts when the cutting direction changes. Therefore, the study on the causes of wire lag and measures to curtail its effects can be a remarkable research prospective.
- There is enormous scope in improving the properties of wire electrodes for enhanced cutting efficiency and longer tool life. The performance of a wire electrode during machining is highly dependent on the wire material, which should satisfy all the desired properties of a wire tool such as electrical conductivity, good mechanical strength, high thermal conductivity, sufficient heat capacity, etc. With the advent of newer materials, the development of novel combinations of wire core material and the coating material is still a key research area.

- The recording of the plasma formation is difficult and can be an interesting area to explore for a deeper understanding of the discharge phenomenon at the wire and workpiece interface. It is also needed to develop a numerical tool for the prediction of instability in sparking conditions.
- Wire breakage affects the environment by increasing energy consumption and machining time. As the wire is very thin, many times the wire is used for a single time, thereafter it to be disposed of, which may be hazardous to the environment. Proper disposal or reusability of used wires is to be extensively explored to achieve sustainable machining.

References

Abhilash, P.M., Chakradhar, D., 2020. ANFIS modelling of mean gap voltage variation to predict wire breakages during wire EDM of Inconel 718. CIRP J. Manuf. Sci. Technol. 31, 153–164. https://doi.org/10.1016/j.cirpj.2020.10.007

Abhilash, P.M., Chakradhar, D., 2020a. Surface integrity comparison of wire electric discharge machined Inconel 718 surfaces at different machining stabilities. Procedia CIRP 87, 228–233. https://doi.org/10.1016/j.procir.2020.02.037

Abhilash, P.M., Chakradhar, D., 2020b. Prediction and analysis of process failures by ANN classification during wire-EDM of Inconel 718. Adv. Manuf. 8, 519–536. https://doi.org/10.1007/s40436-020-00327-w

Abyar, H., Abdullah, A., Akbarzadeh, A., 2018. Analyzing wire deflection errors of WEDM process on small arced corners. J. Manuf. Process. 36, 216–223. https://doi.org/10.1016/j.jmapro.2018.10.002

Abyar, H., Abdullah, A., Akbarzadeh, A., 2019. Prediction algorithm for WEDM arced path errors based on spark variable gap and nonuniform spark distribution models. J. Manuf. Sci. Eng. Trans. ASME 141, 1–11. https://doi.org/10.1115/1.4041779

Almeida, S., Mo, J., Bil, C., Ding, S., Wang, X., 2021. Comprehensive servo control strategies for flexible and high-efficient wire electric discharge machining. A systematic review. Precis. Eng. 71, 7–28. https://doi.org/10.1016/j.precisioneng.2021.02.007

Altpeter, F., Perez, R., 2004. Relevant topics in wire electrical discharge machining control, in: Journal of Materials Processing Technology. pp. 147–151. https://doi.org/10.1016/j.jmatprotec.2003.10.033

Alavala, C.R., 2010. Finite Element Methods.

Arunachalam, C., Aulia, M., Bozkurt, B., Eubank, P.T., 1998. Wire Vibration, Bowing and Breakage in Wire EDM. VDI Berichte 4255, 109–118. https://doi.org/10.1063/1.1355281

Azhari, A., Hamedon, Z., Gebremariam, M.A., 2017. A study on Wire Breakage in Electrical Discharge Machining of Polyurethane Foam, Materials Today: Proceedings.

Babu Rao, T., Gopala Krishna, A., 2013. Simultaneous optimization of multiple performance characteristics in WEDM for machining ZC63/SiCp MMC. Adv. Manuf. 1, 265–275. https://doi.org/10.1007/s40436-013-0029-y

Banerjee, S., Prasad, B.V.S.S.S., 2010. Numerical evaluation of transient thermal loads on a WEDM wire electrode under spatially random multiple discharge conditions with and without clustering of sparks. Int. J. Adv. Manuf. Technol. 48, 571–580. https://doi.org/10.1007/s00170-009-2300-8

Banerjee, S., Prasad, B.V.S.S.S., Mishra, P.K., 1993. A simple model to estimate the thermal loads on an EDM wire electrode. J. Mater. Process. Tech. 39, 305–317. https://doi.org/10.1016/0924-0136(93)90165-3

Banerjee, S., Prasad, B.V.S.S.S., Mishra, P.K., 1997. Analysis of three-dimensional transient heat conduction for predicting wire erosion in the wire electrical discharge machining process. J. Mater. Process. Technol. 65, 134–142. https://doi.org/10.1016/0924-0136(95)02253-8

Banu, A., Ali, M.Y., Rahman, M.A., Konneh, M., 2020. Stability of micro dry wire EDM: OFAT and DOE method. Int. J. Adv. Manuf. Technol. 106, 4247–4261. https://doi.org/10.1007/s00170-020-04923-9

Baumann I, Barthel B, inventor; Berkenhoff and Co KG., assignee. Wire electrode for the spark-erosive cutting of hard metal. United States patent US 6,348,667. 2002.

Beck, J. V, 1981. Transient temperatures in a semi-infinite cylinder heated by a disk heat source. Int J Heat Mass Transf . 24, 1631–1640.

Beckert, M., Klemm, H., 1984. Handbuch der metallographischen Ätzverfahren. Deutscher Verlag für Grundstoffindindustrie, Leipzig, Germany.

Beltrami, I., Bertholds, A., Dauw, D., 1996. A simplified post process for wire cut EDM. J. Mater. Process. Technol. 58, 385–389. https://doi.org/10.1016/0924-0136(95)02212-0

Benedict, G.F., 1987. Non Traditional Manufacturing Processes. New York: Marcel Dekker.

Bergs, T., Tombul, U., Herrig, T., Olivier, M., Klink, A., Klocke, F., 2018. Analysis of characteristic process parameters to identify unstable process conditions during wire EDM, in: Procedia Manufacturing. Elsevier B.V., pp. 138–145. https://doi.org/10.1016/j.promfg.2018.11.018

Bhartiya, D., Rana, P., Singh, M.A., Marla, D., 2020. Multi-Objective Optimization of Wire-Electric Discharge Machined Ultrathin Silicon Wafers Using Response Surface Methodology for Solar Cell Applications. J. Micro Nano-Manufacturing 8, 1–7. https://doi.org/10.1115/1.4049362

Bisaria, H., Shandilya, P., 2018. Study on Effect of Machining Parameters on Performance Characteristics of Ni-rich NiTi Shape Memory Alloy during Wire Electric Discharge Machining. Mater. Today Proc. 5, 3316–3324. https://doi.org/10.1016/j.matpr.2017.11.574

Blanc P, Ly M, Sanchez G, inventor; Thermocompact SA, assignee. Composite wire for electrical discharge machining. United States patent US 8,378,247. 2013.

Briffod J, inventor; Agie Charmilles New Technologies SA, assignee. Zinc or cadmium coated, surface oxidized electrode wire for EDM cutting of a workpiece; and method for forming such a wire. United States patent US 4,977,303. 1990.

Cabanes, I., Portillo, E., Marcos, M., Sánchez, J.A., 2008a. An industrial application for on-line detection of instability and wire breakage in wire EDM. J. Mater. Process. Technol. 195, 101–109. https://doi.org/10.1016/j.jmatprotec.2007.04.125

Cabanes, I., Portillo, E., Marcos, M., Sánchez, J.A., 2008b. On-line prevention of wire breakage in wire electro-discharge machining. Robot. Comput. Integr. Manuf. 24, 287–298. https://doi.org/10.1016/j.rcim.2006.12.002

Caggiano, A., Perez, R., Segreto, T., Teti, R., Xirouchakis, P., 2016. Advanced Sensor Signal Feature Extraction and Pattern Recognition for Wire EDM Process Monitoring, in: Procedia CIRP. Elsevier B.V., pp. 34–39. https://doi.org/10.1016/j.procir.2016.02.181

Carslaw, H. S., Jaeger, J.C., 1959. Conduction of heat in solids. 2nd ed. London: Clarendon Press.

Chaudhary, T., Siddiquee, A.N., Chanda, A.K., 2019. Effect of wire tension on different output responses during wire electric discharge machining on AISI 304 stainless steel. Def. Technol. 15, 541–544. https://doi.org/10.1016/j.dt.2018.11.003

Chen, Z., Huang, Y., Huang, H., Zhang, Z., Zhang, G., 2015. Three-dimensional characteristics analysis of the wire-tool vibration considering spatial temperature field and electromagnetic field in WEDM. Int. J. Mach. Tools Manuf. 92, 85–96. https://doi.org/10.1016/j.ijmachtools.2015.03.003

Chen, Z., Zhang, G., Han, F., Zhang, Y., Rong, Y., 2018. Determination of the optimal servo feed speed by thermal model during multi-pulse discharge process of WEDM. Int. J.

Mech. Sci. 142–143, 359–369. https://doi.org/10.1016/j.ijmecsci.2018.05.006

Chen, Z., Zhang, G., Yan, H., 2018a. A high-precision constant wire tension control system for improving workpiece surface quality and geometric accuracy in WEDM. Precis. Eng. 54, 51–59. https://doi.org/10.1016/j.precisioneng.2018.05.001

Chen, Z., Zhang, Y., Zhang, G., Li, W., 2018b. Modeling and reducing workpiece corner error due to wire deflection in WEDM rough corner-cutting. J. Manuf. Process. 36, 557–564. https://doi.org/10.1016/j.jmapro.2018.10.021

Chu, X., Zeng, X., Zhuang, W., Zhou, W., Quan, X., Fu, T., 2019. Vibration assisted high-speed wire electric discharge machining for machining surface microgrooves. J. Manuf. Process. 44, 418–426. https://doi.org/10.1016/j.jmapro.2019.05.026

Ciwen, H., Jinsheng, Z., Jianyong, L., 2018. Ultra-long Wire Reciprocated-WEDM with Dual Tensile Reels Winded, in: Procedia CIRP. Elsevier B.V., pp. 115–119. https://doi.org/10.1016/j.procir.2017.12.046

Das, S., Joshi, S.S., 2010. Modeling of spark erosion rate in microwire-EDM. Int. J. Adv. Manuf. Technol. 48, 581–596. https://doi.org/10.1007/s00170-009-2315-1

Dauw, D.F., Albert, L., 1992. About the Evolution of Wire Tool Performance in Wire EDM. CIRP Ann. - Manuf. Technol. 41, 221–225. https://doi.org/10.1016/S0007-8506(07)61190-1

Dauw, D.F., Beltrami, I., 1994. High Precision Wire EDM by Online Wire Positioning Control. J. Chem. Inf. Model. 43, 193–197. https://doi.org/10.1017/CBO9781107415324.004

Deb, P., Dutta, P., Choudhuri, B., Deoghare, A.B., 2019. Parametric Analysis of WEDM to Optimize Cutting Parameters for Inconel 800. Mater. Today Proc. 22, 1676–1686. https://doi.org/10.1016/j.matpr.2020.02.185

Dekeyser, W., Snoeys, R., Jennes, M., 1985a. A thermal model to investigate the wire rupture phenomenon for improving performance in EDM wire cutting. J. Manuf. Syst. 4, 179–190. https://doi.org/10.1016/0278-6125(85)90024-X

Dekeyser, W., Snoeys, R., Jennes, M., 1988. Expert system for wire cutting edm, based on pulse classification and thermal modeling, Robotics & Computer-Integrated Manufacturing. 4, 219-224. https://doi.org/10.1016/0736-5845(88)90080-4

Deshmukh, S.S., Jadhav, V.S., Shrivastava, R., 2019. Study Spark Gap of Wire Electric

Discharge Machining on AISI 4140. Mater. Today Proc. 22, 1812–1821. https://doi.org/10.1016/j.matpr.2020.03.015

DiBitonto, D.D., Eubank, P.T., Patel, M.R., Barrufet, M.A., 1989. Theoretical models of the electrical discharge machining process. I. A simple cathode erosion model. J. Appl. Phys. 66, 4095–4103. https://doi.org/10.1063/1.343994

Dixit, U.S., 2009. Finite element methods for engineers.

Ekmekci, B., Tekkaya, A.E., Erden, A., 2006. A semi-empirical approach for residual stresses in electric discharge machining (EDM). Int. J. Mach. Tools Manuf. 46, 858–868. https://doi.org/10.1016/j.ijmachtools.2005.07.020

Ezaki S, Seto H, Hasegawa H, inventor; Tokyo Tungsten Co Ltd Sumitomo Electric Industries Ltd., assignee. Electrode wire for electric spark cutting. United States patent US 5,028,756. 1991.

Farooq, M.U., Ali, M.A., He, Y., Khan, A.M., Pruncu, C.I., Kashif, M., Ahmed, N., Asif, N., 2020. Curved profiles machining of Ti6Al4V alloy through WEDM: Investigations on geometrical errors. J. Mater. Res. Technol. 9, 16186–16201. https://doi.org/10.1016/j.jmrt.2020.11.067

Fedorov, A.A., Blesman, A.I., Postnikov, D. V., Polonyankin, D.A., Russkikh, G.S., Linovsky, A. V., 2018. Investigation of the impact of Rehbinder effect, electrical erosion and wire tension on wire breakages during WEDM. J. Mater. Process. Technol. 256, 131–144. https://doi.org/10.1016/j.jmatprotec.2018.02.002

Fitzpatrick M.E., Fry A.T., Holdway P., Kandil F.A., Shackleton J., Suominen L., 2005. Determination of residual stresses by X-ray diffraction - issue 2. Middlesex (UK): National Physical Laboratory:52.

Fowle FF, inventor; Indiana Steel & Wire Co., assignee. Process of treating zinc-coated wire. United States patent US 1,896,613. 1933.

García Navas, V., Ferreres, I., Marañón, J.A., Garcia-Rosales, C., Gil Sevillano, J., 2008. Electro-discharge machining (EDM) versus hard turning and grinding-Comparison of residual stresses and surface integrity generated in AISI O1 tool steel. J. Mater. Process. Technol. 195, 186–194. https://doi.org/10.1016/j.jmatprotec.2007.04.131

Gamage, J.R., Desilva, A.K.M., 2016. Effect of Wire Breakage on the Process Energy Utilisation of EDM, in: Procedia CIRP. Elsevier B.V., pp. 586–590.

https://doi.org/10.1016/j.procir.2016.02.264

Gonchikar, U, Ravindra, HV, Addamani, R, & Sudhir, P., 2020. Estimation and Comparison of Machining Performances Using Group Method Data Handling Technique and ANN in Wire EDM of Stavax Material, in: Proceedings of the ASME 2020 International Mechanical Engineering Congress and Exposition. https://doi.org/https://doi.org/10.1115/IMECE2020-23435

Gonnissen D, Van Vooren W, NV Bekaert SA, inventor. Electric discharge machining wire. United States patent US 6,875,943. 2005.

Groos H, inventor; Berkenhoff and Co KG, assignee. Wire electrode for the spark erosive cutting. United States patent US 4,766,280. 1988.

Groos H., Barthel B., Noethe T., Dietrich C., inventor; Berkenhoff and Co KG, assignee. Wire electrode for spark erosion cutting. United States patent US 6,781,081. 2004.

Groos H, Barthel B, Noethe T, inventor; Berkenhoff and Co KG., assignee. Wire electrode with a structured interface surface. United States patent US 6,794,597. 2004.

Guo, Z.N., Lee, T.C., Yue, T.M., Lau, W.S., 1997a. Study on the machining mechanism of WEDM with ultrasonic vibration of the wire. J. Mater. Process. Technol. 69, 212–221.

Guo, Z.N., Lee, T.C., Yue, T.M., Lau, W.S., 1997b. A Study of Ultrasonic-aided Wire Electrical Discharge Machining. J. Mater. Process. Technol. 63, 823–828.

Guo, Z.N., Yue, T.M., Lee, T.C., Lau, W.S., 2003. Computer simulation and characteristic analysis of electrode fluctuation in wire electric discharge machining. J. Mater. Process. Technol. 142, 576–581. https://doi.org/10.1016/S0924-0136(03)00662-9

Gupta, K., Jain, N.K., 2014. Analysis and optimization of micro-geometry of miniature spur gears manufactured by wire electric discharge machining. Precis. Eng. 38, 728–737. https://doi.org/10.1016/j.precisioneng.2014.03.009

Guu, Y.H., Hocheng, H., Chou, C.Y., Deng, C.S., 2003. Effect of electrical discharge machining on surface characteristics and machining damage of AISI D2 tool steel. Mater. Sci. Eng. A 358, 37–43. https://doi.org/10.1016/S0921-5093(03)00272-7

Habib, S., Okada, A., 2016. Study on the movement of wire electrode during fine wire electrical discharge machining process. J. Mater. Process. Technol. 227, 147–152. https://doi.org/10.1016/j.jmatprotec.2015.08.015

Hada, K., Kunieda, M., 2013. Analysis of wire impedance in wire-EDM considering

electromagnetic fields generated around wire electrode. Procedia CIRP 6, 244–249. https://doi.org/10.1016/j.procir.2013.03.065

Han, F., Cheng, G., Feng, Z., Isago, S., 2008. Thermo-mechanical analysis and optimal tension control of micro wire electrode. Int. J. Mach. Tools Manuf. 48, 922–931. https://doi.org/10.1016/j.ijmachtools.2007.10.024

Han, F., Cheng, G., Feng, Z., Soichiro, I., 2009. Measurement of wire electrode temperature in WEDM. Int. J. Adv. Manuf. Technol. 41, 871–879. https://doi.org/10.1007/s00170-008-1546-x

Han, W., Kunieda, M., 2021. Research of micro EDM/ECM method in same electrolyte with running wire tool electrode. Precis. Eng. 70, 1–14. https://doi.org/10.1016/j.precisioneng.2021.01.013

Herrero, A., Azcarate, S., Rees, A., Gehringer, A., Schoth, A., Sanchez, J.A., 2008. Influence of Force Components on Thin Wire EDM. Wire 5–8.

Hinduja, S., Kunieda, M., 2013. Modelling of ECM and EDM processes. CIRP Ann. - Manuf. Technol. 62, 775–797. https://doi.org/10.1016/j.cirp.2013.05.011

Hsue WJ, inventor; National Kaohsiung University Of Science, assignee. Vibration assisted wire machining device. United States patent US 16/869,323. 2020.

Huang, J.T., Liao, Y.S., 2000. A wire-EDM maintenance and fault-diagnosis expert system integrated with an artificial neural network. Int. J. Prod. Res. 38, 1071–1082. https://doi.org/10.1080/002075400189022

Huang, J.T., Liao, Y.S., Hsue, W.J., 1999. Determination of finish-cutting operation number and machining-parameters setting in wire electrical discharge machining. J. Mater. Process. Technol. 87, 69–81. https://doi.org/10.1016/S0924-0136(98)00334-3

Hwa Yan, B., Tsai, H.C., Yuan Huang, F., Chorng Lee, L., 2005. Examination of wire electrical discharge machining of Al2O 3p/6061Al composites. Int. J. Mach. Tools Manuf. 45, 251–259. https://doi.org/10.1016/j.ijmachtools.2004.08.015

Ikai, T., Hashigushi, K., Heat input for crater formation in EDM. Proceedings of international symposium for electro-machining—ISEM XI; 1995 April 17-21; Lausanne, Switzerland. Lausanne: Presses polytechniques et universitaires romandes; 1995.

Jain.V.K., 2004. Advanced Machining Processes. Allied Publishers Private Limited, Indian

Institute of Technology, Kanpur,India.

Jahan, M.P., Saleh, T., Rahman, M., Wong, Y.S., 2010. Development, modeling, and experimental investigation of low frequency workpiece vibration-assisted micro-EDM of tungsten carbide. J. Manuf. Sci. Eng. Trans. ASME 132, 1–8. https://doi.org/10.1115/1.4002457

Jain, V.K., Sreenivasa Rao, P., Choudhary, S.K., Choudhary, S.K., 1991. Experimental investigations into traveling wire electrochemical spark machining (TW-ECSM) of composites. J. Manuf. Sci. Eng. Trans. ASME 113, 75–84. https://doi.org/10.1115/1.2899625

Jennes, M., Snoeys, R., Dekeyser, W., 1984. Comparison of Various Approaches to Model the Thermal Load on the EDM-Wire Electrode. CIRP annals 33, 93-98. https://doi.org/10.1016/S0007-8506(07)61387-0

Jianyong, L., Jianmei, G., Liantong, D., Yanhua, C., Dongjiang, S., 2018. Research on the Real-time Wear of Wire Electrode during the Electrical Discharge Machining (EDM) of Precision Micro Hole. Procedia CIRP 68, 565–568. https://doi.org/10.1016/j.procir.2017.12.114

Jilani, S.T., Pandey, P.C., 1982. Analysis and modelling of edm parameters. Precis. Eng. 4, 215–221. https://doi.org/10.1016/0141-6359(82)90011-3

Joshi, S.N., Pande, S.S., 2010. Thermo-physical modeling of die-sinking EDM process. J. Manuf. Process. 12, 45–56. https://doi.org/10.1016/j.jmapro.2010.02.001

Joshi, K., Bhandarkar, U., Samajdar, I., Joshi, S.S., 2018. Microstructural Characterization of Thermal Damage on Silicon Wafers Sliced Using Wire-Electrical Discharge Machining. J. Manuf. Sci. Eng. Trans. ASME 140, 1–14. https://doi.org/10.1115/1.4039647

Kavimani, V., Prakash, K.S., Thankachan, T., 2019. Multi-objective optimization in WEDM process of graphene – SiC-magnesium composite through hybrid techniques. Measurement 145, 335–349. https://doi.org/10.1016/j.measurement.2019.04.076

Kumar, A., Abhishek, K., Vivekananda, K., Maity, K., 2018. Effect of wire electrode materials on die-corner accuracy for Wire Electrical Discharge Machining (WEDM) of Inconel 718, in: Materials Today: Proceedings. Elsevier Ltd, pp. 12641–12648. https://doi.org/10.1016/j.matpr.2018.02.247

Kamei, T., Okada, A., Okamoto, Y., 2016. High-speed Observation of Thin Wire Movement

in Fine Wire EDM. Procedia CIRP 42, 596–600. https://doi.org/10.1016/j.procir.2016.02.266

Kaneko H, Onoue M, inventor; Inoue Japax Research Inc., assignee. Electrode material for travelling-wire type electrical discharge machining. United States patent US 4,424,432. 1984.

Kapoor, J., Singh, S., Khamba, J.S., 2012. High-performance wire electrodes for wire electrical-discharge machining - A review. Proc. Inst. Mech. Eng. Part B J. Eng. Manuf. 226, 1757–1773. https://doi.org/10.1177/0954405412460354

Khan, B., Davis, R., Singh, A., 2019. Effect of input variables and cryogenic treatment in wire electric discharge machining of Ti-6Al-4V alloy for biomedical applications. Mater. Today Proc. 8–12. https://doi.org/10.1016/j.matpr.2019.09.226

Kimura, A., Okamoto, Y., Okada, A., Ohya, J., Yamauchi, T., 2013. Fundamental study on multi-wire EDM slicing of SiC by wire electrode with track-shaped section. Procedia CIRP 6, 232–237. https://doi.org/10.1016/j.procir.2013.03.052

Kinoshita, N., Fukui, M., Gamo, G., 1982. Control of Wire-EDM Preventing Electrode from Breaking. CIRP Ann. - Manuf. Technol. 31, 111–114. https://doi.org/10.1016/S0007-8506(07)63279-X

Kinoshita, N., Fukui, M., Kimura, Y., 1984. Study on Wire-EDM: Inprocess Measurement of Mechanical Behaviour of Electrode-Wire. CIRP Ann. - Manuf. Technol. 33, 89–92. https://doi.org/10.1016/S0007-8506(07)61386-9

Kirwin, R.M., Mahbub, M.R., Jahan, M.P., 2018. Investigating the Effect of Wire Feed Rate and Wire Tension on the Corner and Profile Accuracies During Wire-EDM of Ti-6Al-4V, in: Proceedings of the ASME 2018 13th International Manufacturing Science and Engineering Conference. Texas, USA. https://doi.org/https://doi.org/10.1115/MSEC2018-6540

Klocke, F., Lung, D., Thomaidis, D., Antonoglou, G., 2004. Using ultra thin electrodes to produce micro-parts with wire-EDM. J. Mater. Process. Technol. 149, 579–584. https://doi.org/10.1016/j.jmatprotec.2003.10.061

Koyano, T., Takahashi, T., Tsurutani, S., Hosokawa, A., Furumoto, T., Hashimoto, Y., 2018. Temperature Measurement of Wire Electrode in Wire EDM by Two-color Pyrometer, in: Procedia CIRP. Elsevier B.V., pp. 96–99.

https://doi.org/10.1016/j.procir.2017.12.029

Kruth, J.P., Lauwers, B., Schacht, B., Van Humbeeck, J., 2004. Composite wires with high tensile core for wire EDM. CIRP Ann. - Manuf. Technol. 53, 171–174. https://doi.org/10.1016/S0007-8506(07)60671-4

Kumagai, S., Sato, N., Takeda, K., 2007. Automatic stripping of dielectric-encased wire tool electrode used in electrical discharge machining. J. Manuf. Sci. Eng. Trans. ASME 129, 973–978. https://doi.org/10.1115/1.2738541

Kumar, A., Abhishek, K., Vivekananda, K., Maity, K., 2018. Effect of wire electrode materials on die-corner accuracy for Wire Electrical Discharge Machining (WEDM) of Inconel 718, in: Materials Today: Proceedings. Elsevier Ltd, pp. 12641–12648. https://doi.org/10.1016/j.matpr.2018.02.247

Kumar, B., Bag, S., 2019. Phase transformation effect in distortion and residual stress of thin-sheet laser welded Ti-alloy. Opt. Lasers Eng. 122, 209–224. https://doi.org/10.1016/j.optlaseng.2019.06.008

Kunieda, M., Kojima, H., Kinoshita, N., 1990. On-Line Detection of EDM Spark Locations by Multiple Connection of Branched Electric Wires. CIRP Ann. - Manuf. Technol. 39, 171–174. https://doi.org/10.1016/S0007-8506(07)61028-2

Kuruvila, N, & Ravindra, H., 2011. Parametric Influence and Optimization of Wire EDM on Oil Hardened Non Shrinking Steel, in: Proceedings of the ASME 2011 International Mechanical Engineering Congress and Exposition. Denver, Colorado, USA. https://doi.org/https://doi.org/10.1115/IMECE2011-63379

Lalwani, V., Sharma, P., Pruncu, C.I., Unune, D.R., 2020. Response surface methodology and artificial neural network-based models for predicting performance of wire electrical discharge machining of inconel 718 alloy. J. Manuf. Mater. Process. 4. https://doi.org/10.3390/jmmp4020044

Lambert, J.A., Murphy, K.D., 2002. Modal convection and its effect on the stability of EDM wires. Int. J. Mech. Sci. 44, 207–216. https://doi.org/10.1016/S0020-7403(01)00075-3

Lee JC, inventor; Pung Kuk Edm Wire Manufacturing Co Ltd., assignee. Method of manufacturing zinc-coated electrode wire for electric discharge processors using hot dip galvanizing process. United States patent US 10/540,324. 2006.

Lee JC, inventor; Pung Kuk Edm Wire Manufacturing Co Ltd., assignee. Electrode wire with

multi-coated layers for electrical discharge machining and method of manufacturing the same. United States patent US 10/570,489. 2008.

Liu, Z., Li, R., Jiang, R., Li, X., Zhang, M., 2016. Effects of Al addition on the structure and mechanical properties of Zn alloys. J. Alloys Compd. 687, 885–892. https://doi.org/10.1016/j.jallcom.2016.06.196

Liao, Y.S., Chu, Y.Y., Yan, M.T., 1997. Study of wire breaking process and monitoring of WEDM. Int. J. Mach. Tools Manuf. 37, 555–567. https://doi.org/10.1016/S0890-6955(95)00049-6

Lin, C.T., Chung, I.F., Huang, S.Y., 2001. Improvement of machining accuracy by fuzzy logic at corner parts for wire-EDM, Fuzzy Sets and Systems 122, 499-511. https://doi.org/10.1016/S0165-0114(00)00034-8

Lin, P.D., Liao, T.T., 2009. An effective-wire-radius compensation scheme for enhancing the precision of wire-cut electrical discharge machines. Int. J. Adv. Manuf. Technol. 40, 324–331. https://doi.org/10.1007/s00170-007-1333-0

Luo, Y.F., 1995. An energy-distribution strategy in fast-cutting wire EDM, Journal of Materials Processing Technology.

Luo, Y.F., 1999. Rupture failure and mechanical strength of the electrode wire used in wire EDM. J. Mater. Process. Technol. 94, 208–215. https://doi.org/10.1016/S0924-0136(99)00107-7

Ly M, Sanchez G, inventor; Thermo Compact SA, assignee. Electrode wire for spark erosion. United States patent US 8,338,735. 2012.

Mahapatra, S.S., Patnaik, A., 2007. Optimization of wire electrical discharge machining (WEDM) process parameters using Taguchi method 911–925. https://doi.org/10.1007/s00170-006-0672-6

Maher, I., Sarhan, A.A.D., Hamdi, M., 2014. Review of improvements in wire electrode properties for longer working time and utilization in wire EDM machining. Int. J. Adv. Manuf. Technol. 76, 329–351. https://doi.org/10.1007/s00170-014-6243-3

Maher, I., Sarhan, A.A.D., Marashi, H., 2017. Wire Rupture Optimization in Wire Electrical Discharge Machining using Taguchi Approach. MATEC Web Conf. 95, 07014. https://doi.org/10.1051/matecconf/20179507014

Manjaiah, M., Narendranath, S., Basavarajappa, S., Gaitonde, V.N., 2015. Effect of electrode

material in wire electro discharge machining characteristics of Ti50Ni50-xCux shape memory alloy. Precis. Eng. 41, 68–77. https://doi.org/10.1016/j.precisioneng.2015.01.008

Manjaiah, M., Narendranath, S., Basavarajappa, S., Gaitonde, V.N., 2014. Wire electric discharge machining characteristics of titanium nickel shape memory alloy. Trans. Nonferrous Met. Soc. China (English Ed. 24, 3201–3209. https://doi.org/10.1016/S1003-6326(14)63461-0

Maria, P. and Costa, P., 2010. Image Processing: The Fundamentals.

Mohapatra, K.D., Shaibu, V.B., Sahoo, S.K., 2018. Modeling and Analysis of Wire EDM in a Gear Cutting Process for a 2D Model. Mater. Today Proc. 5, 4793–4802. https://doi.org/10.1016/j.matpr.2017.12.053

Mohri, N., Yamada, H., Furutani, K., Narikiyo, T., Magara, T., 1998. System Identification of Wire Electrical Discharge Machining. CIRP Ann. - Manuf. Technol. 47, 173–176. https://doi.org/10.1016/S0007-8506(07)62811-X

Mori, A., Kunieda, M., Abe, K., 2016. Clarification of Gap Phenomena in Wire EDM Using Transparent Electrodes. Procedia CIRP 42, 601–605. https://doi.org/10.1016/j.procir.2016.02.219

Mouralova, K., Kovar, J., Klakurkova, L., Blazik, P., Kalivoda, M., Kousal, P., 2018. Analysis of surface and subsurface layers after WEDM for Ti-6Al-4V with heat treatment. Meas. J. Int. Meas. Confed. 116, 556–564. https://doi.org/10.1016/j.measurement.2017.11.053

Mouralova, K., Benes, L., Prokes, T., Bednar, J., Zahradnicek, R., Fries, J., 2020. Machining of pure molybdenum using WEDM. Meas. J. Int. Meas. Confed. 163, 108010. https://doi.org/10.1016/j.measurement.2020.108010

Murphy, K.D., Lin, Z., 2000. Influence of spatially nonuniform temperature fields on the vibration and stability characteristics of EDM wires. Int. J. Mech. Sci. 42, 1369–1390. https://doi.org/10.1016/S0020-7403(99)00064-8

Nart, E., Celik, Y., 2013. A practical approach for simulating submerged arc welding process using FE method. JCSR 84, 62–71. https://doi.org/10.1016/j.jcsr.2013.02.005

Nain, S.S., Garg, D., Kumar, S., 2018a. Investigation for obtaining the optimal solution for improving the performance of WEDM of super alloy Udimet-L605 using particle swarm

optimization. Eng. Sci. Technol. an Int. J. 21, 261–273. https://doi.org/10.1016/j.jestch.2018.03.005

Naidu, B.V., Varaprasad, K.C., Rao, K.P., 2020. Experimental analysis on wire spark erosion machining of aluminium hybrid metal matrix composites by Taguchi approach. Mater. Today Proc. 39, 206-210. https://doi.org/10.1016/j.matpr.2020.06.493

Nain, S.S., Garg, D., Kumar, S., 2018b. Evaluation and analysis of cutting speed, wire wear ratio, and dimensional deviation of wire electric discharge machining of super alloy Udimet-L605 using support vector machine and grey relational analysis. Adv. Manuf. 6, 225–246. https://doi.org/10.1007/s40436-017-0192-7

Obara, H., Iwata, Y., 1995. An Attempt to Detect Wire Temperature Distribution During Wire EDM, in: Proceedings of the Eleventh International Symposium for Electro-Machining (ISEM-11). Lausanne, Switzerland.

Okada, A., Konishi, T., Okamoto, Y., Kurihara, H., 2015. Wire breakage and deflection caused by nozzle jet flushing in wire EDM. CIRP Ann. - Manuf. Technol. 64, 233–236. https://doi.org/10.1016/j.cirp.2015.04.034

Okada, A., Uno, Y., Nakazawa, M., Yamauchi, T., 2010. Evaluations of spark distribution and wire vibration in wire EDM by high-speed observation. CIRP Ann. - Manuf. Technol. 59, 231–234. https://doi.org/10.1016/j.cirp.2010.03.073

Okada, A., Uno, Y., Onoda, S., Habib, S., 2009. Computational fluid dynamics analysis of working fluid flow and debris movement in wire EDMed kerf. CIRP Ann. - Manuf. Technol. 58, 209–212. https://doi.org/10.1016/j.cirp.2009.03.003

Owhal, A., Srinivasa Rao, N., Gupta, U., Mahajan, M., 2020. Extension of Wire-EDM Capability for Turning Titanium Alloy and an Experimental Study for Process Optimization by Grey Relational Analysis. Mater. Today Proc. 24, 966–974. https://doi.org/10.1016/j.matpr.2020.04.409

Pandey, P.C., Jilani, S.T., 1986. Plasma channel growth and the resolidified layer in EDM. Precis. Eng. 8, 104–110. https://doi.org/10.1016/0141-6359(86)90093-0

Patel, M.R., Barrufet, M.A., Eubank, P.T., DiBitonto, D.D., 1989. Theoretical models of the electrical discharge machining process. II. The anode erosion model. J. Appl. Phys. 66, 4104–4111. https://doi.org/10.1063/1.343995

Powell R.L., Childs G.E., Thermal Conductivity. Cyrogenics Division, NBS Institute for

Basic Standards.

Pramanik, A., Basak, A.K., 2016. Degradation of wire electrode during electrical discharge machining of metal matrix composites. Wear 346–347, 124–131. https://doi.org/10.1016/j.wear.2015.11.011

Pramanik, A., Basak, A.K., 2018. Sustainability in wire electrical discharge machining of titanium alloy : Understanding wire rupture. J. Clean. Prod. 198, 472–479. https://doi.org/10.1016/j.jclepro.2018.07.045

Pramanik, A., Basak, A.K., 2019. Effect of wire electric discharge machining (EDM) parameters on fatigue life of Ti-6Al-4V alloy. Int. J. Fatigue 128, 105186. https://doi.org/10.1016/j.ijfatigue.2019.105186

Prohaszka, J., Mamalis, A.G., Vaxevanidis, N.M., 1997. The effect of electrode material on machinability in wire electro-discharge machining 69, 233–237.

Prevéy P.S., 1986. X-ray diffraction residual stress techniques. American society for metals. ASM handbook, Ohio. ASM International. 380–92.

Puri, YM, & Deshpande, N., 2006. Parametric Optimization of WEDM of High Chromium High Carbon Die Steel Using ANN, in: Proceedings of the ASME 2006 International Mechanical Engineering Congress and Exposition. Manufacturing Engineering and Textile Engineering. Chicago, Illinois, USA, pp. 167–175. https://doi.org/https://doi.org/10.1115/IMECE2006-14306

Puri, A.B., Bhattacharyya, B., 2003a. Modelling and analysis of the wire-tool vibration in wire-cut EDM. J. Mater. Process. Technol. 141, 295–301. https://doi.org/10.1016/S0924-0136(03)00280-2

Puri, A.B., Bhattacharyya, B., 2003b. An analysis and optimisation of the geometrical inaccuracy due to wire lag phenomenon in WEDM. Int. J. Mach. Tools Manuf. 43, 151–159. https://doi.org/10.1016/S0890-6955(02)00158-X

Qu, J., Shih, A.J., Scattergood, R.O., 2002. Development of the cylindrical wire electrical discharge machining process, part 2: Surface integrity and roundness. J. Manuf. Sci. Eng. Trans. ASME 124, 708–714. https://doi.org/10.1115/1.1475989

Rajurkar, K.P., Wang, W.M., Lindsay, R.P., 1991. On-Line Monitor and Control for Wire Breakage in WEDM. CIRP Ann. - Manuf. Technol. 40, 219–222. https://doi.org/10.1016/S0007-8506(07)61972-6

Rajurkar, K.P., Wang, W.M., McGeough, J.A., 1994. WEDM Identification and Adaptive Control for Variable-Height Components. CIRP annals 43, 199-202. https://doi.org/10.1016/S0007-8506(07)62195-7

Rajurkar, K.P., Wang, W.M., 1997. Improvement of EDM performance with advanced monitoring and control systems. J. Manuf. Sci. Eng. 119, 770–775.

Rajurkar, K.P., Wang, W.M., Zhao, W.S., 1997. WEDM-Adaptive Control with a Multiple Input Model for lndentification of Workpiece Height. CIRP Annals 46, 147-150.

Reed R.P., Mikesell R.P., 1967. Low Temperature Mechanical Properties Of Copper and Selected Copper Alloys. U.S. Department of Commerce, National Bureau of Standards.

Roy, A., Narendranath, S., 2018. Effect of spark gap voltage and wire electrode feed rate on machined surface morphology during Wire EDM process, in: Materials Today: Proceedings. Elsevier Ltd, pp. 18104–18109. https://doi.org/10.1016/j.matpr.2018.06.145

Saha, S., Pachon, M., Ghoshal, A., Schulz, M.J., 2004. Finite element modeling and optimization to prevent wire breakage in electro-discharge machining. Mech. Res. Commun. 31, 451–463. https://doi.org/10.1016/j.mechrescom.2003.09.006

Sanchez, J.A., Plaza, S., Ortega, N., Marcos, M., Albizuri, J., 2008. Experimental and numerical study of angular error in wire-EDM taper-cutting. Int. J. Mach. Tools Manuf. 48, 1420–1428. https://doi.org/10.1016/j.ijmachtools.2008.04.011

Sarkar, S., Sekh, M., Mitra, S., Bhattacharyya, B., 2011. A novel method of determination of wire lag for enhanced profile accuracy in WEDM. Precis. Eng. 35, 339–347. https://doi.org/10.1016/j.precisioneng.2011.01.001

Sen, R., Choudhuri, B., Barma, J.D., Chakraborti, P., 2018. Study the impact of process parameters and electrode material on wire electric discharge machining performances. Mater. Today Proc. 5, 7552–7560. https://doi.org/10.1016/j.matpr.2017.11.427

Seong KC, inventor. Method of manufacturing porous electrode wire for electric discharge machining and structure of the electrode wire. United States patent US 6,306,523. 2001.

Shoda, K., Kaneko, Y., Nishimura, H., M.K., 1992. Adaptive Control of WEDM with On-line Detection of Spark Locations, in: Proceeding of the Tenth International Symposium for Electro-Machining (ISEM-10). Magdeburg, Germany.

Singh, B., Misra, J.P., 2019. Surface finish analysis of wire electric discharge machined

specimens by RSM and ANN modeling. Measurement 137, 225–237. https://doi.org/10.1016/j.measurement.2019.01.044

Singh, R., Pratap Singh, R., Tyagi, M., Kataria, R., 2019. Investigation of dimensional deviation in wire EDM of M42 HSS using cryogenically treated brass wire. Mater. Today Proc. 2–8. https://doi.org/10.1016/j.matpr.2019.08.028

Sneha, P., Mahamani, A., Kakaravada, I., 2018. Optimization of Wire Electric Discharge Machining Parameters in Machining of Ti-6Al-4V Alloy. Mater. Today Proc. 5, 6722–6727. https://doi.org/10.1016/j.matpr.2017.11.330

Taylor R.E., Finch R.A., 1964. The specific heats and resistivities of molybdenum, tantalum, and rhenium. J of the Less Common Metals. 6, 283‑294. https://doi.org/10.1016/0022-5088(64)90124-9.

Tang, A., Li, S., Yang, G., Li, L., Landers, R.G., 2019. Wire Vibration Modeling and Experimental Analysis for Wire Saw Machining. J. Manuf. Sci. Eng. 141, 1–10. https://doi.org/10.1115/1.4045059

Tietz T.E., Wilson J.W., 1961.Mechanical, oxidation, and thermal property data for seven refractory metals and their alloys Sunnyvale (CA): Lockheed Missiles and Space Division, Lockheed Aircraft Corporation; Report No.: NP-11108.

Tomura, S., Kunieda, M., 2009. Analysis of electromagnetic force in wire-EDM. Precis. Eng. 33, 255–262. https://doi.org/10.1016/j.precisioneng.2008.07.004

Tosun, N., Cogun, C., 2003. An investigation on wire wear in WEDM. J. Mater. Process. Technol. 134, 273–278. https://doi.org/10.1016/S0924-0136(02)01045-2

Valencia J.J., Quested P. N., 2008. Thermophysical Properties. ASM Handbook. 15, 468-481. DOI: 10.1361/asmhba0005240

Wang, J., Ravani, B., 2003. Computer aided contouring operation for traveling wire electric discharge machining (EDM) 35, 925–934. https://doi.org/10.1016/S0010-4485(02)00207-5

Yadav, V., Jain, V.K., Dixit, P.M., 2002. Thermal stresses due to electrical discharge machining. Int. J. Mach. Tools Manuf. 42, 877–888. https://doi.org/10.1016/S0890-6955(02)00029-9

Yan, H., Bakadiasa Kabongo, D., Yan, Z., Han, F., Chen, Z., 2020. Sustainable production of high-uniformity workpiece surface quality in wire electrical discharge machining by

fabricating surface microstructure on wire electrode. J. Clean. Prod. 259. https://doi.org/10.1016/j.jclepro.2020.120881

Yan, M.T., Liao, Y.S., 1996. A self-learning fuzzy controller for wire rupture prevention in WEDM. Inter. J. Adv. Manuf. Technol. 11, 267–275.

Yan, M.T., Liao, Y.S., 1996. Monitoring and self-learning fuzzy control for wire rupture prevention in wire electrical discharge machining. Int. J. Mach. Tools Manuf. 36, 339–353. https://doi.org/10.1016/0890-6955(95)00050-X

Yan, M.T., Liao, Y.S., Chang, C.C., 2001. On-line estimation of workpiece height using neural networks and hierarchical adaptive control of WEDM. Inter. J. Adv. Manuf. Technol. 18, 884–891.

Yan, M.T., Huang, C.W., Fang, C.C., Chang, C.X., 2004. Development of a prototype Micro-Wire-EDM machine. J. Mater. Process. Technol. 149, 99–105. https://doi.org/10.1016/j.jmatprotec.2003.10.057

Yan, M.T., Huang, P.H., 2004. Accuracy improvement of wire-EDM by real-time wire tension control. Int. J. Mach. Tools Manuf. 44, 807–814. https://doi.org/10.1016/j.ijmachtools.2004.01.019

Yan, M.T., Chien, H.T., 2007. Monitoring and control of the micro wire-EDM process. Int. J. Mach. Tools Manuf. 47, 148–157. https://doi.org/10.1016/j.ijmachtools.2006.02.006

Yan, M.T., Fang, C.C., 2008. Application of genetic algorithm-based fuzzy logic control in wire transport system of wire-EDM machine. J. Mater. Process. Technol. 205, 128–137. https://doi.org/10.1016/j.jmatprotec.2007.11.091

Yang, X., Xu, C., Kunieda, M., 2010. Miniaturization of WEDM using electrostatic induction feeding method. Precis. Eng. 34, 279–285. https://doi.org/10.1016/j.precisioneng.2009.07.002

Yang, X., Feng, G., Teng, Q., 2012. Temperature field simulation of wire electrode in high-speed and medium-speed WEDM under moving heat source. Procedia CIRP 1, 633–638. https://doi.org/10.1016/j.procir.2012.04.112

Yeo, S.H., Kurnia, W., Tan, P.C., 2008. Critical assessment and numerical comparison of electro-thermal models in EDM. J. Mater. Process. Technol. 203, 241–251. https://doi.org/10.1016/j.jmatprotec.2007.10.026

Zhang, G., Chen, Z., Zhang, Z., Huang, Y., Ming, W., Li, H., 2014. A macroscopic

mechanical model of wire electrode deflection considering temperature increment in MS-WEDM process. Int. J. Mach. Tools Manuf. 78, 41–53. https://doi.org/10.1016/j.ijmachtools.2014.01.004

Zhang, Y., Zhang, Z., Huang, H., Huang, Y., Zhang, G., Li, W., Liu, C., 2018. Study on thermal deformation behavior and microstructural characteristics of wire electrical discharge machining thin-walled components. J. Manuf. Process. 31, 9–19. https://doi.org/10.1016/j.jmapro.2017.10.024

Zhang, G., Li, W., Zhang, Y., Huang, Y., Zhang, Z., Chen, Z., 2020. Analysis and reduction of process energy consumption and thermal deformation in a micro-structure wire electrode electric discharge machining thin-wall component. J. Clean. Prod. 244, 118763. https://doi.org/10.1016/j.jclepro.2019.118763

Zhang, Z., Huang, H., Ming, W., Xu, Z., Huang, Y., Zhang, G., 2016. Study on machining characteristics of WEDM with ultrasonic vibration and magnetic field assisted techniques. J. Mater. Process. Technol. 234, 342–352. https://doi.org/10.1016/j.jmatprotec.2016.04.007

Zhao, Y., Kunieda, M., Abe, K., 2018. A novel technique for slicing SiC ingots by EDM utilizing a running ultra-thin foil tool electrode. Precis. Eng. 52, 84–93. https://doi.org/10.1016/j.precisioneng.2017.11.012

Appendix

Appendix A2

Permission for Figure 2.4

This Agreement between iit guwahati -- sanghamitra das ("You") and Elsevier ("Elsevier") consists of your license details and the terms and conditions provided by Elsevier and Copyright Clearance Center.

License Number	5205390066084
License date	Dec 10, 2021
Licensed Content Publisher	Elsevier
Licensed Content Publication	Journal of Materials Processing Technology
Licensed Content Title	Analysis of three-dimensional transient heat conduction for predicting wire erosion in the wire electrical discharge machining process
Licensed Content Author	S. Banerjee,B.V.S.S.S. Prasad,P.K. Mishra
Licensed Content Date	Mar 1, 1997
Licensed Content Volume	65
Licensed Content Issue	1-3
Licensed Content Pages	9
Start Page	134

End Page	142
Type of Use	reuse in a thesis/dissertation
Portion	figures/tables/illustrations
Number of figures/tables /illustrations	1
Format	both print and electronic
Are you the author of this Elsevier article?	No
Will you be translating?	No
Title	Numerical and Experimental Investigations on Wire Electrode Health during Wire Electric Discharge Machining Process
Institution name	Indian Institute of Technology Guwahati
Expected presentation date	Feb 2022
Portions	Figure 4
Requestor Location	iit guwahati amingaon, north guwahati guwahati, assam 781039 India Attn: iit guwahati
Publisher Tax ID	GB 494 6272 12

Permission for Figure 2.6

This Agreement between iit guwahati -- sanghamitra das ("You") and Elsevier ("Elsevier") consists of your license details and the terms and conditions provided by Elsevier and Copyright Clearance Center.

License Number	5205390983822
License date	Dec 10, 2021
Licensed Content Publisher	Elsevier
Licensed Content Publication	CIRP Annals - Manufacturing Technology
Licensed Content Title	Modelling of ECM and EDM processes
Licensed Content Author	S. Hinduja,M. Kunieda
Licensed Content Date	Jan 1, 2013
Licensed Content Volume	62
Licensed Content Issue	2
Licensed Content Pages	23
Start Page	775
End Page	797

Type of Use	reuse in a thesis/dissertation
Portion	figures/tables/illustrations
Number of figures/tables /illustrations	1
Format	both print and electronic
Are you the author of this Elsevier article?	No
Will you be translating?	No
Title	Numerical and Experimental Investigations on Wire Electrode Health during Wire Electric Discharge Machining Process
Institution name	Indian Institute of Technology Guwahati
Expected presentation date	Feb 2022
Portions	Figure 44
Requestor Location	iit guwahati amingaon, north guwahati guwahati, assam 781039 India Attn: iit guwahati
Publisher Tax ID	GB 494 6272 12

Permission for Figure 2.7

This Agreement between iit guwahati -- sanghamitra das ("You") and Elsevier ("Elsevier") consists of your license details and the terms and conditions provided by Elsevier and Copyright Clearance Center.

License Number	5205391130689
License date	Dec 10, 2021
Licensed Content Publisher	Elsevier
Licensed Content Publication	Wear
Licensed Content Title	Degradation of wire electrode during electrical discharge machining of metal matrix composites
Licensed Content Author	A. Pramanik,A.K. Basak
Licensed Content Date	Jan 15, 2016
Licensed Content Volume	346
Licensed Content Issue	n/a
Licensed Content Pages	8
Start Page	124
End Page	131

Type of Use	reuse in a thesis/dissertation
Portion	figures/tables/illustrations
Number of figures/tables /illustrations	1
Format	both print and electronic
Are you the author of this Elsevier article?	No
Will you be translating?	No
Title	Numerical and Experimental Investigations on Wire Electrode Health during Wire Electric Discharge Machining Process
Institution name	Indian Institute of Technology Guwahati
Expected presentation date	Feb 2022
Portions	Figure 1
Requestor Location	iit guwahati amingaon, north guwahati guwahati, assam 781039 India Attn: iit guwahati
Publisher Tax ID	GB 494 6272 12

Permission for Figure 2.8

This Agreement between iit guwahati -- sanghamitra das ("You") and Elsevier ("Elsevier") consists of your license details and the terms and conditions provided by Elsevier and Copyright Clearance Center.

License Number	5205400073638
License date	Dec 10, 2021
Licensed Content Publisher	Elsevier
Licensed Content Publication	Journal of Cleaner Production
Licensed Content Title	Sustainability in wire electrical discharge machining of titanium alloy: Understanding wire rupture
Licensed Content Author	A. Pramanik,A.K. Basak
Licensed Content Date	Oct 10, 2018
Licensed Content Volume	198
Licensed Content Issue	n/a
Licensed Content Pages	8
Start Page	472
End Page	479

Type of Use	reuse in a thesis/dissertation
Portion	figures/tables/illustrations
Number of figures/tables /illustrations	1
Format	both print and electronic
Are you the author of this Elsevier article?	No
Will you be translating?	No
Title	Numerical and Experimental Investigations on Wire Electrode Health during Wire Electric Discharge Machining Process
Institution name	Indian Institute of Technology Guwahati
Expected presentation date	Feb 2022
Portions	Figure 4
Requestor Location	iit guwahati amingaon, north guwahati guwahati, assam 781039 India Attn: iit guwahati
Publisher Tax ID	GB 494 6272 12

Permission for Figure 2.9

This Agreement between iit guwahati -- sanghamitra das ("You") and Elsevier ("Elsevier") consists of your license details and the terms and conditions provided by Elsevier and Copyright Clearance Center.

License Number	5205400184790
License date	Dec 10, 2021
Licensed Content Publisher	Elsevier
Licensed Content Publication	CIRP Annals - Manufacturing Technology
Licensed Content Title	Evaluations of spark distribution and wire vibration in wire EDM by high-speed observation
Licensed Content Author	A. Okada,Y. Uno,M. Nakazawa,T. Yamauchi
Licensed Content Date	Jan 1, 2010
Licensed Content Volume	59
Licensed Content Issue	1
Licensed Content Pages	4
Start Page	231
End Page	234

Type of Use	reuse in a thesis/dissertation
Portion	figures/tables/illustrations
Number of figures/tables /illustrations	1
Format	both print and electronic
Are you the author of this Elsevier article?	No
Will you be translating?	No
Title	Numerical and Experimental Investigations on Wire Electrode Health during Wire Electric Discharge Machining Process
Institution name	Indian Institute of Technology Guwahati
Expected presentation date	Feb 2022
Portions	Figure 1
Requestor Location	iit guwahati amingaon, north guwahati guwahati, assam 781039 India Attn: iit guwahati
Publisher Tax ID	GB 494 6272 12

Permission for Figure 2.11 and 2.12

This Agreement between iit guwahati -- sanghamitra das ("You") and Elsevier ("Elsevier") consists of your license details and the terms and conditions provided by Elsevier and Copyright Clearance Center.

License Number	5205400692077
License date	Dec 10, 2021
Licensed Content Publisher	Elsevier
Licensed Content Publication	Journal of Materials Processing Technology
Licensed Content Title	Study on machining characteristics of WEDM with ultrasonic vibration and magnetic field assisted techniques
Licensed Content Author	Zhen Zhang,Hao Huang,Wuyi Ming,Zhong Xu,Yu Huang,Guojun Zhang
Licensed Content Date	Aug 1, 2016
Licensed Content Volume	234
Licensed Content Issue	n/a
Licensed Content Pages	11
Start Page	342

End Page	352
Type of Use	reuse in a thesis/dissertation
Portion	figures/tables/illustrations
Number of figures/tables /illustrations	2
Format	both print and electronic
Are you the author of this Elsevier article?	No
Will you be translating?	No
Title	Numerical and Experimental Investigations on Wire Electrode Health during Wire Electric Discharge Machining Process
Institution name	Indian Institute of Technology Guwahati
Expected presentation date	Feb 2022
Portions	Figures 1 and 4
Requestor Location	iit guwahati amingaon, north guwahati guwahati, assam 781039 India Attn: iit guwahati
Publisher Tax ID	GB 494 6272 12

Appendix A3

DFLUX subroutine to incorporate moving heat source characteristics in the thermo-mechanical modeling of the wire electrode

(This subroutine is written for the molybdenum wire at process conditions: V = 85 V, I = 6 A, t_{on} = 16 µs, t_{off} = 2 µs, v = 6 m/s)

```
      SUBROUTINE
DFLUX(FLUX,SOL,KSTEP,KINC,TIME,NOEL,NPT,COORDS,JLTYP,
     1          TEMP,PRESS,SNAME)

      INCLUDE 'ABA_PARAM.INC'

      DIMENSION FLUX (2),TIME(2),COORDS(3)
      CHARACTER*80 SNAME
       REAL vel,X0,Y0,Z0,DX,DY,R,pi,DZ,L,sr
       REAL V, I, TON
       Qmax=11.612*(10**10)
       V=85
       I=6
       TON=0.000016
       vel = 6
       R=2.04E-3
       R=R*(I**0.43)
       R=R*(TON**0.44)
       WRITE(*,*)R,R
       pi = 3.14
       X0 = 0.0    !initial heat source position
       Y0 = 0.00009
       Z0 = 0.00055
       L = vel*TIME(1)
       DX = COORDS(1)-X0
```

```
DY = COORDS(2)-Y0
DZ = Z0-L-COORDS(3)
sr = sqrt(DX**2 + DZ**2)
IF (sr.LT.R.AND.TIME(1).LE.TON) THEN
      FLUX(1) = Qmax*exp(-4.5*(sr**2)/(R**2))
                ELSE IF (TIME(1).GT.TON) THEN
                  FLUX(1) = 0

ENDIF
FLUX(2)=0.0
RETURN
END
```

Appendix A5

Appendix A5.1 Specifications of the Wire cut EDM system

Our(NIQ) Specifications	VENDOR 3 (M/s Mahi Traders, Guwahati)
	Model: ECO 32 **Make: JK Machines**
Technical Specification:	
• X axis Travel of the table : 300-350 mm	**320 mm**
• Y axis Travel of the table : 350-400 mm	**400 mm**
• Maximum Work Table Area : 415x 635 mm	**440 x 680 mm**
• Maximum Work-piece Thickness to cut : 500 mm	**400 mm**
• Maximum taper per 100 mm thickness : $\pm 3^0$	**.± 3^0**
• Work-piece weight to handle : 400-450 kg	**300 Kg**
• Maximum Speed : 80 mm^2/min	**80 mm^2/min**
• Machining accuracy : 0.01 mm	**0.01**
• Least Input Increment : 0.001 mm	**0.001**
• Least Command Input : $\pm$ 0.001 mm	**0001**
• Best Surface Finish : 1.25 To 1.75 µ Ra	**1.25 to 1.75 µ Ra**
• Display : LCD monitor	**LCD**
• Axis control : 4 axis (X,Y,U & V)	**4 axis**
• Resolution : 0.001 mm	**0.001**
• Interpolation : Linear and Circular	**0.18**
• Programming : Incremental	**Linear & Circular**
• Least Input Increment : 0.001 mm	**Incremental**
• Least Command Input : ± 0.001 mm	**0.001 mm**
• Data input / output system : USB, Key board and Mouse.	**0.001 mm** **USB, key board , mouse**
• Power : 3 Phase, 415 V, 50 Hz	**3 Phase, 415 V, 50 Hz**
• Control System : Computer Numerical Control	**LM Guide ways for x and y axis**
• Guide ways : L M Guide ways for x and y Axis	
• Total Machine Load : 1.5 KVA	**1.5 kVA**
• Dielectric fluid : Soft Water (D.M Water) +Gel	**Soft water + Gel**
• Dielectric Tank Capacity : 55 Ltrs	**55 Ltr**

List of publications

Book chapters

1. **Das, S.**, Joshi, S.N. and Dixit U.S., 2021. Modeling and Optimization of EDM-Based Hybrid Machining Processes. In: Kuriachen B., Mathew J. and Dixit U. S. (eds) *Electric Discharge Hybrid-Machining Processes: Fundamentals and Applications*. CRC Press, Taylor and Francis Group.
2. **Das, S.** and Joshi, S.N., 2020. Thermal Modeling and Simulation of Crater Generation on Wire Electrode during Wire EDM Operation. In: Shunmugam M., Kanthababu M. (eds) Advances in Simulation, Product Design and Development (pp. 121-135). Springer, Singapore.https://doi.org/10.1007/978-981-32-9487-5_10.
3. Kumar, J., **Das, S.** and Joshi, S.N., 2020. Three-Dimensional Numerical Modelling of Temperature Profiles on the Wire Electrode During Wire Electric Discharge Machining Process. In Biswal B., Sarkar B., Mahanta P. (eds) Advances in Mechanical Engineering (pp. 359-371). Springer, Singapore.https://doi.org/10.1007/978-981-15-0124-1_32.

Journal papers

1. **Das, S.** and Joshi, S.N., 2020. Estimation of wire strength based on residual stresses induced during wire electric discharge machining. *Journal of Manufacturing Processes*, 53, pp.406-419. https://doi.org/10.1016/j.jmapro.2020.03.015. [*SCI, Elsevier, Impact factor: 5.010, Paper citations: 7*]
2. **Das, S.** and Joshi, S.N., 2021. Measurement and analysis of molybdenum wire erosion and deformation during wire electric discharge machining of Ti-6Al-4V alloy. *Measurement*, *179*, p.109440. https://doi.org/10.1016/j.measurement.2021.109440. [*SCI, Elsevier, Impact factor: 3.927*]
3. Kumar, S., **Das, S.** and Joshi, S.N., 2021. Finite Element Modeling of Thermal Residual Stresses generated during EDM of AISI 1018 Steel. *Journal of The Institution of Engineers (India): Series C*, pp.1-9. https://doi.org/10.1007/s40032-021-00695-7. (not related to thesis work)
4. **Das, S.** and Joshi, S.N., Review of the causes of wire breakage and its mitigation during the wire electric discharge machining (wire-EDM) process. ASME Journal of Manufacturing Science and Engineering. (Under review)

5. **Das, S.** and Joshi, S.N., Prediction of crater induced failure of coated wires during wire EDM of Ti-6Al-4V alloy. Wear. (Under review)

Conference papers

1. **Das S.** and Joshi S. N., Thermal modeling and simulation of crater generation on wire electrode during wire EDM operation, In *7th International & 28th All India Manufacturing Technology, Design and Research Conference (AIMTDR-2018)*, College of Engineering Guindy, Anna University, Chennai, INDIA, December 13th-15th, 2018. (Presented in person).
2. Kumar J., **Das S.** and Joshi S.N., Three-dimensional numerical modeling of temperature profiles on the wire electrode during wire electric discharge machining process, In *International Conference on Recent Innovations and Developments in Mechanical Engineering (ICRIDME-2018)*, NIT Meghalaya, Shillong, India, 8th-10th November, 2018. (Presented in person) **(Best Poster Presentation award)**
3. **Das S.** and Joshi S. N., Causes of wire breakage during wire electric discharge machining process, In *7th International Conference on Advancements and Futuristic Trends in Mechanical and Materials Engineering(AFTMME 2019)*,Indian Institute of Technology Ropar, Punjab, INDIA, December 05th-07th, 2019.(Presented in person).
4. Kumar S., **Das S.** and Joshi S.N., Thermal residual stress analysis during electrical discharge machining of AISI 1018 steel, In *7th International Conference on Advancements and Futuristic Trends in Mechanical and Materials Engineering*(*AFTMME 2019*),Indian Institute of Technology Ropar, Punjab, INDIA, December 05th-07th, 2019.(Presented in person).
5. **Das S.** and Joshi S. N., Effect of Spark Discharges on Wire Cross Sections During Wire Electric Discharge Machining of Ti-6Al-4V Alloy, In *International Conference on Advancements and Futuristic Trends in Mechanical and Materials Engineering*(*AFTMME 2020*), **S**ociety of Materials & Mechanical Engineers, December 19th-20th, 2020.(Presented in person).
6. **Das S.** and Joshi S. N., Experimental investigations into erosion of zinc coated brass wire electrode during wire electric discharge machining of Ti-6Al-4V alloy, In 8*th International & 29th All India Manufacturing Technology, Design and Research*

Conference (*AIMTDR-2021*), PSG College of Technology, Coimbatore and PSG Institute of Technology and Applied Research, Coimbatore, INDIA, December 9th-11th, 2021. (Presented in person).

7. Gautom U., **Das S.** and Sarma D.K., Prediction of Surface Roughness on Dry Turning using Two Different Cutting Tool Nose Radius, In *5th International & 26th All India Manufacturing Technology, Design and Research Conference (AIMTDR-14)*,Department of Mechanical Engineering, Indian Institute of Technology Guwahati, Guwahati, INDIA, December 12th-14th, 2014. (Presented in person).